

Reconstruction of late Quaternary marine and terrestrial environmental conditions of Northwest Africa and Southeast Australia

A multiple organic proxy study using marine sediments

Raquel A. Lopes dos Santos

ISBN: 978-94-6203-218-7

Cover design by: John Cluderay

Printed by Wöhrmann Print Service; Zutphen

Reconstruction of late Quaternary marine and terrestrial environmental conditions of Northwest Africa and Southeast Australia

A multiple organic proxy study using marine sediments

Reconstructie van laat-Kwartair mariene en terrestrische milieucondities van Noordwest Afrika en Zuidoost Australië

Een studie van mariene sedimenten met meerdere organische proxies
(met een samenvatting in het Nederlands)

Reconstrução do ambiente marinho e terrestre do Noroeste Africano e Sudeste Australiano durante o Quaternário tardio

Uso de múltiplos indicadores orgânicos em sedimentos marinhos
(com um sumário em Português)

Proefschrift

ter verkrijging van de graad van doctor aan de Universiteit Utrecht op gezag van de rector magnificus, prof.dr. G.J. van der Zwaan, ingevolge het besluit van het college voor promoties in het openbaar te verdedigen op maandag 17 december 2012 des middags te 12.45 uur

door

Raquel Alfama Lopes dos Santos

geboren op 10 oktober 1979 te Mindelo, Cabo Verde

Promotoren: Prof. dr. ir. S. Schouten

Prof. dr. ir. J.S. Sinninghe Damsté

The research in this thesis was funded through a VICI grant by the Netherlands Organisation for Scientific Research (NWO-ALW)

“Measure what is measurable and make measurable what cannot now be measured.”

(Galileo)

“...
Fazê nos lar
Lugar mas sabe qu’tem na mundo
Fazê nh’infancia
Um jardim de felecidade

‘Judá-me crescê
Cu tudo amor e amizade
Dá-me’ bô carinho e bô ternura
‘O mãe querida que Deus dá-me

Dá-me leite d’bô peito sagrado
Mamãe querida
Dá-me bô sustento bençoade
Papai querido

‘Judá-me vivê nhas ilusão
Nhas fantasia
...”

(Manuel de Novas)

Aos os meus pais Loty e Ruy
pelo vosso imenso amor e suporte
em todas as etápas da minha vida

Table of contents

| | | |
|--|--|-----|
| Chapter 1 | Introduction | 7 |
| Part I Past sea temperatures | | |
| Chapter 2 | Glacial–interglacial variability in Atlantic meridional overturning circulation and thermocline adjustments in the tropical North Atlantic | 17 |
| Chapter 3 | Comparison of organic and inorganic proxies for reconstruction of late Quaternary sea-surface temperature variability from offshore southeastern Australia | 31 |
| Part II Past primary productivity | | |
| Chapter 4 | Relationship between primary productivity and Sahara dust input in the eastern tropical North Atlantic during the late Quaternary | 47 |
| Chapter 5 | Late Quaternary productivity changes from offshore southeastern Australia: a biomarker approach | 61 |
| Chapter 6 | A late Quaternary sedimentary record of steryl alkyl ethers from offshore southeastern Australia | 77 |
| Part III Past vegetation changes | | |
| Chapter 7 | Wet phases in the Sahara/Sahel region and human migration patterns in North Africa | 89 |
| Chapter 8 | A novel method for the rapid analysis of levoglucosan in soils and sediments | 103 |
| Chapter 9 | Abrupt vegetation change follows the late Quaternary megafaunal extinction in southeastern Australia | 109 |
| References | | 118 |
| Summary | | 136 |
| Samenvatting | | 138 |
| Resumo | | 141 |
| Acknowledgements | | 144 |
| Curriculum Vitae | | 146 |

Chapter 1

Introduction

1.1 Climate change and vulnerable regions

Currently, large efforts are undertaken to document and understand global and regional climate change and to define probabilities on how climate will evolve in the future. Climate is normally defined as the ‘average weather’, i.e. the 30 year average of temperature, precipitation and wind (IPCC, 2007). The Intergovernmental Panel on Climate Change (IPCC) recognizes climate change as a change in these conditions that can be identified using statistical tests and that persists for an extended period, typically decades or longer. It refers to any change in climate, whether it is caused by natural processes or as a result of human activity (IPCC, 2007).

One current feature of climate change is the global warming. The current global warming is marked by observations of increases in global average air and ocean temperatures, widespread melting of snow and ice and rising of global average sea level (e.g. IPCC, 2007; Mann et al., 2008; Kemp et al., 2011). It has been suggested that most of the recent observed global warming is caused by increasing greenhouse gas levels, especially CO₂, that start around the same time as industrialization (Canadell et al., 2007; IPCC, 2007; Le Quéré et al., 2009), suggesting human activities as the main cause of this warming. However, to exactly identify the causes of global warming and its impact, knowledge of regional climate change from a network of locations around the world is required.

Africa and Australia are two continents that are strongly affected by climate change. The IPCC 2007 report predicts that climate change in parts of Africa will aggravate the water stress currently faced in some countries, while other countries will start experience water stress, particularly in Northwestern (NW) Africa (Boko et al., 2007). Temperatures are expected to increase 3-4 °C for the period 2080-2099 in comparison to 1980-1999 (Fig. 1.1). In North and Southeastern (SE) Australia, water security problems are expected and increased salinity in the Murray river together with a decrease in streamflow of the Murray-Darling river system, the largest river in Australia, is likely to happen (Hennessy et al., 2007). Temperatures are expected to rise up to 3 °C for the period 2080-2099 in comparison to 1980-1999 (Fig. 1.1).

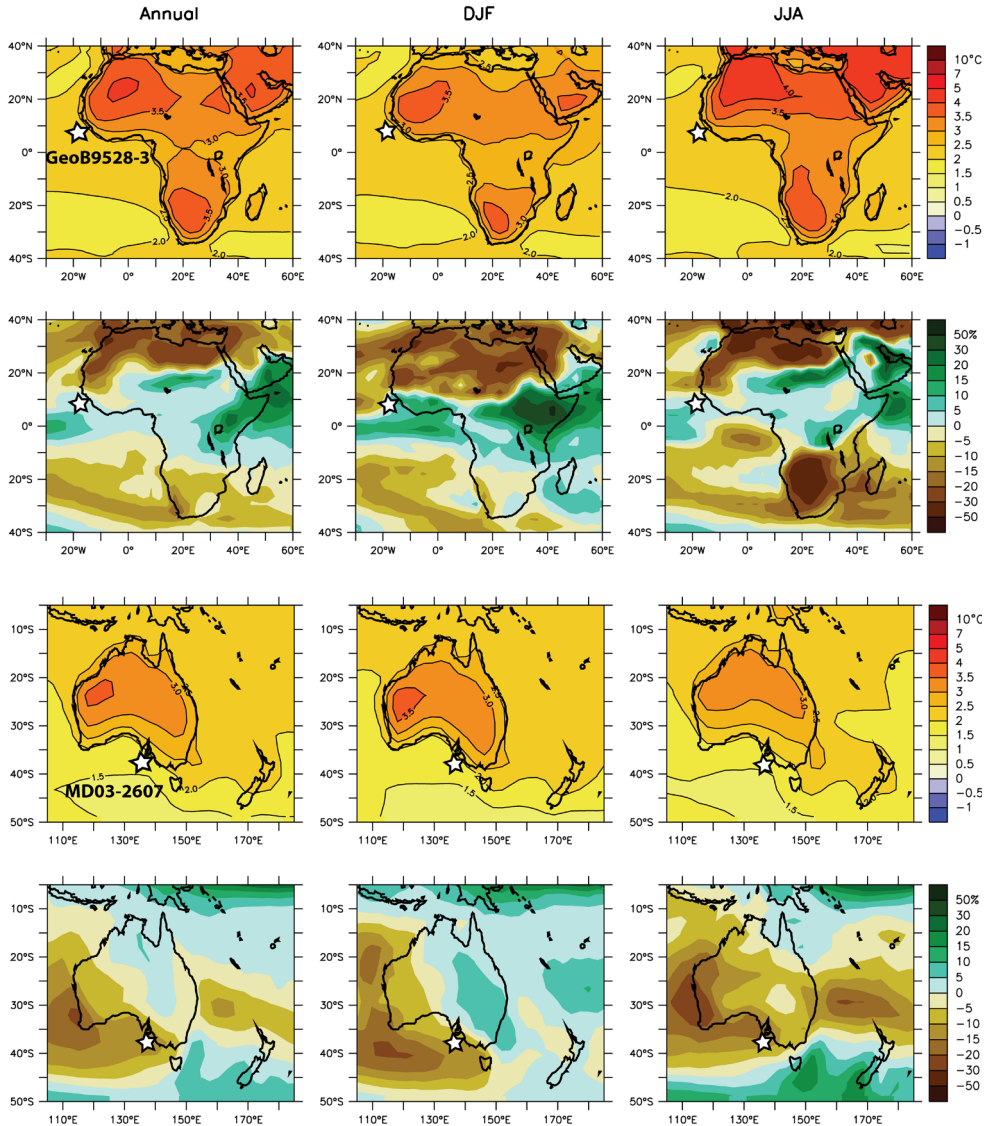


Fig. 1.1: Projected changes in temperature and precipitation over Africa and Australia between 1980-1999 and 2080-2099, averaged from 21 model simulations. First column: annual changes, second column: December to February changes, last column: June to August changes. Stars represent the location of the two sites studied in this thesis. Graphs from IPCC 2007 report (Christensen et al., 2007).

The potential vulnerability to climate change, that will lead to reduced water supply for e.g. irrigation and high loss in biodiversity, makes NW Africa and SE Australia important areas to investigate the impact of future climate change. Unfortunately, uncertainties between

climate models exist for the impact of climate change on NW Africa and SE Australia: where certain models show an increase in precipitation, others show a decrease (Boko et al., 2007; Hennessy et al., 2007). In order to test these model results and examine the magnitude and consequences of future climate change, it is important to reconstruct past climate changes and its variability over longer time scales. However, instrumental records cover less than 10^{-7} of earth's climatic history (Bradley, 1999) and thus provide an incomplete perspective of past conditions on Earth. Therefore, there has been a strong increase in paleoclimatic research over the last decades, in particular for the Quaternary period as it enables to place the modern climate change under boundary conditions, such as continental configurations and the presence of ice sheets, close to those prevailing today. The Quaternary is the geologic period that covers the last 1.8-2 Ma up to present day (Bradley, 1999). It is also the time interval in which modern humans first appeared and spread over the different continents (Stanley, 1999). The Quaternary is divided in two epochs: the Pleistocene, which covers the interval from 2 Ma up to 0.01 Ma, and the Holocene, which covers the past 10 ka. The late Quaternary is an informal geologic term that covers somewhere from the middle Pleistocene (0.7-0.1 Ma) to the most recent times (Alverson et al., 1999, Pether, 2012).

1.2 Climate changes during the late Quaternary

1.2.1 Global climate changes

During the late Quaternary, glacial-interglacial cycles have provided a strong imprint on global climate as identified in the deuterium isotopic composition from ice cores, an indicator for temperature changes (Jouzel et al., 2007) (Fig. 1.2). These oscillations between glacial and interglacial conditions at approximately 100 ka periodicity have been occurring for the last 900 ka. The exact cause of this cyclicity is not yet well known but it is maybe triggered by changes in Earth's orbital configuration called Milankovitch cycles. As the Earth rotates around its axis and orbits around the Sun, several quasi-periodic variations named eccentricity, obliquity and precession occur at mean periods of 100, 41 and 23 ka, respectively (Milankovitch, 1941; Berger, 1978; Imbrie and Imbrie, 1979). The precession and obliquity cycles can also be recognized in the deuterium record of the ice cores (Fig. 1.2).

These glacial-interglacial cycles recognized in the deuterium record can also be recognized in reconstructed atmospheric CO_2 concentrations from ice cores (Fig. 1.2) (Luthi et al., 2008 and references there in). This orbital-scale CO_2 changes are mainly explained by a removal of CO_2 during glacial periods from the atmosphere and export of this carbon to deep oceans. Two main mechanisms have been used to explain this process: first, the biological pump hypothesis (Broecker, 1982), that infers an increase in photosynthesis and productivity in the Antarctic and tropical upwelling waters during glacials, leading to a higher production of organic matter, a part of which would sink to the deep oceans. The second mechanism is an increase in the CO_3^{2-} content in surface waters, especially from Antarctic, due to changes in deep water circulation during glacials (Broecker and Pen, 1989). The CO_3^{2-} would combine

chemically with the atmospheric CO_2 producing HCO_3^- . However, it is unclear which mechanism is the underlying cause for the observed $p\text{CO}_2$ variations.

In the marine environment, the stacked record of $\delta^{18}\text{O}$ of shells of benthic foraminifera (Lisiecki and Raimo, 2005) follows the same trend as the deuterium isotope records of Antarctica (Fig. 1.2) because it mainly reflects the glacial-interglacial changes in the global ice volume. These isotopic changes are the base of a chronology named Marine Isotopic Stages (MIS), widely used nowadays in paleoclimatic studies to date time periods of climate events reconstructed from different locations.

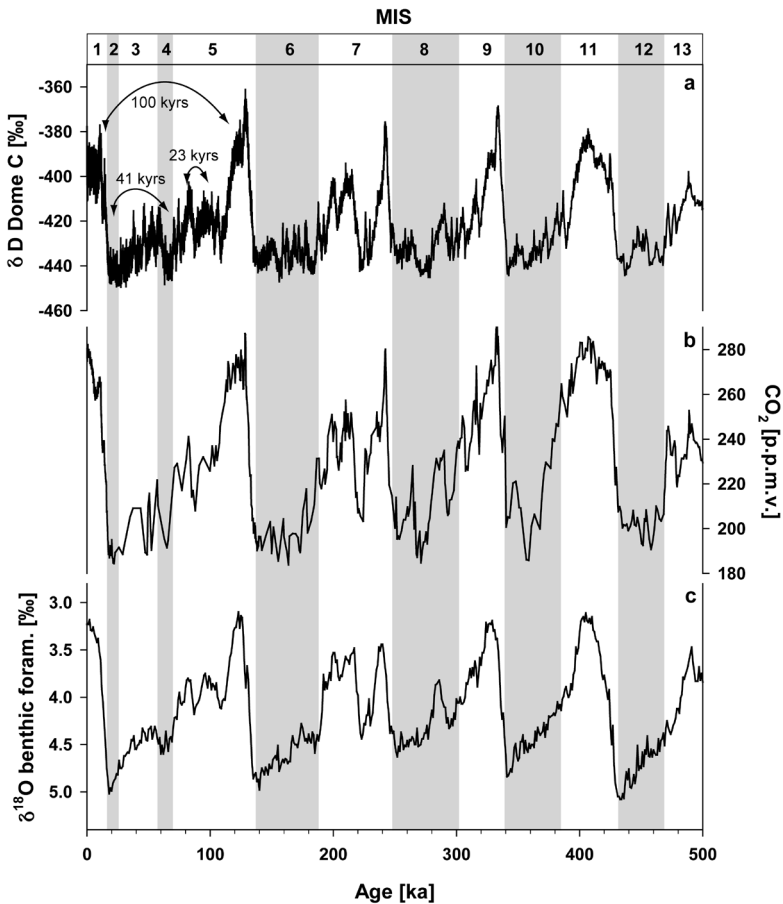


Fig. 1.2: Late Quaternary continental, atmospheric and marine climate records. a) δD of ice core Dome C in Antarctica (Jouzel et al., 2007), b) compilation of CO_2 records from Antarctica ice cores (Petit et al., 1999; Monnin et al., 2001; Pepin et al., 2001; Raynaud et al., 2005; Siegenthaler et al., 2005), c) stacked $\delta^{18}\text{O}$ of benthic foraminifera (Lisiecki and Raymo, 2005). The arrows show the 23, 41 and 100 ka oscillations. The numbers (1-13) show the different marine isotopic stages (MIS). Grey bars show the glacials.

1.2.2 The late Quaternary period in NW Africa

Paleoclimate reconstructions show that NW Africa has experienced repeated climatic changes during the late Quaternary, inducing substantial changes in the hydrology and vegetation cover. Glacial periods in NW Africa were extremely arid evidenced by decreased monsoon levels, drought-resistant vegetation, southward migration of the Sahara-Sahel boundary, decreased river discharge as well as low sea-level and lake levels (Livingstone, 1975; Dupont et al., 2000; Gasse et al., 2000; Hooghiemstra et al., 2006; Shanahan et al., 2006; Mulitza et al., 2008; Niedermeyer et al., 2010; Pierau et al., 2010). In contrast, interglacial periods were characterized by wetter conditions reflected in a more humid type of vegetation, northward position of the Sahara-Sahel boundary, higher river discharge, sea level and lake levels. Some climatic changes towards more drier and cooler periods can also be recorded during short term events like the Younger Dryas and Heinrich events with paleoenvironmental changes similar to glacial periods (deMenocal et al., 2000a; Mulitza et al., 2008; Niedermeyer et al., 2010). Additionally, extreme climatic events also happened during the Holocene with interchangeable wet and dry phases (Gasse et al., 2000). Indeed, one of the most striking wet event during the Holocene is the African Humid period (ca 6-14.5 ka - Ritchie et al., 1985; deMenocal et al., 2000) where the Sahara was nearly fully vegetated and north Africa was characterized by numerous lakes. The end of the humid period was abrupt and followed by the onset of a drier period until most recent times (Gasse et al., 2000; deMenocal et al., 2000).

Besides continental climate events, several atmospheric and oceanographic changes along the coast of NW Africa occurred during the late Quaternary which drove part of the continental climate changes. Glacial periods were characterized by stronger winds (Sarnthein et al., 1982; Flores et al., 2000) that lead to an increase in upwelling and dust transport to the ocean along the coast of NW Africa (Sicre et al., 2000; Flores et al., 2000; Freudenthal et al., 2002). Strong changes in the ocean currents, sea surface temperature (SST) and primary productivity were also noted during the late Quaternary (Sarnthein et al., 1982; Freudenthal et al., 2002; Zhao et al., 2006). However, due to complexity of the wind and oceanic currents in this area, these changes were not uniform along the NW Africa coast and several uncertainties remain.

1.2.3 The late Quaternary period in SE Australia

Late Quaternary climate changes in SE Australia are, in comparison to NW Africa, much less understood because paleoenvironmental studies from this area are limited. Most evidence comes from lake levels, pollen and periglacial features and suggests that the climate of SE Australia was cooler, drier and possibly windier during glacials (Bowler et al., 1976 and references therein; Singh, 1983). Although contrasting records of higher lake levels during Last Glacial Maximum (LGM; ca. 21 Ka) in some lakes in SE Australia are reported,

they can be a consequence of increased run-off due to augmented snowfall and decreased evaporation (Galloway, 1965; Harrison, 1993). Interglacials and parts of MIS 3 were in general characterized by wetter conditions with high lake levels and wetter forest types (Harrison, 1993; Harle, 1997; Williams et al., 2006). Significant vegetation changes happened during the last 50 ka. However, it is not always clear if these are due to climate changes or human impact on the ecosystems (Miller et al., 2005; Williams et al., 2006; Murphy et al., 2012; Rule et al., 2012). For instance, a sharp change in vegetation with different photosynthetic pathways (from C_4 to C_3 plants) was recorded around 40-45 ka in SE Australia (Miller et al., 2005; Rule et al., 2012) and proposed to be caused by burning events induced by humans or by alterations in the Australian monsoon system. Additionally, vegetation changes occurred throughout the Holocene that are also explained by increased burning events and changes in the water balance (Williams et al., 2006).

Besides these variations in the continental climate, atmospheric and oceanographic changes also occurred along the coast of SE Australia. Indeed, some disagreement exists in the positioning of the sub-tropical front during the LGM in this area. This front separates subtropical and subantarctic waters and is mainly defined by the strength of the westerlies (Belkin and Gordon, 1996). Due to this uncertainty, the intensity of the southern westerlies in SE Australia during the LGM is not clear. Oceanographically, during the late Quaternary strong changes in the SST and primary productivity occurs in this area on a glacial-interglacial time-scale (Gingele and De Deckker, 2005; Calvo et al., 2007). For example, an increase in productivity during glacial is suggested due to the increase in the westerly winds (Gingele and De Deckker, 2005). However, some uncertainties still exist in the paleoceanography of the region, e.g. distribution of ocean currents during LGM due to a lack of understanding on the subtropical front position at this period.

In summary, substantial uncertainty on the late Quaternary paleoclimate of NW Africa and SE Australia still exists and, thus, reconstructions of past changes in continental climate as well as oceanography are needed. A promising approach for paleoenvironmental reconstructions is the analyses of organic proxies in marine cores that provide insights into both continental and oceanographic changes (e.g. Ohkouchi et al., 1997; Madureira and Piccinini, 1999). This approach is increasingly applied in the last decade due to the development of analytical tools that enables the accurate identification and characterization of organic compounds.

1.3 Organic proxies in marine sediment cores

Biomarkers are sedimentary organic compounds resistant to degradation and, therefore, showing relatively minor change in their structure in comparison to their parent organic molecule produced by specific organisms (Peters et al., 2005). Their chemical structure allows to trace back target source organisms and/or environmental parameters at the moment of deposition. Thus, they have been frequently used as proxies for paleoenvironmental reconstructions. A proxy is a measurable variable used to infer the value of an unobservable

variable such as temperature, salinity, nutrient and oxygen content, CO₂ concentration, wind speed and productivity (Fischer and Wefer, 1999). The most commonly applied organic proxies based on lipid biomarkers are those used for sea temperatures (e.g. Prah and Wakeham, 1987; Schouten et al., 2002, Rampen et al., 2012), vegetation (Eglinton and Hamilton, 1967; Freeman et al., 1990) and primary productivity (see in Table 1.1).

SST proxies are based on three groups of compounds. The long-chain alkenones are produced by haptophytes (Volkman et al., 1980) and are used to define the U^K₃₇ index (Brassell et al., 1986; Prah and Wakeham, 1987), the first organic proxy developed for SST estimates. Glycerol dialkyl glycerol tetraethers (GDGTs) are compounds produced by Thaumarchaeota (Sinninghe Damsté et al., 2002) and are used in the TEX₈₆ index (Schouten et al., 2002, Kim et al., 2010). Finally, long-chain diols produced by eustigmatophyte algae (Volkman et al., 1992), are used to define the most recent organic SST proxy, the LDI index (Rampen et al., 2012).

Several lipid biomarkers have been used in the past decades to reconstruct primary productivity of specific algal groups (see table 1.1 for examples) such as diatoms, haptophytes, dinoflagellates and eustigmatophytes (e.g. Volkman et al., 1980; 1992; 1998). Primary productivity reconstructions are of great interest because of their link to the carbon cycle and to the atmospheric and oceanographic conditions. Therefore, its reconstruction at different settings is very needed.

Recently, for the terrestrial climate, a range of proxies have been developed. For instance, precipitation using δD of *n*-alkanes (Xie et al., 2000; Schefuß et al., 2005), air mean annual temperatures using branched GDGTs (Weijers et al., 2007) and vegetation reconstructions using the $\delta^{13}C$ of *n*-alkyl compounds (e.g. Huang et al., 1995). The latter proxy is used to reconstruct C₃-C₄ vegetation shifts (Freeman et al., 1990; Bird et al., 1995; Huang et al., 1995). This is particularly important because the distributions of these plant types are related directly to climatic conditions through adaptation of their photosynthetic pathways (Tippel and Pagani, 2007).

Thus, for both continental climate as well as marine environments a range of organic proxies are available. Interestingly, the terrestrial biomarkers are also found in marine sediment cores as they are transported by river and dust and subsequently preserved in the sediments. Thus, marine cores provide excellent archives for both continental and marine proxies and they usually give longer and better dated records than continental archives. As a number of proxies are only recently developed, the application of some of these proxies is still at its infancy. Furthermore, most of the time these proxies are not applied simultaneously what prevents a proper comparison between them, in case they reconstruct a similar parameter, or a comparison between marine and continental climate change. A multi-proxy approach in paleoclimate reconstructions is, therefore, increasingly used to enable a reliable interpretation of the proxies.

Table 1.1: Major molecular organic (lipids) proxies used in paleoenvironmental research.

| Compound | Source organism | Parameter | Reference |
|--|--------------------------|--------------------------------------|--|
| Alkenones | Haptophytes | Haptophyte productivity, SST | Brassell et al., 1986; Prahl and Wakeham, 1987 |
| Alkenones ($\delta^{13}C$) | Haptophytes | CO ₂ | Jasper and Hayes, 1990 |
| Alkenones (δD) | Haptophytes | Salinity | Englebrecht and Sachs, 2005 |
| GDGTS | Thaumarchaeota | SST | Schouten et al., 2002 |
| 1,15 and 1,13 Long-chain diols | Eustigmatophytes | SST, eustigmatophytes productivity | Volkman et al., 1992; Rampen et al., 2012 |
| 1,14 Long-chain diols | <i>Proboscia</i> diatoms | <i>Proboscia</i> productivity | Sinninghe Damsté et al., 2003 |
| Loliotide and iso-loliotide | Diatoms | Diatom Productivity | Repeta, 1989 |
| Isorenieratene | Green sulfur bacteria | Euxinic conditions | Repeta et al., 1989 |
| Highly Branched isoprenoids | Diatoms | Diatom Productivity | e.g. Volkman et al., 1994; Sinninghe Damsté et al., 1999 |
| Sterols | Phytoplankton | Algal productivity | e.g. Boon et al., 1979; Robinson et al., 1984 |
| Branched GDGTS | Bacteria | Soil input, air temperature, soil pH | Hopmans et al., 2004; Weijers et al., 2007 |
| Long-chain <i>n</i>-alkanes ($\delta^{13}C$) | Higher plants | Changes in vegetation | Eglinton and Hamilton, 1967; Freeman et al., 1990 |
| Long-chain <i>n</i>-alkanes (δD) | Higher plants | Precipitation | Xie et al., 2000 |

1.4 Scope and framework

The research presented in this thesis focuses on the application of multiple organic proxies for the reconstruction of paleoceanographic and continental climate conditions of NW Africa and SE Australia during the late Quaternary. In particular, three climate parameters were reconstructed: sea water temperature, marine primary productivity and continental vegetation changes. To this end, two sediment cores from offshore NW Africa and SE Australia were analysed in detail using multiple marine and terrestrial organic proxies to generate millennial-scale climate records of the late Quaternary.

Part I covers the reconstruction of sea temperatures using organic proxies. **Chapter 2** describes the late Quaternary changes in sea surface and sub-surface temperatures in the Guinea Plateau region in NW Africa. Surface sediment analysis showed that $U^{K'}_{37}$ relates to annual mean SST, while TEX^H_{86} records thermocline temperatures. The late Quaternary sediment record of $U^{K'}_{37}$ and TEX^H_{86} showed an antiphase behavior between surface and sub-surface temperatures during periods of Atlantic Meridional Overturning Circulation (AMOC) slowdown. Thus, comparison of these records with proxies for AMOC demonstrated, for the first time, that AMOC slowdown induced a thermocline adjustment, especially in the eastern tropical Atlantic, on millennial time scales. This finding was supported by modeling studies. In **Chapter 3** a multi-proxy approach based on the established proxies $U^{K'}_{37}$ and TEX^H_{86} and a novel proxy, the Long-chain Diol index (LDI), was used to reconstruct changes in SST from the Murray Canyons area near SE Australia during the late Quaternary. All three proxies showed similar SST trends over the glacial-interglacial cycles reflecting global temperature changes. However, differences in absolute temperatures were noted between the three different proxies. Comparison with temperatures reconstructed from foraminiferal assemblages showed that the LDI likely reflect summer SST, while $U^{K'}_{37}$ recorded mean annual SST and TEX^H_{86} winter SST. During interglacials the temperature difference between TEX^H_{86} and $U^{K'}_{37}$ strongly decreased, suggesting a seasonal change of the growth season of the Thaumarchaeota or the influence of the warm Leeuwin current during winter.

Part II discusses the reconstruction of the primary productivity based on several biomarker lipids. **Chapter 4** identifies factors controlling primary productivity in the eastern tropical north Atlantic at the Guinea Plateau region. Biomarker records for haptophytes (alkenones), dinoflagellates (dinosterol) and eustigmatophytes (long-chain 1,15-diols) showed a significant correlation to the total organic matter and a link between iron concentrations and accumulation rates with some productivity proxies suggests that primary productivity at this latitude is possibly controlled by ocean fertilization by the Sahara dust during arid periods. **Chapter 5** reconstructs past changes in primary productivity in the Murray Canyons area, offshore SE Australia. During glacial periods, the study site is characterized by relatively high primary productivity based on total organic carbon and alkenones (biomarker for haptophytes productivity) records. This is likely due to the stronger westerly winds at these times. In contrast, during interglacials and MIS 3 the area is characterized by high productivity of *Proboscia* diatoms based on the 1,14-diol index. This high productivity of

Proboscia diatoms is concomitant with high diatom productivity in equatorial tropical oceans and maybe a consequence of input of nutrient-rich Southern Ocean waters. **Chapter 6** shows for the first time a continuous late Quaternary sedimentary record of steryl alkyl ethers, compounds that have no known biological source. The sediments from offshore SE Australia are characterized by a large range of different isomers, i.e. C₂₇₋₃₀ steroid moieties containing one or two double bond, ether-bound to C₁₀₋₁₁ alkyl moieties, which distribution remains fairly constant over time. The sedimentary record suggests a link between the production of these compounds and a sharp decrease in SST on a millennial time-scale, confirming previous suggestions that these compounds indicate cooler waters.

Part III of this thesis comprises the reconstruction of vegetation changes on the continent using terrestrial biomarkers. In **Chapter 7**, the variability in the types of terrestrial vegetation (C₃ vs. C₄ plants) based on stable carbon isotopic composition of *n*-alkanes was used to reconstruct past humidity/aridity of NW Africa. The strong correlation of the stable carbon isotopic composition record of the *n*-alkanes with proxies for deep water circulation showed that the AMOC strength induced wet periods and an expansion of C₃ plants in central North Africa, that were coincident to major human migration. **Chapter 8** describes the development and validation of a rapid method to analyze levoglucosan, a biomarker for biomass burning, in geological marine sediments using high performance liquid chromatography/electrospray ionization/mass spectrometry. Compared to previous methods it does not require derivatization or extensive work up and allows to separate levoglucosan from other biomass burning products. This method was used to reconstruct a biomass burning record of SE Australia in **Chapter 9**. In addition, this last chapter describes the variability in C₃ vs. C₄ vegetation based on stable carbon isotopic composition of *n*-alkanes from the Murray-Darling basin in SE Australia. The results showed that, during the LGM and penultimate glacial maximum, arid conditions favored C₃ plants that, for the LGM, were associated with high biomass burning. During times of presumed increases in summer monsoon, an expansion of C₄ plants was noted. An abrupt vegetation change from C₄ to C₃ plants was observed following the main period of the late Quaternary megafaunal extinction in Australia, suggesting that this abrupt vegetation change was possibly caused by a reduction in herbivory or by increased burning events.

In summary, the research described in this thesis showed the benefit in the application of multiple organic proxies in marine sediment records, leading to a comprehensive reconstruction of the paleoenvironmental conditions both of the continent as well as the ocean. This has led to a significant improvement in the understanding of the cause and effect of environmental changes in marine and continental areas of NW Africa and SE Australia. Furthermore, the research helps to explain differences in behavior of temperature proxies at different settings leading to a better application of these proxies in the future.

Chapter 2

Glacial–interglacial variability in Atlantic meridional overturning circulation and thermocline adjustments in the tropical North Atlantic

Raquel A. Lopes dos Santos, Matthias Prange, Isla S. Castañeda, Enno Schefuß, Stefan Mulitza, Michael Schulz, Eva M. Niedermeyer, Jaap S. Sinninghe Damsté, Stefan Schouten
Published in *EPSL* 300 (2010) 407-414

Abstract

Changes in the strength of Atlantic meridional overturning circulation (AMOC) are known to have profound impacts on global climate. Coupled modelling studies have suggested that, on annual to multi-decadal time scales, a slowdown of AMOC causes a deepening of the thermocline in the tropical Atlantic. However, this process has been poorly constrained by sedimentary geochemical records. Here, we reconstruct surface ($U_{37}^{K'}$ Index) and thermocline (TEX_{86}^H) water temperatures from the Guinea Plateau Margin (Eastern tropical Atlantic) over the last two glacial–interglacial cycles (~192 ka). These paleotemperature records show that periods of reduced AMOC, as indicated by the $\delta^{13}C$ benthic foraminiferal record from the same core, coincide with a reduction in the near-surface vertical temperature gradient, demonstrating for the first time that AMOC-induced tropical Atlantic thermocline adjustment exists on longer, millennial time scales. Modelling results support the interpretation of the geochemical records and show that thermocline adjustment is particularly pronounced in the eastern tropical Atlantic. Thus, variations in AMOC strength appear to be an important driver of the thermocline structure in the tropical Atlantic from annual to multi-millennial time scales.

2.1. Introduction

The ocean is a fundamental component of the Earth's climate due to its capacity to store and transport large amounts of heat. The Atlantic meridional overturning circulation (AMOC) transports heat through warm (and saline) surface currents from the tropics to the polar and subpolar North Atlantic where heat is released to the atmosphere producing a southward current of cold water in the deep Atlantic (Ganachaud and Wunsch, 2003). It is widely accepted that past variations in AMOC induced substantial changes in the global temperature distribution, wind fields and the hydrologic cycle (Rahmstorf, 2002). Additionally, some climate models predict a slowdown of the AMOC for increased future atmospheric CO₂ concentrations (Gregory et al., 2005). Therefore, it is crucial to gain deeper insight into past AMOC variations and their impact on ocean properties.

Previous studies, using coupled climate models and observational data, showed that an anticorrelated variation between surface and subsurface temperature in the tropical North Atlantic is a distinctive signature of AMOC variability on (multi-)decadal time scales (Chiang et al., 2008; Zhang, 2007) that is clearly distinguishable from the response pattern of external radiative forcing (Zhang, 2007). The physics behind these temperature variations have been investigated in previous studies: upon AMOC slowdown, strengthened northeast trade winds, associated with a southward displacement of the Atlantic intertropical convergence zone, tend to cool the surface of the tropical North Atlantic mainly due to enhanced evaporative latent heat fluxes (Chiang et al., 2008; Zhang, 2007), a process that cannot be simulated with uncoupled ocean-only models. Simultaneously, subsurface waters in the tropical Atlantic warm due to reduced import of relatively cold water into the tropical Atlantic from the south and reduced warm-water export to the north (Chiang et al., 2008). This goes along with a deepening of the permanent (Huang et al., 2000; Rahmstorf, 2002) and tropical (Haarsma et al., 2008) thermoclines, accomplished by rapid baroclinic wave adjustment processes (Zhang, 2007).

Although this process is well documented on (multi-)decadal time scales, it is not known how important this pattern of tropical upperocean temperature is on longer, millennial time scales, both from a modelling perspective as well as in geochemical records. Here, we use a combined geochemical and modelling approach to investigate the impact of AMOC changes on surface and subsurface temperature variations in the eastern tropical North Atlantic on multi-millennial time scales and assess the potential of this temperature difference for reconstructing past AMOC variability.

2.2. Study location and regional setting

The geochemical records were derived from marine sediment core GeoB9528-3 (09°09.96'N, 17°39.81'W; 3057 m water depth; Fig. 2.1) retrieved from the Guinea Plateau Margin which spans the last 192 ka (thousand years) (Castañeda et al., 2009). The oceanographic system of the Guinea coast region (NW Africa) is strongly influenced by

deep water masses including the North Atlantic Deep Water (NADW) and also by several other surface and subsurface flows (Fig. 2.1). The main surface current that connects the tropical North Atlantic with the extratropics is the Canary Current (CC), which comes from the North Atlantic. It is characterized by cool, wide and slow water flow towards the equator throughout the year (Batteen et al., 2000; Wooster et al., 1976). On average, this current is about 500 m deep underlain by South Atlantic Central Water (SACW) and deeper by North Atlantic Central Water (NACW) (Wooster et al., 1976). The Antarctic Intermediate Water (AAIW) is found around 800 m depth with a salinity between 34.6 and 34.9 at the latitude of the study area. Below 1500 m, the North Atlantic Deep Water (NADW) is found with a salinity between 34.9 and 35 (Mulitza et al., 2006). This region is influenced by several other surface and subsurface currents including the North Equatorial Current (NEC) (Fig. 2.1), which is a broad westward flowing current, found around 7°N to about 20°N, mainly fed by cooler waters from the northeast Atlantic (Schott et al., 2002). The Equatorial Under Current (EUC), an eastward flowing current characterized by relatively high temperature and salinity, transports heat and salt to the study area in subsurface layers of ~100 m depth (Peterson and Stramma, 1991). Near the southern boundary of the NEC, the North Equatorial Counter Current (NECC), an eastward flow, is sometimes present (Richardson and Walsh, 1986). The main source of the NECC is the retroflexion from the upper layers (100 m) of the North Brazil Current (NBC), starting between 5° and 8°N (Bourles et al., 1999; Schott et al., 2002; Wilson et al., 1994). The NBC also contributes to the intermediate layers of the NECC/NEUC system (Wilson et al., 1994) and eventually to the Caribbean Current. The Guinea Dome is a thermal upwelling dome in the northeastern tropical Atlantic with the core located near 10°N, 22°W and linked to a cyclonic circulation composed of the NECC, NEUC, and NEC (Mazeika, 1967). Sediment core GeoB9528-3 is located outside the Guinea Dome (Fig. 2.1).

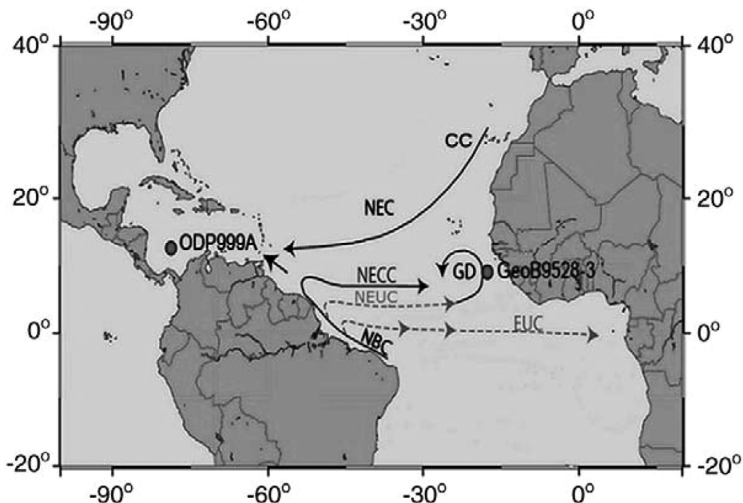


Fig. 2.1: Location of core GeoB9528-3 in Northwest Africa and core ODP 999A (Schmidt et al., 2006)

in the Cariaco basin. The black arrows indicate the major surface ocean currents in this area and the dashed arrows the main subsurface currents. CC—Canary Current, NEC—North Equatorial Current, NECC—North Equatorial Counter Current, GD—Guinea Dome, NEUC—North Equatorial Under Current, EUC—Equatorial Under Current, NBC—North Brasil Current. Figure based on Schott et al. (2002a).

2.3. Materials and methods

2.3.1. Geochemical analyses of core GeoB9528-3

Sediment core GeoB9528-3 was sampled at 5-cm intervals for organic geochemical analyses. The age model of this core is based on oxygen isotope stratigraphy of *Cibicides wuellerstorfi* and covers the interval from ~7 to 192 ka. The age model has been previously published by Castañeda et al. (2009). The $\delta^{13}\text{C}$ measurements of *C. wuellerstorfi* of this core is also described by Castañeda et al. (2009) and is used as a proxy for changes in deep water circulation. Sediment samples from the core were freeze-dried, homogenized and extracted as described by Castañeda et al. (2009). After extraction, each sample was separated into an apolar, ketone and polar fraction via alumina column chromatography using solvent mixtures of 9:1 (v/v) hexane:DCM, 1:1 hexane:DCM, and 1:1 DCM: MeOH, respectively. The alkenones were analysed for $\text{U}^{\text{K}'}_{37}$ as described previously (Castañeda et al., 2009). The polar fractions were analyzed using high-pressure liquid chromatography (HPLC). The conditions for $\text{TEX}_{86}^{\text{H}}$ analysis of the sediments from GeoB9528-3 were described by Schouten et al. (2007). Since the location is in a tropical area, we used the $\text{TEX}_{86}^{\text{H}}$ proxy, which is applicable in high temperature settings ($>15\text{ }^{\circ}\text{C}$), and converted it into temperature values using the calibration of Kim et al. (2010):

$$\text{TEX}_{86}^{\text{H}} = \log \left(\frac{[\text{GDGT} - 2] + [\text{GDGT} - 3] + [\text{Cren}']}{[\text{GDGT} - 1] + [\text{GDGT} - 2] + [\text{GDGT} - 3] + [\text{Cren}']} \right)$$

$$\text{Temp} [^{\circ}\text{C}] = 68.4 (\text{TEX}_{86}^{\text{H}}) + 38.6$$

2.3.2. NW Africa surface sediment analysis

In addition to sediment core GeoB9528-3, we also examined 12 surface sediment samples collected from NW Africa near the core location (Table 2.1) to obtain information on the modern distribution of $\text{U}^{\text{K}'}_{37}$ and $\text{TEX}_{86}^{\text{H}}$ ratios. The $\text{TEX}_{86}^{\text{H}}$ temperatures from these surface sediments were derived from Kim et al. (2010). The $\text{U}^{\text{K}'}_{37}$ analysis of the NW Africa surface sediment samples were done as described in Niedermeyer et al. (2009) and converted into temperature using the calibration of Müller et al. (1998).

Table 2.1: Summary table of core names locations and reconstructed temperature data from NW Africa surface sediments.

| Sample (GeoB) | Latitude [°N] | Longitude [°W] | U ^K ₃₇ [°C] | TEX ^H ₈₆ [°C] |
|---------------|---------------|----------------|-----------------------------------|-------------------------------------|
| 9501 | 16°50.38 | 16°43.92 | 22.9 | 21.2 |
| 9506 | 15°36.48 | 18°20.48 | 24.0 | 23.2 |
| 9508 | 15°29.89 | 17°56.44 | 24.1 | 22.9 |
| 9510 | 15°24.98 | 17°39.24 | 23.7 | 22.2 |
| 9512 | 15°20.22 | 17°22.01 | 23.8 | 22.8 |
| 9520 | 13°49.76 | 17°35.45 | 23.1 | 22.4 |
| 9521 | 13°50.90 | 17°29.42 | 23.6 | 22.8 |
| 9525 | 12°38.39 | 17°52.76 | 24.6 | 22.7 |
| 9528 | 09°10.02 | 17°39.79 | 26.9 | 23.7 |
| 9529 | 09°21.19 | 17°22.13 | 27.0 | 23.7 |
| 9534 | 08°54.03 | 14°56.15 | 26.6 | 24.1 |
| 9535 | 08°52.53 | 14°57.62 | 26.8 | 24.0 |

2.3.3. Model experiment

To establish the equilibrated SST and subsurface temperature response in the tropical Atlantic to an AMOC shutdown, simulations were performed with the coupled atmosphere-ocean model ECBILT-CLIO. For our sensitivity experiments, we used the global atmosphere-ocean model ECBILT-CLIO version 3 (www.knmi.nl/onderzk/CKO/ecbilt.html). The coupled model derives from the atmosphere model ECBILT (Opsteegh et al., 1998) and the ocean/sea-ice model CLIO (Goosse and Fichefet, 1999). The atmospheric component solves the quasigeostrophic equations and ageostrophic correction terms in T21-resolution using three layers. The ocean component is a state-of-the-art free-surface primitive equation general circulation model which includes parameterization for downsloping currents, eddy-flux parameterization for sub-gridscale horizontal mixing (Goosse et al., 1999), and a vertical mixing scheme based on the Mellor-Yamada (Mellor and Yamada, 1982) level 2.5 model (Goosse et al., 1999). These sophisticated parameterizations are of utmost importance for the simulation of the tropical thermocline which would largely be eroded by simplistic mixing with too high diffusivity. The ocean grid has a horizontal resolution of 3 degrees and 20 levels in the vertical (6 levels within the topmost 100 m). Sea-ice dynamics involves a viscous-plastic rheology. There is no local flux correction in ECBILT-CLIO. However, precipitation over the Atlantic and Arctic basins is artificially reduced by 8.5% and 25%, respectively, and homogeneously redistributed over the North Pacific. The implementation of this regional flux adjustment considerably improves the simulation of the modern climate and produces a realistic AMOC (e.g. Prange and Schulz, 2004).

From a 5000 year control run with modern boundary conditions (Prange and Schulz, 2004), three freshwater hosing experiments (with different magnitudes of globally uncompensated freshwater forcing to the North Atlantic between 50°N and 70°N: 0.1 Sv, 0.2 Sv, 0.5 Sv) were branched off. The hosing experiments were designed to elucidate the relationship between AMOC and the tropical thermocline. Freshwater hosing is a convenient and common method to slow down the AMOC in numerical climate models (e.g. Stouffer et al., 2006). We do not imply, however, that anomalous North Atlantic freshwater fluxes were the only possible forcing mechanism of late Quaternary AMOC variations in reality. All hosing experiments were integrated for another 500 years, i.e. long enough for the AMOC and the tropical thermocline to equilibrate (Fig. 2.2). The last 100 years of each experiment were used for further analysis.

In order to quantify a relationship between AMOC strength (i.e. volume flux of NADW) and surface–subsurface temperature difference ΔT , we use the following approach: a considerable portion of the meridional overturning in the North Atlantic immediately recirculates north of 20°N (see Figure 1 in Prange and Schulz (2004)) and, hence, does not contribute to the southward flow of NADW in the tropical and South Atlantic. Therefore, a better measure of NADW volume flux– which is also commonly used and which we have taken in this study is the maximum of the meridional overturning streamfunction in the South Atlantic at 30°S (also referred to as the net export of NADW). Note that negative values are associated with the southern overturning cell and are not related to the NADW flux; therefore, negative values were set to zero.

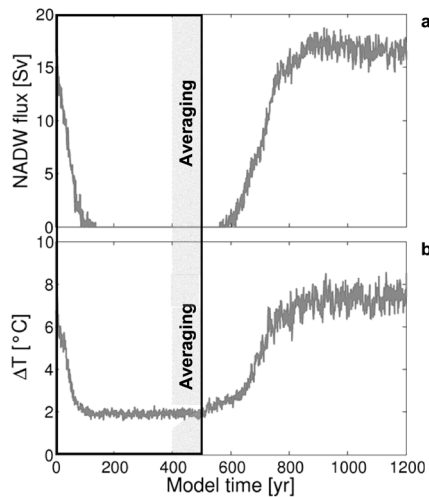


Fig. 2.2: Time series from the 0.5-Sv freshwater-hosing experiment as an example of experimental design and analysis. a, NADW volume flux (i.e. AMOC strength) calculated as described in the text. b, Surface–subsurface temperature difference ΔT , where the subsurface temperature is taken at 100 m as described in Section 2.4.3. Time 0 corresponds to the end of a 5000-year control run with modern boundary conditions and marks the beginning of the freshwater-hosing experiment. Freshwater was injected into the North Atlantic for 500 years (thick box). Averages from the last 100 years (shaded bar) were taken to construct the graph in Fig. 2.7.

2.4. Results and discussion

2.4.1. U_{37}^K and TEX_{86}^H temperature reconstructions in the eastern tropical North Atlantic

Two organic geochemical proxies, U_{37}^K and TEX_{86}^H , were applied to reconstruct water temperatures of the eastern tropical North Atlantic. Both the U_{37}^K index, based on the ratio of di- and tri-unsaturated long chain ketones produced by haptophyte algae (Prah and

Wakeham, 1987), and the initial $\text{TEX}_{86}^{\text{H}}$ proxy (Schouten et al., 2002), which is based on glycerol dialkyl glycerol tetraethers (GDGTs) produced by Marine Group 1 Crenarchaeota, are usually thought to reflect SST (Kim et al., 2008; Schouten et al., 2002). To confirm this, we analyzed surface sediments collected on a transect along the NW African coast (Table 2.1) for $\text{U}^{\text{K}'}_{37}$ and compared this with $\text{TEX}_{86}^{\text{H}}$ values (Kim et al., 2010) for the same set of samples. This showed that the $\text{U}^{\text{K}'}_{37}$ index corresponds well to annual mean SST (Locarnini et al., 2006) (Fig. 2.3). However, $\text{TEX}_{86}^{\text{H}}$ temperatures are substantially lower compared to $\text{U}^{\text{K}'}_{37}$ -based SST, and are similar or slightly lower than thermocline temperatures from around 30 m depth (Fig. 2.3). The difference between $\text{U}^{\text{K}'}_{37}$ and $\text{TEX}_{86}^{\text{H}}$ for a number of sites is around 1.5 °C, which may be explained by the calibration errors of the two proxies (Kim et al., 2008; 2010; Müller and Fischer, 2001). However, for sites closer to the equator (<10°N) this difference is larger and up to ~3 °C (Table 2.1 and Fig. 2.3). There could be several explanations for these cooler $\text{TEX}_{86}^{\text{H}}$ temperatures in comparison to the $\text{U}^{\text{K}'}_{37}$. First, the $\text{TEX}_{86}^{\text{H}}$ record could be influenced by input from soil derived isoprenoid GDGTs (Weijers et al., 2006). The branched and isoprenoid tetraether (BIT) index (Hopmans et al., 2004) provides a method to assess the relative amount of soil organic matter input and thus possible influences on the $\text{TEX}_{86}^{\text{H}}$ record (Hopmans et al., 2004). In general, $\text{TEX}_{86}^{\text{H}}$ is considered to be applicable in settings where the BIT index is <0.3 (Weijers et al., 2006). However, BIT values in the surface sediments were always <0.1 (Kim et al., 2008). These low BIT values were expected since the coring site is remote from the coast and river inputs. Thus, soil-derived GDGTs can be ruled out as an influence on the $\text{TEX}_{86}^{\text{H}}$ in this region. A second explanation for the difference in temperature values between the $\text{TEX}_{86}^{\text{H}}$ and $\text{U}^{\text{K}'}_{37}$ proxies could be due to differences in the growth season between the source organisms (Huguet et al., 2006). Indeed, there are large seasonal variations in SST at the sites > 10°N but at latitudes below 10°N, including our core site GeoB9528-3, seasonal variation alone cannot explain the full temperature difference between the two proxies (Fig. 2.3). A third explanation could be lateral transport of GDGTs from colder areas to the region of NW Africa. However, alkenones have been shown to be affected more by long-distance lateral transport than crenarchaeol (Mollenhauer et al., 2005, 2007; Shah et al., 2008). The fact that the $\text{U}^{\text{K}'}_{37}$ values in the surface sediments correspond well to SST argues against a substantial effect of lateral transport in this area. Variations in upwelling intensity could be another factor influencing $\text{TEX}_{86}^{\text{H}}$ temperatures as suggested by previous studies (Kim et al., 2008; Wuchter et al., 2006). However, the pattern of cooler $\text{TEX}_{86}^{\text{H}}$ temperatures in comparison to $\text{U}^{\text{K}'}_{37}$ is observed in surface sediments located near the permanent upwelling cell of NW Africa, which is centered at ~20–25°N, but we also observe this pattern at sites located outside of the upwelling cell. Therefore, it seems that at site GeoB9528-3, upwelling is not the main cause of this temperature difference. The fifth and, in our view, the most likely explanation to explain the cooler $\text{TEX}_{86}^{\text{H}}$ temperatures compared to $\text{U}^{\text{K}'}_{37}$, is that $\text{TEX}_{86}^{\text{H}}$ reflects a deeper and cooler water mass in comparison to the $\text{U}^{\text{K}'}_{37}$ index. Indeed, Crenarchaeota can reside deeper in the water column (Karner et al., 2001) and, thus, can potentially reflect temperatures of deeper water masses (Huguet

et al., 2007) compared to haptophyte algae, which must remain within the photic zone. Previous studies have shown that TEX_{86} reflects subsurface rather than surface temperatures in the Santa Barbara Basin (Huguet et al., 2007) and, importantly, in the nearby Benguela upwelling region (Lee et al., 2008). In the latter study, it was found that TEX_{86} in suspended particulate matter was fairly uniform in the upper water layer and similar to TEX_{86} values in the surface sediments. TEX_{86} temperatures were substantially lower than SST, indicating a predominant contribution of crenarchaeota living in colder deeper waters. This deeper depth production may be to avoid competition for e.g., ammonia (Martens-Habbenha et al., 2009). Future seasonal studies of Crenarchaeota abundance and crenarchaeotal lipid fluxes will be fundamental to better understand the TEX_{86} . However, it is reasonable to assume that in the eastern tropical Atlantic, $\text{TEX}_{86}^{\text{H}}$ is reflecting subsurface temperatures, likely around the thermocline, rather than annual mean surface temperatures.

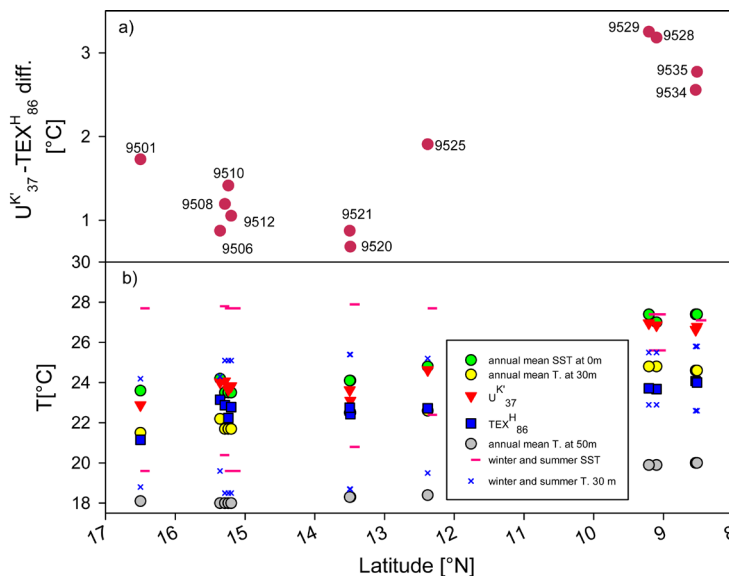


Fig. 2.3: U^{K}_{37} -derived SST, $\text{TEX}^{\text{H}}_{86}$ -derived temperatures and ΔT ($U^{\text{K}}_{37} - \text{TEX}^{\text{H}}_{86}$) differences in surface sediment samples from the northwest African margin at different latitudes. a) The $U^{\text{K}}_{37} - \text{TEX}^{\text{H}}_{86}$ temperature difference plotted against latitude. The GeoB station numbers are listed next to the data points and GeoB station locations are listed in Table 2.1. Note that the surface sediment samples collected from latitudes of 8–10°N, including site GeoB9528-3, display the greatest difference between the U^{K}_{37} and $\text{TEX}^{\text{H}}_{86}$ records. b) Comparison of winter, summer and annual mean SST at 0 m (Locarnini et al., 2006) and water column temperatures at 30 and 50 m (Locarnini et al., 2006) with U^{K}_{37} and $\text{TEX}^{\text{H}}_{86}$ (Kim et al., 2010) reconstructed temperatures for GeoB stations plotted against latitude. Note that U^{K}_{37} derived temperatures (red triangles) agree well with SST (green circles). In contrast, $\text{TEX}^{\text{H}}_{86}$ -derived temperatures (blue squares) indicate cooler temperatures compared to SST and display a better agreement with water column temperatures at 30 m (yellow circles).

2.4.2. Millennial scale temperature records from the eastern tropical North Atlantic

The pattern of cooler $\text{TEX}_{86}^{\text{H}}$ temperature estimates compared to U^{K}_{37} is also consistently found for the sedimentary record of GeoB9528-3 (Fig. 2.4). The difference between the two proxies is up to 7 °C, for certain time intervals, which is much larger than the present seasonal temperature variations. Thus, it seems unlikely that seasonality is the main factor leading to this temperature difference at this latitude.

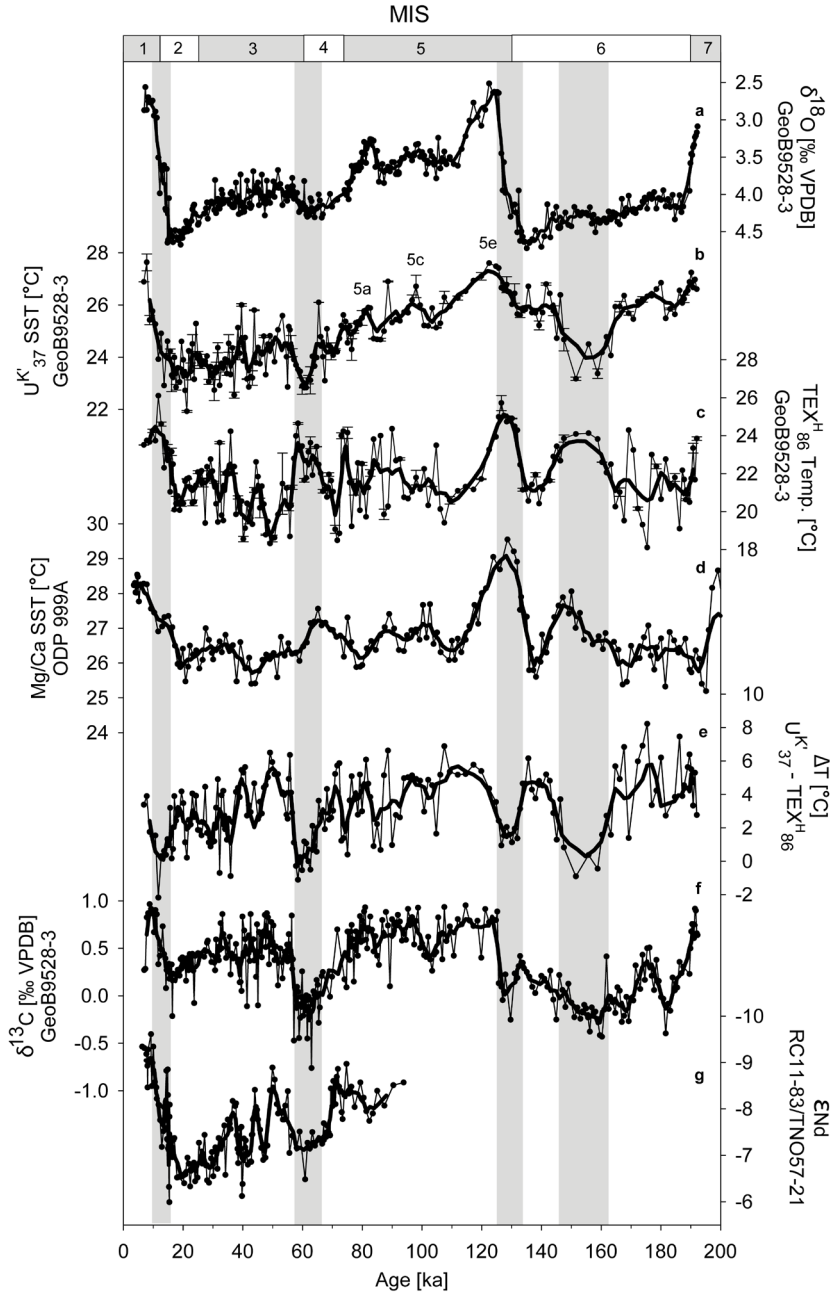


Fig. 2.4: Comparison of geochemical records from eastern and western tropical Atlantic. a, $\delta^{18}\text{O}$ of *C. wuellerstorfi* of eastern Atlantic core GeoB9528-3 (Castañeda et al., 2009); b, $U^{K'}_{37}$ (Castañeda et al., 2009) and c, TEX^H_{86} records of core GeoB9528-3; the error bars on the $U^{K'}_{37}$ and TEX^H_{86} records represent the standard deviation of multiple runs; d, Mg/Ca record from core ODP 999A from western Atlantic (Schmidt et al., 2006); e, Difference of $U^{K'}_{37}$ and TEX^H_{86} -derived temperatures (ΔT) for GeoB9528-3; f, $\delta^{13}\text{C}$ of *C. wuellerstorfi* of core GeoB9528-3 (Castañeda et al., 2009) and g, Nd isotope ratios of core RC11-83/TNO57-21 from south Atlantic (Piotrowski et al., 2005). Shaded bars indicate periods of minor thermal stratification ($\Delta T < 2^\circ\text{C}$). The records show that depleted benthic $\delta^{13}\text{C}$ values (f) and increased neodymium isotope ratios (g), indicating that low AMOC strength, correspond to reduced ΔT (e). In all panels, the bold line represents the smoothed data points obtained by using a 5 point running mean whereas the black circles represent all available data points.

Since BIT values are always below 0.3 (Fig. 2.5), soil organic matter input has not influenced the TEX^H_{86} record. This suggests that TEX^H_{86} records subsurface temperatures over the last ~192 ka at this site. The $U^{K'}_{37}$ SST corresponds well to the general trends observed in the $\delta^{18}\text{O}$ record of the benthic foraminifera *C. wuellerstorfi* (Castañeda et al., 2009) (Fig. 2.4a, b), displaying the warmest temperatures during interglacials, Marine Isotope Stages (MIS) 1 and 5e, and the coolest temperatures during MIS 2, 4 and 6.

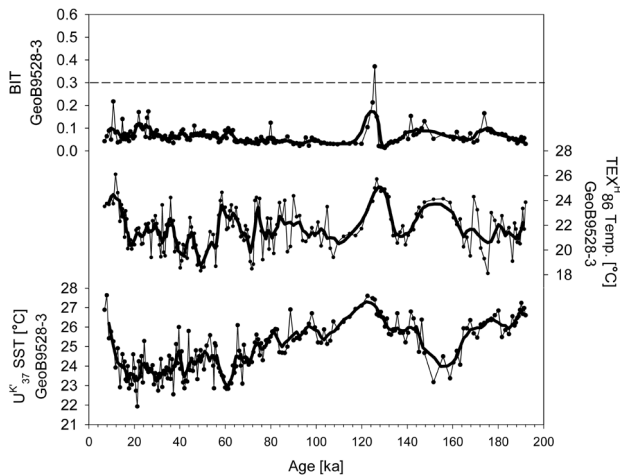


Fig. 2.5: BIT index values of core GeoB9528-3 together with the TEX^H_{86} and $U^{K'}_{37}$ records of the same core. The dashed line represents a BIT value of 0.3. Nearly all samples in GeoB9528-3 have a BIT value of < 0.3 and thus soil organic matter input is not biasing the TEX^H_{86} record.

Previous studies noted similarities in SST between these two interglacial periods in the equatorial eastern Atlantic (Hippler et al., 2006; Weldeab et al., 2007) with the coolest SSTs during MIS 2 and MIS 6 (Weldeab et al., 2007). Interestingly, during these cold intervals, the TEX^H_{86} record registers warm conditions in the thermocline (Fig. 2.4b, c). Enhanced subsurface temperatures are especially pronounced during the transitions from MIS 6 to 5, 4

to 3, and 2 to 1, as well as during MIS 6 (shaded bars, Fig. 2.4). The transitions were paralleled by sea-level rise and presumably meltwater input into the North Atlantic, originating from a decaying Laurentide ice sheet (Carlson et al., 2007; Chang et al., 2008; Hippler et al., 2006; Piotrowski et al., 2005, 2008). An exception is the subsurface warming during MIS 6, for which there is no evidence for large-scale sea-level rise and associated meltwater injection into the North Atlantic. When comparing the $\delta^{13}\text{C}$ of *C. wuellerstorfi* from GeoB9528-3 (Castañeda et al., 2009) and a neodymium isotope (ϵNd) record (Piotrowski et al., 2008) from the South Atlantic, both proxies for deep-water ventilation (Lynch-Stieglitz et al., 2007), we find that depleted $\delta^{13}\text{C}$ values and increased ϵNd , indicating low AMOC strength, correspond to smaller temperature differences (ΔT) between $\text{U}^{\text{K}'}_{37}$ and $\text{TEX}^{\text{H}}_{86}$ (Fig. 2.4e, f, g) thus reflecting thermocline warming during these periods.

Remarkably, there is also a significant correspondence (linear regression $r^2=0.54$; $p<0.001$) between the $\text{TEX}^{\text{H}}_{86}$ temperature record and the Mg/Ca SST record from ODP site 999A from the Caribbean basin on the western side of the tropical Atlantic (Schmidt et al., 2006) (Fig. 2.4c,d). This is in agreement with the study of Schmidt et al. (2004), showing that during periods of AMOC slowdown, widespread surface cooling in the tropical North Atlantic is not reflected in the western Caribbean. Instead, SST warming occurs here due to the accumulation of warm and saline water in response to AMOC slowdown. This all suggests that AMOC is an important driver of the tropical thermocline adjustment processes.

2.4.3. Modeling tropical thermocline adjustment

Further support for the interpretation of the geochemical records comes with our modeling experiment to simulate the impact of AMOC slowdown on surface and thermocline temperatures in the eastern tropical Atlantic. The GeoB9528-3 core top data suggest that $\text{TEX}^{\text{H}}_{86}$ reflects temperatures at around 30 m depth (Fig. 2.3), which is close to the present day maximum vertical temperature gradient (Fig. 2.6). Consequently, water temperature at this depth is particularly sensitive to vertical movements of the tropical thermocline, resulting in large variations of $\text{TEX}^{\text{H}}_{86}$ temperatures in response to AMOC-induced thermocline shifts. To capture this $\text{TEX}^{\text{H}}_{86}$ signal by the climate model and hence to allow for a reasonable data-model comparison, we “measure” temperature changes at a depth close to the modeled (rather than the observed) maximum vertical temperature gradient. As shown in Fig. 2.6, the modelled tropical thermocline at the location of core GeoB9528-3 occurs somewhat deeper than in reality (the maximum vertical temperature gradient is at a depth of ~ 100 m in the model). In order to make modeled subsurface temperature variations comparable to the $\text{TEX}^{\text{H}}_{86}$ reconstruction, we therefore use the ocean-model temperature at 100 m to calculate changes of the surface–subsurface temperature difference (ΔT) in the freshwater-hosing experiments (cf. Fig. 2.7c).

In a first hosing experiment with 0.5 Sv freshwater forcing, NADW formation completely stops (Fig. 2.2). An overall surface cooling, in comparison to modern SST, of the tropical North Atlantic is simulated, except for the western Caribbean, where SST slightly (~ 0.2 °C; statistically significant at the 0.01 significance level) increases (Fig. 2.7a).

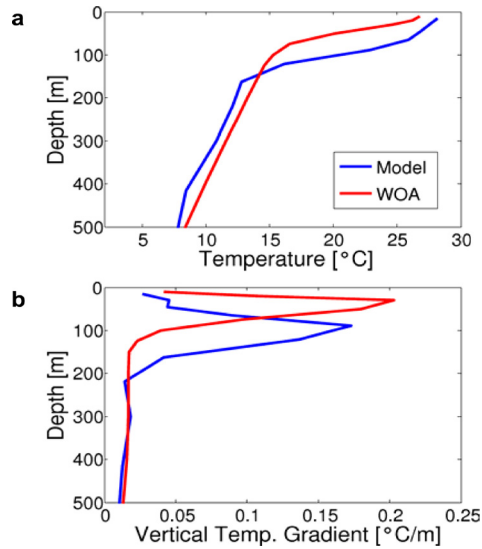


Fig. 2.6: Upper-ocean temperature stratification in the northeast tropical Atlantic at core location GeoB9528-3. a, profiles of annual-mean temperature in observed climatology (red) and ECBILT-CLIO modern control run (blue; calculated from long-term mean). b, corresponding vertical gradients. Data source: Locarnini et al. (2006).

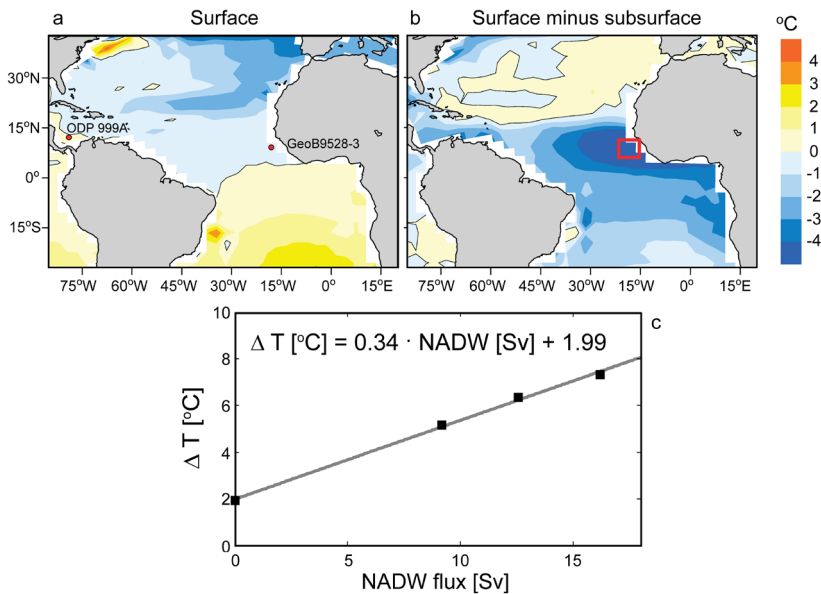


Fig. 2.7: Oceanic temperature response to AMOC changes simulated using a coupled climate model. a, SST difference between control run with 16.2 Sv (1 Sv=106 m³ s⁻¹) of North Atlantic Deepwater (NADW) export (modern conditions) and a run with deepwater formation completely shut down by

a strong freshwater injection into the subpolar North Atlantic. The positions of sediment cores ODP Site 999A and GeoB9528-3 are marked by red dots. b, Same as in (a) but for the surface–subsurface temperature difference anomaly, where the subsurface temperature is calculated as a vertical average over 30–200 m depth. c, relationship between absolute surface–subsurface temperature difference in the tropical northeast Atlantic around site GeoB9528-3 (area averaged over the red square indicated in b) and NADW flux, where the subsurface temperature is taken at 100 m (i.e. at the depth of the maximum vertical temperature gradient in the model as described in Section 2.4.3). NADW flux is defined as the maximum of the meridional overturning stream function in the South Atlantic at 30°S (see Section 2.3.3 for details). Different NADW fluxes have been obtained by varyingly strong freshwater injections. All results correspond to 100-year averaged equilibrated annual means.

The cooling takes place only in a thin layer; below ~30 m (eastern tropical North Atlantic) to 100 m (western equatorial Atlantic) the ocean warms. Maximum warming indeed occurs around the depth of the tropical thermocline, pointing to an important role of vertical shifts in the position of the thermocline in subsurface warming. This subsurface warming leads to a substantially reduced surface–subsurface temperature difference in comparison to the control case, particularly in the eastern tropical Atlantic (Fig. 2.7b). These model results are thus in agreement with our $\text{TEX}_{86}^{\text{H}}$ record showing eastern tropical Atlantic subsurface warming in phase with Caribbean SST warming and AMOC slowdown. Further model experiments with moderate AMOC slowdowns reveal that the magnitude of the surface–subsurface temperature difference at site GeoB9528-3 (Fig. 2.7b) scales nearly linearly with the magnitude of the AMOC anomaly (Fig. 2.7c).

In the tropical North Atlantic, the thermocline adjustments can be ascribed to the mechanisms described above (Chiang et al., 2008; Haarsma et al., 2008; Zhang, 2007). While weakened southeast trades during times of reduced AMOC may contribute to thermocline deepening in the eastern tropical South Atlantic (McIntyre and Molino, 1996), northeasterly wind anomalies over the eastern tropical North Atlantic would counteract tropical thermocline deepening here and, hence, can be ruled out as a possible driver for the observed thermocline adjustment. Our model results suggest that reconstructed surface–subsurface temperature differences may be taken as a measure of AMOC variability also on timescales much longer than decadal, and that ideal locations for reconstructing surface–subsurface temperature differences may be found in the eastern tropical North Atlantic (Fig. 2.7b). Our simulations allow for a rough estimate of the AMOC variability associated with these temperature variations (Fig. 2.7c), although the exact number is uncertain due to uncertainties in the temperature proxies and model details and changing boundary conditions including greenhouse gases, orbital parameters and glacial ice sheets (which may influence thermocline depth through mechanisms other than AMOC changes (Paul and Schafer Neth, 2003), but are not considered here). Using the geochemical records and the modeled relation between ΔT and NADW flux (Fig. 2.7c), we estimate that (multi-)millennial AMOC changes were roughly on the order of 10 Sv. While this absolute number should be interpreted carefully, it does suggest that the AMOC changes were quite substantial. These variations in tropical thermocline depth, in

turn, are likely to have a substantial impact on biological productivity in the euphotic zone (McIntyre and Molfino, 1996) and interannual tropical Atlantic climate variability (Haarsma et al., 2008). However, care has to be taken in interpreting this quantitative estimate as both the model and record of temperature differences across the thermocline are subject to the aforementioned uncertainties.

2.5. Conclusions

In the northeastern tropical Atlantic, $\text{TEX}_{86}^{\text{H}}$ turns out to be a proxy for subsurface temperature. In combination with a surface paleothermometer like U_{37}^{K} , this allows for reconstructing past changes in tropical thermocline structure. Our sediment records and model results support the notion that a slowdown of the AMOC results in a deepening of the tropical Atlantic thermocline and that this also holds on (multi-) millennial and glacial–interglacial time scales. The depth–adjustment of the thermocline results in a change in the temperature difference between surface and subsurface. The model experiments suggest that the reconstructed temperature changes of up to 7 °C may be indicative of AMOC variations on the order of 10 Sv. Accordingly, the eastern tropical North Atlantic appears to be a particularly sensitive region for thermocline adjustments caused by the variability in AMOC strength. Sediment records from this area may thus be particularly useful for constraining past AMOC variability and its impact on the tropical Atlantic Ocean.

Acknowledgments

We thank two anonymous reviewers and editor P. Delaney for comments which improved the manuscript. We thank Marianne Baas, Ellen Hopmans, Jort Ossebaar and Michiel Kienhuis for analytical assistance with the organic geochemical analyses, and Monika Segl for assistance with the foraminiferal isotope analyses. Research funding was provided by NEBROC-2 and a VICI grant to SS from the Netherlands Organization of Scientific Research. ES, MP, SM, MS and EMN have been funded through the DFG-Research Center/Excellence Cluster “The Ocean in the Earth System”. Samples from GeoB9528-3 were supplied through the assistance of MARUM at the University of Bremen.

Chapter 3

Comparison of organic and inorganic proxies for reconstruction of late Quaternary sea-surface temperature variability from offshore southeastern Australia

Raquel A. Lopes dos Santos, Michelle I. Spooner, Timothy T. Barrows, Patrick De Deckker, Jaap S. Sinninghe Damsté and Stefan Schouten
In revision for *Paleoceanography*

Abstract

Several proxies have been developed to reconstruct past sea-surface temperature (SST) but each of them can give a signal of different seasons and are associated with different uncertainties. Therefore, a multi-proxy approach is often required to understand these effects and precisely reconstruct SST. Here, we reconstruct SST for the last ~135 ka from offshore southeastern Australia using three independent organic proxies ($\text{TEX}_{86}^{\text{H}}$ based on glycerol dialkyl glycerol tetraethers, UK'_{37} based on alkenones and LDI based on long-chain diols) and foraminiferal faunal assemblages obtained from a core located in the Murray Canyons area. The organic proxy records show similar trends, with highest temperature (20-25°C) during the last interglacial and lowest temperature (8-12°C) during Last Glacial Maximum. However, differences are noted in absolute SST estimates obtained by the organic proxies and these differences varied over time. Comparison with SST reconstructions based on the modern analogue of foraminiferal assemblages shows that LDI inferred-temperatures compare well with the temperature of the warmest month, $\text{TEX}_{86}^{\text{H}}$ with the temperature of the coolest month and UK'_{37} with mean annual temperature. An increase in $\text{TEX}_{86}^{\text{H}}$ estimates relative to the other proxies during deglaciations and interglacials suggest that either winter temperatures rapidly warmed, possibly due to an invigoration of the Leeuwin Current over the core site, or that there was a change in the growth season of the *Thaumarchaeota*, the source organism of $\text{TEX}_{86}^{\text{H}}$. Our study shows the benefits of a multi-proxy approach in the interpretation of SST proxies, leading to a more robust knowledge of past ocean temperature changes.

3.1 Introduction

Accurate sea-surface temperature (SST) reconstruction from low- to high-latitude environments is a primary objective for paleoceanographic studies since SST is a crucial element of global climate. Several proxies have been used to reconstruct SST and are either based on inorganic (shells or skeletons) or organic (lipids) fossil remains. Both kinds of proxy have different uncertainties associated with them and, therefore, a multi-proxy approach is often used to constrain these uncertainties. An approach commonly used in the past has been the use of oxygen isotope composition of planktonic foraminifera tests to estimate temperature (Urey, 1947; Fischer and Wefer, 1999 and references cited therein). However, other factors such as ice volume, the state of preservation of the tests, species-dependent vital effects as well as sea-water composition, such as carbonate ion concentration and salinity, influence the $\delta^{18}\text{O}$ values of carbonates (e.g. Spero et al., 1997; Pearson et al., 2001; Lea et al., 2002). Another common technique is based on the analysis of fossil species assemblages (Imbrie and Kipp, 1971; Hutson, 1977; Pflaumann et al., 1996; Malmgren and Nordlund, 1997; Waelbroeck et al., 1998), but estimates based on this approach can be compromised by selective dissolution and lack of modern analogues (Barrows and Juggins, 2005). In addition, planktonic foraminiferal assemblages can reflect environmental variables other than sea surface temperature and transfer function approaches have also been used to assess thermocline depth (Andreasen and Ravelo, 1997), mixed layer depth (Spooner et al., 2005) and productivity (Mix, 1989). The Mg/Ca ratios of planktonic foraminifera have been shown to be a useful proxy for SST reconstructions (Nürnberg et al., 1996). However, these ratios can also be affected by carbonate ion concentration, pH, salinity, species-dependent vital effects and test dissolution (e.g. Brown and Elderfield, 1996; Lea et al., 2002; Eggins et al., 2004; Ferguson et al., 2008). All these foraminiferal proxies have been used to reconstruct mean annual SST, but studies have shown that they sometimes better record a seasonal or a subsurface temperature (e.g. Barrows and Juggins, 2005; Haarmann et al., 2011).

The main advantage of organic proxies for paleothermometry in comparison to inorganic ones is that they are not substantially influenced by sea water chemistry. The first organic proxy developed for SST estimation is the $\text{U}^{\text{K}'}_{37}$ index (Prahl and Wakeham, 1987), based on the relative abundance of di- and tri-unsaturated alkenones produced by haptophyte algae (Brassell et al., 1986). Culture and core top studies have shown that this index correlates well with mean annual SST (Müller et al., 1998). However, it has also been shown that physiological growth factors including nutrient and light limitation can affect the $\text{U}^{\text{K}'}_{37}$ index (Herbert, 2003 and references cited therein). Furthermore, diagenesis may influence the $\text{U}^{\text{K}'}_{37}$ (Hoefs et al., 1998; Gong and Hollander, 1999). A more recently developed SST proxy, the $\text{TEX}^{\text{H}}_{86}$, is based on the relative abundance of Glycerol Dialkyl Glycerol Tetraethers (GDGTs) (Schouten et al., 2002; Kim et al., 2010) produced by Thaumarchaeota (Sinninghe Damsté et al., 2002). This proxy has the advantage, compared to the $\text{U}^{\text{K}'}_{37}$, that it can be applied at temperatures >28 °C and in sediments up to 145 Ma old where alkenones are rarely found. Furthermore, it seems to be less affected by diagenesis (Schouten et al., 2004;

Kim et al., 2009). However, contributions of GDGTs from land can substantially affect the $\text{TEX}_{86}^{\text{H}}$ (Weijers et al., 2006) and additionally, as Thaumarchaeota occur throughout the water column (Karner et al., 2001; Herndl et al., 2005), $\text{TEX}_{86}^{\text{H}}$ has been reported to sometimes reflect subsurface temperatures (i.e. below the wind mixed layer) instead of SST (Huguet et al., 2007; Lee et al., 2008; Lopes dos Santos et al., 2010; Rommerskirchen et al., 2011). The latest introduced organic proxy for SST, the LDI (Long-chain Diol Index), has been recently described by Rampen et al. (2012) and is based on the relative distribution of 1,13 and 1,15 long-chain diols produced by algae, likely eustigmatophyte (Volkman et al., 1992). This proxy shows a strong correlation with SST in marine surface sediments. Application on a sediment core from the southeastern Atlantic showed SST patterns for the last 43 ka in agreement with other SST proxies and known climate events (Rampen et al., 2012). However, factors other than temperature that can affect this proxy have not yet been investigated in any detail. Finally, although all these organic proxies are calibrated against annual mean SST using core top sediments, they have been found to be biased towards a certain season at certain locations (e.g. Ternois et al., 1997; Herfort et al., 2006; Castañeda et al., 2010; Huguet et al., 2011). The application of multiple proxies can potentially yield more insight in these seasonal biases as well as other factors affecting SST reconstructions.

In this study, we applied multiple SST proxies to a sediment record from the Murray Canyons Group area offshore southeastern Australia (Fig. 3.1). This area has been the subject of several paleoceanographic studies (Gingele et al., 2004; Gingele and De Deckker, 2005; Calvo et al., 2007; Gingele et al., 2007; Moros et al., 2009; De Deckker et al., 2012; Lopes dos Santos et al., 2012) although SST reconstructions have been limited. Presently, the SST of western and southern Australian coastal waters is under the influence of the Leeuwin current (LC), which is Australia's longest warm water current, and its extensions: the South Australia and Zeehan currents (Ridgway and Condie, 2004) (Fig. 3.1). Ridgway and Condie (2004) showed that under modern day conditions, the LC (or its extensions) first penetrates the southern shelf of Australia and reaches the core area in May with the strongest influence in austral winter, i.e. July, especially during La Niña phases. Several paleoceanographic studies have reconstructed the strength and impact of the LC on millennial-time scales (Wells and Wells, 1994; Li et al., 1996; Li and McGowran, 1998; Martinez et al., 1999; Li et al., 1999; Gingele et al., 2001; Barrows and Juggins, 2005; Moros et al., 2009; Spooner et al., 2011) but most of these studies focused on the western coast of Australia and it is not clear whether the LC reached South Australian coastal waters during glacial periods. Wells and Wells (1994) suggested that the LC was absent during glacials due to an intensification of the West Australian Current and due to higher addition of the Indonesian Throughflow waters into the South Equatorial current instead of the LC. However, Barrows and Juggins (2005) and Spooner et al. (2011) showed that the LC did not cease but only decreased its flow during glacials and probably reached latitudes as far as 32°S (see Fig.3.1). Most studies have found this current to be much more intense during interglacials than during glacials and to reach southeastern Australia or even the west coast of Tasmania (Wells and Wells, 1994; Ridgway

and Condie, 2004; Moros et al., 2009; De Deckker et al., 2012).

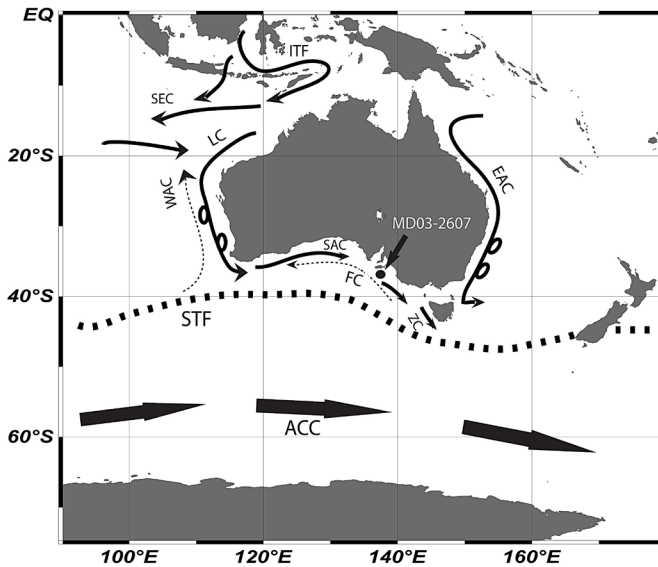


Fig. 3.1: Location of core MD03-2607 offshore southeastern Australia (black dot) together with the modern position of the subtropical front (STF - dashed line) and the main currents around Australia (arrows). ITF – Indonesian Throughflow, LC – Leeuwin Current, SAC – South Australia Current, FC – Flinders Current (dotted arrow means subsurface current), ZC – Zeehan Current, WAC – West Australia Current (dotted arrow means subsurface current), EAC – East Australia Current, SEC – South Equatorial Current, ACC – Antarctic Circumpolar Current.

We use a multi-proxy approach to reconstruct SST offshore southeastern Australia for the last ~135 ka. We compare organic proxy records with foraminiferal assemblages from the same sediment core which allow us to infer the impact of seasonal contrasts on these proxy records and the influence of the LC which mainly impacts austral winter.

3.2 Material and Methods

Sediment core MD03-2607 was recovered during the AUSCAN 2003 cruise (MD131) from the Murray Canyons group area in offshore southeastern Australia at $36^{\circ}57.64' \text{S}$; $137^{\circ}24.39' \text{E}$ (Fig. 3.1) and 865 m water depth (Hill and De Deckker, 2004). A description of the core and its mineralogical content was published in Gingele et al. (2004). The age model of this core was recently revised by Lopes dos Santos et al. (2012) and is based on the ^{14}C dates of mixed planktonic foraminiferal assemblages and optically stimulated luminescence dating of single grains or small aliquots of sand-sized quartz for the past ~35 ka, with older tie-points based on correlation of the $\delta^{18}\text{O}$ record of the planktonic foraminifera *Globigerina bulloides* with stacked isotope records of Lisiecki and Raymo (2005).

3.2.1 Sampling of core MD03-2607

Initial onboard analysis, during the 2003 AUSCAN cruise, indicated higher sedimentation rates towards the base of the core MD03-2607 (~30 m long) and this was considered during sampling. For biogeochemical analyses, only the first 15 m of the core was sampled with a resolution of 5 cm intervals for the first 3 m and at 10 cm for the rest 12 m. A total of 172 samples were analysed. For the relative foraminiferal abundance counts the entire core was sampled, however, for this study only data of the first 15 m are reported. The Holocene section was sampled every 5 cm but sections with higher sedimentation rates were increased to a sampling rate of 20 cm, 30 cm and 60 cm. Foraminifera counts were made for a total of 116 samples.

3.2.2 Organic proxy analysis

Sediment samples were freeze-dried, homogenized and extracted using an Automated Solvent Extractor (ASE) 200, DIONEX; 100°C and 7.6×10^6 Pa with a mixture of dichloromethane (DCM): methanol (MeOH) (9:1, v:v) to obtain a total lipid extract (TLE). Internal standards (squalane, nonadeca-1-one, C_{46} GDGT) were added to the TLE, which was subsequently separated into an apolar, ketone and polar fraction in an alumina oxide column (Al_2O_3), using *n*-hexane/DCM 9:1, *n*-hexane/DCM 1:1 and methanol/DCM 1:1 as eluents, respectively. The ketone fractions, containing the alkenones, were analyzed by gas chromatography (GC) and gas chromatography/mass spectrometry (GC/MS) as described previously (Lopes dos Santos et al., 2012). One aliquot of the polar fraction was analysed for GDGTs by filtration through a polytetrafluoroethylene (PTFE) filter and analysed using high performance liquid chromatography/mass spectrometry (HPLC/MS) following Schouten et al. (2007). Another aliquot of the polar fraction was analysed for long-chain diols by silylation using bis(trimethylsilyl)trifluoroacetamide (BSTFA) and pyridine before being analysed by GC/MS following Rampen et al. (2012).

U^{K'}₃₇ analyses: Alkenone identification and analyses was previously described in Lopes dos Santos et al. (2012). The U^{K'}₃₇ was calculated using the equation described by Prahl and Wakeham (1987). SST values were estimated using the global core top calibration of Müller et al. (1998) covering a temperature range of 0 to 27°C and that was reported to have a calibration error of 1.5°C.

LDI analyses: Compound identification of the long-chain diols was conducted using a Thermofinnigan Trace GC Ultra connected to Thermofinnigan DSQ MS operated at 70 eV, with a mass range *m/z* 50-800 and 3 scans *s*⁻¹. The capillary column was a silica column (25 m x 0.32 mm) coated with CP Sil-5 (film thickness = 0.12 μm). The initial oven temperature started at 70°C and increased at a rate of 20°C *min*⁻¹ to 130°C, and subsequently at a rate of 4°C *min*⁻¹ to the final temperature of 320°C, which was held for 10 min. The relative abundance of diols was measured using single ion monitoring of *m/z* 299, 313, 327 and 341 with a dwell time of 100 ms. The LDI index was calculated using equation [1], as described by Rampen et al. (2012):

$$LDI = \frac{[C_{30}1,15 - \text{diol}]}{[C_{30}1,15 - \text{diol}] + [C_{28}1,13 - \text{diol}] + [C_{30}1,13 - \text{diol}]} \quad [1]$$

and converted into SST [2] using the global core top calibration of Rampen et al. (2012), covering a temperature range of -3 to 27°C and reported to have a calibration error of 2°C:

$$SST = \frac{LDI - 0.095}{0.033} \quad [2]$$

TEX₈₆^H analyses: The polar fractions were analyzed for GDGTs using HPLC-APCI-MS following Schouten et al. (2007). TEX₈₆^H was calculated using the equation [3] described by Kim et al. (2010) and equation [4] was used to estimate temperature values. This global core top calibration, covering a temperature range of -3 to 30°C, was reported to comprise a calibration error of 2.5°C (Kim et al., 2010):

$$TEX_{86}^H = \log \left(\frac{[GDGT - 2] + [GDGT - 3] + [Cren']}{[GDGT - 1] + [GDGT - 2] + [GDGT - 3] + [Cren']} \right) \quad [3]$$

$$\text{Temp [}^\circ\text{C]} = 68.4 (TEX_{86}^H) + 38.6 \quad [4]$$

3.2.3 Planktonic foraminifera analyses and modern analogue technique

The species nomenclature used in this study follows the taxonomy of Saito et al. (1981). Counts of planktonic foraminifera were made on splits of the >150 μm fraction removing small juvenile specimens. Each sample was split by an Otto-micro splitter until ~ 400 species were present in the final split. The number of fragments of the tests was also recorded to give an indication of the preservation status of the foraminifera in the sample.

SST were estimated from the planktonic foraminiferal assemblage data using the modern analogue technique, in conjunction with a database from Southern Hemisphere core tops, AUSMAT-F4 with a final training set containing 1303 core top samples (Barrows and Juggins, 2005). The annual SST (Tmean) and the temperature of the warmest (Tmax) and coolest months (Tmin) were estimated, with each estimate calculated as the mean of the 10 best analogues from the global database. The distance to the nearest analogue, the mean distance and the standard deviation were also calculated to assess the quality of the analogue. The relatively most precise variable, based on this Southern Hemispheric calibration covering a temperature range of -1 to 30°C, is Tmean with a root mean squared error of prediction (RMSEP) of 0.8 °C based on a five-fold leave-out cross-validation (Note that this is a different method for error calculation than those for the organic proxies which is based on global calibration errors). Tmax also has a low RMSEP of 0.9°C, whereas, Tmin SST has relatively the greatest error with a RMSEP of 1°C (Barrows and Juggins, 2005). The quality of SST estimates is measured by the squared chord distance, with distances of <0.2 indicating good analogues. For further details, see Barrows and Juggins (2005).

3.3 Results

The $\text{TEX}_{86}^{\text{H}}$ (blue line, Fig. 3.2b) follows the same trend as the U_{37}^{K} (red line Fig. 3.2b; from Lopes dos Santos et al., 2012) and $\delta^{18}\text{O}$ (Fig 3.2a; from Lopes dos Santos et al., 2012) records but absolute SSTs are generally lower than U_{37}^{K} , by up to 6°C , except during deglaciations and interglacials (Marine Isotope stages (MIS) 1 and 5e) where they are similar to U_{37}^{K} temperatures. The lowest SSTs of about 8°C are recorded during the LGM and MIS 4, and the Antarctic Cold Reversal (ACR) event is visible as an interruption of the deglacial warming trend. The LDI-derived SST (green line, Fig. 3.2b) has a similar trend as the other SST records but absolute values are consistently higher than those of U_{37}^{K} and $\text{TEX}_{86}^{\text{H}}$ temperatures, except during deglaciation periods where temperature estimates are similar to those of U_{37}^{K} and $\text{TEX}_{86}^{\text{H}}$. The highest temperature of $\sim 25^{\circ}\text{C}$ was recorded during the last interglacial period and the lowest temperature of $\sim 13^{\circ}\text{C}$ was recorded during LGM. The LDI also shows an interruption of the deglacial warming trend during the ACR.

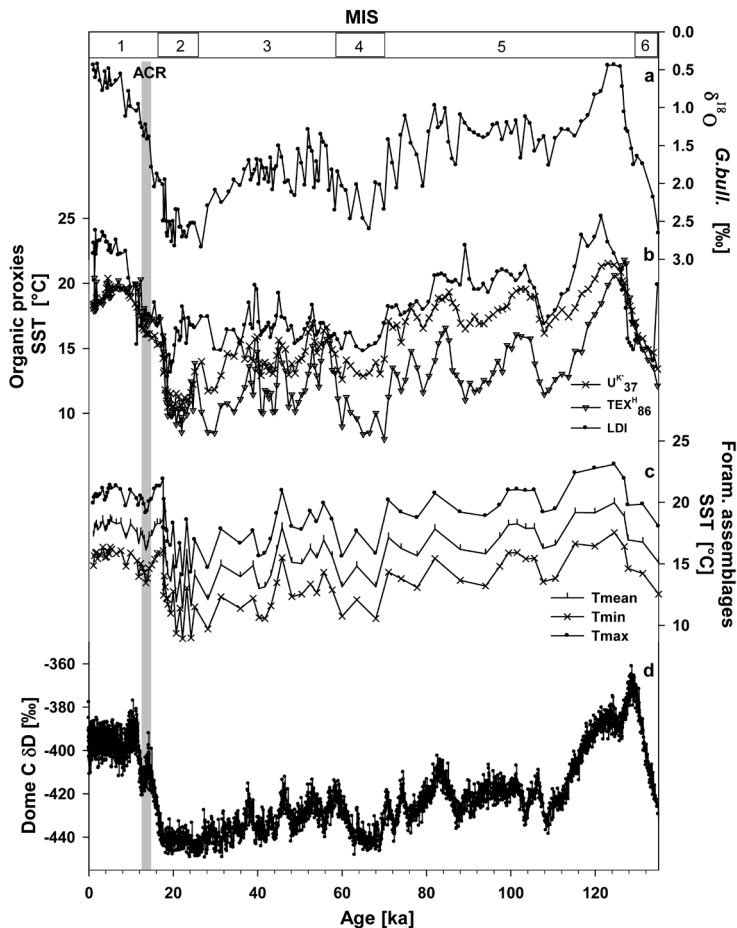


Fig. 3.2: Comparison between planktonic foraminiferal oxygen-isotopes and SST reconstructions from core MD03-2607, together with the Dome C deuterium isotope record, as a proxy for air temperature in Antarctica. a) $\delta^{18}\text{O}$ record of *Globigerina bulloides* (Lopes dos Santos et al., 2012), b) LDI SST

(dots), $\text{TEX}_{86}^{\text{H}}$ SST (triangles) and $\text{U}^{\text{K}'}_{37}$ SST (crosses - $\text{U}^{\text{K}'}_{37}$ SST from Lopes dos Santos et al., 2012), c) modern analogue technique SST reconstructions for warm months (dots), cold months (crosses) and mean annual (vertical lines), and d) δD from the EPICA ice core, Dome C (Jouzel et al., 2007). Shaded bar is the Antarctic Cold Reversal (ACR). MIS = Marine Isotope Stage.

The foraminiferal assemblages provide a mean annual SST estimate of $\sim 20^{\circ}\text{C}$ during the last interglacial period, slightly warmer than the present interglacial SST of $\sim 19^{\circ}\text{C}$ (Fig. 3.2c). The lowest mean annual SST (T_{mean}) was recorded during LGM with $\sim 11^{\circ}\text{C}$. The SST of the warmest month (T_{max}) inferred from the foraminifer assemblages are $\sim 22\text{--}23^{\circ}\text{C}$ during the interglacials with SST of $\sim 14^{\circ}\text{C}$ during the LGM (Fig. 3.2c). The coldest month SST (T_{min}) was $\sim 18^{\circ}\text{C}$ during interglacials and $\sim 9^{\circ}\text{C}$ during LGM and MIS 6 (Fig. 3.2c). All the foraminiferal assemblage-derived SST records showed a sharp cooling of approximately 3°C during the ACR.

3.4 Discussion

3.4.1 Comparison of SST estimates

The organic proxy SST records all broadly follow the trend of the $\delta^{18}\text{O}$ record of *G. bulloides* (Lopes dos Santos et al., 2012) and all are generally in line with changes in Antarctic temperature shifts as can be seen by the δD record of the EPICA Dome C ice core (Fig. 3.2d) (Jouzel et al., 2007), suggesting that the SST in the Murray Canyons Group area follows Southern Hemisphere climate variations as previously suggested for the last 30 ka (Calvo et al., 2007). The coherent changes between the organic proxy SST records are demonstrated by the significant correlation between them ($r^2=0.62\text{--}0.66$, $p<0.001$), with only $\text{TEX}_{86}^{\text{H}}$ and LDI showing a weaker but still significant ($r^2=0.37$, $p<0.001$) correlation (Fig. 3.3).

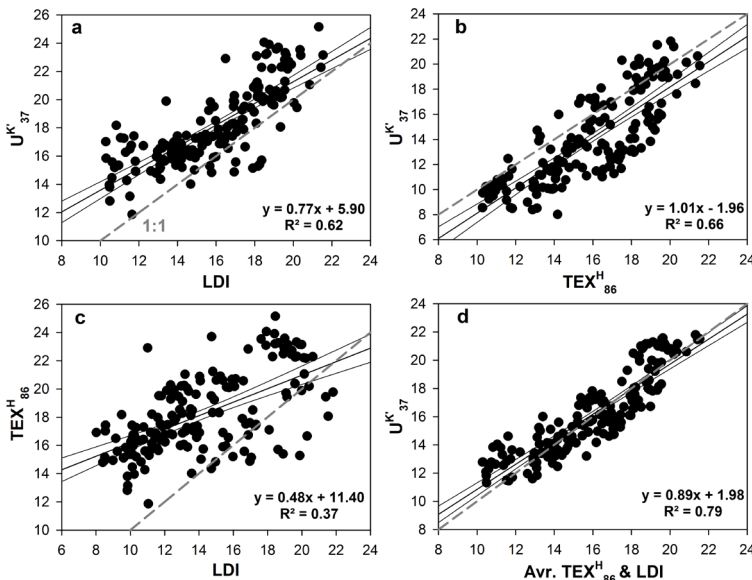


Fig. 3.3: Correlation and confidence interval (95%) between organic proxy SST estimates for core MD03-2607. a) correlation between $U^{K'}_{37}$ and LDI, b) between $U^{K'}_{37}$ and TEX^H_{86} , c) between TEX^H_{86} and LDI and d) between $U^{K'}_{37}$ and the average of the TEX^H_{86} and LDI. Dashed line is the 1:1 line.

Importantly, the timing of the SST changes does not differ substantially between the organic proxies and the foraminiferal temperature records, suggesting that the former are not strongly affected by lateral transport or selective degradation. A similar observation was made for the western Mediterranean where SST reconstruction during the penultimate glacial-interglacial cycle, based on the Mg/Ca ratio of planktonic foraminifera, showed trends coherent with both $U^{K'}_{37}$ and TEX^H_{86} (Huguet et al., 2011).

A striking observation is that the magnitude of temperature variations and absolute temperature values between the organic proxies are different. For some part, this difference between the SST estimates is within calibration errors of the proxies. The calibration error for $U^{K'}_{37}$ was reported to be 1.5°C (Müller et al., 1998), 2.5°C for TEX^H_{86} (Kim et al., 2010) and 2.0°C for LDI (Rampen et al., 2012), and may result in systematic errors of <3°C between different proxy records. However, for large parts of the record, differences between the three proxies are >3°C, which need to be explained by different factors. Furthermore, these differences are variable and not systematic in nature, and, thus, cannot be explained by calibration issues only. Each proxy can be affected by a variety of parameters other than temperature. For instance, soil organic matter input by rivers may affect GDGT distributions in coastal marine sediments and thus TEX^H_{86} (Weijers et al., 2006). However, the Branched Isoprenoid Tetraether index (BIT index), a proxy for soil organic matter input in the marine environment (Hopmans et al., 2004), was always < 0.3, suggesting that TEX^H_{86} was not substantially affected by soil organic matter input (cf. Weijers et al., 2006). The LDI and $U^{K'}_{37}$ are not expected to be influenced by soil organic matter input as they are likely to be uniquely sourced by algae. Lateral transport and selective degradation is unlikely to be an important issue as discussed above. Light and nutrient limitation can affect some of these proxies (e.g. Herbert, 2003 and references cited therein], but it is not clear how they would affect the proxies such that they would cause the observed differences in SST.

The proxies, most likely, record the growth temperature of their source organisms and, therefore, the different SST estimates might be influenced by the difference in the depth habitat of the organisms. Thaumarchaeota are chemoautotrophic nitrifiers (Könneke et al., 2005; Wuchter et al., 2006a; Park et al., 2010) and occur throughout the water column (e.g. Karner et al., 2001; Herndl et al., 2005) and, therefore, TEX^H_{86} may record lower temperatures of deeper water masses than the LDI and $U^{K'}_{37}$ proxies as proposed previously (e.g. Lee et al., 2008; Lopes dos Santos et al., 2010). However, TEX^H_{86} temperatures are not always lower than the $U^{K'}_{37}$; for example, during the deglaciations, TEX^H_{86} temperatures are similar to those of the LDI and $U^{K'}_{37}$. This suggests that Thaumarchaeota may have been migrating between the surface and the subsurface in the water column during specific periods. For the LDI and $U^{K'}_{37}$ proxies, the same reconstructed temperatures would be expected as both proxies are based on compounds produced by photosynthetic algae. However, the LDI is

recording higher temperatures than $U^{K'}_{37}$, a feature which is difficult to explain by differences in depth habitat.

Thus, most factors known to affect the different proxies are unlikely to explain the differences observed between their SST estimates. One last explanation for the dissimilarity between the reconstructed-SST estimates may be differences in the growing season of the source organisms of each of the proxies, which is discussed in more detail below.

3.4.2 The influence of seasons on the organic proxy records

To examine the impact of seasonality on the organic proxies, we compared SST estimates from the uppermost core sample with various SSTs of the present day system (Fig. 3.4). The LDI gives a temperature estimate of 22°C, which is 4°C higher than the SST recorded during austral summer at our core site (Locarnini et al., 2010). TEX^{H}_{86} and $U^{K'}_{37}$ provide a temperature estimate of 18°C that matches modern austral summer SST but is 2°C higher than annual mean SST. Interestingly, the SST estimates based on the foraminiferal assemblage are also generally higher than modern SST but close to the estimated uncertainties (Fig. 3.4), with the Tmax and Tmin ~1°C higher than the modern warmest and coolest temperature, respectively, while Tmean is also ~1°C higher than modern SST (Fig. 3.4). Most likely, these reconstructed high temperatures indicate that the uppermost sediment of our core does not represent modern conditions: indeed, our age model suggests it is ~1 ka old, and thus may be from a warmer period in the past. If we assume that the core top sample has a 1-2°C offset compared to modern conditions, it would suggest that the LDI may represent austral summer temperatures and TEX^{H}_{86} and $U^{K'}_{37}$ represent annual mean or austral fall temperatures, while the SST estimates from foraminiferal assemblages would fit the seasonal SST distribution at the Murray Canyon area (Fig. 3.4).

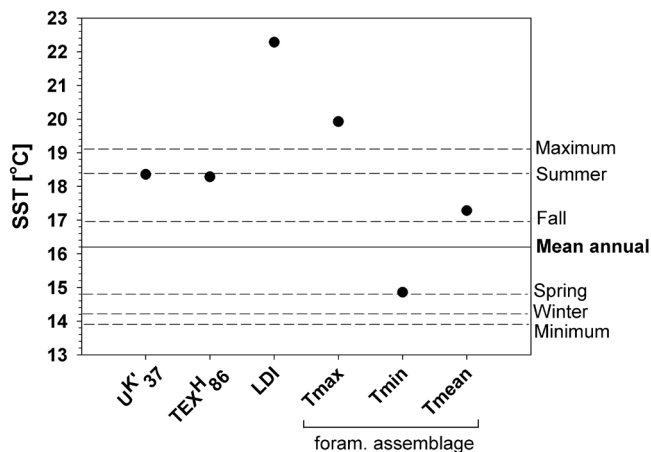


Fig. 3.4: Measured and proxy reconstructed SST (from the core top) at core site MD03-2607. Modern austral seasonal SST, mean annual SST and minimum and maximum SST (Locarnini et al., 2010) are shown as lines together with reconstructed SST based on organic proxies and based on foraminifera assemblages.

To test the potential impact of seasonality on the organic proxies on geological time scales, we compared the organic proxy-derived SST records with those obtained from the foraminiferal assemblage (Fig. 3.5).

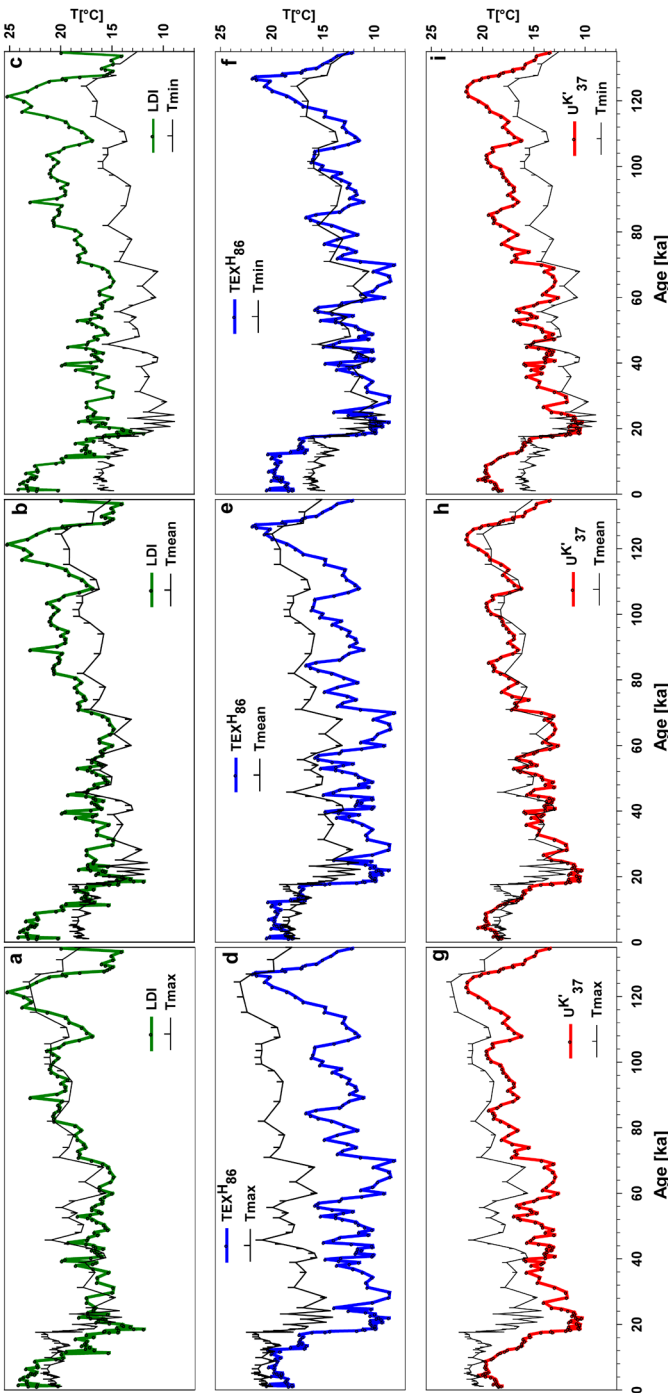


Fig. 3.5: Comparison of paleotemperatures reconstructed with organic proxies with those reconstructed with the modern analogue technique of foraminifera assemblages from core MD03-2607. LDI SST together with foraminifer SST reconstruction for the warmest months (Tmax; a), annual (Tmean; b) and coldest months (Tmin; c), TEX^H₈₆ SST together with foraminifer SST reconstruction in the same order as described for LDI (d-f) and U^K₃₇ SST (from Lopes dos Santos et al., 2012) with SST reconstruction using assemblages in the same order described above (g-i).

This shows that the LDI-reconstructed SSTs follow a similar trend and have similar absolute values as the warmest month SSTs (Tmax) reconstructed from foraminiferal assemblages throughout most of the core (Fig. 3.5a-c). In contrast, $\text{TEX}_{86}^{\text{H}}$ -reconstructed SSTs are more in agreement with the coolest month SSTs (Tmin), except during interglacials where $\text{TEX}_{86}^{\text{H}}$ temperature estimates are 4-5°C warmer than Tmin (Fig. 3.5d-f). Finally, U_{37}^{K} -reconstructed SSTs are in good agreement with the mean annual SSTs (Tmean) reconstructed using the foraminiferal assemblages (Fig. 3.5g-i). Together, this strongly suggests that LDI and $\text{TEX}_{86}^{\text{H}}$ proxies may reflect SST of a particular season, i.e. warm austral summer and cold austral winter, respectively, while U_{37}^{K} records the mean annual SST. Further support for this interpretation comes from the fact that the averaged temperature of both LDI and $\text{TEX}_{86}^{\text{H}}$ yields a SST record that correlates well with the U_{37}^{K} record (Fig. 3.6, 3.3d).

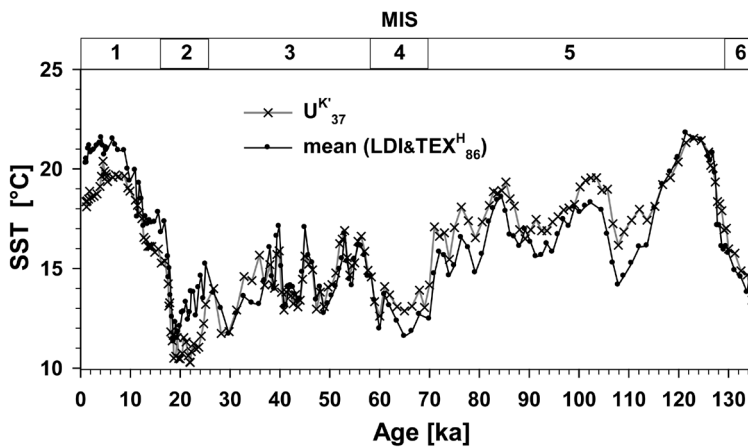


Fig. 3.6: Comparison of the U_{37}^{K} SST record (crosses - Lopes dos Santos et al., 2012) with the mean of the LDI and $\text{TEX}_{86}^{\text{H}}$ SST estimates (dots).

Previous studies have shown that $\text{TEX}_{86}^{\text{H}}$ can record seasonal SSTs rather than an annual mean SST. For example, Herfort et al. (2006) showed that the TEX_{86} recorded mainly winter temperatures in the southern North Sea, whereas for the Mediterranean it was shown that $\text{TEX}_{86}^{\text{H}}$ likely recorded summer temperatures (Menzel et al., 2006; Leider et al., 2010; Castañeda et al., 2010; Huguet et al., 2011). The seasonal bias towards winter temperatures in the North Sea (Herfort et al., 2006) was attributed to the higher abundance of Thaumarchaeota during this season in this area (Wuchter et al., 2006; Pitcher et al., 2011). During winter, the concentration of ammonia, which fuels the chemoautotrophic Thaumarchaeota, are high and algal productivity is low, and thus competition for ammonia is limited. At our site it is possible that the growth season of Thaumarchaeota is also related to high ammonia levels and less competition with algae. Indeed, on average chlorophyll abundances are generally low during austral winter compared to austral fall and spring (Conkright et al., 2002). However, for a better understanding of the influence of seasonality in the $\text{TEX}_{86}^{\text{H}}$ proxy, ecological

studies of Thaumarchaeota as well as sediment trap studies from the Murray Canyons Group area are needed.

For $U^{K'}_{37}$, a seasonal bias has sometimes been observed (Ternois et al., 1997; Castañeda et al., 2010; Leider et al., 2010), but it generally shows a stronger relationship with the mean annual SST (e.g. Müller et al., 1998; Herbert, 2003 and references cited therein; Mohtadi et al., 2011) as observed at our core site. For the LDI, no studies have been done yet on seasonal biases. However, a slightly stronger correlation of LDI values with summer SST compared to annual mean was reported by Rampen et al. (2012) for marine surface sediments, tentatively suggesting that the source organisms, likely eustigmatophyte algae (Volkman et al., 1992), may preferentially proliferate during summer months. Our LDI record also suggests that the source algae for the diols are more abundant during austral summer, although this season's chlorophyll concentrations are relatively low in comparison to the fall season (Conkright et al., 2002). Sediment trap studies are clearly needed to confirm a seasonality effect for this new proxy.

3.4.3 Convergence of TEX^H_{86} and $U^{K'}_{37}$ SST estimates during deglaciations

A striking observation is that the temperature differences between the organic proxies, in particular the TEX^H_{86} and $U^{K'}_{37}$, are much smaller during deglaciations and interglacials. Comparison to the $U^{K'}_{37}$ SST record of the nearby core MD03-2611 (~80 km far) shows a similar record as our $U^{K'}_{37}$ SST confirming that the $U^{K'}_{37}$ is giving a regionally consistent pattern while TEX^H_{86} follows this pattern only during deglaciation and interglacials.

Two explanations can be proposed for this decrease in difference between the reconstructed temperatures using the $U^{K'}_{37}$ and TEX^H_{86} at our site. First, it could be that the Thaumarchaeota changed their growth season during deglaciations and interglacials and was more reflective of annual mean temperatures, matching the $U^{K'}_{37}$ temperature estimates. Indeed, a relatively lower temperature difference between TEX^H_{86} and $U^{K'}_{37}$ was also recorded during interglacials in the Mediterranean and was explained by a change in growth season for the Thaumarchaeota (Huguet et al., 2011). A similar pattern where Thaumarchaeota may have been changing their behavior during interglacials may have occurred here, although ecological and sediment trap studies are required to confirm this hypothesis.

Secondly, it could be that winter temperatures, as recorded by the TEX^H_{86} at this site, were relatively warm during deglaciations causing a decrease in the differences in TEX^H_{86} and $U^{K'}_{37}$ SST. However, the warmer austral winter temperature is not apparent in the T_{min} record inferred from foraminiferal assemblages (Fig. 3.5f), possibly because T_{min} reflects the coldest month while TEX^H_{86} may reflect winter temperatures of a different month or a whole season. Possibly, the TEX^H_{86} reflects temperatures from the winter months influenced by warmer water masses (e.g. the LC current), while T_{min} does not record this influence. Indeed, seasonality recorded by the difference between T_{mean} and T_{min} inferred by the foraminiferal assemblage is almost constant over the last 135 ka, in contrast to the difference between the $U^{K'}_{37}$ and TEX^H_{86} proxies (Fig. 3.7). This suggests that these two SST

reconstructions, T_{min} and TEX^H_{86} , are registering different seasonal conditions and are likely affected by different factors.

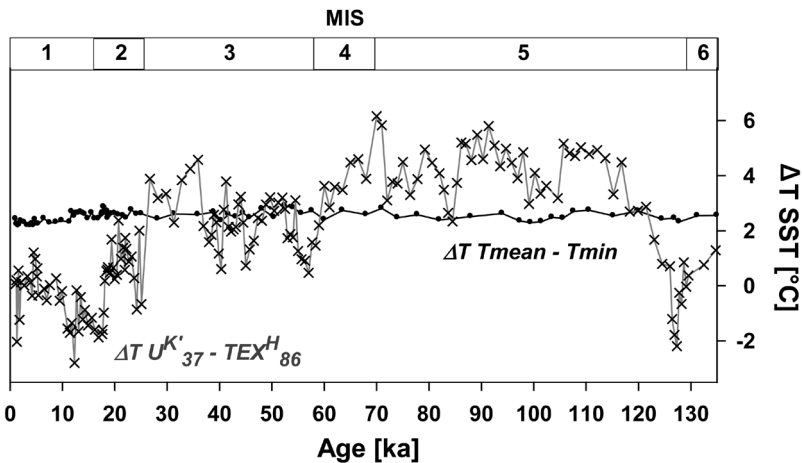


Fig. 3.7: Reconstructed seasonality based on the difference between the mean annual and coolest months from the foraminiferal assemblages (dots) and the difference between $U^{K'}_{37}$ and TEX^H_{86} (crosses).

If the relatively high TEX^H_{86} SSTs do indicate a warming of austral winter SST in southeastern Australia, then it is likely reflecting the input of warm waters from the LC (and extensions) during these periods. If so, this suggests that the LC reached the core site during deglaciations, interglacials and, possibly, during MIS 2 and parts of MIS 3 (Fig. 3.2b). De Deckker et al. (2012) also recorded the presence of the LC in the nearby core MD03-2611 during these periods based on the analysis of planktonic foraminifera groups. The TEX^H_{86} SST estimates converge to those of the $U^{K'}_{37}$ at ~ 25 ka, suggesting the presence of the LC from this time period at the core site in the last glacial-interglacial cycle. As the LC is prevented from reaching southern Australia when the Subtropical Front (STF) was in its northern position (Moros et al., 2009; De Deckker et al., 2012), our results support a southern position of the STF during deglaciations and interglacial but also during early MIS 2 and parts of MIS 3, as suggested previously by other studies (Sikes et al., 2009; Bard and Rickaby, 2009; De Deckker et al., 2012). Indeed, *G. ruber* and *G. sacculifer* were found in the glacial sediments of our core which indicates the presence of subtropical water. However, care has to be taken in reconstructing the LC influence in southeastern Australia and STF position based on the TEX^H_{86} , due to the uncertainties in interpreting the TEX^H_{86} as a winter temperature signal and in interpreting the front as a purely temperature defined feature.

3.5 Conclusions

Sea-surface temperatures from the Murray Canyons Group area offshore southeastern

Australia were reconstructed for the last 135 ka using three independent organic proxies, which showed coherent patterns over glacial-interglacial time scales. Comparison between the temperature proxies and seasonal SST estimates obtained from foraminiferal assemblages showed that LDI seems to be related to austral summer month SST, $\text{TEX}_{86}^{\text{H}}$ to austral winter month SST and $\text{U}_{37}^{\text{K}'}$ to the mean annual SST. This unique multi-proxy approach enabled us to evaluate the seasonal biases on sea-surface temperature proxies. The reduced difference between $\text{TEX}_{86}^{\text{H}}$ and $\text{U}_{37}^{\text{K}'}$ SST estimates during the deglaciations are either due to a change in the growth season of Thaumarchaeota or due to a reduced seasonal SST contrast and, possibly, shows the impact of the LC during the coolest months at the Murray Canyons Group area, as the LC mainly affects winter temperatures offshore southeastern Australia.

Acknowledgements

Research funding was provided by a VICI grant to SS from the Netherlands Organization of Scientific Research. Core MD03-2607 was obtained with a National Oceans Office and Australian Research Council grant, both awarded to PDD. Y. Balut from IPEV was instrumental in obtaining the core. M.I.S. was the recipient of an ANU postgraduate award.

Chapter 4

Relationship between primary productivity and Sahara dust input in the eastern tropical North Atlantic during the late Quaternary

Raquel A. Lopes dos Santos, Aline Govin, Isla S. Castañeda, Matthias Zabel, Enno Schefuß, Stefan Mulitza, Jaap S. Sinninghe Damsté, Stefan Schouten
In preparation

Abstract

During the late Quaternary, primary productivity in the NW African coastal waters experienced significant changes due to upwelling and ocean fertilization by Saharan dust, driven by variations in wind strength. Here, we evaluate the relationship between primary productivity and iron supply from Sahara dust in sediments from the Guinea Plateau Margin. We reconstruct a late Quaternary record of total organic carbon (TOC) and specific biomarker lipids (dinosterol for dinoflagellates, C_{37} alkenones for haptophytes and C_{30} *n*-alkyl 1,15-diol for eustigmatophytes) and compared this to iron concentrations and accumulation rates and geochemical proxies for NW African aridity changes. During the past 192 ka, TOC and biomarker lipids concentrations and accumulation rates show minima during Marine Isotope Stages (MIS) 1 and 5.5 (interglacials) and increased levels throughout glacials, MIS 3 and 5.4. Our results indicate a positive correlation between sedimentary Fe and biomarker accumulation rates, suggesting a link between iron content and primary productivity in particular during periods of high aridity on the continent. This study suggests that productivity in oligotrophic eastern tropical North Atlantic is considerably influenced by the fertilization effect of the Sahara dust.

4.1 Introduction

Reconstruction of primary productivity is essential to better understand the past carbon cycle and to assess the factors controlling productivity on geological time scales. Past primary productivity has been inferred from the accumulation of certain metals sensitive to organic carbon fluxes (e.g. Dymond et al., 1992), from the ratio of radionuclides scavenged from the water column (e.g. Kumar et al., 1995), from microfossil assemblages (e.g. Mix, 1989a) or from the accumulation of biologically produced substances such as organic carbon, carbonates, opal and lipid biomarkers (e.g. Lyle et al., 1988; Bareille et al., 1991; Hinrichs et al., 1999). The latter has been increasingly used to reconstruct primary productivity in highly productive upwelling areas (e.g. Repeta et al., 1992; Schubert et al., 1998; Hinrichs et al., 1999; Sicre et al., 2000; Zhao et al., 2006) because it provides details on algal groups community changes.

The eastern Atlantic along the NW African coast is, at present, a highly productive area (van Camp et al., 1991) where primary productivity is mainly controlled by nutrient availability, which in turn is determined by upwelling, river discharge and dust input from the Sahara desert area (Sprenkel et al., 2000; Nave et al., 2001; Bouimetarhan et al., 2009). From these nutrient sources, the dust input from the Sahara desert is the one that can have the strongest impact in open marine waters furthest away from the coast. Indeed, phytoplankton productivity was shown to be stimulated in the tropical and sub-tropical north Atlantic due to the Fe and P fertilization effect of Sahara dust (Mills et al., 2004; Sedwick et al., 2005). It was shown that Fe stimulates the productivity of diazotrophs, as these organisms contain the iron-rich nitrogen fixing enzyme nitrogenase (Mills et al., 2004; La Roche et al., 2005). The stimulation of diazotrophs leads to an increasing production of ammonia and, subsequently, nitrate, thereby, stimulating phytoplankton productivity.

Based on a variety of approaches, many studies (Bertrand et al., 1996; Martinez et al., 1999a; Flores et al., 2000; Sicre et al., 2000; Zhao et al., 2000; Sicre et al., 2001; Freudenthal et al., 2002; Moreno et al., 2002; Nave et al., 2003; Zhao et al., 2006; Romero et al., 2008; Zarriess and Mackensen, 2010; Crosta et al., 2012) reconstructed past productivity variations and their forcing along the NW African coast on geological time scales, mainly at latitudes above 12°N (Fig. 4.1). The longest paleoproductivity record, which is based on biomarker lipid concentrations and accumulation rates (AR), covers the last 160 ka at 20°N (ODP 658; Fig. 4.1) and suggests significant changes in phytoplankton productivity (Zhao et al., 2006). To evaluate the role of nutrient input from the continent through dust on primary productivity, Zhao et al. (2006) compared algal lipid biomarkers with those of aeolian transported terrestrial biomarkers. They attributed the generally high productivity at this site to strong upwelling and the variations therein to fertilization effects due to dust input from the Sahara region. Other paleoproductivity records indicate that primary productivity is highly variable along the NW African coast. For example, some studies suggest minimum values of primary productivity during the Last Glacial Maximum (LGM, ~21 ka) (Zhao et al., 2000 – ODP658; Sicre et al., 2001 – SU94-11k; Zarriess and Mackensen, 2010 - GeoB9526, 9527; Fig. 4.1). It was

suggested that this was due to a decrease in the Mauritanian upwelling area as a consequence of lower sea levels during the LGM (Martinez et al., 1999a). Furthermore, although the trade winds were stronger during LGM, reduced seasonality and stronger westward winds were likely decreasing the upwelling intensity (Martinez et al., 1999a). In contrast, other studies have concluded that the LGM was characterized by relatively high productivity in the eastern tropical Atlantic, due to increased dust input as well as increased upwelling (Sicre et al., 2000 – SU94-20b; Flores et al., 2000 – Camel-1; Freudenthal et al., 2002 – GeoB4223, 4228, 4240; Fig. 4.1). Most studies indicate that interglacial periods are intervals of relatively low productivity (Sicre et al., 2000 – SU94 – 20b; Freudenthal et al., 2002 – GeoB4223, 4228, 4240; Nave et al., 2003 – GeoB4240, 4241, 4242, Fig. 4.1). Weaker trade winds likely led to a decrease in the strength of the upwelling system and hence in primary productivity during interglacial periods in comparison to glacial times (Sicre et al., 2000; Freudenthal et al., 2002; Nave et al., 2003). However, a few studies have reported high productivity in some places along the NW African coast during parts of interglacials (Flores et al., 2000; Zhao et al., 2006; Crosta et al., 2012 – GeoB4905-4). Such increases in productivity could result from an increase in the upwelling area on the shelf or the occasional westward-blowing winter winds could have enhanced upwelling at latitudes below 20 °N of NW African coast (Bertrand et al., 1996). Alternatively, a more humid continental climate over Africa during interglacial periods (e.g. Drake et al., 2011) led to a stronger river discharge and nutrient input that could stimulate productivity at latitudes below 15 °N on the NW African margin (Zarries and Mackensen, 2010; Crosta et al., 2012). Finally, several studies indicate relatively high primary productivity values during Marine Isotope Stage (MIS) 3 as well as during deglaciations (Martinez et al., 1999a; Flores et al., 2000; Nave et al., 2003; Zhao et al., 2006; Romero et al., 2008 – GeoB7926). Dry continental climate conditions, stronger trade winds and increased upwelling were proposed to explain the high productivity off NW Africa during these time intervals.

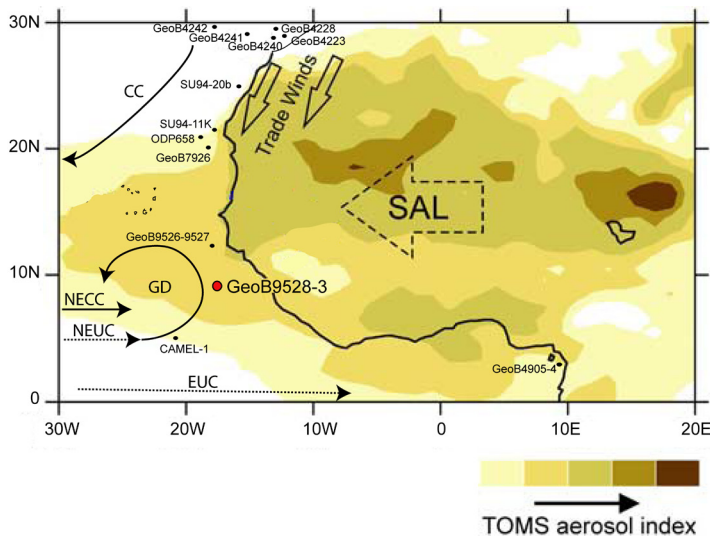


Fig. 4.1: Map of NW African coast showing the location of core GeoB9528-3 (red dot) and other sites discussed in this study, together with the Total Ozone Mapping Spectrometer (TOMS) averaged aerosol concentrations for the years 1997-2005 as an indicator for dust input. Arrows in the continent indicate principal wind direction of trade winds and Sahara Air Layer (SAL). Arrows in the ocean indicate surface currents (full lines) and subsurface currents (dashed lines). CC – Canary current, GD – Guinea dome, NECC – North equatorial counter current, NEUC – North equatorial under current, EUC – Equatorial under current. Figure adapted from Mulitza et al. (2008) and Schott et al. (2002a).

To better understand these regional differences in productivity along NW African margin, we constructed a productivity record from the eastern tropical North Atlantic, offshore NW Africa at 9 °N, for the past 192 ka. This region is rarely investigated and, to the best of our knowledge, no long-term productivity record exists so far (Fig. 4.1). At this site today, there is no large upwelling cell (Mittelstaedt, 1983; 1991; Bouimetarhan et al., 2009) and chlorophyll concentrations (Table 4.1 – Conkright et al., 2002) show no seasonal trend and relatively low values compared to the higher latitudes where upwelling exists, suggesting oligotrophic conditions. Because the site is located relatively far from the African coast, the impact of river discharge is also expected to be minor. Indeed, sediments at this site are characterized by low amounts of fluviially-transported terrestrial biomarkers, i.e. branched glycerol dialkyl glycerol tetraethers, throughout the last two glacial-interglacial cycles (Lopes dos Santos et al., 2010). Thus, neither upwelling nor riverine input are expected to strongly control primary productivity on glacial-interglacial time scales at the core location. However, the study site does receive a large amount of dust transported from the Sahara region (Fig. 4.1) and, as explained above, Sahara dust input to the eastern tropical north Atlantic likely stimulates primary productivity by supplying both Fe and P (Mills et al., 2004). Here, we present records of total organic carbon (TOC) and three different biomarker lipids as indicators for algal productivity. C_{37} alkenones were used as biomarkers for haptophyte algae (Volkman et al., 1980; Marlowe et al., 1984), while dinosterol and long-chain 1,15 *n*-alkyl diols are used as biomarkers for dinoflagellates (Boon et al., 1979; Volkman et al., 1998) and eustigmatophyte algae (yellow-green algae) (Volkman et al., 1992; Versteegh et al., 1997), respectively. In addition, we reconstructed the impact of iron fertilization through aeolian input by comparing our productivity records with proxies for Fe input (sedimentary Fe contents) and for continental humidity conditions over Africa (Fe/K and Al/Si ratios).

Table 4.1: Seasonal chlorophyll values [$\mu\text{g/l}$] at NW Africa coast at a longitude of 17 °W (from Conkright et al., 2002).

| Season | 25°N | 20°N | 9 °N |
|--------|------|------|------|
| Winter | 2.9 | 3.9 | 0.01 |
| Spring | 0.03 | 5.1 | 0.4 |
| Summer | 0.6 | 3.0 | 0.5 |
| Fall | 0.2 | 2.6 | 0.5 |

4.2 Material and methods

4.2.1 GeoB9528-3 core location and age model

Sediment core GeoB9528-3 was recovered during the Meteor-cruise M65/1 Dakar, in 2005 from the Guinea Plateau Margin at 9°9.96N, 17°39.81W (Fig. 4.1) and 3057 m water depth (Mulitza et al., 2006). The core was sampled at 2.5 cm intervals for foraminiferal isotope analyses (for construction of the age model) and at 5 cm intervals for biogeochemical analyses using 10 cc cut syringes. The age model is based on oxygen isotope stratigraphy of the benthic foraminifer *Cibicidoides wuellerstorfi* and has been previously published by Castañeda et al. (2009).

4.2.2 Total organic carbon

The percentage of TOC was determined using a Thermofinnigan Delta Plus isotope ratio mass spectrometer after high temperature combustion with a Carlo Erba Instruments Flash 1112 Elemental Analyser. Sediments for these analyses were acidified with 2 M HCl in silver capsules and dried overnight in a 60°C oven. The TOC contents were calibrated against the laboratory standards, benzoic acid ($C_{org} = 68.8\%$) and acetanilide ($C_{org} = 71.09\%$). AR of TOC was calculated using the formula $AR = LSR [cm\ ka^{-1}] \times DBD [g\ cm^{-3}] \times C [gOC\ gsed.^{-1}]$, where LSR = linear sedimentation rates derived from linear interpolation of tie points of the age model (Castañeda et al., 2009), DBD = dry bulk density and C = concentration of total organic carbon.

4.2.3 Extraction and fractionation

Sediments were freeze-dried, homogenized with a mortar and pestle and extracted using an Automated Solvent Extractor (ASE 200, DIONEX; 100°C and 7.6×10^6 Pa with a mixture of dichloromethane (DCM): methanol (MeOH) (9:1, v:v) to obtain a total lipid extract (TLE). Internal standards (squalane, nonadecanone) were added to the TLE and separated into an apolar, ketone and polar fraction using alumina column chromatography and solvent mixtures of 9:1 hexane:DCM, 1:1 hexane:DCM, and 1:1 DCM:MeOH, respectively. Squalane was subsequently added as internal standard to the polar fraction, which was then derivatized with bis-trimethylsilyltrifluoroacetamide (BSTFA) in pyridine. The ketone and polar fractions were analyzed by gas chromatography (GC) and gas chromatography/mass spectrometry (GC/MS).

4.2.3.1 GC analysis

The ketone fractions were analyzed by GC – Hewlett Packard 6890, on a 50 m, silica column with 0.32 mm of inner diameter and coated with CP Sil-5 (thickness=0.12µm). The carrier gas was helium. The oven was programmed from 70°C at injection, then increased by 20°C min⁻¹ to 200°C and next by 3°C min⁻¹ until 320°C. The final temperature of 320°C was held for 30 min. For quantification of alkenone concentrations, nonadecanone was used as internal standard.

The derivatized polar fractions were analyzed on a Hewlett Packard 6890 GC with a 25 m silica column, 0.32 mm of inner diameter and coated with CP Sil-5 (thickness=0.12 μ m). The carrier gas was helium. The oven was programmed from 70°C at injection, to 130°C at a rate of 18°C min⁻¹, followed by an increase of 3°C min⁻¹ until 320°C and holding this temperature for 10 min. Quantification of dinosterol and the C₃₀ 1,15-diol were performed by comparison of peak areas with that of the squalane internal standard. AR of the compounds was calculated as described for TOC.

4.2.3.2 GC/MS

Compound identification was conducted using a ThermoFinnigan Trace GC Ultra connected to ThermoFinnigan DSQ MS operated at 70 eV, with a mass range m/z 50-800 and 3 scans per second. The capillary column is the same as described for the GC analyses of the polar fractions. The temperature program initiated at 70°C, increased first at a rate of 20°C min⁻¹ to 130°C, and next at a rate of 4°C min⁻¹ to the final temperature of 320°C, which was held for 10 min.

4.2.4 Major element concentrations and ratios

The intensities of major elements were measured every 1 cm with the X-ray Fluorescence (XRF) Core Scanner II (AVAATECH Serial No. 2) of the MARUM - University of Bremen. Scanner data were collected over a 1.2 cm² area with a down-core slit size of 10 mm (generator settings of 10 kV, current of 0.30 mA, sampling time of 20 s). Raw data spectra were processed by the analysis of X-ray spectra by Iterative Least square software (WIN AXIL) package from Canberra Eurisys.

In addition, 87 freeze-dried, powdered and homogenized sediment samples (2-5 g of dry sediment), that were taken along the length of core Geob9528-3, were analysed for their major element concentrations by energy dispersive polarization X-ray Fluorescence (EDP-XRF) spectroscopy, using a SPECTRO XEPOS instrument (Wien et al., 2005). See Govin et al. (2012) for details on the method. Using a log-ratio regression approach (Weltje and Tjallingii, 2008), powdered measurements and scanner data were combined to derive high-resolution calibrated proportions of the elements Ca, Fe, Al, Si, Ti and K. The MATLAB routine developed by David Heslop (personal communication) was used with Ca as a common denominator of the log-ratio regressions (mean r² of 0.96).

In order to calculate Fe accumulation rates, high-resolution Fe concentrations were derived from calibrated proportions. Using a Monte-Carlo simulation (10,000 iterations), we performed a linear regression between the EDP-XRF Fe concentrations and scanner calibrated Fe proportions at the same depths (Fig. 4.2). The regression includes the 1s uncertainties on both Fe concentrations (3 % of the Fe value, estimated from replicate measurements) and Fe proportions (\pm 0.8 %, root mean square deviation between EDP-XRF Fe proportions and scanner Fe proportions). Fe AR was calculated as described for TOC.

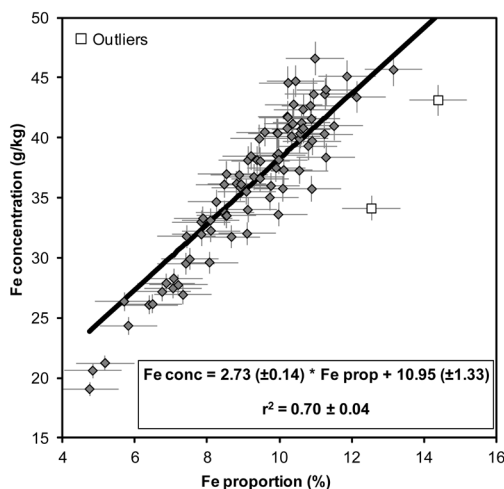


Fig. 4.2: Calibration of Fe concentrations in core GeoB9528-3. The regression (black line) is performed with a Monte-Carlo simulation (10,000 iterations) between the Fe concentrations (Y-axis) measured on powdered samples and the scanner calibrated Fe proportions (X-axis) for the same depths (grey diamonds). Two outliers (open square) were excluded from the regression. Error bars highlight 1 σ uncertainties on Fe concentrations and Fe calibrated proportions (see text).

4.3 Results

4.3.1 Sedimentation rates, TOC and algal biomarker concentrations and AR

The sedimentation rate in core GeoB9528-3 was 3.4 cm ka⁻¹ until ~83 ka, followed by an increase to ~7 cm ka⁻¹ for periods < 83 ka (Fig. 4.3g). The TOC content ranged from 0.3 to 1.6 % with the lowest values noted at ~ 124 and 10 ka during MIS 5.5 and 1 (Fig. 4.3a, b). The highest TOC content was recorded at ~ 48 ka during MIS 3. TOC AR had a similar pattern as TOC, except for the break at 83 ka due to the change in LSR, and ranged from 0.07 $\mu\text{g m}^{-2} \text{yr}^{-1}$ during MIS 5.5 to 0.9 $\mu\text{g m}^{-2} \text{yr}^{-1}$ during MIS 3 (Fig. 4.3b). Sediments in core GeoB9528-3 contain biomarkers of several different algal groups including diatoms, haptophyte algae, eustigmatophytes and dinoflagellates. Loliolide and isololiolide (anoxic degradation products of the fucoxanthin in diatoms - Repeta, 1989), were detected in ~30 samples with abundances that were too low to be accurately quantified. Concentrations of C₃₇ alkenones (C_{37:2} + C_{37:3}), which is a proxy for haptophyte algal productivity (Volkman et al., 1980), ranged from 0.08 during MIS 1 (~10 ka) and 5.5 (124 ka) to 3.4 $\mu\text{g g}^{-1}$ during MIS 6 at 187 ka (Fig. 4.3c). Alkenone AR ranged from 2 to 81 $\mu\text{g m}^{-2} \text{yr}^{-1}$ with the lowest values during MIS 1 and 5.5 and highest value at ~80 ka (Fig. 4.3c). The concentration record of dinosterol (a biomarker for dinoflagellates, Boon et al., 1979), was more variable than that of TOC and alkenones. The concentrations ranged from not detectable to 0.5 $\mu\text{g g}^{-1}$ (Fig. 4.3d). Dinosterol was not detected in sediments deposited in MIS 1 and MIS 5.5 and the highest concentration was recorded during MIS 6 at 169 ka. The dinosterol AR record has maxima of

13 $\mu\text{g m}^{-2} \text{yr}^{-1}$ during MIS 3 at ~ 38 ka, at ~ 64 ka during MIS 4 and at ~ 169 ka during MIS 6 (Fig. 4.3d). Long chain C_{30} and C_{32} *n*-alkyl 1,15-diols, biomarkers for eustigmatophyte algae (Volkman et al., 1992), were found in all sediments, but it was not possible to accurately quantify the C_{32} 1,15-diol due to co-elutions. Concentrations of the C_{30} 1,15-diol ranged from 0.03 $\mu\text{g g}^{-1}$ during MIS 1 (~ 10 ka) and MIS 5.5 (~ 124 ka) to 0.5 $\mu\text{g g}^{-1}$ during MIS 3 (~ 47 ka), 5 (~ 107 ka) and 6 (~ 188 ka) (Fig. 3e). C_{30} 1,15-diol AR ranged from a minimum of $\sim 0.6 \mu\text{g m}^{-2} \text{yr}^{-1}$ during MIS 1 and MIS 5.5 to a maximum of 30 $\mu\text{g m}^{-2} \text{yr}^{-1}$ during MIS 3. MIS 2 was also characterized by high C_{30} 1,15-diol AR (Fig. 4.3e).

4.3.2 Elemental composition

To produce a high resolution Fe concentration record we calibrated the Fe proportions from XRF measurements with measured Fe concentrations obtained from a selection of samples (see methods). The linear regression used for calibrating Fe concentrations has a mean r^2 of 0.7 ± 0.04 (Fig. 4.2). The sedimentary Fe concentrations range from 24 to 55 g kg^{-1} and had a minimum during the interglacials MIS 1 and 5.5 and a maximum during MIS 4 at 64 ka (Fig. 4.3f). Fe AR ranged from 0.6 $\text{g m}^{-2} \text{yr}^{-1}$ at MIS 5.5 to 2 $\text{g m}^{-2} \text{yr}^{-1}$ < 83 ka. The Fe/K ratio, a proxy for aridity (Mulitza et al., 2008), ranged from 2.4 during MIS 5 at 121 ka to a maximum of 7 during interglacials at 10 and 128 ka (Fig. 4.3h). The Al/Si, another proxy for aridity (Mulitza et al., 2008), ranged from 0.32 during MIS 5 at 126 ka to 0.58 during MIS 1 and some intervals of MIS 5 and 6 (Fig. 4.3h).

4.4 Discussion

4.4.1 Assumptions in primary productivity records

As discussed in the introduction, marine biomarker concentration and accumulation records are frequently used to reconstruct primary productivity (e.g. Schubert et al., 1998; Hinrichs et al., 1999; Zhao et al., 2006). However, it should be noted that the reliability of marine biomarkers to reconstruct productivity changes is limited by several uncertainties in particular the dilution by inorganic sediment and preservation effects. The dilution effect can be partially accounted using the AR of the compounds. The AR records of the biomarkers are generally quite similar to the absolute concentrations (Fig. 4.3) as the LSR only shows a major change at 83 ka, suggesting that dilution by inorganic material are only partially affecting the reconstructed productivity records. Variations in the degree of preservation of organic matter can also cause variations in biomarker concentrations independent of productivity changes. However, the core is located at 3 km depth where bottom water oxygen concentrations likely have not varied to a large degree, i.e. reaching suboxic levels, over glacial-interglacial times. Furthermore, sedimentation rates were relatively constant, except for a major break at 83 ka, and thus sedimentary oxygen exposure time likely has not varied substantially. Indeed, a higher sedimentation rate is observed for sediments < 83 ka, but concentrations are not elevated compared to sediments older than 83 ka (Fig. 4.3). Thus, we assume that preservation did not play a major role in our organic biomarker records. Finally,

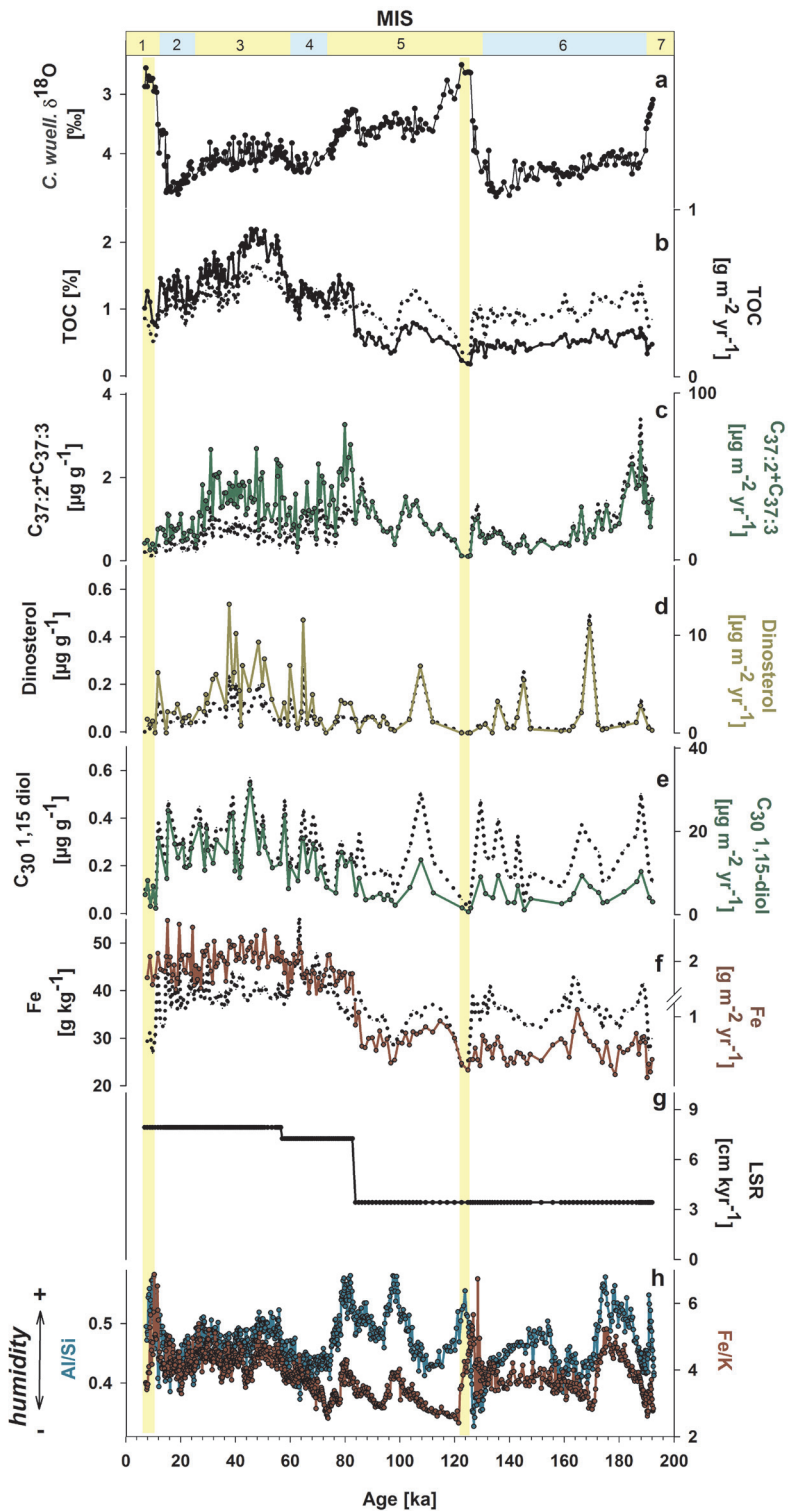


Fig. 4.3: Geochemical records of core GeoB9528-3. a) Oxygen isotope of benthic foraminifer *Cibicidoides wuellerstorfi* (Castañeda et al., 2009), b) TOC percentage (dashed line) and TOC AR (black plain line), c) alkenones concentration (dashed line) and alkenones AR (green plain line), d) dinosterol concentration (dashed line) and dinosterol AR (yellow plain line), e) C_{30} 1,15-diol concentration (dashed line) and C_{30} 1,15-diol AR (green plain line), f) Iron concentration (dashed line) and Fe AR (red plain line), g) linear sedimentation rates, h) Al/Si and Fe/K ratios. MIS = Marine Isotope Stages. Yellow bars highlight interglacial periods.

the TOC record can also be biased by terrestrial input. However, our core site is quite far from the coast (> 300 km) and the input of soil derived branched tetraethers is low (Lopes dos Santos et al., 2010) so organic matter input from the continental area is not expected to strongly contribute to the TOC and is mostly reflecting marine OC. Thus, based on the above discussion we assume that variations in AR of the biomarkers and TOC are reasonably reflecting past productivity changes.

4.4.2 Glacial-interglacial primary productivity changes

The TOC and the three different biomarker AR records (Fig. 4.3) show broad similarities compared to each other, i.e. low AR during MIS 1 and 5.5 and relatively higher values during glacials (MIS 2, 4 and 6), MIS 3 and 5.4. Direct correlation of these records shows that concentrations as well as AR of all biomarkers correlate significantly with TOC ($p < 0.01$; Table 4.2). This correlation may be because general productivity, reflected in TOC, varied in a similar fashion as that of haptophyte, dinoflagellate and eustigmatophyte productivity for the last 192 ka. However, some differences are observed between the different algal groups. For example, haptophyte productivity has a maximum at around 80 and 187 ka whereas dinoflagellate and eustigmatophyte productivity records (Fig. 4.3c, d, e) do not show a strong increase in productivity. Similar to our observations, sometimes opposite trends between alkenones, dinosterol and C_{30-32} 1, 15 diols concentrations and AR were also noted off NW Africa by Zhao et al. (2006) on a glacial-interglacial time-scales. For instance, they observed maximum alkenone concentrations and AR at ~87 and 160 ka, periods where no strong increase in diols and dinosterol were reported. This pattern may suggest some successions between the different algal groups, possibly due to nutrient competition, where haptophytes possibly compete with the other two algal groups.

Our primary productivity records show clear minima during interglacial periods (Fig. 4.3). This is in agreement with records from latitudes above 20°N (Sicre et al., 2000; Freudenthal et al., 2002; Nave et al., 2003), where weaker trade winds led to a decrease in the strength of the upwelling system. Additionally, elevated productivity levels during glacials and MIS 3 recorded at our core site are also in agreement with previous studies along the coast of NW Africa above 20°N (Sicre et al., 2000; Freudenthal et al., 2002; Nave et al., 2003; Zhao et al., 2006). Indeed, low productivity during interglacials and high productivity periods during glacials, MIS 3 and 5.4 were also noted in the oligotrophic area of the Sierra Leone Rise (Flores et al., 2000). The high productivity periods were explained as a consequence of a

shallower nutricline due to an intensification of the equatorial Atlantic divergence (Flores et al., 2000). However, as these periods were characterized by stronger winds (Flores et al., 2000) other factors such as Fe fertilization by dust input, may have played a role as well.

4.4.3 Sahara dust fertilization effect in primary productivity

To evaluate the role of the Saharan dust input we constructed a Fe concentration and AR record for our core since Sahara dust is the main source of this element to the eastern tropical North Atlantic (Gao et al., 2001). In general, the Fe concentration and AR record show broadly similar trends to the TOC and biomarker concentrations and AR, with local minima during MIS 5.5 (Fig. 4.3). Indeed, Fe AR showed a significant correlation ($p < 0.01$) with TOC and the biomarkers AR (Table 4.2b). The good correlations could be the result of the large break in MAR at ~83 ka which affect all AR records. However, a significant correlation between TOC and Fe concentrations also exists (Table 4.2a), suggesting a real link between organic matter accumulation and Fe. The good correlation between Fe and productivity proxies indicate that Fe stimulated productivity, possibly by inducing nitrogen fixation leading to an enhanced supply of bioavailable nitrogen (Falkowski, 1997). It should be noted that phosphorous has also been proposed to be the element in the Sahara dust that stimulate the nitrogen fixation (Sanudo-Wilhelmy et al., 2001). However, Mills et al. (2004) showed that nitrogen fixation in eastern tropical North Atlantic is co-limited by these two elements. As only a small part of the Fe in the dust can be used by phytoplankton (Wu et al., 2001), the bioavailable Fe is rapidly used what makes Fe a limiting nutrient for phytoplankton grow at these area. The correlations observed here provide evidence that iron fertilization may have played a role in past productivity changes. However, an alternative explanation for the significant correlation between Fe and TOC in marine sediments is the recent idea that Fe promotes OC preservation (Lalonde et al., 2012). It was suggested that reactive Fe phases (defined as the solid iron phases that are reductively dissolved by sodium dithionite) promote the preservation of organic matter by inhibiting microbial degradation due to the strong association between the Fe and the OC (Lalonde et al., 2012). Unfortunately, this hypothesis cannot be assessed using our data.

The higher Fe concentrations, and thus of Sahara dust, could have been caused by increasing wind strength during arid periods. To assess the continental aridity for these periods, Fe/K and Al/Si ratios were used because it has been shown that they are efficient proxies for continental aridity off NW Africa (Mulitza et al., 2008). During the interglacials, minimum productivity coincides with the lowest values of Fe concentrations (Fig. 4.3f) and high Fe/K and Al/Si ratios suggesting more humid conditions (Fig. 4.3h). Therefore, our results suggest that during warm and wetter periods, less dust from the Sahara is transported to the core site, thereby limiting productivity. Vice versa, periods of higher productivity, such as glacial and MIS 3 and 5.4, coincide with periods of higher Fe concentration during more arid periods. Thus, Sahara dust may have been transported during arid periods to the eastern tropical Atlantic, stimulating productivity.

Table 4.2: Pearson correlation between the concentrations (a) and mass accumulation rates (b) of the biomarkers, organic carbon and Fe. ^a correlation coefficient, ^b P value and ^c number of data points.

| (a) | Alkenone [$\mu\text{g/g}$] | Dinosterol [$\mu\text{g/g}$] | C30 1,15-diol [$\mu\text{g/g}$] | Fe [g/kg] |
|-----------------------------------|------------------------------|--------------------------------|-----------------------------------|----------------------|
| OC [g/g] | 0.26 ^a | 0.31 | 0.58 | 0.51 |
| | <0.001 ^b | <0.001 | <0.001 | <0.001 |
| | 193 ^c | 89 | 89 | 192 |
| Alkenone [$\mu\text{g/g}$] | | 0.18 | 0.33 | 0.000618 |
| | | 0.09 | <0.001 | 0.99 |
| | | 89 | 89 | 192 |
| Dinosterol [$\mu\text{g/g}$] | | | 0.39 | 0.17 |
| | | | <0.001 | 0.11 |
| | | | 89 | 88 |
| C30 1,15-diol [$\mu\text{g/g}$] | | | | 0.54 |
| | | | | <0.001 |
| | | | | 88 |

| (b) | Alkenone AR | Dinosterol AR | C30 1,15-diol AR | Fe AR |
|------------------|---------------------|---------------|------------------|--------|
| TOC AR | 0.49 ^a | 0.51 | 0.77 | 0.89 |
| | <0.001 ^b | <0.001 | <0.001 | <0.001 |
| | 192 ^c | 88 | 89 | 191 |
| Alkenone AR | | 0.37 | 0.48 | 0.35 |
| | | <0.001 | <0.001 | <0.001 |
| | | 88 | 89 | 192 |
| Dinosterol AR | | | 0.54 | 0.40 |
| | | | <0.001 | <0.001 |
| | | | 88 | 88 |
| C30 1,15-diol AR | | | | 0.74 |
| | | | | <0.001 |
| | | | | 88 |

Although our results suggest Fe fertilization may be an important controller of the productivity at the Guinea Plateau Margin, it should be noted that other factors may also control productivity at this latitude. For example, the nutrient concentration of the thermocline waters can change as it can be sourced from either the North Atlantic (low nutrient) during glacials or the South Atlantic (high nutrient) source during interglacials, thereby having an impact on primary productivity (Francois et al., 1990). However, all the biomarker AR records show relatively low productivity during interglacials contradicting the expected effect of nutrient diffusion from the thermocline. Another possible factor is nutrient variations by changes in the ocean current dynamics, as this area is strongly affected by different currents (Mulitza et al., 2006 – Fig. 4.1). Indeed, Flores et al. (2000) suggested that an intensification of the north equatorial current and equatorial divergence induced a shallowing of the nutricline and

increased productivity during the MIS 6, 5.2, 5.4, 4 and 2. However, at the moment we cannot evaluate this hypothesis for our core site.

4.5 Conclusions

Our late Quaternary biomarker records for specific algal groups (haptophytes, dinoflagellates and eustigmatophytes) in the eastern tropical Atlantic show similar patterns for the last 192 ka, suggesting that similar factors controlled their productivity. Sometimes, the productivity response between the algal groups differs, possibly due to competition effects. From the significant correlation of the biomarker AR with that of Fe AR, we suggest that Fe fertilization by Saharan dust is a factor controlling primary productivity at the Guinea Plateau margin especially during arid periods when reorganizations in the thermohaline circulation led to stronger winds and higher input of Saharan dust to the study site.

Acknowledgements

We thank Marianne Baas, Jort Ossebaar and Michiel Kienhuis for analytical assistance with the organic geochemical analyses. Research funding was provided by NEBROC-2 and a VICI grant to SS from the Netherlands Organization of Scientific Research (NWO). ES and SM have been funded through the DFG-Research Center/Excellence Cluster “The Ocean in the Earth System”. We thank the XRF Core Scanner Lab at the MARUM – Center for Marine Environmental Sciences, University of Bremen, Germany.

Chapter 5

Late Quaternary productivity changes from offshore Southeastern Australia: a biomarker approach

Raquel A. Lopes dos Santos, Daniel Wilkins, Patrick De Deckker and Stefan Schouten
Published in *Pal3* 363-364 (2012) 48-56

Abstract

Reconstructions of primary productivity at low latitudes have been the focus of several studies to better understand how the export of nutrient-rich, intermediate Southern Ocean (SO) waters influences productivity at these latitudes. This was triggered by the general observation of minima in the planktonic foraminiferal $\delta^{13}\text{C}$ values during deglaciations, which was interpreted as an isotopic signal of intermediate SO waters, together with a concomitant increase in diatom productivity at some equatorial sites. However, the impact of these SO waters on productivity at higher latitudes are not well constrained. Here, we compare a high-resolution planktonic foraminiferal $\delta^{13}\text{C}$ record with total organic carbon and biomarker records for *Proboscia* diatoms and haptophytes in marine sediments from offshore Southeastern Australia. The planktonic foraminiferal $\delta^{13}\text{C}$ record shows distinct minima during deglaciations and the Marine Isotope Stage 4/3 transition, tentatively suggesting that ^{13}C -depleted SO waters reached the coast of Southeastern Australia. However, it did not result in increased productivity during these periods. Instead, the highest primary productivity period, as indicated by total organic carbon and alkenone accumulation rates, occurred during the Last Glacial Maximum while *Proboscia* diatoms mainly proliferated during interglacials and Marine Isotope Stage 3 matching periods of increased diatom productivity in some sites of the Eastern Equatorial Pacific. Our study suggests that increased primary productivity offshore Southeastern Australia was mainly due to stronger westerly winds during glacial periods while *Proboscia* diatom productivity was probably controlled by the transport of silicic acid to this area.

5.1 Introduction

Understanding the long-term oceanographic controls on primary productivity in lower latitudes of the southern hemisphere has been the aim of numerous studies. In particular, studies have focused on understanding the role of Sub-Antarctic Mode Water (SAMW) and Antarctic Intermediate Water (AAIW) in controlling productivity at lower latitudes (Toggweiler et al., 1991; Brzezinski et al., 2002; Matsumoto et al., 2002; Sarmiento et al., 2004; Crosta et al., 2007; Calvo et al., 2011). This was triggered by the general observation of minima in planktonic foraminiferal $\delta^{13}\text{C}$ values during deglaciations, which is commonly interpreted as an isotopic signal of ^{13}C -depleted, CO_2 -rich, deep Southern Ocean (SO) waters transported through intermediate water masses such as the SAMW and AAIW (Spero and Lea, 2002; Pena et al., 2008; Calvo et al., 2011; Hayes et al., 2011; Horn et al., 2011). These periods of isotopic minima are contemporaneous with elevated diatom productivity in the Equatorial Pacific (Calvo et al., 2011; Hayes et al., 2011), suggesting that the influx of nutrients, in particular silicic acid, by intermediate waters stimulated diatom productivity at the lower latitudes. However, the impact of these nutrient-rich intermediate waters at higher latitudes is less well constrained.

In the southern hemisphere, most palaeoproductivity studies are focused on equatorial, Antarctic or upwelling regions (Romero et al., 2003; Willmott et al., 2010; Calvo et al., 2011) but few exist from offshore Southeastern Australia (Gingele and De Deckker, 2005). However, offshore Southeastern Australia, and more specifically, the Murray Canyons area probably receives intermediate waters from the SO that originate from the Sub-Antarctic and Antarctic region as discussed by Passlow et al. (1997) from offshore Victoria (37°S, 137°E) to the east of the canyons area, suggesting that this area may be useful to evaluate the impact of SO waters on past productivity. A reconstruction of late Quaternary fluctuation in primary productivity in the Murray Canyons area was previously done by Gingele and De Deckker (2005), relying mainly on sediment records of carbonate content, total organic carbon (TOC) and the stable isotopic composition of planktonic foraminifera. These authors found that increased productivity, inferred from elevated TOC contents, occurred during periods of insolation minima. Gingele and De Deckker (2005) also reported the absence of biogenic silica in sediments, possibly due to dissolution, and therefore could not reconstruct past diatom productivity. Additionally, their $\delta^{13}\text{C}$ and TOC records were in relatively low resolution for some time periods, making recognition of, for example, minima in $\delta^{13}\text{C}$ of planktonic foraminifera difficult.

In the present study, we re-examined the Murray Canyons core MD03-2607 studied by Gingele and De Deckker (2005) and substantially increased the resolution of TOC, $\delta^{13}\text{C}$ and $\delta^{18}\text{O}$ of planktonic foraminifera records. In addition, we used organic biomarker records for haptophyte algae (alkenones) and relative abundance of *Proboscia* diatoms (Diol index, Rampen et al., 2008) to reconstruct past productivity. Alkenones are established biomarkers to measure past haptophyte algae abundance (e.g. Volkman et al., 1980). The Diol index is the ratio of long chain 1,14 diols produced by *Proboscia* diatoms (Sinninghe Damsté et al.,

2003), relative to long chain 1,15 diols (or 1,13 diols) that are produced by eustigmatophytes (Volkman et al., 1992). *Proboscia* diatoms grow in the early stages of upwelling when nutrient concentrations strongly increase (Koning et al., 2001; Smith, 2001). The Diol index has been used to reconstruct variations in past *Proboscia* diatom productivity in the Arabian Sea and in the SO and related to changing nutrient conditions (Rampen et al., 2008; Willmott et al., 2010). We compare our productivity records with the stable carbon isotopic signal in planktonic foraminifera to identify the timing of the advection of water masses from the SO into the Southeastern Australia region and its influence on (past) productivity levels.

5.2 Core location and regional setting

Piston core MD03-2607 ($36^{\circ}57.64' S$; $137^{\circ}24.39' E$) was acquired in the Murray Canyons area at 865 m water depth, east of Sprigg Canyon (Fig. 5.1). This sediment core was retrieved from a gently sloping plateau, which is separated from the main shelf break by the upper Sprigg Canyon to avoid any significant erosion or deposition of turbidites (Hill and De Deckker, 2004; Gingele and De Deckker, 2005).

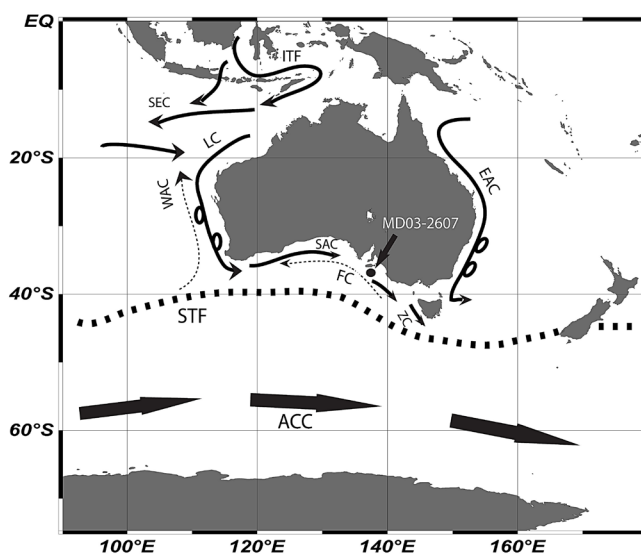


Fig. 5.1: Location of core MD03-2607 offshore Southeastern Australia (black dot) together with the modern position of the subtropical front (STF — dashed line) and the main currents around Australia (arrows). ITF — Indonesian Troughflow, LC — Leeuwin Current, SAC — South Australia Current, FC — Flinders Undercurrent (dotted arrow means subsurface current), ZC — Zeehan Current, WAC — West Australia Current (dotted arrow means subsurface current), EAC — East Australia Current, SEC — South Equatorial Current, ACC — Antarctic Circumpolar Current. Map was generated with the Ocean Data View software.

The Murray Canyons Group is a vast system of deep-sea canyons located offshore

southern Australia that descend to ~5000 m water depth (Hill and De Deckker, 2004) and is influenced by several deep, intermediate and surface water masses. The Circumpolar Deep Water (CPDW), a water mass derived from the Antarctic Circumpolar Current, is the main deep current in the area and is divided into lower CPDW and upper CPDW. Together, the CPDW flows from ~4000 to 1100 m depth (Passlow et al., 1997). Two intermediate water masses were identified around this area: the Antarctic Intermediate Water (AAIW) flowing around 1100–850 m depth and the Sub-Antarctic Mode Water (SAMW) flowing around 850–450 m depth (Passlow et al., 1997). Apart from these water masses, two coastal currents with opposite direction occur in the area: the Leeuwin Current (LC) and its extension (the South Australia Current — SAC), flowing eastward and the Flinders Undercurrent (FC) that flows westward. The LC is a warm surface current that flows southward along the coast of Western Australia, then turns eastward and continues towards the Great Australian Bight. It is strongest in winter, when eastward local winds prevail, but during summer this current weakens and the SAC enhances in the western Great Australian Bight (Middleton and Bye, 2007). The LC is particularly prominent offshore southern Australia during La Niña years (De Deckker et al., 2012). The FC originates from SO waters and has its maximum amplitude at around 600 m depth. It is stronger in summer when the LC is weaker and, together with favourable winds, it can induce weak to moderate coastal upwelling (Middleton and Bye, 2007). This is particularly evident east of the Murray Canyons area along the Bonney coast.

5.3 Methods

5.3.1 Chronology and stable isotopic composition of foraminifera

The age model of the upper part of the core was derived from 13 Optically Stimulated Luminescence (OSL) (Table 5.1) and 22 Accelerator Mass Spectrometry (AMS) radiocarbon (^{14}C) dates (Table 5.2) measured from the upper 430 cm (~35 ka) of core MD03-2607 (Wilkins, 2009). Following the procedures described in Wilkins et al. (2012), OSL dates were measured on single grains or very small aliquots of sand-sized quartz (63–90 μm) loaded into discs containing a 10×10 array of 300 μm wells using the modified single-aliquot regenerative dose (SAR) protocol of Olley et al. (2004). Lithogenic radionuclide activities were measured by high resolution gamma spectrometry on 7 bulk sediment samples, with 4 of these samples also measured by alpha spectrometry. Dose rates were calculated using the equations of Stokes et al. (2003), iteratively adjusting for the small excess of ^{230}Th and ^{231}Pa until the sample age was stable.

AMS ^{14}C dates were measured on planktonic foraminifera (mixed *Globigerina bulloides* and *Globigerinoides ruber*) from 19 sample depths (Table 5.2). Results are presented as calibrated ages corrected for the regional marine reservoir using the Marine04 dataset in Calib 5.0.1 (ages <26.0 ka) or the polynomial of Bard (1998) for ages >26.0 ka (Stuiver and Reimer, 1993; Bard, 1998; Reimer and Reimer, 2001; Hughen et al., 2004). Benthic foraminifera (mixed *Cibicidoides mundulus* and *Cibicidoides wuellerstorfi*) were also dated

from sediment at 175 cm depth. An additional planktonic sample from the top of a nearby multi-core (MC03) was dated at the AMS facility at the Australian Nuclear Science and Technology Organization to obtain a ¹⁴C age from the modern sediment water interface (Fink et al., 2004).

Table 5.1: Average water content, supported and unsupported dry dose rate, environmental dose rate, equivalent dose (D_e) and age for OSL samples from selected horizons in core MD03-2607.

| Sample depth (cm) | Measured water content (%) | Modeled water content (%) | Supported dry dose rate (mGy/ka) | Unsupported dry dose rate (mGy/ka) | Environmental dose rate (Gy/ka) | Equivalent dose ^a (Gy) | Sample age (ka) |
|----------------------------|----------------------------|---------------------------|----------------------------------|------------------------------------|---------------------------------|-----------------------------------|-----------------|
| 0 - 1 | 51 | 64 ± 5 | 58.8 ± 12 | 4.1 ± 0.3 | 0.34 ± 0.03 | 0.39 ± 0.04 | 1.07 ± 0.16 |
| 24.5 - 25.5 | 52 | 60 ± 5 | 63.5 ± 12 | 4.7 ± 0.3 | 0.37 ± 0.03 | 0.91 ± 0.13 | 2.38 ± 0.41 |
| 32.5 - 33.5 | 51 | 58 ± 5 | 66.4 ± 16 | 5.5 ± 0.3 | 0.40 ± 0.03 | 1.25 ± 0.24 | 3.11 ± 0.67 |
| 49.5 - 50.5 | 49 | 59 ± 5 | 74.0 ± 17 | 6.3 ± 0.4 | 0.44 ± 0.04 | 1.74 ± 0.22 | 3.94 ± 0.61 |
| 63.5 - 64.5 ^b | 48 | 56 ± 5 | 76.1 ± 15 | 9.1 ± 0.5 | 0.46 ± 0.04 | 14.92 ± 0.35 | 24.06 ± 2.16 |
| 74.5 - 75.5 | 47 | 54 ± 5 | 77.3 ± 11 | 10.0 ± 0.5 | 0.47 ± 0.04 | 2.55 ± 0.19 | 5.37 ± 0.61 |
| 99.5 - 101.5 | 44 | 49 ± 5 | 93.6 ± 27 | 22.8 ± 1.0 | 0.60 ± 0.05 | 5.98 ± 0.81 | 9.98 ± 1.61 |
| 124.5 - 125.5 | 45 | 50 ± 5 | 109 ± 25 | 25.8 ± 1.2 | 0.69 ± 0.06 | 7.83 ± 0.43 | 11.35 ± 1.11 |
| 149.5 - 150.5 | 49 | 54 ± 5 | 124 ± 29 | 34.3 ± 1.5 | 0.76 ± 0.06 | 11.86 ± 0.34 | 15.52 ± 1.30 |
| 174.5 - 175.5 ^c | 72 | 75 ± 5 | 197 ± 43 | 44.3 ± 1.9 | 1.05 ± 0.08 | 13.39 ± 1.72 | 12.75 ± 1.89 |
| 199.5 - 200.5 | 75 | 79 ± 5 | 272 ± 31 | 44.6 ± 1.9 | 1.40 ± 0.09 | 24.75 ± 0.94 | 17.60 ± 1.36 |
| 239.5 - 240.5 | 74 | 76 ± 5 | 291 ± 31 | 53.0 ± 2.3 | 1.54 ± 0.10 | 30.51 ± 0.79 | 19.72 ± 1.39 |
| 279.5 - 280.5 | 62 | 66 ± 5 | 271 ± 28 | 58.1 ± 2.5 | 1.53 ± 0.10 | 29.98 ± 3.19 | 19.58 ± 2.48 |

^a The D_e error term incorporates curve fitting errors and an additional 2.5% systematic measurement error.

^b Suspected turbidite.

^c Confirmed turbidite.

Table 5.2: Calibrated radiocarbon results from core MD03-2607 and multi-core MC03.

| Sample depth and dated material | Sample Code | pMC ^a | $\delta^{13}\text{C} \text{‰}$ ^b | Conventional age(¹⁴ C yr BP) | Calibrated date ^c ($\Delta\text{R } 461 \pm 29$) ^c ($\Delta\text{R } 1,060 \pm 70$) ^d |
|----------------------------------|-------------|------------------|---|--|--|
| MC-03 0.5 cm <i>G. bulloides</i> | OZH 736 | 83.37 ± 0.71 | -1.2 ± 0.2 | 1,460 ± 705 | (modern) ^d |
| 0.5 cm planktonic ^f | ANUA 29624 | 73.10 ± 1.73 | -0.5 ± 0.2 | 2,600 ± 190 | 1,090 ± 200 ^d |
| 25 cm <i>G. bulloides</i> | ANUA 29003 | 61.38 ± 1.37 | 0.0 ± 0.2 | 4,010 ± 180 | 2,690 ± 250 ^d |
| 40 cm planktonic | ANUA 29625 | 61.12 ± 1.42 | 0.2 ± 0.2 | 4,045 ± 185 | 2,740 ± 260 ^d |
| 50 cm planktonic | ANUA 29004 | 53.19 ± 1.20 | -0.5 ± 0.2 | 5,155 ± 180 | 4,140 ± 260 ^d |
| 75 cm planktonic | ANUA 29626 | 41.48 ± 1.01 | -0.1 ± 0.2 | 7,155 ± 195 | 6,530 ± 230 ^d |
| 85 cm planktonic | ANUA 29627 | 39.23 ± 0.96 | -0.3 ± 0.2 | 7,600 ± 195 | 7,040 ± 230 ^d |
| 95 cm planktonic | ANUA 29630 | 30.13 ± 0.83 | -0.3 ± 0.2 | 9,720 ± 220 | 9,280 ± 280 ^d |
| 100 cm planktonic | ANUA 29631 | 28.41 ± 0.76 | -0.4 ± 0.2 | 10,190 ± 215 | 9,880 ± 280 ^d |
| 140 cm planktonic | ANUA 31203 | 20.71 ± 0.53 | -1.1 ± 0.2 | 12,730 ± 205 | 14,260 ± 345 ^e |
| 150 cm planktonic | ANUA 29005 | 18.53 ± 0.51 | -0.7 ± 0.2 | 13,620 ± 220 | 15,560 ± 335 ^e |
| 165 cm planktonic | ANUA 29628 | 15.54 ± 0.45 | -0.7 ± 0.2 | 15,040 ± 235 | 17,570 ± 425 ^e |
| 175 cm planktonic | ANUA 29006 | 12.47 ± 0.38 | 0.0 ± 0.2 | 16,810 ± 240 | 19,550 ± 255 ^e |
| 175 cm planktonic | ANUA 30504 | 10.44 ± 0.30 | 0.0 ± 0.2 | 18,240 ± 230 | 20,470 ± 265 ^e |
| 175 cm benthic | ANUA 30503 | 11.02 ± 0.29 | 0.0 ± 0.2 | 17,800 ± 210 | 20,980 ± 345 ^e |
| 200 cm planktonic | ANUA 29007 | 14.07 ± 0.40 | 0.3 ± 0.2 | 15,840 ± 225 | 18,730 ± 210 ^e |
| 240 cm planktonic | ANUA 29008 | 11.43 ± 0.34 | 0.4 ± 0.2 | 17,510 ± 240 | 20,030 ± 115 ^e |
| 260 cm planktonic | ANUA 29629 | 10.74 ± 0.33 | -0.4 ± 0.2 | 18,010 ± 245 | 20,710 ± 320 ^e |
| 280 cm planktonic | ANUA 29009 | 9.95 ± 0.32 | 0.0 ± 0.2 | 18,630 ± 260 | 21,630 ± 390 ^e |
| 300 cm planktonic | ANUA 31204 | 9.34 ± 0.25 | 0.4 ± 0.2 | 19,130 ± 215 | 22,240 ± 225 ^e |
| 360 cm planktonic | ANUA 31205 | 7.02 ± 0.33 | 0.2 ± 0.2 | 21,420 ± 380 | 25,140 ± 490 ^e |
| 430 cm planktonic | ANUA 29010 | 2.17 ± 0.14 | 0.0 ± 0.2 | 30,850 ± 500 | 35,910 ± 500 ^e |

^a Percent Modern Carbon (pMC) has been corrected for machine background and carbonate preparation background. ^b $\delta^{13}\text{C}$ corrections are from material measured by Gingele et al. (2004). ^c All radiocarbon ages were calibrated in Calib 5.0.1 (Stuiver and Reimer, 1993), assuming a sample age-span of 100 years, and applying the Marine04 dataset of Hughen et al. (2004) for ages <26.0 ka, and the polynomial of Bard (1998) for ages >26.0 ka. ^d Dates corrected with the core-top reservoir age from MC03 (equivalent to a ΔR of 1060 ± 70 years) prior to calibration. ^e A regionally corrected marine reservoir of 461 ± 29 yr has been subtracted from the corrected radiocarbon age prior to calibration. ^f Planktonic samples consisted primarily of *G. bulloides* supplemented with *G. ruber*. The benthic sample was composed of *Cibicides mundulus* and *C. wuellerstorfi*.

Samples were dissolved in an evacuated glass reaction chamber with supersaturated (105% v/v) phosphoric acid, the resultant gas was cryogenically purified, with CO₂ transferred to glass vessels along with ultra-high-purity H₂ and graphitized overnight at 550 °C with 3–6 mg of iron powder catalyst (Vogel, 1984). The resulting graphite was pressed into a 1 mm central hole in aluminum sample holders and plugged from behind with a short length of aluminum wire as reported by Fifield et al. (1994). The percentage of modern carbon (pMC) of each of the graphite targets was measured with the 14UD Pelletron Tandem Accelerator of the Department of Nuclear Physics at the ANU (Fifield et al., 1994). Uncertainties in pMC values are reported with an additional 2% error added in quadrature to the uncertainty due to counting statistics in order to account for accelerator reproducibility.

The age model of the lower part of the core was based on oxygen isotope stratigraphy of *G. bulloides* tuned to a stacked benthic foraminifer record (Lisiecki and Raymo, 2005).

Although the oxygen isotopic stratigraphy of benthic foraminifera is preferred for tuning the age model, as temperature variations are minimal, there were insufficient benthic foraminifera present throughout the core to obtain a continuous record. Previous stable isotope analyses on foraminifera were published in Gingele et al. (2004); however, additional analyses were required in order to improve the age resolutions and the $\delta^{13}\text{C}$ record, especially for Marine Isotope Stages (MIS) 5 and 6. The sediment core was therefore sampled at 5 cm intervals for foraminiferal tests for the first 200 cm and at ~ 10 cm interval for the remainder of the core. A minimum of 10 calcite tests, previously cleaned, were softly crushed to open their chambers and to homogenize the material. Samples weighing from 40 to 60 μg were analyzed on a Thermo Finnigan MAT253 with Kiel IV device with a precision of $<0.1\%$ against the NBS19 standard. All samples were analyzed in duplicate with a maximum value of standard deviation of $\sim 0.4\%$. Comparison of the oxygen isotope record of *G. bulloides*, i.e. the combined data from Gingele et al. (2004) and those generated here, with the stacked record of Lisiecki and Raymo (2005) and a benthic foraminifera record from a core east of New Zealand (Elderfield et al., 2010) show a number of similar features which were used as tie points for the age model (Fig. 5.2). The age model was used to calculate sedimentation rates.

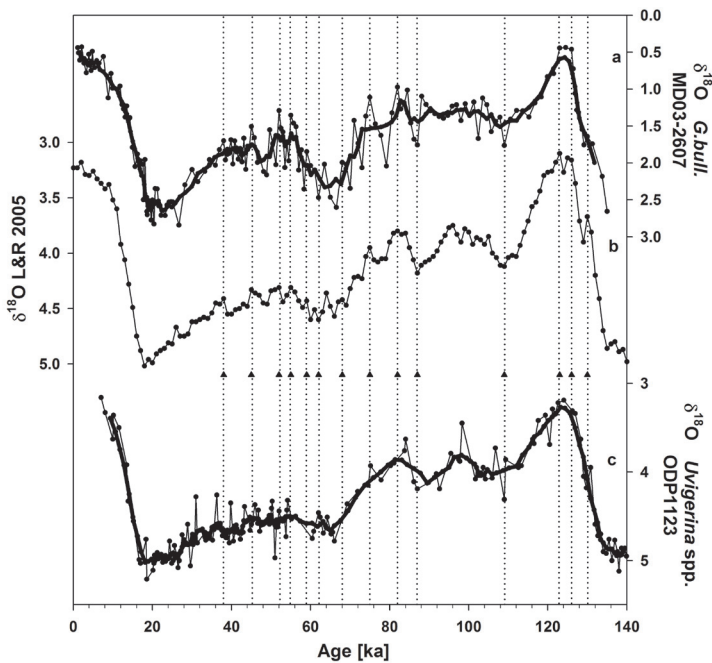


Fig. 5.2: Comparison of the age model stratigraphy of core MD03-2607. a) $\delta^{18}\text{O}$ of *Globigerina bulloides* of core MD03-2607 located offshore Southeastern Australia. b) Global stack of benthic foraminifera (Lisiecki and Raymo, 2005). c) $\delta^{18}\text{O}$ of benthic foraminifera *Uvigerina* spp. from core ODP1123 (Elderfield et al., 2010), east of New Zealand. The thicker line represents smoothed line of 5 points mean; triangles and dotted vertical lines represent tie points used to tune $\delta^{18}\text{O}$ record of core MD03-2607 to that of Lisiecki and Raymo (2005).

5.3.2 Total organic carbon measurements

Samples for TOC measurements were taken approximately every 10 cm through most of the core. The sediments were acidified with 2 M HCl overnight to remove carbonate, neutralized using distilled water and freeze dried. TOC was determined using a Flash 2000 organic elemental analyzer with a thermal conductivity detector. Mass accumulation rates of TOC was estimated based on sedimentation rates and assuming a dry bulk density of 0.8 [g/cm³] and a sediment porosity of 0.72. The dry bulk density value is based on a previous study with multicores from the area (Schmidt et al., 2010) and is assumed not to vary substantially over the depth of the core (~15 m).

5.3.3 Biomarker analyses

Sediment core MD03-2607 was sampled at 5 cm intervals for the first 300 cm and 10 cm for the rest of the core for biomarker analyses. Sediment samples were freeze-dried, homogenized and extracted using an Automated Solvent Extractor (ASE) 200, DIONEX; 100 °C and 7.6×10⁶ Pa with a mixture of dichloromethane (DCM):methanol (MeOH) (9:1, v:v) to obtain a total lipid extract (TLE). Internal standards (squalane, nonadeca-1-one, C₄₆ Glycerol Dialkyl Glycerol Tetraether — GDGT) were added to the TLE and subsequently each TLE was separated into an apolar, ketone and polar fraction. The ketone fractions were analyzed by gas chromatography (GC) and gas chromatography/mass spectrometry (GC/MS) and the polar fractions were analyzed by GC/MS.

5.3.3.1 Gas Chromatography analyses

The ketone fractions were analyzed by a Hewlett Packard 6890 GC, fitted with a 50 m, silica column with 0.32 mm of diameter and coated with CP Sil-5 (thickness=0.12 μm). The carrier gas was helium. The oven was programmed from 70 °C at injection, then increased by 20 °C min⁻¹ to 200 °C and next by 3 °C min⁻¹ until 320 °C. The final temperature of 320 °C was held for 30 min. Concentrations of alkenones were calculated using nonadeca-1 – one as internal standard. U^K₃₇ was calculated using the equation described by Prahl and Wakeham (1987) and SST values were estimated using the calibration of Müller et al. (1998) as this is the most commonly used global core top calibration, including in our study site (Calvo et al., 2007). Mass accumulation rates of the alkenones were estimated as described for TOC.

5.3.3.2 Gas Chromatography/Mass Spectrometry analyses

Compound identification of alkenones and long chain diols was conducted using a Thermo Finnigan Trace Ultra GC connected to ThermoFinnigan DSQ MS operated at 70 eV, with a mass range m/z 50–800 and 3 scans s⁻¹. The column is a 25 m, silica column with 0.32 mm of diameter and coated with CP Sil-5 (thickness=0.12 μm). The temperature program initiated at 70 °C, increased first at a rate of 20 °C min⁻¹ to 130 °C, and next at a rate of 4 °C min⁻¹ to the final temperature of 320 °C, which was held for 10 min. The relative abundances of diols were measured using the same GC/MS operated in single ion mode, monitoring ions of m/z 299, 313 and 327, with a dwell time of 100 ms and ionization energy of 70 eV. The

Diol index was calculated using the equation described by Rampen et al. (2008):

$$\text{Diol index} = \frac{[C_{28} + C_{30} \text{ 1,14} - \text{diol}]}{[C_{28} + C_{30} \text{ 1,14} - \text{diol}] + [C_{30} \text{ 1,15} - \text{diol}]}$$

5.4 Results and discussion

5.4.1 Age model of core MD03-2607 and sedimentation rates

The thirteen OSL dates are shown in Table 5.1. Excluding a suspected poorly bleached sample at 63 cm, the 5 OSL dates from the top 75 cm of the core are consistent with a linear sedimentation rate of 0.17 mm yr⁻¹, implying the loss of approximately 19 cm of sediment from the top of the profile during coring. The three dates between 100 and 150 cm indicate a slower rate of deposition during the early Holocene and the end of MIS 2 (average of 0.07 mm yr⁻¹). The period immediately following the Last Glacial Maximum (LGM), dates between 20 and 15 ka, is characterized by the most rapid sediment deposition (up to 0.29 mm yr⁻¹). Planktonic foraminifera specimens used for ¹⁴C dating consist of either monospecific *G. bulloides* or mixed *G. bulloides* and *G. ruber*, and are thus representative of the Flinders Undercurrent or a mixed surface/intermediate water age (Moros et al., 2009). Comparison of the ¹⁴C dates with OSL dating shows that during the mid to late Holocene, the OSL dates consistently underestimate the ¹⁴C dates adjusted with the published regional reservoir correction, with an average discrepancy of 1250±340 years (Wilkins, 2009). The age offset is within statistical uncertainty of the reservoir age calculated from the core-top sample from multi-core MC03 (1460±70 ¹⁴C yr BP). We therefore used a reservoir age correction of 1460±70 years rather than the published regional marine reservoir of 461±29 years (Reimer and Reimer, 2001) to obtain consistent AMS ¹⁴C and OSL dates for the Holocene. During the LGM and the deglaciation, the ¹⁴C dates were corrected with the published regional marine reservoir of 461±29 years.

The δ¹⁸O record of *G. bulloides* clearly shows similar variations to those of the stacked benthic foraminifera record (Lisiecki and Raymo, 2005), spanning from MIS 1 to the latest part of MIS 6 (Fig. 5.2). Our revised age model for MD03-2607 also compares well with the age model of Gingele and De Deckker (2005). The good correspondence of the δ¹⁸O record of the planktonic foraminifera *G. bulloides* with the stacked benthic foraminiferal isotope records and the consistent AMS ¹⁴C and OSL dates confirms that resedimentation caused by turbid layers (see Table 5.1) was likely not a major issue for this core (cf. Gingele and De Deckker, 2005).

Sedimentation rates of sediments from the deeper part of the core were in general 0.1 mm yr⁻¹ with peaks during interglacials and MIS 3 of up to 0.2 mm yr⁻¹. The highest peak in the sedimentation rate was during LGM, where values of 0.3–0.8 mm yr⁻¹ were recorded (Fig. 5.3h). The higher sediment rates during the LGM are probably due to the sea level lowstand at that time, through which the Murray River mouth was closer to the site (see Gingele and De Deckker, 2005). Our calculated sedimentation rates compare well with those

of Gingele and De Deckker (2005), although our higher resolution record now yields more detailed sedimentation rate changes.

5.4.2 Carbon isotope record of foraminifera

The $\delta^{13}\text{C}$ record of *G. bulloides* shows distinct sharp minima associated with the deglaciation periods antecedent to MIS 5e and 1, and the MIS4/3 transition (yellow bars, Fig. 5.3c). Minima in stable carbon isotopic values of planktonic foraminifera can in principle be caused for a variety of reasons. For instance, the input of terrestrial organic matter and subsequent oxidation can lower the $\delta^{13}\text{C}$ of dissolved inorganic carbon. However, the $\delta^{13}\text{C}$ of the sedimentary organic carbon was relatively constant at -22 to -23% (Lopes dos Santos et al., unpublished data) suggesting that the input of terrestrial organic matter did not substantially change over time. A lower primary productivity and low nutrient concentrations can lead to a decrease in CO_2 uptake, leading to a decrease in $\delta^{13}\text{C}$ of dissolved inorganic carbon and thus to a decrease in the planktonic $\delta^{13}\text{C}$ record. However, as will be discussed below, the productivity records do not match the planktonic foraminifera record. Thus, we suggest that these minima probably represent an isotopic signal of SO waters which contain ^{13}C -depleted CO_2 (Spero and Lea, 2002; Pena et al., 2008; Calvo et al., 2011; Hayes et al., 2011). Indeed, the timing and distribution of the deglacial carbon isotope are consistent with those of other planktonic foraminifera records used elsewhere to infer the influx of SO waters (Spero and Lea, 2002; Pena et al., 2008; Calvo et al., 2011; Hayes et al., 2011). This suggests that the Murray Canyons Group area received an influx of SO waters, during the deglaciations and the MIS4/3 transition. Gingele and De Deckker (2005) also reported minima in their $\delta^{13}\text{C}$ record of *G. bulloides* but, due to the lower resolution of their record, the first two isotopic minima were not apparent in their record. These minima in planktonic $\delta^{13}\text{C}$ record is not directly interpreted as upwelling per se in this study since it has evidence based on barium concentrations that deeper waters can be brought up in the canyons, but not up to the surface.

5.4.3 Sea-surface temperature record

We generated a sea-surface temperature (SST) record based on the U_{37}^{K} of the alkenones (Prahl and Wakeham, 1987; Müller et al., 1998). The uppermost core sample shows a temperature of $18\text{ }^\circ\text{C}$ in agreement with the modern SST range in this area ($14\text{--}18\text{ }^\circ\text{C}$) (Locarnini et al., 2010). The U_{37}^{K} SST record shows a good correspondence with our $\delta^{18}\text{O}$ record of *G. bulloides* (Fig. 5.3a, b), displaying the warmest temperature of $\sim 21\text{ }^\circ\text{C}$ during the last interglacial (MIS 5e), slightly warmer than the present interglacial with $\sim 20\text{ }^\circ\text{C}$ (MIS 1). The lowest temperature was recorded during the LGM with a temperature of $\sim 10\text{ }^\circ\text{C}$. The last deglaciation was characterized by a warming of $\sim 10\text{ }^\circ\text{C}$ with a clear interruption from 16 to 13 ka, comparable with the interruption reported in the U_{37}^{K} SST record of the nearby core MD03-2611, which is ca. 80 km south-east of our core (Calvo et al., 2007).

5.4.4 Productivity in the Murray Canyons area

Several proxies were used to reconstruct a high-resolution productivity record offshore Southeastern Australia. We first generated a high-resolution record of % TOC and TOC accumulation rates (TOC AR) as an indicator for general productivity as well as biomarker records for specific algae, i.e. alkenone concentrations and accumulation rates (alkenone AR) and the Diol index. The potential controls on the productivity records are subsequently discussed.

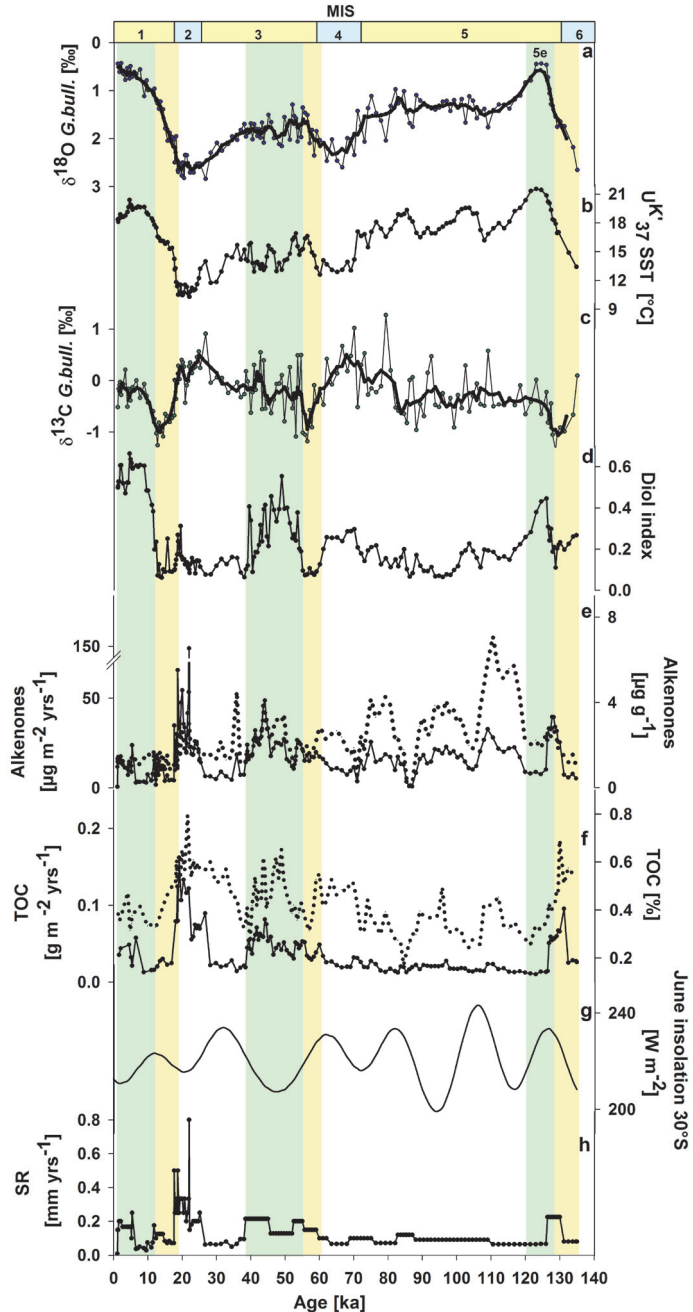


Fig. 5.3: Geochemical records from core MD03-2607. (a) $\delta^{18}\text{O}$ of *Globigerina bulloides*. Thick line represents the smoothed 5 points mean. (b) U_{37}^{K} SST. (c) $\delta^{13}\text{C}$ of *G. bulloides*. Thick line represents the smoothed 5 points mean. (d) Diol index. (e) Alkenone concentration (dotted line) and accumulation rates (plain line). (f) Total Organic Carbon (TOC) percentage (dotted line) and accumulation rates (plain line). (g) June insolation minima at 30°S. (h) Sedimentation Rate (SR). MIS stands for Marine Isotope Stages. Yellow shaded bars are periods of minima in planktonic $\delta^{13}\text{C}$ suggesting influence of Southern Ocean waters and green shaded bars are peak periods in diol index suggesting blooms in *Proboscia* diatoms.

5.4.4.1 General productivity

TOC varied from 0.2 to 0.8% with maxima during the LGM and minima at 85 ka. The TOC AR shows a relatively similar pattern as % TOC suggesting that the TOC record is not strongly affected by dilution of inorganic material. The TOC AR had maximum values of 0.2 and 0.1 $\text{g m}^{-2} \text{yr}^{-1}$ at the LGM and the penultimate deglaciation, followed by lower peaks during MIS 1 and 3 (Fig. 5.3f). This is similar to the findings of Gingele and De Deckker (2005), who found higher TOC contents during the LGM and the penultimate deglaciation. This increase of TOC AR could in principle be caused by increased terrigenous carbon input from the Murray–Darling River as the sea level stand was lower and the core site was then closer to the river mouth (Gingele et al., 2004). However, Gingele and De Deckker (2005) did not find elevated C/N ratios during these times, suggesting no increased input of terrestrial organic matter. Additionally, $\delta^{13}\text{C}$ values of sedimentary organic matter during glacials were rather constant at -22 to -23‰ (Lopes dos Santos et al., unpublished data), values corresponding to those of marine organic matter (Meyers, 1994) and suggesting no substantial increase in the delivery of terrestrial OC. Based on this, we assume that the TOC reflects mainly marine OC.

A comparison of the TOC records with the planktonic foraminiferal carbon isotope record shows that most maxima in TOC do not match with minima in $\delta^{13}\text{C}$, suggesting that an influx of deep SO waters did not have a large influence on general productivity. Gingele and De Deckker (2005) inferred that the increased TOC during glacials may be due to stronger winds as they found a correlation between their TOC record and June insolation minima at 30°S. Indeed, we also find a reasonable match between maxima in our high-resolution TOC record and insolation minima (Fig. 5.3f, g), suggesting that stronger winds could play a role in the increased productivity. During insolation minima, the anticyclonic center lies over central Australia and the westerlies occur over this region (Sturman and Tapper, 1996). The stronger winds have the potential to bring aeolian dust to our core site (Gingele and De Deckker, 2005; Gingele et al., 2007), thereby fertilizing the surface waters, as well as enhancing the mixing of waters from below the surface thereby providing an influx of deeper nutrient-rich waters, as postulated by Passlow et al. (1997) for core E55-6 offshore Victoria. Unfortunately, the *n*-alkane's record at this site seems to be more related to fluvial input as it correlates with the BIT index (Hopmans et al., 2004), a proxy for soil input organic matter mainly transported by rivers. Thus, further studies, reconstructing e.g. aeolian input, are needed to provide evidence for this hypothesis.

5.4.4.2 Haptophyte productivity

Alkenone concentrations ranged from 0.1 to 7 $\mu\text{g g}^{-1}$ with the lowest values at 86 ka and highest values at 110 ka (Fig. 5.3e). The alkenone AR shows a similar pattern as the alkenone concentration although the maximum during LGM is much more dominant due to the larger SR at this time. In principle, biomarker concentrations can be substantially affected not only by production but also by the degree of preservation. For example, an increase in the SR can decrease the time that the biomarkers are exposed to the oxygen, leading to an increased preservation and concentration. However, as the highest concentrations are observed during periods of low SR, we assume that the alkenones are not substantially affected by preservation. In agreement with the TOC, the maxima in alkenone concentration and AR do not match minima in the foraminiferal carbon isotope record, suggesting that influx of deep SO waters apparently did not stimulate haptophyte algal productivity to any great extent. In contrast, the increased haptophyte productivity is mainly during insolation minima, possibly due to stronger offshore winds such as the westerlies, as well as winds from inland Australia that may have increased the input of nutrients to this site.

5.4.4.3 *Proboscia* diatom productivity

Finally, we investigated the sediments for potential biomarkers of diatoms. Only 1,14-diols, derived from *Proboscia* diatoms (Sinninghe Damsté et al., 2003), were present in relatively high amounts, while other potential diatom biomarkers, such as highly branched isoprenoids (Volkman et al., 1994), were not detected and only low amounts of the somewhat more ambiguous diatom biomarker loliolide (Klok et al., 1984) were detected. We therefore used the Diol index, based on the relative abundance of 1,14-diol versus 1,15-diols, which has been shown to be a suitable recorder of the relative abundance of *Proboscia* diatoms (Rampen et al., 2008). The Diol index clearly shows maxima during MIS 1, 3 and 5e and minimum values during deglaciation periods (Fig. 5.3d). In contrast to the other productivity records, there is no apparent correlation of the Diol index with insolation minima and, in fact, *Proboscia* diatom productivity was relatively greater during the warm periods.

Comparison with the foraminiferal carbon isotope record shows that peaks in the Diol index lag the start of each of the $\delta^{13}\text{C}$ minima by about 10 ka, suggesting that *Proboscia* productivity increased only after the influx of ^{13}C -depleted SO waters diminished. Interestingly, our *Proboscia* diatom productivity matches some diatom productivity records from the Eastern Equatorial Pacific: indeed, higher opal flux burial rates during the Holocene as seen in core V21-40 (Bradt Miller et al., 2006) (Fig. 5.4c) and during MIS 3 in core TR163-19 (Kienast et al., 2006), both located in the Eastern Equatorial Pacific, display an excellent match with our diol record (Fig. 5.4b and d). These similar trends suggest that possibly these areas, as well as the Murray Canyons area, simultaneously received input of nutrients, particularly silicic acid, during interglacials which stimulated diatom productivity. A possible scenario which can explain the seemingly contemporaneous elevated diatom productivity in the Equatorial Pacific and *Proboscia* diatom productivity in Southeastern Australia is the transport of nutrients as silicic acid from SO waters. However, if this was the case, then we

would expect a match between the maxima in our Diol index record and carbon isotope minima in planktonic foraminifera, a phenomenon that we do not observe. This potentially suggests that the SO waters which reached Southeastern Australia during deglaciations did not contain sufficient nutrients to stimulate productivity offshore Southeastern Australia.

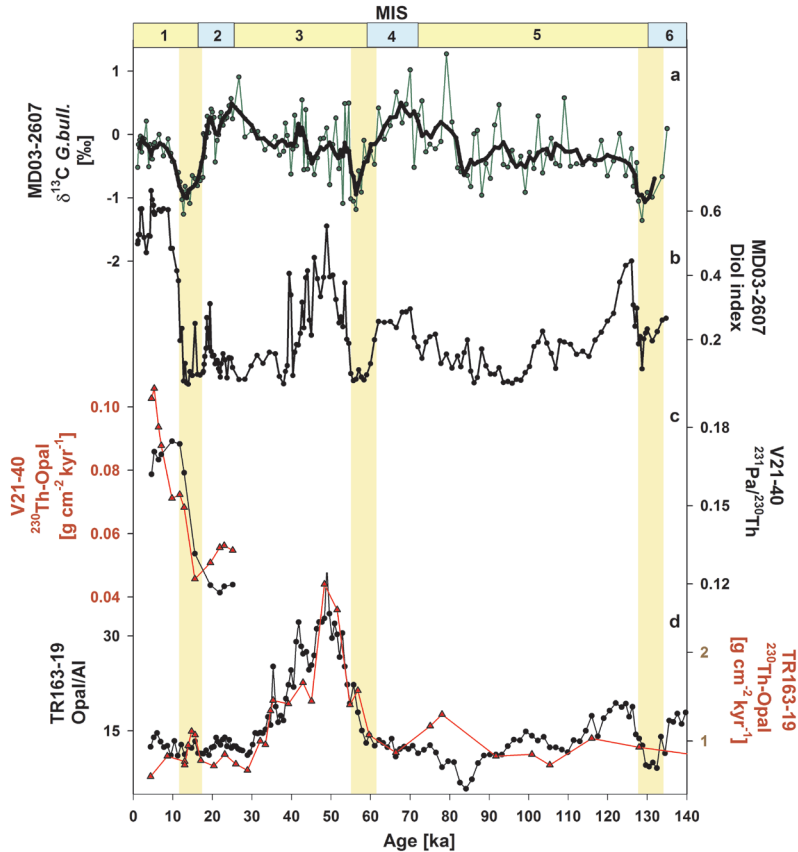


Fig. 5.4: Geochemical records from offshore Southeastern Australia and from selected cores from different latitudes. (a) $\delta^{13}\text{C}$ of *G. bulloides* from core MD03-2607. (b) Diol index record from core MD03-2607. (c) $^{231}\text{Pa}/^{230}\text{Th}$ in black and ^{230}Th -normalized opal flux in red from core V21-40 in East Equatorial Pacific (Bradtmiller et al., 2006). (d) Biogenic opal/aluminium ratios in black and ^{230}Th -normalized opal flux in red of core TR163-19 in the Eastern Equatorial Pacific (Kienast et al., 2006). MIS (=Marine Isotope Stages). Yellow shaded bars represent periods of minima in planktonic $\delta^{13}\text{C}$.

It should be noted that *Proboscia* diatoms are able to build thin frustules and thus can thrive at relatively low concentration of silicic acid (Goering and Iverson, 1981). Indeed, their frustules may be more prone to dissolution in comparison to those of other diatoms (Koning et al., 2001), thus providing an explanation why no diatom frustules were found at this site. Consequently, the amount of silicic acid in the SO waters that reached Southeastern

Australia during interglacials and MIS 3 was probably relatively low, but nevertheless sufficient enough to support an increased *Proboscia* diatom productivity, but possibly not of other diatom groups. This suggests that silicic acid, presumably derived from the SO, was predominantly transported to the equatorial Pacific and only to a minor extent to offshore Southeastern Australia during these periods. This could possibly explain the apparent enigma that *Proboscia* diatom productivity was stimulated while no minima in $\delta^{13}\text{C}$ planktonic foraminifera record were apparent.

5.5 Conclusions

High resolution records of past productivity offshore Southeastern Australia show strong variations for the last ~135 ka. The highest primary productivity is observed during the LGM and is, possibly, linked to the stronger winds (e.g. the westerlies), causing an increased dust supply from inland Australia to the core site, as well as mixing of the water column that would have brought nutrient-rich waters to the surface. Diatom productivity at the Murray Canyons Group area seems to be limited, as the only specific biomarkers for diatoms found were long chain 1,14 diols and no silica frustules were found in the sediments. The reconstructed *Proboscia* diatom productivity, based on the Diol index, was higher during interglacials and MIS 3, concomitant with diatom productivity increases in the equatorial Pacific, but not with minima in the planktonic foraminiferal record, an indicator for SO water influx. This can tentatively be explained by a minor input of silicic acid transport from the SO as *Proboscia* diatoms only require low amounts of silica. Further studies on past changes in ocean currents are needed for a better understanding of the mechanism which transports nutrients from the SO to lower latitudes.

Acknowledgments

We thank Sebastiaan Rampen, Anhelique Mets and Judith Shelley for analytical assistance. Mrs Judith Shelley prepared some of the additional planktonic foraminifers that were analyzed at NIOZ. Research funding was provided by a VICI grant to SS from the Netherlands Organization of Scientific Research. Core MD03-2607 was obtained with a National Oceans Office grant and an Australian Research Council grant, both awarded to PDD. Y. Balut from IPEV was instrumental in obtaining the core. DW acknowledges help from J. Olley [CSIRO Canberra] and L.K. Fifield [ANU] with dating procedures and provision of facilities. Dating by DW was funded by ARC grant (DP034493) and AINSE grant (AINGRA07037).

Chapter 6

A late Quaternary sedimentary record of steryl alkyl ethers from offshore southeastern Australia

Raquel A. Lopes dos Santos, Patrick De Deckker, Jaap S. Sinninghe Damsté and Stefan Schouten
Published in *Organic Geochemistry*, *In press*

Abstract

Steryl alkyl ethers (SAE) have been reported from marine sediments ranging in age from the Holocene to the Lower Cretaceous, and their production has been linked to upwelling of cold, nutrient-rich waters. However, the lack of continuous stratigraphic records for these compounds has complicated validation of the precise connection of their production, sedimentary distribution and survival with climatic conditions. Here, we report an SAE record that spans the last ~135 ka from a sediment core taken offshore southeastern Australia in the Murray Canyons Group region. The SAE are composed predominantly of C₂₇₋₃₀ steroid moieties with one or two double bonds, ether-bound to C₁₀₋₁₁ alkyl moieties. Some of these SAE are identical to those reported in marine sediments, whereas others have not been identified previously. The SAE do not exhibit any systematic change in their distribution over the past 110 ka but sediments older than 110 ka possess a different assemblage of SAE with higher amounts of constituents containing a C₁₁ alkyl moiety. The SAE accumulation rates increase rapidly during glacial episodes and for intervals characterized by a sharp decline in sea-surface temperature. These results suggest that SAE may be related to marine eukaryotes that thrive when there is an influx of cold, deep waters in the Murray Canyons Group region, likely triggered by stronger westerlies over southeastern Australia forcing deeper waters to reach the surface during glacials.

6.1 Introduction

Steryl alkyl ethers (SAE) are unusual compounds present in modern and ancient sediments (e.g. Boon and de Leeuw, 1979; Brassell et al., 1980; 2009; Schouten et al., 2000; 2005), that are considered as “orphan” biomarkers since their biological sources are as yet unknown. They were first reported in Walvis Bay sediments (Boon and de Leeuw, 1979) and tentatively identified by comparison with a published mass spectrum of cholesteryl 1-hexadecyl ether (Funasaki and Gilbertson, 1968). Schouten et al. (2005) unambiguously identified the dominant sedimentary SAEs in sediments of the South East Atlantic Ocean and the Arabian Sea using chemical degradation and synthesis of authentic standards. SAEs in Pleistocene sediments from South East Atlantic Ocean consisted of C_{27-29} steroidal moieties with one double bond, which are ether bounded at positions 3 and 5 to C_{8-12} alkyl chains, while sediments from the Arabian Sea contain C_{27-29} steroidal moieties with 1-2 double bonds that are ether bounded to C_{10} alkyl chain at position 5 (Schouten et al., 2005). A comprehensive overview of the occurrence and distribution of SAEs in sediments from the lower Cretaceous, Tertiary and Quaternary periods was recently compiled by Brassell (2009). SAEs with C_{27-29} steroidal moieties attached to C_{8-12} alkyl chains were by far the most ubiquitous but an unusual SAE composed of a $C_{26.2}$ steroidal moiety ether bounded to a C_{10} alkyl was recognized in Quaternary sediments from the Japan Trench (Boon and de Leeuw, 1979; Brassell et al., 1980; Wefer et al., 1998; Schouten et al., 2000; Marlow et al., 2001; Schefuß et al., 2001; Brassell et al., 2004; Schouten et al., 2005; Brassell, 2009).

The biological origin of SAEs is presently unknown. Most of the locations where these compounds were found are highly productive upwelling areas in which phytoplankton tends to be dominated by diatoms or sites characterized by a high productivity of diatoms. Hence, diatoms have been suggested as the likely source of SAEs (Schouten et al., 2000). However, analysis of ca. 120 strains of predominantly marine diatoms did not reveal the presence of SAEs (Schouten et al., 2005). Alternatively, it was suggested that they could be products formed during zooplankton herbivory on food sources containing sterols, similarly to the processes described for steryl chlorine esters (Harradine et al., 1996; Pearce et al., 1998). However, the distribution of the steroidal moieties of the SAEs is different from that of free sterols (Brassell, 2009 and references cited therein), suggesting that SAEs may represent a direct biological input (Schouten et al., 2000). Brassell (2009) raised the possibility that SAEs may be storage lipids of phytoplankton or zooplankton. Additionally, he also suggested that SAEs may be a reflection of the biological changes occurring as a response to upwelling of cold bottom waters (Brassell, 2009). However, up to now there has not been a continuous sedimentary record of SAEs enabling a more detailed assessment of the climatic controls on SAE distribution and abundances.

Here, we analyzed the abundance and distribution of SAEs in sediments from a single core covering the last ~135 ka from the Murray Canyons Group area, offshore southeastern Australia (see Hill and De Deckker, 2004). This area is characterized by increased productivity during periods of insolation minima due to stronger westerlies and winds from

inland Australia that can bring aeolian dust and enhance mixing of waters from below the surface (Gingele and De Deckker, 2005; Gingele et al., 2007; De Deckker et al., 2012). We compared the SAE record with proxy records for sea surface temperature and productivity to investigate climatic controls on their occurrence and distribution.

6.2 Material and Methods

6.2.1 Sampling and extraction

Sediment core MD03-2607 (30 m long) was recovered during the AUSCAN 2003 cruise (MD131) from the Murray Canyons Group offshore southeastern Australia at 36° 57.64' S; 137° 24.39' E (Fig. 6.1) in 865 m deep waters (Hill and De Deckker, 2004). A description of the core and its mineralogical content were published elsewhere (Gingele et al., 2004). The age model (based on ^{14}C and OSL dating and $\delta^{18}\text{O}$ record of planktonic foraminifera), $U^{K'}_{37}$, sea surface temperature (SST) record, alkenone and total organic carbon records for the first 15 m of the core were described previously (Gingele and De Deckker, 2005; Lopes dos Santos, 2012). Core MD03-2607 was sampled for biomarker analyses at 5 cm intervals for the first 3 m and 10 cm for the rest of the 12 m. Sediment samples were freeze-dried, homogenized and extracted using an Automated Solvent Extractor (ASE 200, DIONEX; 100°C and 7.6×10^6 Pa) with a mixture of dichloromethane (DCM): methanol (MeOH) (9:1, v:v) to obtain a total lipid extract (TLE). Internal standards were added to the TLE and subsequently each sample was separated into an apolar, ketone and polar fraction using Al_2O_3 column chromatography as described previously (Lopes dos Santos et al., 2012). For this work, the apolar fractions were analyzed for SAEs by gas chromatography (GC) and gas chromatography/mass spectrometry (GC/MS). Furthermore, polar fractions of selected sediments were derivatized using bis(trimethylsilyl)trifluoroacetamide (BSTFA) and pyridine before being analysed for the distribution of sterols using GC and GC/MS.

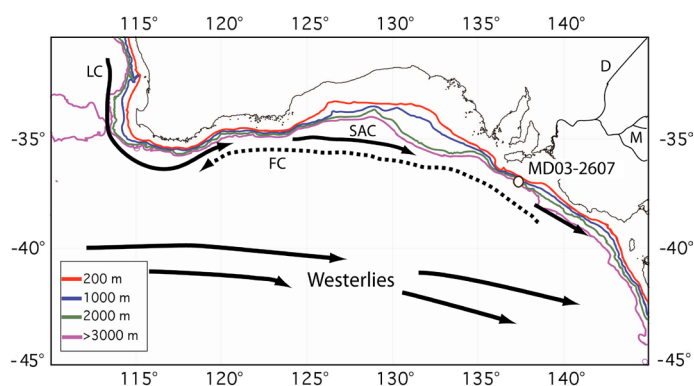


Fig. 6.1: Location of core MD03-2607 offshore southeastern Australia together with the present day ocean currents and the position of the Westerlies. Colored lines show bathymetry around Australia. LC – Leeuwin Current, SAC – South Australia Current, FC - Flinder Current, D – Darling River, M - River Murray.

6.2.2 GC and GC/MS analysis

The apolar fractions were analyzed by a Hewlett Packard 6890 gas chromatograph, on a 25 m, silica column with 0.32 mm of diameter and coated with CP Sil-5 (thickness=0.12 μm). The carrier gas was Helium. The oven was programmed from 70°C at injection, and then increased by 20 °C min^{-1} to 130 °C and subsequently by 4°C min^{-1} until 320°C. The final temperature of 320°C was held for 10 min. Concentrations of SAEs were determined using the squalane internal standard. The pseudo Kovats indices of the SAEs were determined using the retention times of co-injected C_{38} and C_{40} *n*-alkane standards with pseudo Kovats indices of 3800 and 4000, respectively, as described by Schouten et al. (2005). An estimation of mass accumulation rates of SAEs was made using the concentration and sedimentation rates based on the sediment depth and age and assuming a dry bulk density of 0.8 [g/cm^3] and a sediment porosity of 0.72. The value for dry bulk density is based on a previous study with multicores from the area (Schmidt et al., 2010) and were assumed not to substantially vary over the depth of the record (~15 m).

Mass spectral identification of the sterols and SAEs was conducted using a Thermo Finnigan Trace Gas Chromatograph (GC) Ultra connected to Thermofinnigan DSQ mass spectrometer operated at 70 eV, with a mass range m/z 50-800 and a cycle time of 3 scans s^{-1} . The capillary column and temperature program used was the same as described for the GC analyses. Identification of the SAEs are based on published mass spectra and Kovats retention indices reported by Schouten et al. (2005).

6.3 Results and discussion

6.3.1 SAE distributions

GC and GC/MS analysis of apolar fractions from sediments from offshore southeastern Australia show the dominance of long-chain C_{27} to C_{33} *n*-alkanes, with an odd over even carbon number predominance. In a number of sediments, substantial amounts of SAEs are detected (Fig. 6.2). Interpretation of full scan mass spectral data and inspection of mass chromatograms of m/z 369, 383, 397, 411, diagnostic for SAEs (Schouten et al., 2005), show that the SAEs are dominated by C_{27-30} steroidal moieties containing one or two double bonds ether bound to a C_{10} alkyl chain (Fig. 6.3). Only in sediments older in age than 110 ka, a different distribution, i.e. with a substantially increased amount of SAEs containing a C_{11} alkyl moiety, is apparent (Fig. 6.3).

Since mass spectrometry alone does not allow the exact identification of the position at which the alkyl chain is ether-bound (Schouten et al., 2005), we calculated the pseudo Kovats indices of the different SAEs (Table 6.1) and compare them with those described by Schouten et al. (2005). The pseudo Kovats index of the dominant $\text{C}_{27:1}$ - C_{10} SAE (**1b**) is identical to that of cholest-5-enyl 3 β -(5-decanyl) ether (Table 6.1). This SAE has also been reported in Holocene sediments of the Arabian Sea and Pleistocene sediments of South East Atlantic Ocean (Schouten et al., 2005). In addition, an earlier eluting isomer of a $\text{C}_{27:1}$ - C_{10} SAE (**1a**) was also previously reported in Miocene sediments from the Monterey Formation (Schouten

et al., 2005). Its structure is unknown but, based on its early retention time compared to authentic standards, Schouten et al. (2005) suggested that the alkyl chain may be branched rather than linear. Additionally, a $C_{27:2}$ - C_{10} SAE (**Id**) is present in the southeastern Australia sediments in minor amounts (Fig. 6.3). $C_{27:2}$ - C_{10} SAEs have been reported previously for many other sites, e.g. Arabian Sea, South East Atlantic Ocean, Japan Trench, Iceland-Faroe Ridge and Falkland Plateau (Schouten et al., 2000; Schefuß et al., 2001; Brassell, 2009). A $C_{27:1}$ - C_{11} SAE (**Ic**) is detected only in sediments older than 110 ka (Fig. 6.3) and elutes earlier than the $C_{27:1}$ - C_{11} SAE reported in South East Atlantic Ocean sediments (Schouten et al., 2005), suggesting that it has a different, possibly branched, structure of the alkyl chain.

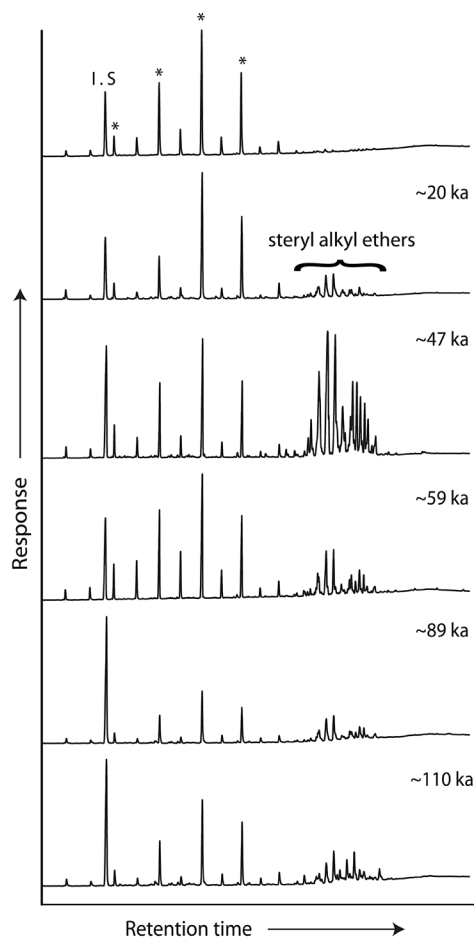


Fig. 6.2: Gas chromatograms of selected apolar fractions from sediment extracts of core MD03-2607. The first panel is a representative chromatogram of the samples where steryl alkyl ethers were not detected. I.S. stands for internal standard (squalane), * *n*-alkanes.

SAEs with C_{28} sterol moieties comprise either C_{28} steroid moieties with one or two double

bonds attached to a C_{10} alkyl moiety (**IIa, b, c, e, f**) or a $C_{28:1}$ steroidal moiety linked to a C_{11} alkyl chain (**IIId**) (Fig. 6.3). All $C_{28:1}$ - C_{10} SAEs have different Kovats indices in comparison to those reported in Schouten et al. (2005). $C_{28:1}$ - C_{10} and $C_{28:2}$ - C_{10} SAEs have been previously reported in sediments from Arabian Sea, South East Atlantic Ocean, Japan Trench, Monterey Formation and Falkland Plateau (Brassell et al., 1980; Schefuß et al., 2001; Brassell, 2009). A $C_{28:1}$ - C_{11} SAE (**IIId**) is found in sediments older than 110 ka (Fig. 6.3); this SAE has not been reported previously. Two $C_{29:1}$ - C_{10} SAEs (**IIIa, b**) are detected in our sediment core (Fig. 6.3) and both elute earlier than 24-ethyl-cholest-5-enyl 3 β -(5-decanyl) ether reported by Schouten et al. (2005). Comparison of the retention times suggest that one of them, the $C_{29:1}$ - C_{10} SAE with Kovats index 3923 (**IIIa**), is likely the pseudo-homologue of the early eluting $C_{27:1}$ - C_{10} SAE (with Kovats index of 3724 - **Ia**) given that the difference in their retention times is comparable with that between cholest-5-enyl 3 β -(5-decanyl) ether and 24-ethyl-cholest-5-enyl 3 β -(5-decanyl) ether (Schouten et al., 2005). Also, two $C_{29:2}$ - C_{10} (**IIIId, e**) and a $C_{29:1}$ - C_{11} (**IIIc**) (in sediments > 110 ka) SAEs are present in southeastern Australia sediments, which, until now, have not been previously reported.

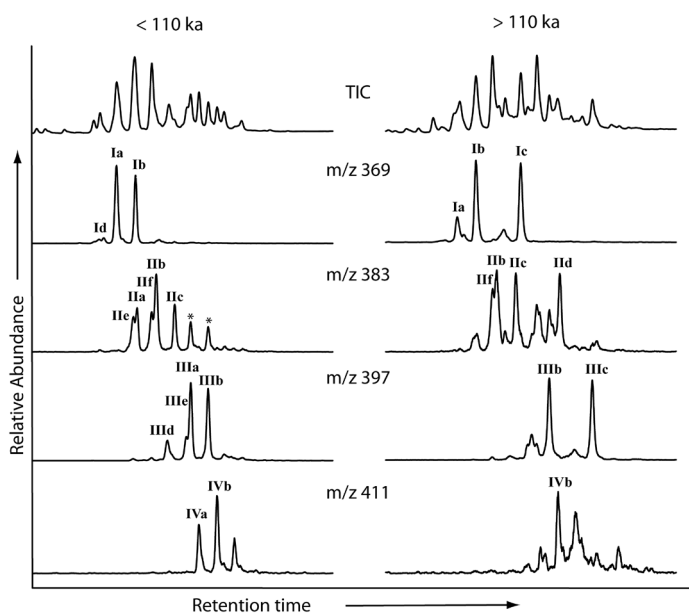


Fig. 6.3: Total ion chromatogram and mass chromatograms of m/z 369, 383, 397 and 411 of steryl alkyl ethers from southeastern Australia sediments at ~47 ka (left) and ~110 ka (right). This illustrates that sediments <110 ka have a different distribution than the older sediments. Structure numbers refer to steryl alkyl ethers listed in Table I. * refers to crosstalk of C_{29} steryl alkyl ethers.

Interestingly, two $C_{30:1}$ - C_{10} SAEs are identified in the southeastern Australia sediments (Fig. 6.3, Table 6.1) in the sediments younger than 110 ka. The mass spectra of these SAEs (Fig. 6.4) comprise fragment ions m/z 69, 97, 139, 229 and 271 which are characteristic fragments

of trimethylsilylated dinosterol (Boon et al., 1979), although the fragment ion m/z 139 is relatively higher than in that of dinosterol. This tentatively suggests that these SAEs might comprise dinosterol as the sterol moiety. To the best of our knowledge this represents the first report of an SAE containing a 4-methyl steroidal moiety.

Table 6.1: Composition and relative retention times of the dominant steryl alkyl ethers in sediments of core MD03-2607. n.d - not determined.

| Compound | Steroid moiety | Alkyl moiety | Position O-bond on alkyl moiety | Pseudo-Kovats index |
|----------|------------------------|-----------------|---------------------------------|---------------------|
| Ia | C _{27:1} | C ₁₀ | n.d | 3724 ^a |
| Ib | C _{27:1} | C ₁₀ | 5 | 3775 ^b |
| Ic | C _{27:1} | C ₁₁ | n.d | 3886 |
| Id | C _{27:2} | C ₁₀ | n.d | 3700 |
| IIa | C _{28:1} | C ₁₀ | n.d | 3779 |
| IIb | C _{28:1} | C ₁₀ | n.d | 3831 |
| IIc | C _{28:1} | C ₁₀ | n.d | 3879 |
| IId | C _{28:1} | C ₁₁ | n.d | 3962 |
| IIe | C _{28:2} | C ₁₀ | n.d | 3768 |
| IIIf | C _{28:2} | C ₁₀ | n.d | 3818 |
| IIIa | C _{29:1} | C ₁₀ | n.d | 3923 |
| IIIb | C _{29:1} | C ₁₀ | n.d | 3969 |
| IIIc | C _{29:1} | C ₁₁ | n.d | 4081 |
| IIId | C _{29:2} | C ₁₀ | n.d | 3863 |
| IIIe | C _{29:2} | C ₁₀ | n.d | 3912 |
| IVa | 4-Me C _{30:1} | C ₁₀ | n.d | 3947 |
| IVb | 4-Me C _{30:1} | C ₁₀ | n.d | 3994 |

^a previously detected in the Monterey Formation (Schouten et al., 2005)

^b previously detected in southeastern Atlantic and the Arabian Sea and confirmed by an authentic standard (Schouten et al., 2005)

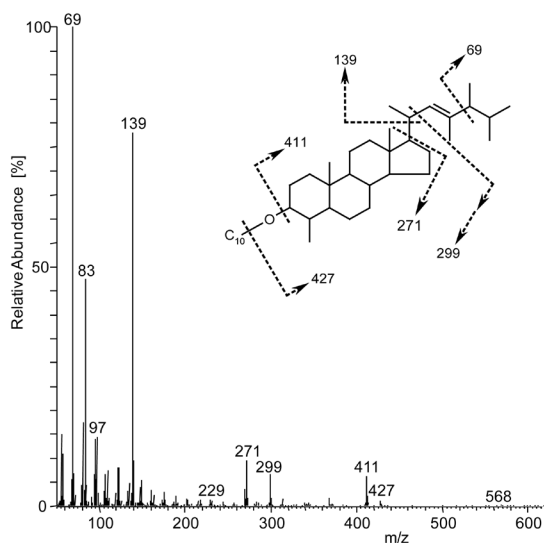


Fig. 6.4: Mass spectrum of a 4-methyl C_{30:1}-C₁₀ (IVb) steryl alkyl ether in southeastern Australia sediments, tentatively identified as a dinosterol derivative based on the fragmentation pattern shown.

Information on the sources of SAE can potentially be gained by comparison with the free sterol distribution. Unfortunately, in most sediments, abundance of sterols are low hindering a proper quantitative evaluation of sterol distributions. Comparison for a selected number of sediments show that the SAEs have a distinctively different distribution in comparison to the sterols (Fig. 6.5). Sterols are dominated by the 24-ethyl-cholestanol and 24-ethyl-cholesterol (β -sitosterol), with smaller amounts of 24-ethyl-cholest-5,22-dienol (stigmasterol), cholesterol, dinosterol and finally C_{28} sterols. In contrast, the SAEs are dominated by components containing a $C_{27:1}$ steroidal moiety, followed by $C_{28:1}$ and $C_{29:1}$ and finally 4-methyl $C_{30:1}$ steroidal moieties. Thus, there is a substantial difference in the distribution of steroid moieties between sterols and SAE, in particular with respect to the C_{29} sterols which are more dominant in the free sterols (Fig. 6.5). These large differences, as observed previously (Schouten et al., 2000; 2005; Brassell, 2009), suggest that free sterols are an unlikely direct source for production of the SAEs, for instance as a result of zooplankton feeding on algae. The recognition of SAEs containing dinosterol moieties is significant not only as the first confirmation of 4-methyl SAEs but also because it provides the first instance wherein the steryl moiety in SAEs has restricted biological affinities, i.e. it is only produced by dinoflagellates (although this sterol has also been found in low amounts in a few diatoms; Volkman et al., 1993). It would therefore suggest that dinoflagellates may also synthesize SAEs. Nevertheless, it is striking that the most recent documentation of SAEs is in sediments from Holocene age (Schouten et al., 2000), while they have not been found in cultures of dinoflagellates or diatoms, nor have these compounds been reported yet from suspended particulate matter.

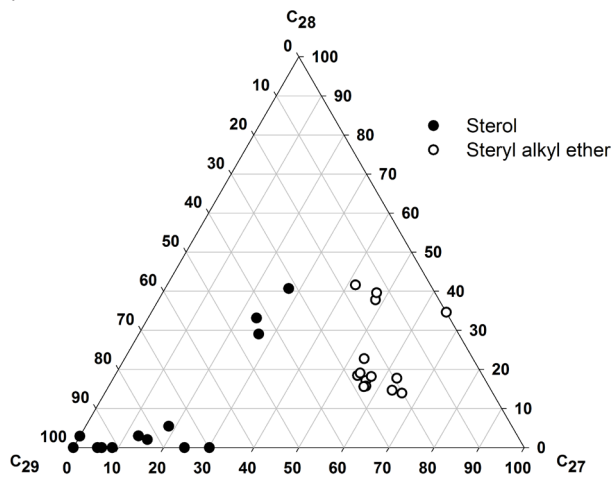


Fig. 6.5: Ternary diagram of relative abundance of C_{27} , C_{28} and C_{29} homologues of free sterols and steryl alkyl ethers in selected sediments.

In summary, sediments offshore southeastern Australia have a different SAEs distribution in comparison to those at other locations, although some of these SAEs have been also identified previously (Schouten et al., 2005). In addition, no SAEs with a C_{12} alkyl chain

are detected, compounds that have been reported in sediments from the South East Atlantic Ocean (Schouten et al., 2005). The distribution of SAEs in southeastern Australia sediments does not change except for sediments >110 ka, which contain relatively more SAEs with a C₁₁ alkyl chain. This suggests that, for most of the sediment record, the organisms responsible for SAE production, either directly or indirectly, did not change substantially in composition.

6.3.2 SAE accumulation rates and relation with environmental changes

The sedimentary records of the total SAE concentration as well as accumulation rate for the last ~135 ka (Fig. 6.6) have similar trends, suggesting that changes in sedimentation rates did not strongly affect the records. The records show that these compounds are present in low abundance or below detection limit for most of the time, but show large transient changes in abundances in distinct periods (shaded bars in Fig. 6.6).

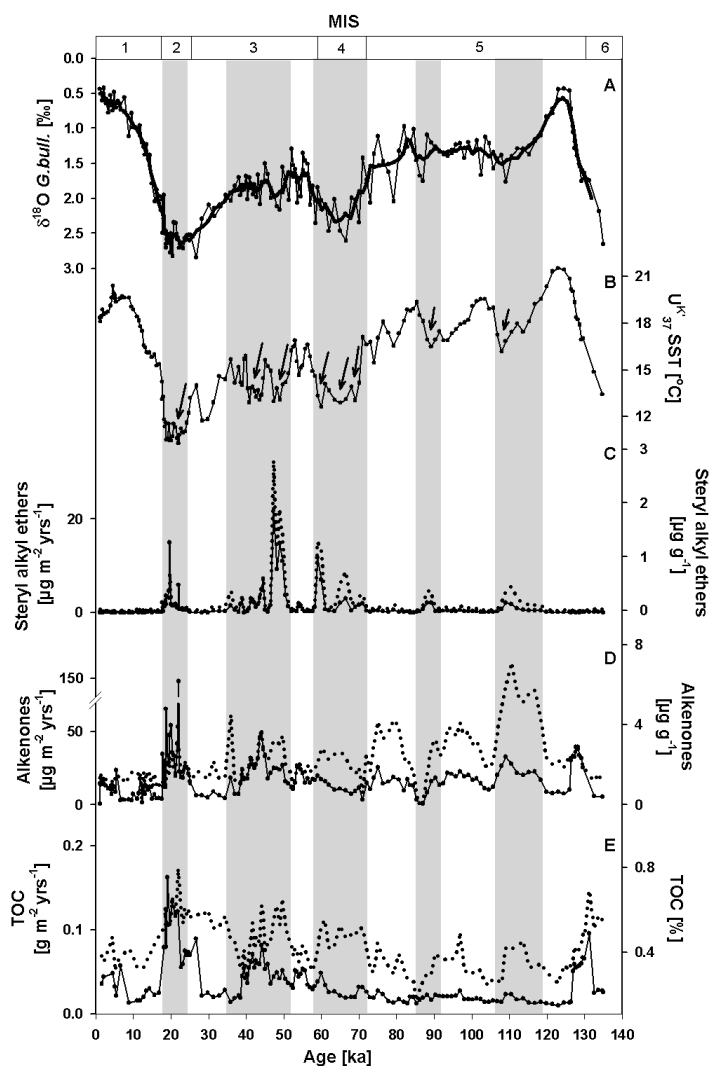


Fig. 6.6: Geochemical records of core MD03-2607 together with temperature record of Antarctica. A) $\delta^{18}\text{O}$ record of planktonic foraminifer *G. bulloides* (Gingele et al., 2004; Lopes dos Santos et al., 2012), B) $U^{K'}_{37}$ sea surface temperature (Lopes dos Santos et al., 2012), C) Total steryl alkyl ethers concentration (dotted line) and mass accumulation rate (plain line), D) Alkenones concentration (dotted line) and mass accumulation rate (plain line) (Lopes dos Santos et al., 2012) and E) TOC percentage (dotted line) and mass accumulation rate (plain line) (Lopes dos Santos et al., 2012). MIS stands for marine isotope stages. Arrows indicate rapid decreases in $U^{K'}_{37}$ temperatures. Shaded bars indicate periods of increased steryl alkyl ethers concentration and accumulation rates.

Five main periods of abrupt increase in SAE accumulation rates are observed with the highest during glacials, i.e. Marine Isotope Stages (MIS) 2 and 4, and also during the warmer MIS 3. The profile of SAE normalized to organic carbon showed similar timing of abrupt increase, suggesting that the production of these compounds is enhanced as a proportion of the organic matter during these periods. During interglacials, the SAEs are below detection limit. In principle, this pattern supports the hypothesis of Brassell (2009) that the presence of SAEs indicates relatively cold waters since the periods of high accumulation rates of SAE coincide with periods with SSTs $<20^\circ\text{C}$ based on $U^{K'}_{37}$ -reconstructed temperatures (Fig. 6.6). Noticeably, the spikes in SAE accumulation rates are often coincident with sharp drops in the $U^{K'}_{37}$ SST and increased $\delta^{18}\text{O}$ values of the planktonic foraminifer *Globigerina bulloides* in the same core (Fig. 6.6), both being indicative of decreased SST in this region. Indeed, a correlation exists between the SAE accumulation rate and $U^{K'}_{37}$ SST ($R^2=0.16$, $P<0.0001$), although this relatively weak correlation suggests no strong direct linear relationship. Thus, SAE production during the late Quaternary offshore southeastern Australia seems to be triggered during glacial periods and part of MIS 3, especially when temperatures were low or dropping.

Since glacial periods offshore southeastern Australia are characterized by stronger winds in comparison to interglacials that can bring nutrient-rich water near the surface (Passlow et al., 1997; Gingele and De Deckker, 2005; Gingele et al., 2007; De Deckker et al., 2012), it may be that the SAEs are connected to input of cold waters as suggested previously (Brassell, 2009). This could also explain the seemingly contradictory presence of SAEs in the relatively warm Arabian Sea during the Holocene since this area is presently characterized by strong upwelling of colder bottom waters (Smith et al., 1998). Nevertheless, SAEs are not continuously present in the glacial periods of our record while, in some episodes of rapid cooling (e.g. at 25 ka or 135 ka), no spike in SAE abundance is noticeable. Thus, it seems that cold temperatures themselves or rapid cooling is not the only variable explaining the production of SAEs.

To investigate the potential source of the SAEs, we compared their sedimentary record with those of organic carbon and alkenones (from Lopes dos Santos et al., 2012; Fig. 6.6), the latter as indicator for haptophyte algal biomass (Volkman et al., 1980). Indeed, there is some correlation of SAE abundance with the abundance of haptophytes ($R^2=0.11$, $P<0.0001$) and organic carbon ($R^2=0.06$, $P=0.002$), but the correlation is rather weak and there is no

clear match between spikes in the records of SAEs and alkenones. This suggests that the organisms synthesizing these compounds, directly or indirectly, behave differently than e.g. haptophytes. The source of SAEs remains, therefore, enigmatic.

6.4. Conclusion

SAEs in sediments from offshore southeastern Australia are dominated by C₂₇₋₃₀ steroidal moieties containing one or two double bonds and ether-bound to C₁₀₋₁₁ alkyl moieties. Similar SAEs have been reported at other locations although in different distributions. The sedimentary record of SAEs accumulation rates shows no clear correlation with organic matter or alkenone accumulation rates, but does seem to be related to abrupt decreases in sea surface temperature. Although our results support the relation between the production of SAEs and the influx of colder waters, more studies are required to confirm this hypothesis and to determine the biological sources of SAE.

Acknowledgements

We thank two anonymous reviewers and Dr. J. Maxwell for comments which improved the manuscript. Research funding was provided by a VICI grant to SS from the Netherlands Organization of Scientific Research. Core MD03-2607 was obtained with an Australian National Oceans Office grant and Australian Research Council grant, both awarded to PDD. Y. Balut from IPEV was instrumental in obtaining the core.

Chapter 7

Wet phases in the Sahara/Sahel region and human migration patterns in North Africa

Isla S. Castañeda, Stefan Mulitza, Enno Schefuß, Raquel A. Lopes dos Santos, Jaap S. Sinninghe Damsté, Stefan Schouten
Published in *PNAS* 106 (2009) 20159-20163

The carbon isotopic composition of individual plant leaf waxes (a proxy for C_3 vs. C_4 vegetation) in a marine sediment core collected from beneath the plume of Sahara-derived dust in northwest Africa reveals three periods during the past 192,000 years when the central Sahara/Sahel contained C_3 plants (likely trees), indicating substantially wetter conditions than at present. Our data suggest that variability in the strength of Atlantic meridional overturning circulation (AMOC) is a main control on vegetation distribution in central North Africa, and we note expansions of C_3 vegetation during the African Humid Period (early Holocene) and within Marine Isotope Stage (MIS) 3 (~50–45 ka) and MIS 5 (~120–110 ka). The wet periods within MIS 3 and 5 coincide with major human migration events out of sub-Saharan Africa. Our results thus suggest that changes in AMOC influenced North African climate and, at times, contributed to amenable conditions in the central Sahara/Sahel, allowing humans to cross this otherwise inhospitable region.

The Sahara desert is known to have undergone major, and possibly abrupt, hydrological fluctuations and was vegetated at times in the past (deMenocal et al., 2000; Kuper and Kröpelin, 2006). During a wet phase in the Early Holocene known as the African Humid Period (AHP), the region currently occupied by the Sahara desert was vegetated, contained forests, grasslands, and permanent lakes, and was occupied by human populations (Kuper and Kröpelin, 2006). When the AHP ended at ~5.5 ka, the Sahara was transformed into a hyperarid desert (deMenocal et al., 2000). On orbital time scales, the large hydrological fluctuations in North Africa are linked to changes in the African monsoon, which is related to precession-forced variability in low-latitude summer insolation (Claussen et al., 1999; deMenocal et al., 2000). The abrupt transitions between humid and arid conditions observed in marine and terrestrial paleoclimate records from North Africa, however, cannot be explained solely by gradual orbital forcing (deMenocal et al., 2000); thus, other nonlinear feedback processes are required to explain the abrupt climate responses to orbital forcing. Vegetation and sea surface temperatures (SSTs) are two parameters that have often been cited as factors contributing to abrupt climate change in North Africa (Claussen et al., 1999; Schefuß et al., 2003). However, relatively little information exists regarding the type and extent of past vegetation in the Sahara/Sahel region, and at present, there are no paleoclimate records from below the summer dust plume (located between 0°N and 12°N and west of 10°W). Such records are critical for reconstructing past environmental conditions in North Africa, validating climate models, and assessing feedbacks between vegetation, orbital forcing, SSTs, and precipitation. Furthermore, human migration events have often been linked to climatic change (Behrensmeyer, 2006), and the dynamic shifts that occurred in continental Africa between desert, grassland, and woodland environments likely have influenced hominin and faunal migration patterns.

Past Vegetation Shifts in the Central Sahara/Sahel Region

To better understand past vegetation changes in the Sahara/Sahel region, we studied marine sediment core GeoB9528-3 (09°09.96'N, 17°39.81'W; 3,057-m water depth) retrieved from the Guinea Plateau Margin, spanning the last 192 ka (SI Text and Fig. S7.1). This site receives dust from central North Africa near the boundary of the Sahara with the Sahel (Fig. 7.1 and SI Text), which is transported westward by the African Easterly Jet (AEJ), and thus serves as an excellent recorder of past vegetation changes in the central Sahara/Sahel region. We measured the carbon isotopic composition ($\delta^{13}\text{C}$) of long-chain *n*-alkanes with 29 (C_{29}) and 31 (C_{31}) carbon atoms (the two most abundant homologues) derived from plant leaf waxes, which are preserved in marine sediments and provide information on the relative contribution from C_3 and C_4 plants. The C_3 photosynthetic pathway is the most common and is used by nearly all trees, cool-season grasses, and cool-season sedges, whereas C_4 photosynthesis is used by warm-season grasses and sedges. African vegetation consists primarily of C_4 grasses and C_3 shrubs and trees (Still et al., 2003; Lloyd et al., 2008). In tropical Africa, aridity is recognized as the dominant control on the large-scale distribution of C_3 versus C_4 vegetation

on longer time scales (Scheffuß et al., 2003). C_4 plants are enriched in $\delta^{13}C$ compared with C_3 plants; thus, past changes in African continental hydrology can be inferred from the n -alkane $\delta^{13}C$ record (Scheffuß et al., 2003). Our record shows substantial changes of $>5\text{‰}$ in both $\delta^{13}C_{29}$ and $\delta^{13}C_{31}$ over the last 192 ka, suggesting large scale changes in vegetation (Fig. 7.2). The $\delta^{13}C$ of n -alkanes can be used to estimate the percentage of C_4 vegetation contribution to each n -alkane based on binary mixing models that assume C_{29} end-member values of -34.7‰ (-35.2‰ for C_{31}) and -21.4‰ (-21.7‰ for C_{31}) for C_3 and C_4 vegetation, respectively (see SI Text and Tables S7.1 and S7.2). We note, however, that there is likely a considerable error associated with the absolute $\%C_4$ estimates (maximum error estimated at $\pm 20\%$; see SI Text) because of uncertainty in the end-member values. Nevertheless, these uncertainties do not affect interpretation of the general trends where relatively enriched (depleted) n -alkane $\delta^{13}C$ values indicate increased (decreased) inputs from C_4 plants. Thus, the overall trends in the n -alkane $\delta^{13}C$ records provide important information on past vegetation shifts in central North Africa.

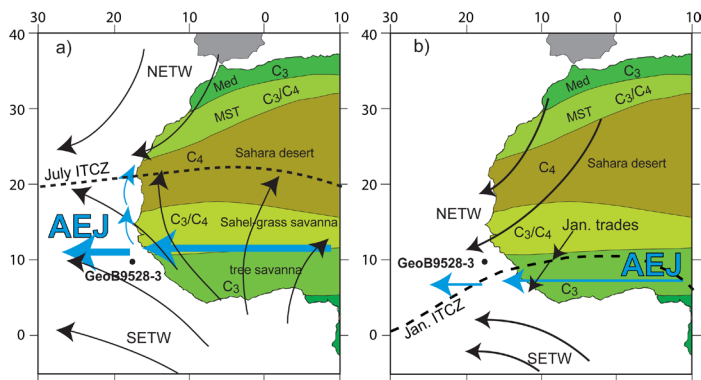


Fig. 7.1: Location of gravity core GeoB9528-3 offshore Guinea and modern vegetation zones of Northwest Africa (White, 1983). From north to south the main vegetation zones are Mediterranean (MED) (C_3 dominated), Mediterranean–Saharan transitional (MST) (mixed C_3 and C_4 plants), Sahara desert (C_4 dominated), Sahel-grass savanna (mixed C_3 and C_4 plants), and tropical rainforest (C_3 dominated). Three main wind systems influence the region of Northwest Africa, the Northeast trade winds (NETW), the Southeast trade winds (SETW), and the AEJ (also known as the Saharan Air Layer), and transport dust and plant leaf waxes from the African continent to the Atlantic. The NETW and the SETW converge at the Intertropical Convergence Zone (ITCZ; the meteorological equator). (a) During Northern Hemisphere summer, when the ITCZ is located at its most northerly position (surface expression at $\sim 20^\circ\text{N}$), the SETW are strongest and dust sourced in the Sahara and the Sahel is raised by easterly winds into the mid-altitude flow (~ 3 km) of the AEJ and transported beyond the continental margin between 10°N and 25°N . The AEJ is strongest during Northern Hemisphere summer when it is located at 10 – 12°N (Nicholson and Grist, 2003). (b) In Northern Hemisphere winter, the ITCZ migrates southwards ($\sim 5^\circ\text{N}$) and the NETW are dominant. The AEJ is weaker in Northern Hemisphere winter and is located at ~ 0 – 5°N (Nicholson and Grist, 2003). At this time, dust in the southern Sahara (the

alluvial plains of Niger, Chad, and Faya Largeau) is uplifted by the low-altitude (500–1,500 m) NETW and deposited along wide areas off Africa between 2°N and 15°N (Huang et al., 2000a), with the main axis of the dust plume located at ~5°N. The Gulf of Guinea receives material sourced in the southern Sahara during Northern Hemisphere winter, which is transported over long distances and deposited offshore.

Plant leaf waxes (*n*-alkanes) can be transported to marine sediments by wind or water; however, fluvial transport is not likely at site GeoB9528-3 because the coring site is located offshore with no major rivers close by (SI Text). No major latitudinal shift of the wind belts occurred between the Last Glacial Maximum (LGM) and the present (Sarnthein et al., 1981); although wind strength varied in the past (Sarnthein et al., 1981; Grousset et al., 1998), the direction of the AEJ remained constant (Grousset et al., 1998) as did the geologic source terrane for terrigenous sediments to Northwest Africa (Cole et al., 2009). Thus, the direction of the AEJ likely remained constant during previous glacial and interglacial periods and the *n*-alkane record of GeoB9528-3 provides a continuous vegetation record of the Sahara/Sahel region. Furthermore, we note that the uppermost sample of GeoB9528-3 (~7 ka) has a $\delta^{13}\text{C}_{29}$ value of -27.6‰, which is in good agreement with surface sediments collected offshore Northwest Africa from 9–12°N latitude, which have $\delta^{13}\text{C}_{29}$ values of -27‰ to -27.5‰ and are thought to be derived from dust from the Sahel/Sahara region (Huang et al., 2000a).

During the past 200 ka, the *n*-alkane $\delta^{13}\text{C}$ records of GeoB9528-3 indicate great variability with a contribution of 39–78% C_4 plants to the C_{29} *n*-alkane and a contribution of 54–99% C_4 plants to the C_{31} *n*-alkane (Fig. 7.2). Our data show that for the majority of the past 192 ka, central North Africa was dominated by C_4 vegetation, indicating arid conditions similar to or even more severe than at present (Fig. 7.2). However, several pronounced periods of increased contributions of C_3 vegetation are observed in the early Holocene, within Marine Isotope Stage (MIS) 3 (~50–45 ka) and during MIS 5 (~120–110 ka). The expansion of C_3 plants during the early Holocene coincides with the African Humid Period (AHP) when the Sahara was vegetated (deMenocal et al., 2000; Kuper and Kröpelin, 2006), supporting the idea that our record reflects vegetation in the Sahara/Sahel region. Remarkably, two intervals within MIS 5 and MIS 3 are characterized by even greater contributions of C_3 vegetation compared with the AHP. The distribution of C_3 and C_4 vegetation in tropical Africa strongly depends on precipitation (Scheffuß et al., 2003). Thus, the episodic expansions of C_3 vegetation in our record likely reflect wetter conditions in the Sahel/Sahara region, whereas dominance of C_4 plants, indicated by enriched *n*-alkane $\delta^{13}\text{C}$ values, reflect arid conditions such as those of the present day. Although wet conditions during MIS 3 are not captured by grain size records from offshore Mauritania (Tjallingii et al., 2008), this site is not situated directly under the path of the AEJ and likely does not capture the climate signal from further inland. In contrast, GeoB9528-3 is situated underneath the AEJ, and our *n*-alkane record also is a direct indicator of continental vegetation. Higher C_4 contributions are noted throughout much of MIS 6 and during MIS 4, and at these times cooler U_{37}^{K} -based SSTs are observed (Fig. 7.2), consistent with previous studies of tropical Africa that found increased abundances of

C₄ vegetation, and thus arid conditions, at times when cool SSTs were present in the tropical Atlantic (Scheffuß et al., 2003). In comparison with the AHP, conditions were relatively more arid during the LGM, but LGM aridity was not nearly as severe as conditions during MIS 6 and MIS 4 (Fig. 7.2).

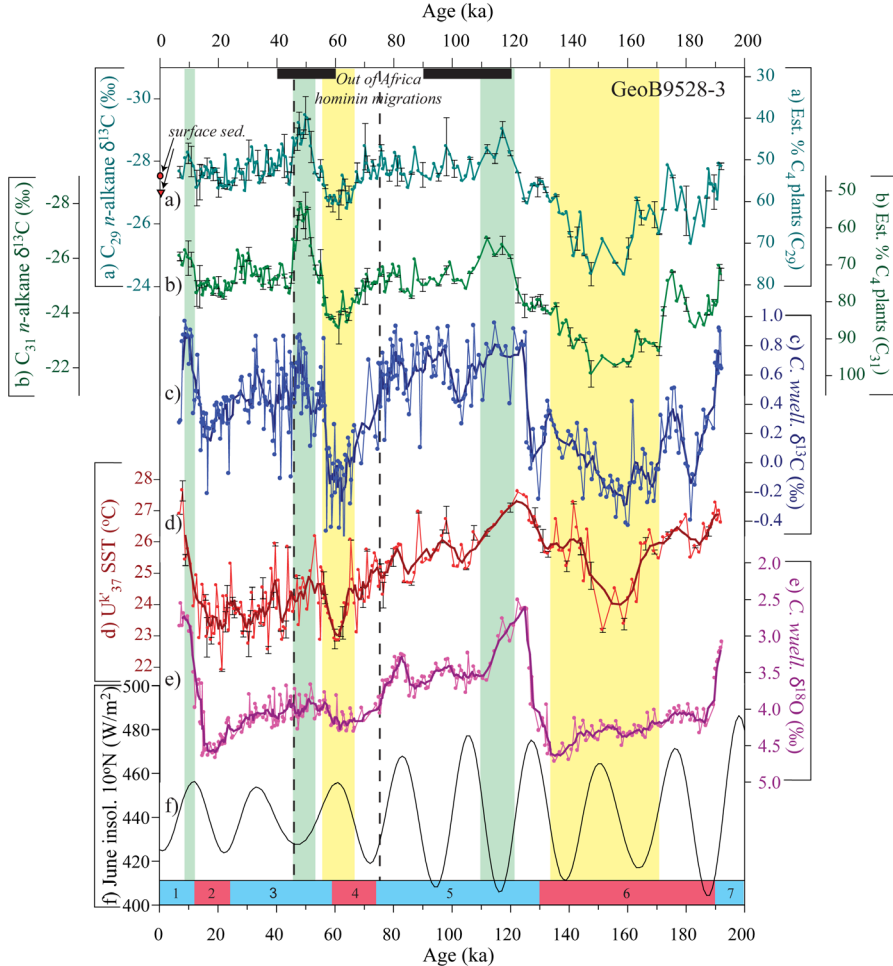


Fig. 7.2: Geochemical records from GeoB9528-3. In traces c–e, the thick line represents the smoothed data (five-point running mean). In traces a, b, and d, the error bars represent the standard deviation of replicate analyses. All isotope data are reported in standard delta notation (‰) against the VPDB standard. The black bars at the top of the graph indicate documented human migrations out of Africa (Stringer, 2000; Osborne et al., 2008). The vertical dashed lines indicate periods of major extinctions and turnovers of hominin populations at ~75 and ~45 ka (Shea, 2008). Wet intervals during the AHP, within MIS 3 and during MIS 5 are indicated by green shading. Arid intervals during MIS 6 and MIS 4 are indicated by yellow shading. The bar at the bottom indicates MIS 1–7. Trace a shows carbon isotope ($\delta^{13}\text{C}$) values of the C₂₉ *n*-alkane. On the right side of the graph, the estimated %C₄ plants is shown for the C₂₉ *n*-alkane, based on a binary mixing model assuming end-member values of -34.7‰ and

-21.4‰ for C₃ and C₄ vegetation, respectively. On the left side of the graph, δ¹³C values of C₂₉ *n*-alkanes in surface sediments collected in the vicinity of GeoB9528-3 are shown. The red circle represents a δ¹³C value of -27.5‰ for site GIK16757-1 (8°58.60 N, 16°56.48 W) and the red triangle represents a δ¹³C value of -27‰ found at sites GIK16405-1 (12°25.37 N, 21°25.37 W) and GIK16408-2 (9°47.88 N, 21° 27.24W) (Huang et al., 2000a). Trace b shows δ¹³C values of the C₃₁ *n*-alkane. On the right side of the graph, the estimated %C₄ plants is shown for the C₃₁ *n*-alkane, based on a binary mixing model assuming end-member values of -35.2‰ and -21.7‰ C₃ and C₄ vegetation, respectively. Trace c shows the δ¹³C of the benthic foraminifer *C. wuellerstorfi*. The precision of these measurements is ±0.05‰ based on replicates of an internal limestone standard. Trace d shows alkenone (U^K₃₇) SST reconstruction for GeoB9528-3 (see SI Text for methods). Trace e shows the δ¹⁸O of the benthic foraminifer *C. wuellerstorfi*. The precision of these measurements is ±0.07‰ based on replicates of an internal limestone standard. Trace f shows June insolation at 10°N (Berger and Loutre, 1991).

Causal Mechanisms for Vegetation Change and Hydrological Variability in Central North Africa

Several mechanisms can be invoked to explain the apparent episodic expansion (contraction) of C₃ (C₄) vegetation in the Sahara/Sahel region. Numerous studies have documented the influence of orbital forcing on North African climate and humid conditions during the AHP and MIS 5, which coincide with periods of maximum northern low-latitude summer insolation (Kutzbach and Street-Perrott, 1985; deMenocal et al., 2000; Tjallingii et al., 2008). However, the likely wettest intervals of our *n*-alkane δ¹³C records, at ~120–110 and 50–45 ka, both coincide with relatively low values of summer insolation (Berger and Loutre, 1991) and it is only during the AHP that maximum summer insolation and wet conditions are observed (Fig. 7.2).

For shorter, millennial-scale climate changes, several recent studies have shown that a reduction in the strength of Atlantic meridional overturning circulation (AMOC, which transports warm upper waters to the north and returns cold, deep water to the south) may trigger arid events in North Africa (Mulitza et al., 2008; Tjallingii et al., 2008). This process may also play a role in the observed longer-term vegetation changes. The proposed mechanism by which changes in AMOC control hydrological conditions in North Africa is related to the position of the monsoonal rain belt over the African continent. Weakening of AMOC, which can be triggered by freshwater input from the high latitudes (Chang et al., 2008; Chiang et al., 2008), leads to reduced deep-water formation rates in the North Atlantic (McManus et al., 2004). AMOC weakening also causes SST cooling in the North Atlantic region (Chang et al., 2008; Chiang et al., 2008) and is accompanied by a strengthening of the combination with advection of cold air from the high latitudes, causes a southward shift of the North African monsoonal rain belt (Chiang et al., 2008; Mulitza et al., 2008), leading to drying in North Africa. It is hypothesized that intensification of the AEJ occurs in conjunction with a southward shift of the monsoonal rain belt, driven by the meridional temperature gradient between the Sahel and the cool Guinea coast, resulting in increased moisture transport from the African continent (Mulitza et al., 2008).

We examined the impact of AMOC on the distribution of C_3 and C_4 vegetation in the Sahara/Sahel region by comparing the n -alkane $\delta^{13}C$ records to the $\delta^{13}C$ of the benthic foraminifer *Cibicidoides wuellerstorfi*, hereafter referred to as $\delta^{13}C_{\text{benthic}}$. Although ^{13}C is a nutrient proxy, it is known that $\delta^{13}C$ minima coincide with reductions in AMOC strength in the deep North Atlantic (McManus et al., 2004) and thus $\delta^{13}C_{\text{benthic}}$ primarily is a measure of the strength of AMOC and deep-water ventilation (Duplessy and Shackleton, 1985; Vidal et al., 1997). Throughout the past 200 ka, a remarkably close correlation is observed between $\delta^{13}C_{\text{benthic}}$ and the n -alkane $\delta^{13}C$ records (Fig. 7.2, SI Text, and Fig. S7.2), indicating a strong connection between variability in AMOC strength and vegetation type in the Sahara/Sahel region. More enriched $\delta^{13}C_{\text{benthic}}$ values, suggesting increased AMOC strength and a relatively stronger influence of North Atlantic deep water (NADW) at the study location, correlate with expansions of C_3 vegetation, whereas more depleted $\delta^{13}C_{\text{benthic}}$ values, suggesting a relatively weaker AMOC, correlate with expansions of C_4 vegetation (Fig. 7.2). Links between the strength of AMOC and millennial scale arid events have been observed in a sedimentary record from offshore Mauritania (Tjallingii et al., 2008), whereas slowdowns of AMOC are observed to trigger droughts in the Sahel during Heinrich events (Mulitza et al., 2008; Carto et al., 2009). Interestingly, our data suggest that the strength of AMOC is a dominant influence on hydrological conditions in the Sahara/Sahel over longer time scales (Fig. 7.2). Maximum NADW formation is observed during stage 5d (Duplessy and Shackleton, 1985), which supports a link between overturning circulation and vegetation type in the Sahara/Sahel region, and may also explain why the greatest inputs of C_3 vegetation do not coincide with summer insolation maxima.

Wet Conditions in the Central Sahara/Sahel and Hominin Migrations Out of Africa

The influence of AMOC on vegetation type in North Africa is of particular interest because this region may have played a key role in the dispersal of anatomically modern humans, which originated in sub-Saharan Africa at ~195 ka (McDougall et al., 2005), into Europe and Southwest Asia (Stringer, 2000). A major dispersal period occurred between 130 and 100 ka (Stringer, 2000; Osborne et al., 2008), which coincides with a major expansion of C_3 vegetation from ~120–110 ka (Fig. 7.2), and thus wetter conditions in the Sahara region, supporting the hypothesis that the Sahara could have provided a dispersal route out of Africa (Osborne et al., 2008). Our interpretation is supported by other paleoclimate evidence and climate models suggesting a significant expansion of wetter conditions in the Sahara from 130 to 120 ka (Gaven et al., 1981; deNoblet et al., 1996; Rohling et al., 2002; Armitage et al., 2007; Osborne et al., 2008). When the S5 sapropel was deposited in the Mediterranean Sea (~124–119 ka), fossil rivers in the Libyan and Chad basins of North Africa were active and provided northward drainage routes for precipitation delivered to central Saharan mountain ranges (Rohling et al., 2002). In addition, recent evidence suggests that an uninterrupted freshwater corridor existed from the central Sahara to the Mediterranean from 130 to 117 ka (Osborne et al., 2008).

The most depleted n -alkane $\delta^{13}C$ values of the entire record are noted within MIS 3, from

~50–45 ka (Fig. 7.2), suggesting a major expansion of C_3 plants. Interestingly, this interval coincides with a second major dispersal period of hominins out of Africa, dated to ~60–40 ka, mainly based on studies of mtDNA (Stringer, 2000; Forster et al., 2001; Mellars, 2006). Additionally, mtDNA evidence suggests that a back migration into Africa from southwestern Asia occurred at ~45–40 ka, and it is thought that this event resulted from a climatic change that allowed humans to enter the Levant (Olivieri et al., 2006). Thus, as with the first out of Africa migration during MIS 5, our data suggest that a second period of hominin migration at ~60–40 ka may have been facilitated by amenable climate conditions in the central Sahara. This interpretation is supported by paleoclimate evidence suggesting that groundwater recharge occurred in the northern Sahara during MIS 3 (Zuppi and Sacchi, 2004) while a Ba/Ca record from the Gulf of Guinea displays increased values at ~55 ka, suggesting less saline surface waters (Weldeab et al., 2007). Furthermore, in the Eastern Mediterranean Levant region there is evidence for extinctions and turnovers of hominin populations at ~75 and ~45 ka, and these events are hypothesized to be caused by shifts to cooler and more arid conditions (Shea, 2008). The n -alkane $\delta^{13}\text{C}$ records indeed provide strong evidence for shifts to relatively more arid conditions, indicated by expansions of C_4 vegetation, initiating at ~75 and ~45 ka, suggesting that similar climate patterns prevailed in both the central Sahara and the Levant regions.

Overall, our results show that variability in the strength of AMOC played a key role in the evolution of climatic conditions in central North Africa during the last 200 ka. Amenable conditions in the central Sahara that were capable of supporting C_3 vegetation existed only during discrete and relatively brief time intervals when enhanced AMOC may have triggered vegetation change, thereby playing a crucial role in driving hominin migrations.

Materials and Methods

Core GeoB9528-3 was sampled at 5-cm intervals for molecular isotopic analyses. Freeze-dried sediment samples were extracted with a DIONEX Accelerated Solvent Extractor (ASE 200) using a solvent mixture of 9:1 dichloromethane (DCM) to methanol (MeOH). After extraction, a known amount of the internal standard squalane was added and the extract was separated into apolar, ketone, and polar fractions via alumina pipette column chromatography using solvent mixtures of 9:1 (vol/vol) hexane/DCM, 1:1 (vol/vol) hexane/DCM, and 1:1 (vol/vol) DCM/MeOH, respectively. Compound-specific $\delta^{13}\text{C}$ analyses were performed on the aliphatic fraction with an Agilent 6800 GC coupled to a ThermoFisher Delta V isotope ratio monitoring mass spectrometer. Isotope values were measured against calibrated external reference gas. The $\delta^{13}\text{C}$ values for individual compounds are reported in the standard delta notation against the Vienna Pee Dee Belemnite (VPDB) standard. A total of 81 of the 193 samples analyzed were run in duplicate or triplicate with a reproducibility of on average 0.24‰ for the C_{29} n -alkane and 0.18‰ for the C_{31} n -alkane. The average reproducibility of the squalane internal standard was 0.15‰ ($n=288$). Methods describing the $\delta^{18}\text{O}$ and $\delta^{13}\text{C}$ analyses of *C. wuellerstorfi* can be found in Mulitza et al. (2008), and

methods describing the U^{K'}₃₇ SST analyses can be found in SI Text.

Acknowledgments

We thank Marianne Baas, Jort Ossebaar, and Michiel Kienhuis for assistance with the organic geochemical and isotopic analyses; Monika Segl and Christina Kämmler for assistance with the foraminiferal isotope analyses; two anonymous reviewers for detailed comments that improved this manuscript; and members of the University of Bremen Geosciences Department and the Center for Marine Environmental Sciences for samples from GeoB9528-3. This work was supported by Netherlands Bremen Oceanography 2. E.S. and S.M. are supported by the Deutsche Forschungsgemeinschaft Research Center/Excellence Cluster “The Ocean in the Earth System.”

Supporting Information

SI Text

Age Model of GeoB9528-3. The age model of GeoB9528-3 was constructed by visual correlation of the benthic foraminifer *C. wuellerstorfi* $\delta^{18}\text{O}$ record with the $\delta^{18}\text{O}$ records of marine sediment core MD95-2042 (Shackleton et al., 2004) and the global benthic $\delta^{18}\text{O}$ stack of Lisiecki and Raymo (2005). The software package AnalySeries 1.1 (Paillard et al., 1996) was used to perform peak-to-peak correlation, which was done on the smoothed (five-point running mean) $\delta^{18}\text{O}$ records. The $\delta^{18}\text{O}$ record of GeoB9528-3 was first correlated to the record of MD95-2042 (Shackleton et al., 2004) in the time interval spanning from 0 to ~140 ka, and the older part of the record was correlated to the global benthic stack (Lisiecki and Raymo, 2005) in the time interval from ~140 to 192 ka (Fig. S7.1). The benthic $\delta^{18}\text{O}$ record of GeoB9528-3 exhibits a close correlation with both the records of MD95-2042 (Shackleton et al., 2004) ($R^2 = 0.91$) and the global benthic stack (Lisiecki and Raymo, 2005) ($R^2 = 0.93$) (Fig. S7.1), attesting to the strength to the chronology.

Long-Chain *n*-Alkane $\delta^{13}\text{C}$ Values for C_3 and C_4 Plants. To estimate the past contribution of C_3 and C_4 vegetation to the different *n*-alkanes, we compiled a list of *n*-alkane $\delta^{13}\text{C}$ values reported for C_3 and C_4 plants in the literature (Table S7.1 and Table S7.2) (Collister et al., 1994; Chikaraishi and Naraoka, 2003; Bi et al., 2005; Rommerskirchen et al., 2006). The mean values of C_{29} *n*-alkanes are -34.7‰ ($n = 50$) and -21.4‰ ($n = 49$) for C_3 and C_4 plants, respectively. The mean values of C_{31} *n*-alkanes are -35.2‰ ($n = 52$) and -21.7‰ ($n = 50$) for C_3 and C_4 plants, respectively. We use these mean end-members for C_3 and C_4 plants to create a binary mixing models to estimate the contribution of C_4 plants to the C_{29} and C_{31} *n*-alkanes, respectively. There is likely substantial error associated with the ‰C_4 estimates. The largest *n*-alkane $\delta^{13}\text{C}$ standard deviation of 2.6, which is reported for the C_{29} and C_{31} *n*-alkanes of C_3 plants (Table S7.1 and Table S7.2), translates to a maximum error estimate of

$\pm 20\%$ C_4 plants. However, for the purpose of our study, the overall trends in the n -alkane $\delta^{13}C$ records are more important than the $\%C_4$ estimates because relatively enriched (depleted) n -alkane $\delta^{13}C$ values indicate increased (decreased) inputs from C_4 plants. Therefore, shifts to relatively enriched or depleted n -alkane $\delta^{13}C$ values provide important information on past vegetation shifts in central North Africa.

A Dust Source for Long-Chain Odd-Numbered n -Alkanes. Long-chain, odd-numbered n -alkanes (C_{25} – C_{35}) are a main component of plant epicuticular leaf waxes (Eglinton and Hamilton, 1967), and these compounds are generally well preserved in sediments. The carbon isotopic composition of n -alkanes can be used to distinguish between plants using the different photosynthetic pathways because C_4 plants, such as warm-season grasses, possess a CO_2 concentrating mechanism, which causes them to be isotopically enriched in ^{13}C compared with C_3 plants, which include most trees, cool-season grasses, and sedges. A third photosynthetic pathway, the CAM pathway, has isotopic values intermediate between those of C_3 and C_4 plants but CAM plants are not a significant component of northwest African vegetation (Winter and Smith, 1996).

Although long-chain n -alkanes are produced by higher plants, these compounds are also found in petroleum. However, the n -alkane carbon preference index (CPI) (Bray and Evans, 1961), which is used to examine odd over even carbon number predominance, can be used to distinguish terrestrial plant from petroleum sources. Terrestrial plants are characterized by CPIs of >3 , whereas mature hydrocarbons have CPIs of ~ 1 (Bray and Evans, 1961). Core GeoB9528-3 is characterized by high CPI values, which range from 3.5 to 8.3 with a mean value of 6.2, indicating a source from terrestrial higher plants throughout the entire record (Eglinton and Hamilton, 1967).

Plant leaf waxes (n -alkanes) can be transported to marine sediments by wind or water (runoff or riverine inputs); however, fluvial transport is not likely at site GeoB9528-3. The coring site is located offshore on the continental slope with no major rivers in close vicinity. Furthermore, we analyzed core GeoB9528-3 for branched glycerol dialkyl glycerol tetraethers (GDGTs), which are lipids produced by soil bacteria that are transported solely by runoff/riverine input (Weijers et al., 2007). However, branched GDGTs were not detected in GeoB9528-3. Thus, the main supply of n -alkanes to GeoB9528-3 is via wind erosion.

Origin of Dust and Associated Leaf Wax n -Alkanes Transported to Site GeoB9528-3.

The main source of n -alkanes to site GeoB9528-3 is from the central Africa near the boundary of the Sahara with the Sahel (Fig. 7.1). Isotopic mapping of n -alkanes in dust (Schefuß et al., 2003a) and surface sediments (Huang et al., 2000a) collected off the coast of Northwest Africa supports this hypothesis. The isotopic pattern in surface sediments of Northwest Africa depends in the latitudinal distribution of vegetation and the transport pathways of the wind systems. Enriched n -alkane $\delta^{13}C$ values, indicating high C_4 contributions, are noted in both dust and surface sediments offshore Northwest Africa between ~ 0 and $10^\circ N$ (Huang et al.,

2000a; Schefuß et al., 2003a), although at this latitude the adjacent continent is covered by tree savanna or rainforest, which is C₃ dominated. This pattern is attributed to long-distance transport of Saharan dust to offshore Northwest Africa (Huang et al., 2000a; Schefuß et al., 2003a). Modeling of backwards trajectories indicates that the dust reaching 10°N (near the location of GeoB9528-3) originates from central Africa near the boundary of the Sahara with the Sahel (Schefuß et al., 2003a). Thus, this region of central North Africa is likely the main source of *n*-alkanes to site GeoB9528-3.

Relationship Between $\delta^{13}\text{C}_{\text{benthic}}$ and *n*-Alkane $\delta^{13}\text{C}$. Throughout the past 200 ka, a significant negative linear relationship is observed between $\delta^{13}\text{C}_{\text{benthic}}$ and the *n*-alkane $\delta^{13}\text{C}$ records of GeoB9528-3 (Fig. S7.2; R²= -0.79 for the C₂₉ *n*-alkane and -0.82 for the C₃₁ *n*-alkane), indicating a strong association between AMOC strength and vegetation type in the Sahara/Sahel region.

Alkenone SST Estimates. Molecular identification of the C_{37:2} and C_{37:3} alkenones was performed on a Thermo Finnigan Trace Gas Chromatograph Ultra coupled to Thermo Finnigan DSQ mass spectrometer. A 25-m CP Sil-5 fused silica capillary column was used (25 m x 0.32 mm; film thickness= 0.12 μm) with helium as the carrier gas. The column was directly inserted into the electron impact ion source of the DSQ quadrupole mass spectrometer. Mass scans were made in the range of $m/z = 50\text{--}800$ with three scans per s and an ionization energy of 70 eV. The temperature program initiated at 70 °C, increased first at a rate of 20 °C per min to 130 °C, and next at a rate of 4 °C min to the final temperature of 320 °C, which was held for 10 min. For quantification, samples were analyzed on an HP 6890 GC using a 50-m CP Sil-5 column (0.32-mm diameter, film thickness of 0.12 μm) and helium as the carrier gas. The oven program initiated at 70 °C and increased by a rate of increased by 20 °C per min to 200 °C and next by a rate of 3 °C per min until 320 °C. The final temperature of 320 °C was held for 25 min. Compound concentrations were determined by relating chromatogram peak areas to the concentration of the internal standard. The U^K₃₇ Index, defined as $C_{37:2}/(C_{37:2} + C_{37:3})$, was used to estimate SSTs (Prah et al., 1988). U^K₃₇ values were converted to SSTs by using the core top calibration of Müller et al. 1998. Of the 193 samples analyzed, 74 were run in duplicate and 18 were run in triplicate. The reproducibility of these analyses is always better than $\pm 0.6^\circ\text{C}$.

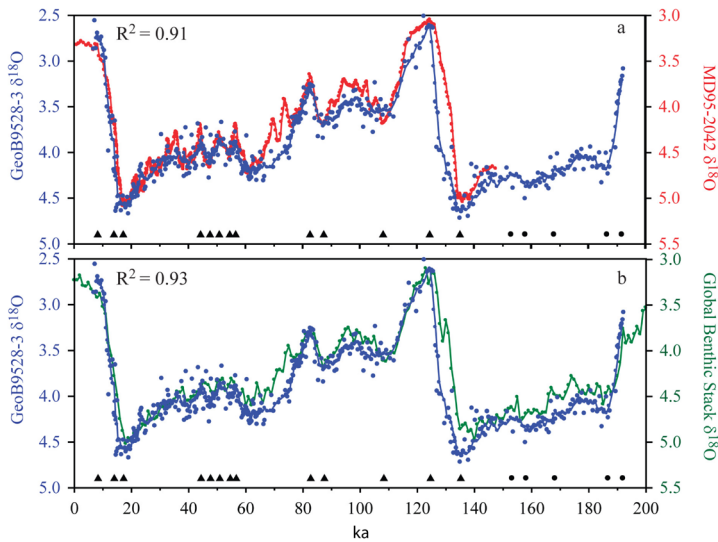


Fig. S7.1: Age model of Geob9528-3. The benthic (*C. wuellerstorfi*) $\delta^{18}\text{O}$ record of Geob9528-3 is shown in blue. The blue circles indicate all $\delta^{18}\text{O}$ measurements while the blue line represents the smoothed data (five-point running mean). The triangles at the bottom of the graph indicate the tie points to the benthic record of MD95-2042 (Shackleton et al., 2004), and the circles indicate the tie points to the global benthic stack (Lisiecki and Raymo, 2005). (a) Cross-correlation between the $\delta^{18}\text{O}$ records of Geob9528-3 and MD95-2042 (plotted in red) (Shackleton et al., 2004). (b) Cross-correlation between the $\delta^{18}\text{O}$ record of Geob9528-3 and the global benthic stack (plotted in green) (Lisiecki and Raymo, 2005).

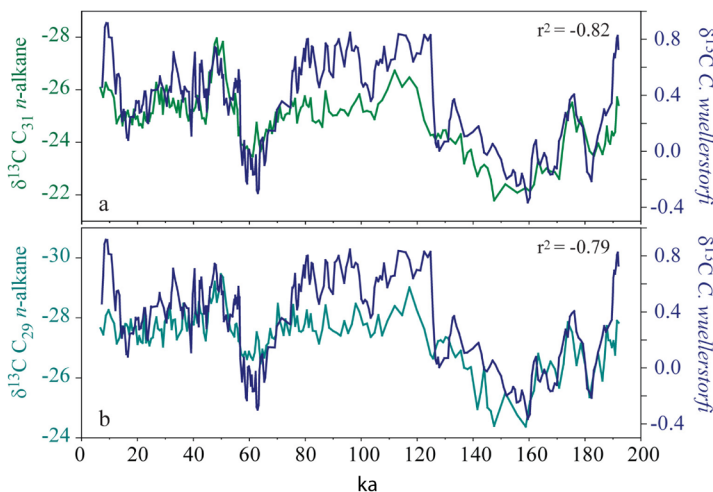


Fig. S7.2: Cross-correlation between the n -alkane $\delta^{13}\text{C}$ records and the $\delta^{13}\text{C}$ record of *C. wuellerstorfi* of Geob9528-3. The benthic (*C. wuellerstorfi*) $\delta^{13}\text{C}$ record of Geob9528-3 is shown in dark blue. In a, the $\delta^{13}\text{C}_{31}$ record is plotted in green, and in b, the $\delta^{13}\text{C}_{29}$ record is plotted in light blue.

Table S7.1: Carbon isotopic values ($\delta^{13}\text{C}$) of the C_{29} and C_{31} n -alkanes of C_3 plants

| Plant | Type | $\delta^{13}\text{C}_{29}$, $n = 50$ | $\delta^{13}\text{C}_{31}$, $n = 52$ | Ref. |
|--|------|---------------------------------------|---------------------------------------|------|
| <i>Psidium cattleionum</i> | C3 | -38.6 | -38.8 | 4 |
| <i>Jacobinia cornea</i> | C3 | -36.1 | -36.2 | 4 |
| <i>Cyperus diffusus</i> | C3 | -36.2 | -36.5 | 4 |
| <i>Dendrocalamus stricus</i> | C3 | -35.3 | -36.4 | 4 |
| <i>Cyprus alternifolius</i> | C3 | -34.2 | -35.3 | 4 |
| <i>Fagus sylvatica</i> | C3 | | | 4 |
| <i>Acer campestre</i> | C3 | -35.0 | -35.0 | 4 |
| <i>Magnolia delabayi</i> | C3 | -34.0 | -34.3 | 4 |
| <i>Quercus turneri</i> | C3 | -32.9 | -35.7 | 4 |
| <i>Quercus rober</i> | C3 | -36.4 | -36.9 | 4 |
| <i>Euphorbia pulcherrima</i> Willd. | C3 | -38.0 | -37.4 | 5 |
| <i>Codiaeum variegatum</i> (L.) Bl. Var. <i>pictum</i> M.-A. forma <i>crispum</i> Pax | C3 | | -35.1 | 5 |
| <i>Ficus altissima</i> Bl. | C3 | -33.9 | -36.1 | 5 |
| <i>Ficus microcarpa</i> Linn. f. | C3 | -31.0 | -33.4 | 5 |
| <i>Osmanthus fragrans</i> Lour. | C3 | -35.7 | -37.0 | 5 |
| <i>Kigelia africana</i> (am.) Benth. | C3 | -33.1 | -33.3 | 5 |
| <i>Syzygium cumini</i> (L.) Skeels | C3 | -37.2 | -35.5 | 5 |
| <i>Swietenia mahagoni</i> (L.) Jacq. | C3 | -34.1 | -35.9 | 5 |
| <i>Pistia stratiotes</i> | C3 | -36.6 | -37.1 | 5 |
| <i>Caryota mitis</i> Lour. | C3 | | -35.5 | 5 |
| <i>Cinnamomum burmanni</i> (Nees) Bl. | C3 | -33.3 | -37.2 | 5 |
| <i>Araucaria cunninghamii</i> Sweet | C3 | -30.1 | -30.5 | 5 |
| <i>Altemanthera dentata</i> 'Rubiginosa' | C3 | -36.6 | -37.2 | 5 |
| <i>Altemanthera versicolor</i> Regel | C3 | -36.7 | -37.5 | 5 |
| <i>Altemanthera bettzickiana</i> (Regel) Nichols | C3 | -36.5 | -37.2 | 5 |
| <i>Holmskioldia sanguinea</i> Retz. | C3 | -35.3 | -33.8 | 5 |
| <i>Quercus acutissima</i> | C3 | -34.7 | -34.8 | 6 |
| <i>Camellia sasanqua</i> | C3 | -31.3 | -33.1 | 6 |
| <i>Chamaecyparis obtusa</i> | C3 | -30.6 | -30.0 | 6 |
| <i>Pinus thunbergii</i> | C3 | -33.5 | -34.1 | 6 |
| <i>Colocasia esculenta</i> | C3 | -33.2 | -34.0 | 6 |
| <i>Lycoris radiata</i> | C3 | -28.0 | -28.4 | 6 |
| <i>Albizia julibrissin</i> | C3 | -35.9 | -37.8 | 6 |
| <i>Benthamidia japonica</i> | C3 | -36.5 | -36.5 | 6 |
| <i>Cryptomeria japonica</i> | C3 | -32.3 | -30.4 | 6 |
| <i>Acer carpiniifolium</i> | C3 | -35.5 | -35.4 | 6 |
| <i>Acer argutum</i> | C3 | -35.9 | -36.4 | 6 |
| <i>Phragmites communis</i> | C3 | -34.6 | -38.1 | 6 |
| <i>Benthamidia japonica</i> | C3 | -38.8 | -37.3 | 6 |
| <i>Prunus jamasakura</i> | C3 | -34.2 | -33.5 | 6 |
| <i>Cryptomeria japonica</i> | C3 | -32.9 | -32.5 | 6 |
| <i>Acer carpiniifolium</i> | C3 | -37.3 | -37.1 | 6 |
| <i>Acer argutum</i> | C3 | -35.6 | -36.0 | 6 |
| <i>Taraxacum officinale</i> | C3 | -37.0 | -36.4 | 6 |
| <i>Plantago asiatica</i> | C3 | -39.6 | -39.8 | 6 |
| <i>Artemisia princeps</i> | C3 | -36.5 | -35.2 | 6 |
| <i>Acer palmatum</i> | C3 | -40.5 | -41.8 | 6 |
| <i>Quercus mongolica</i> | C3 | -33.4 | -32.2 | 6 |
| <i>Quercus dentata</i> | C3 | -33.5 | -34.4 | 6 |
| <i>Manihot utilissima</i> | C3 | -30.8 | -32.0 | 6 |
| <i>Bromus</i> sp. | C3 | -35.7 | -36 | 7 |
| <i>Festuca orthophylla</i> | C3 | -30.3 | -31.3 | 7 |
| <i>Festuca orthophylla</i> | C3 | -31.2 | -32.2 | 7 |
| Average | | -34.7 | -35.2 | |
| SD | | 2.6 | 2.6 | |

Table S7.2: Carbon isotopic values ($\delta^{13}\text{C}$) of the C_{29} and C_{31} n -alkanes of C_4 plants

| Plant | Type | $\delta^{13}\text{C}_{29}$, $n = 49$ | $\delta^{13}\text{C}_{31}$, $n = 50$ | Ref. |
|---|------|---------------------------------------|---------------------------------------|------|
| <i>Saccharum officinarum</i> | C4 | -24.5 | -23.4 | 4 |
| <i>Miscanthus sacchariflorum</i> | C4 | -18.4 | -18.4 | 4 |
| <i>Zea mays</i> | C4 | | -20.5 | 4 |
| <i>Zea mays</i> (L) | C4 | -21.3 | -22.1 | 5 |
| <i>Amaranthus tricolor</i> (L) | C4 | -25.8 | -23.4 | 5 |
| <i>Amaranthus paniculatus</i> (L) | C4 | -25.4 | -22.9 | 5 |
| <i>Imperata cylindrica</i> var. <i>major</i> (Ness) C.E. Hubb | C4 | -21.0 | -19.2 | 5 |
| <i>Bothriochloa ischaemum</i> Keng | C4 | -21.0 | -22.1 | 5 |
| <i>Zoysia japonica</i> Stued | C4 | -24.1 | -23.4 | 5 |
| <i>Saccharum sinense</i> Roxb. | C4 | -15.3 | -16.7 | 5 |
| <i>Zea mays</i> | C4 | -20.9 | -21.7 | 6 |
| <i>Zoysia japonica</i> | C4 | -24.1 | -24.2 | 6 |
| <i>Miscanthus sinensis</i> (1) | C4 | -17.2 | -17.3 | 6 |
| <i>Saccharum officinarum</i> (1) | C4 | -20.6 | -20.7 | 6 |
| <i>Miscanthus sinensis</i> (2) | C4 | -17.5 | -18.6 | 6 |
| <i>Saccharum officinarum</i> (2) | C4 | -20.0 | -19.3 | 6 |
| <i>Sorghum bicolor</i> | C4 | -18.9 | -19.6 | 6 |
| <i>Aristida adscensionis</i> | C4 | -24.9 | -25.3 | 7 |
| <i>Aristida barbicollis</i> | C4 | -21.4 | -23.9 | 7 |
| <i>Aristida congesta</i> | C4 | -22.9 | -24.3 | 7 |
| <i>Aristida graciliflora</i> | C4 | -23.9 | -24.1 | 7 |
| <i>Aristida meridionalis</i> | C4 | -22.4 | -22.8 | 7 |
| <i>Aristida meridionalis</i> | C4 | -21.4 | -21.9 | 7 |
| <i>Stipagrostis ciliata</i> | C4 | -21.7 | -19.8 | 7 |
| <i>Stipagrostis hirtigluma</i> | C4 | -25 | -23.2 | 7 |
| <i>Stipagrostis uniplumis</i> | C4 | -24.5 | -25.9 | 7 |
| <i>Chloris gayana</i> | C4 | -22.5 | -23.4 | 7 |
| <i>Chloris virgata</i> | C4 | -19.6 | -20.2 | 7 |
| <i>Chloris virgata</i> | C4 | -20.6 | -21.7 | 7 |
| <i>Enneapogon</i> sp. | C4 | -23 | -22.7 | 7 |
| <i>Enneapogon cenchroides</i> | C4 | -19.4 | -20.9 | 7 |
| <i>Enneapogon cenchroides</i> | C4 | -18.3 | -20.1 | 7 |
| <i>Eragrostis nindensis</i> | C4 | -22.7 | -24.6 | 7 |
| <i>Eragrostis superba</i> | C4 | -20.8 | -21.8 | 7 |
| <i>Eragrostis tremula</i> | C4 | -25.1 | -25.9 | 7 |
| <i>Eragrostis violacea de winter</i> | C4 | -18.1 | -19.6 | 7 |
| <i>Eragrostis viscosa</i> | C4 | -19.6 | -21.8 | 7 |
| <i>Schmidtia kalahariensis</i> | C4 | -22 | -22.9 | 7 |
| <i>Sporobolus ioclados</i> | C4 | -21.8 | -22.4 | 7 |
| <i>Sporobolus pyramidalis</i> | C4 | -22 | -22.1 | 7 |
| <i>Bothriochloa insculpta</i> | C4 | -19.2 | -18.7 | 7 |
| <i>Brachiana erucitormis</i> | C4 | -20.4 | -20.9 | 7 |
| <i>Digitaria milaniana</i> | C4 | -18.9 | -19.5 | 7 |
| <i>Hyparrhenia filipendula</i> | C4 | -21.9 | -21.9 | 7 |
| <i>Loudetia simplex</i> | C4 | -18.6 | -18.2 | 7 |
| <i>Panicum</i> sp. | C4 | -22.6 | -23 | 7 |
| <i>Panicum arbusculum</i> | C4 | -22 | -24 | 7 |
| <i>Panicum maximum</i> | C4 | -20.8 | -19.4 | 7 |
| <i>Panicum maximum</i> | C4 | -24.2 | -24.5 | 7 |
| <i>Themeda triandra</i> | C4 | -21.3 | -19.6 | 7 |
| Average | | -21.4 | -21.7 | |
| SD | | 2.4 | 2.3 | |

Chapter 8

A novel method for the rapid analysis of levoglucosan in soils and sediments

Ellen C. Hopmans, Raquel A. Lopes dos Santos, Annelieke Mets, Jaap S. Sinninghe Damsté, Stefan Schouten

In revision for *Organic Geochemistry*

Abstract

We have developed a novel method, based on high performance liquid chromatography-mass spectrometry, for the rapid and quantitative analysis of levoglucosan in geological samples. Compared with previous methods it does not require derivatization or extensive work up. The validity of the method is demonstrated by application to soil samples collected from a burned dune area and a late Quaternary marine sediment.

8.1 Introduction

Biomass burning has a large impact on vegetation on land and is also a significant source of aerosol particles, which can have a significant impact on global climate (e.g. Crutzen and Andrea, 1990). Biomass burning has been substantially increasing in industrial times due to human activity. However, in the geological past there have also been biomass burning events as a result of early human activity or natural causes (e.g. Bird and Cali, 1998).

There are several tracers for reconstructing past biomass burning events from ancient sediments and soils, including microscopic examination of charcoal or soot particles and the analysis of specific compounds like polycyclic aromatic hydrocarbons (e.g. Denis et al., 2012). An important compound generated during biomass burning of wood is levoglucosan (1,6-anhydro- β -D-glucopyranose; Simoneit, 2002 and references therein). It is specific for biomass burning as it is only generated by combustion of woody material, which contains sugars such as cellulose (e.g. Elias et al., 2001).

The most commonly used technique to quantitatively analyze levoglucosan, particularly in geological material, is gas chromatography-mass spectrometry (GC-MS) after derivatization to form e.g. trimethylsilyl derivatives (Schkolnik and Rudich, 2006 and references therein). However, the method is relatively time-consuming as it requires fractionation of the extract and appropriate derivatives, which can be labile on long term storage. In addition to GC-MS, some high performance liquid chromatography (HPLC) methods, combined with, amongst others, MS detection, have been developed. They do not require derivatization of levoglucosan (Schkolnik and Rudich, 2006 and references therein). In particular, Gambaro et al. (2008) developed a HPLC-electrospray ionization (ESI)-MS² method with a reportedly high sensitivity (detection limit 0.3 pg on column). However, the method was applied only to melted water from ice cores, which contain relatively little matrix vs. typical geochemical samples, while the applied LC separation technique gave virtually no retention for levoglucosan and thus no efficient separation capability.

We have developed a novel HPLC-MS² method for rapidly and quantitatively analyzing levoglucosan in complex sedimentary matrices and demonstrate its applicability for rapid analysis of soils and marine sediments.

8.2 Material and methods

Standards (levoglucosan, mannosan and galactosan) were from Sigma-Aldrich (St. Louis, MO). In 2011, soil samples were collected from a coastal dune area (52° 42.41' N; 4° 40.20' E) near the town of Schoorl, the Netherlands, where a large vegetation fire occurred in 2009. Finally, a marine sediment was taken from core MD03-2607 (36° 57.64' S; 137° 24.39' E) from the Murray Canyons area, offshore southeast Australia at 250 cm below sea floor and dated at 20.4 ka (Gingele and De Deckker, 2005).

The samples were freeze-dried, homogenized and extracted with MeOH, using an automated solvent extractor (ASE) 350, DIONEX at 100 °C and 1500 psi. In order to remove

salts from the marine sediment extract, it was dissolved in MeCN and filtered over a small 1 cm Na₂SO₄ Pasteur pipette column. Tests with soil extracts showed that this small column did not result in significant loss of levoglucosan, with an average recovery of 101 ± 8% (n=3). To evaluate the efficacy of different extraction solvents, one of the dune soil samples was extracted (3 x) with MeOH or dichloromethane (DCM):MeOH (9:1, v:v) using the above ASE conditions. Extracts were dissolved in MeCN containing 0.01% triethylamine (TEA) and filtered using a regenerated cellulose 0.45 mm filter (Alltech, Deerfield, IL).

The extracts were analyzed using an Agilent 1100 series LC instrument (Agilent, San Jose, CA) coupled to a Thermo TSQ Quantum ultra EM triple quadrupole mass spectrometer with an Ion Max Source with ESI probe (Thermo Electron Corporation, Waltham, MA) operated in negative ion mode. Separation was achieved with a Luna NH₂ column (150 mm × 2 mm i.d., 3 μm; Phenomenex, Torrance, CA) maintained at 25 °C. The compounds were eluted (0.2 ml min⁻¹) with an isocratic mixture of 92.5% A:7.5% B for 10 min followed by back-flushing with an isocratic mixture of 70% A:30% B for 20 min, and re-equilibration at starting conditions for 20 min. Eluent A was 0.01% TEA in MeCN and B 0.01% TEA in water. Detection of levoglucosan was achieved by selected reaction monitoring (SRM) and settings were optimized via direct infusion of a levoglucosan standard solution. ESI settings were: capillary temperature 300 °C, sheath gas (N₂) pressure 50 (arbitrary units), auxiliary gas (N₂) pressure 5 (arbitrary units) and spray voltage -4 kV. Argon (collision pressure 1 mTorr) was used as collision gas. SRM transitions monitored (collision energy in brackets) were *m/z* 161 (peak width Q1 0.2) to *m/z* 71 (15 V), *m/z* 85 (15 V), *m/z* 101 (12 V) and *m/z* 113 (11 V) (peak width Q3 0.7) with 0.1 s dwell time per transition.

Levoglucosan was quantified by integrating the peak area in the total ion chromatogram (addition of all transitions monitored) and comparison of the area with an external standard curve.

8.3 Results and discussion

We first optimized conditions for MS by infusion of a standard levoglucosan solution under negative ion ESI-MS conditions to confirm the suitability of the SRM transitions described by Gambaro et al. (2008), i.e. *m/z* 161 to *m/z* 71, 85, 101 and 113. We then developed a new separation method, based on hydrophilic interaction chromatography (HILIC). Under these conditions a retention time of 4.9 min for levoglucosan was obtained [vs. 1.5 min for Gambaro et al. (2008)], well removed from the injection peak and thus potentially more suitable for analysis of levoglucosan in geological samples with complex matrices. In addition, levoglucosan was separated from its structural isomers mannosan and galactosan (Fig. 8.1a). This allowed calculation of e.g. the ratio of levoglucosan/(mannosan+galactosan) which can potentially be diagnostic for the type of burned biomass, i.e. hardwood versus softwood and grass (e.g. Fabbri et al., 2009). Finally, the stability of the Luna NH₂ column up to pH 11 allowed direct modification of the mobile phase with TEA to pH 8-9 to enhance negative ion formation in the ESI source. The method therefore does not require post-column

addition of NH_4OH applied by Gambaro et al. (2008), making it relatively easier and more robust.

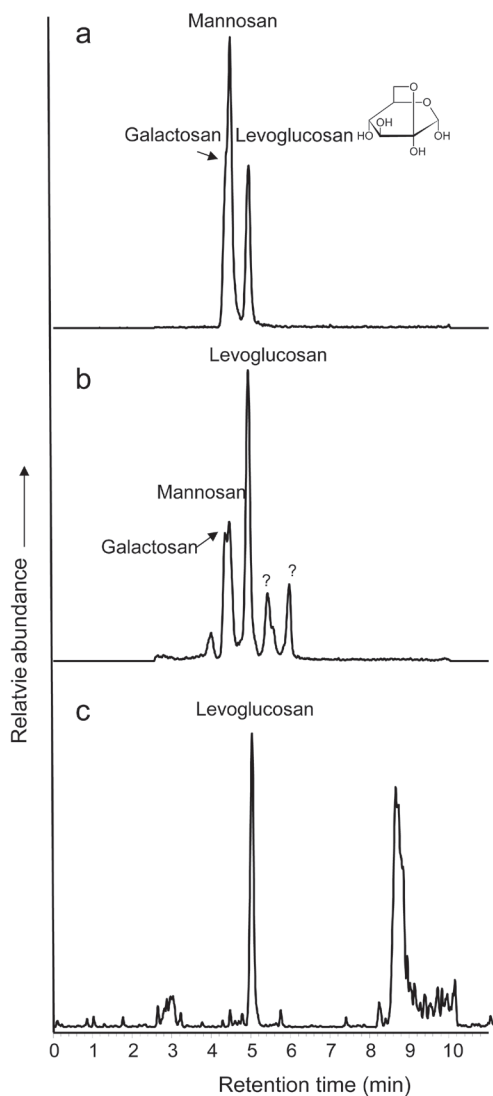


Fig. 8.1: HPLC-ESI-MS² total ion chromatogram of (a) standard mixture of levoglucosan, mannosan and galactosan, (b) MeOH extract of a soil from a burned dune area (c) MeOH extract of a 20.4 ka marine sediment from offshore southeast Australia (ESI spray switched on between 2.5 and 10 min).

The sensitivity of the method was tested by injection of varying amounts of levoglucosan to give a linear response between 0.05 and 5 ng on column ($r^2=0.99$) and a detection limit of ca. 25 pg on column. The method is therefore less sensitive than that of Gambaro et al. (2008), mainly due to the use of MeCN in the mobile phase instead of MeOH. Although

MeOH improves the ionization of levoglucosan, it substantially reduces retention on the column, so is not suitable for samples with a complex matrix. Nevertheless, the detection limit is better than that of GC-MS methods (ca. 100 pg injected on column; Simpson et al., 2004).

To evaluate suitable extraction solvents, we extracted a soil sample from a burned dune area likely to contain a high level of levoglucosan. We first tried extraction with MeOH, as it is commonly used for levoglucosan extraction (e.g. Elias et al., 2001). Indeed, levoglucosan was readily detected at a concentration of 2.62 ± 0.13 (n=3) $\mu\text{g g}^{-1}$ soil (Fig. 8.1b). We also evaluated DCM:MeOH (9:1), as this mixture is regularly used for ASE extraction of geochemical samples and DCM:MeOH has successfully been used for levoglucosan extraction from air filters (Pashynska et al., 2002). An identical concentration of 2.61 ± 0.28 $\mu\text{g g}^{-1}$ soil vs. MeOH extraction was obtained, so both extraction solvents seem equally suitable.

We then tested the method with an ancient sample, from a marine sediment from a core from the Murray Canyons area, offshore southeast Australia and dated at ca. 20.4 ka (Gingele and DeDecker, 2005). This area received dust from nearby Murray-Darling River Basin and thus potentially carries vegetation fire signals. Indeed, we detected levoglucosan (243 pg g^{-1} sediment; Fig. 8.1c), showing that our method is also suitable for analyzing fossilized levoglucosan in marine sediments.

8.4 Conclusions

We have developed a novel HPLC-MS² method for the measurement of levoglucosan in soils and sediments. The method is relatively rapid as it does not require extensive sample clean-up or derivatization, enabling rapid generation of high resolution records of levoglucosan, and therefore biomass burning, from sedimentary archives.

Acknowledgements

The Netherlands Organization for Scientific Research (NWO) is thanked for financial support through a VICI grant to S.S. The research received partial funding from the European Research Council under the European Union's Seventh Framework Program [FP7/2007-2013)/ERC grant agreement no. 226600].

Chapter 9

Abrupt vegetation change follows the late Quaternary megafaunal extinction in southeastern Australia

Raquel A. Lopes dos Santos, Patrick De Deckker, Ellen C. Hopmans, Anhelique Mets, Jaap S. Sinninghe Damsté and Stefan Schouten
In preparation

Abstract

A large megafaunal extinction occurred in Australia at 50-45 ka ago, possibly resulting from a sudden vegetation change due to anthropogenic burning. Recently, however, it was proposed that this sudden vegetation change may be the consequence rather than the cause of this extinction event. Here, we reconstruct past vegetation changes and biomass burning in southeastern Australia using the stable carbon isotopic composition of plant wax *n*-alkanes and the accumulation rates of levoglucosan, respectively, in marine sediments from the Murray Canyons Group area at a location offshore the mouth of the river system that drains the Murray-Darling Basin. An extensive period (68-31 ka) of generally high (60-70%) C₄ plant abundance was punctuated by a sharp decrease in C₄ vegetation (30%) at ~ 43 ka and increased levels of biomass burning. This interval directly followed the main period of human arrival and megafaunal extinction in Australia and lasted ~5 kyrs. It was likely caused by substantially reduced herbivory and/or increased burning events that allowed an increase in C₃ vegetation. This suggests human activity not only to be the driver of the megafaunal extinction but also as the cause of a major ecosystem shift in southeastern Australia.

9.1 Introduction

In Australia, ~90% of megafauna (animals > 40 kg) became extinct between 50 and 45 ka (Roberts et al., 2001; Grün et al., 2010), a period that coincides with the human colonization of Australia (~55-44 ka) (Bowler et al., 2003). However, the actual cause of this late Quaternary megafaunal extinction (LQME) is not clear and has been debated for over a century (Wilkinson, 1885; Prescott et al., 2012; Rule et al., 2012). Climate change has been suggested (Wroe and Field, 2006; Webb, 2008; Murphy et al., 2012) as a possible cause, but the arrival of humans is often inferred as the main driver of this extinction (Miller et al., 1999; 2005; Turney et al., 2008; Prideaux et al., 2007; 2009). Overhunting (Turney et al., 2008; Prideaux et al., 2009) and vegetation changes induced by extensive burning engendered by humans (Miller et al., 2005) are two anthropogenic mechanisms proposed as the driver of the LQME. Dietary reconstructions from the remains of one of these extinct megafauna species (*Genyornis newtoni*) suggest sudden vegetation changes towards an increase in C₃ plants as the cause of the extinction of these animals, which were adapted to an enriched C₄ plant diet (Miller et al., 2005). It has been suggested that the imposition of an aboriginal burning regime in Australia was one of the causes for these vegetation changes (Miller et al., 2005) since vegetation reorganization is commonly reported after anthropogenic fires (Jones, 1969; Stephens et al., 2007). However, it has been recently suggested that in northeastern Australia this sudden vegetation change followed the LQME rather than preceding it and is possibly a consequence of relaxation in herbivory that allowed the accumulation of new vegetation (Rule et al., 2012). The main uncertainty is the timing of vegetation change in Australia, as paleovegetation records from central and southeastern Australia are mainly based on pollen studies (Harle, 1997; Kershaw et al., 1991), reporting changes in a limited number of taxa and local regions, or stable carbon isotope composition of the remains of *Dromaius novaehollandiae* (emu) and *Genyornis newtoni* (Miller et al., 2005; Johnson et al., 1999), carrying uncertainties in the indirect dating (sand grains enclosing eggshells and eggshell organic matter) of the remains. A well-dated and continuous paleovegetation record is therefore needed to constrain the timing of vegetation change in Australia.

Here we reconstruct a continuous C₃-C₄ plant vegetation record based on stable carbon isotopic composition of long chain *n*-alkanes derived from plant leaf waxes and preserved in soils and sediments (Eglinton and Hamilton, 1967). We also reconstruct a biomass burning record based on the accumulation rates (AR) of levoglucosan, a biomarker exclusively produced by extensive burning of vegetation (Simoneit, 2002). We analyzed sediment core MD03-2607, recovered from the Murray Canyons Group region offshore southeastern Australia at 36°57.64'S, 137°24.39'E (Fig. 9.1) at 865 m water depth (Hill and De Deckker, 2004). This core is located offshore the mouth of the River Murray which links with the Darling River. Both rivers and their tributaries drain the large Murray Darling Basin (MDB) that covers 1.10⁶ km², reflecting a substantial part of southeast Australia that hosted many of the megafauna which became extinct.

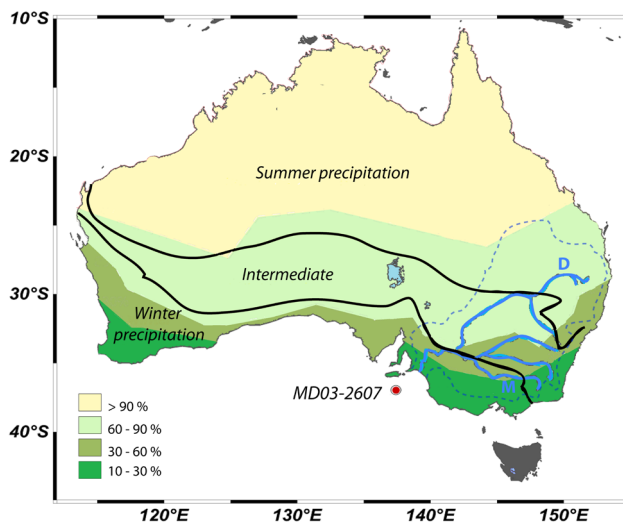


Fig. 9.1: Map of Australia illustrating the modern distribution of the vegetation cover in terms of percentages of C_4 grass relative to C_3 grass (colored areas reproduced from Hattersley, 1983) and the nature of precipitation, together with the location of core MD03-2607 offshore of the mouth of the River Murray. The blue lines show the River Murray (M) and Darling River (D) and their major tributaries. The dashed line represents the MD basin. The black continuous lines represent the approximate boundaries of areas influenced by summer and/or winter rainfall (reproduced from Magee et al., 2004).

9.2 Results and discussion

The age model of the sediment core is based on 22 ^{14}C dates of planktonic foraminifera, 13 optically stimulated luminescence (OSL) dates and cross correlation of the $\delta^{18}\text{O}$ record of planktonic foraminifera *Globigerina bulloides* tests with stacked isotope records (Gingele et al., 2004; Lopes dos Santos et al., 2012) (Fig. S9.1). To constrain the timing of vegetation changes recognized in the core, we obtained two additional ^{14}C dates of planktonic foraminifera from levels originally considered to have been deposited at 39.9 and 41.7 ka (by inference with the stacked isotope record of Lisiecki and Raymo (2005)), which returned calibrated ages of 36.8 ± 0.6 and 39.8 ± 0.8 ka using the Marine09.14c dataset in Calib.6 (Stuiver and Reimer, 1993; Reimer et al., 2009). These dates support the previously published age model considering the uncertainty in ^{14}C age reservoir and ^{14}C -age calendar conversion for such old sediments (see Table S9.1).

The C_{27} - C_{33} n -alkanes in core MD03-2607 show a high odd-over-even carbon number predominance (Carbon Preference Index ranging from 2 to 9) typical for n -alkanes derived from terrestrial land plants (Bray and Evans, 1961). They can in principle have been derived from aeolian input, mainly from central Australia or from riverine material transported by the river system draining the MDB (Gingele et al., 2004; 2007). The weighted average $\delta^{13}\text{C}$ value of the odd-numbered C_{27} - C_{33} n -alkanes in the most recent sediment sample of the core

is -28.4 ‰, a value that, when converted to % C₄ plants based on a binary mixing model with end-member values of -35.2‰ for C₃ and -21.7‰ for C₄ vegetation (Castañeda et al., 2009), corresponds to ~50% C₄ plants. The reconstructed percentage biomass should be interpreted with care as the end-members used in this study is an average of *n*-alkane isotopic values of vegetation from the all world and not specific for Australian vegetation. Furthermore, the reconstructed percentage reflects the contribution of C₄ to the *n*-alkanes pool which may be different from the actual vegetation as the amount of *n*-alkanes can vary with different vegetation types (Diefendorf et al., 2011). Nevertheless, our estimate, seems to reasonably reflect the average % C₄ grass species relative to C₃ grass for the central part of the MDB which varies from ~30 to ~60% (Fig. 9.1; based on Hattersley, 1983). In addition, the δ¹³C value compares reasonably well with δ¹³C values of the C₂₇-C₃₃ *n*-alkanes for contemporary soils collected from the central MDB (Fig. S9.2, Table S9.2), suggesting that the *n*-alkanes in the marine sediments are primarily derived from higher plant material from the MDB and transported by the river system. If aeolian transport would be the main source of sedimentary *n*-alkanes, a higher % C₄ plant would be expected since aeolian transport is typically from the dry central Australia which are predominantly C₄ grasses (Fig. 9.1). Additional support for southeastern Australia being the main source of *n*-alkanes comes from the good match (r²=0.4, P<0.001) between the AR of the *n*-alkanes and the Branched Isoprenoid Tetraether (BIT) index (Fig. 9.2c, d), a proxy for the input of river-borne soil organic matter in the marine environment (Hopmans et al., 2004; Kim et al., 2006), suggesting that the *n*-alkanes are mainly sourced from the MDB for most of the late Quaternary.

The δ¹³C record of the *n*-alkanes in the core (Fig. 9.2f) varies from -26 to -30 ‰ throughout the core and, when converted to % C₄ plant contributions, this corresponds to a variation from ~35-70 % of C₄ plant contribution throughout the past 135 ka. The highest percentage of C₄ plants is observed between 58-44 ka (Fig. 9.2f – yellow bar), a period that overlaps with human ‘colonization’ of Australia and the LQME. A higher percentage of C₄ plants during 65-45 ka has also been inferred from the stable carbon isotopic composition of eggshells from large fossil ratite birds from the southern margin of Lake Eyre (Johnson et al., 1999). This was interpreted as a signal of highly effective summer monsoonal rains, as in Australia, C₃ plants, including C₃ grasses, are more common in regions dominated by winter rainfall, whereas the abundance of C₄ grasses is linked to the intensity of the summer monsoonal precipitation (Fig. 9.1 - Johnson et al., 1999; Hattersley, 1983). Indeed, an expansion of humid conditions has also been recorded in the northeastern Australia from pollen studies during this period (Rule et al., 2012). Thus, assuming that summer precipitation controls C₄ vegetation abundance, our record suggests a more intense summer precipitation across the MDB during 58-44 ka. Interestingly, during the two coldest periods, at ~135 ka [=Marine Isotope Stage 6] and during the Last Glacial Maximum (LGM) at ~20 ka [=Marine Isotope Stage 2], a strong decrease in % C₄ plant contributions is recorded. A decrease in C₄ plants during the LGM was also found near Lake Eyre (Johnson et al., 1999), which these authors attributed to low temperatures and reduced summer monsoon precipitation. Indeed, if the

$\delta^{13}\text{C}$ record is representing a monsoon intensity signal, it may also reflect a weaker influence of the summer monsoonal rains and more arid periods during glacials. This is in agreement with other studies based on pollen analyses and modeling (Rule et al., 2012; Kershaw, 1986; Marshall and Lynch, 2006).

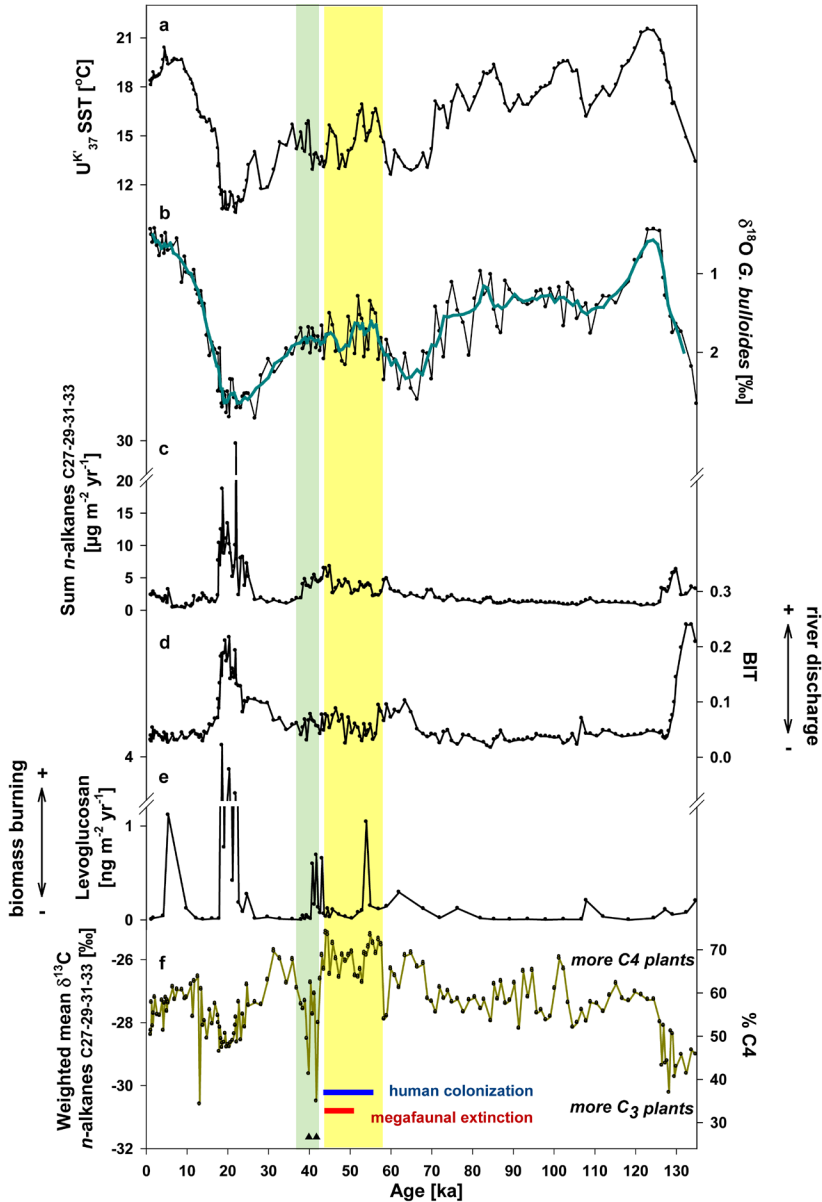


Fig. 9.2: Geochemical records from core MD03-2607. a) U^{K}_{37} SST (Lopes dos Santos et al., 2012); b) $\delta^{18}\text{O}$ of *G. bulloides* (Gingele et al., 2004; Lopes dos Santos et al., 2012), c) *n*-alkanes AR, d) BIT index, e) levoglucosan AR, and f) weighted average isotopic composition of C_{27} - C_{33} *n*-alkanes. The red

line indicates the main period of megafaunal extinction in Australia (Roberts et al., 2001), the blue line indicates the period of human arrival in Australia (Bowler et al., 2003). Black triangles show the two samples used for additional ^{14}C dating (see Table S9.1). Green and yellow shaded bars show the periods of sharp vegetation change and the period with the highest % of C_4 plants, respectively.

A sharp and temporary decrease in % C_4 plants is recorded between ~43-37 ka (Fig 9.2f – green bar). A sharp vegetation change around this time, with an increase of sclerophyll taxa and decrease of rainforest near Lynch's Crater, has also been reported in northeastern Australia (Rule et al., 2012), suggesting that the vegetation change was an event taking place over large parts of Australia. Furthermore giving the dating uncertainties, the shift in the $\delta^{13}\text{C}$ of the eggshells (Miller et al., 2005) may have been contemporaneous with the shift in $\delta^{13}\text{C}$ of the *n*-alkanes in this study and the vegetation change in northeastern Australia (Rule et al., 2012). In any case, our well-dated vegetation record clearly shows that vegetation change followed the LQME of 50-45 ka rather than being contemporaneous.

The observed abrupt and temporary vegetation change at ~43-37 ka in our record is not in line with the reconstructed changes in monsoonal rainfall intensity for central and northern Australia (Magee et al., 2004; van der Kaars and De Deckker, 2002). Additionally, this period was not characterized by a strong decrease in temperatures according to the $\delta^{18}\text{O}$ of planktonic foraminifera and U^{K}_{37} sea surface temperatures for our core (Fig. 9.2a, b) (Lopes dos Santos et al., 2012), assuming that the continental temperatures behaved in parallel with oceanic temperatures. This implies that climate change was not the main cause of the observed vegetation change. Potentially, it may be due to aboriginal or natural burning as previously suggested (Rule et al., 2012; Miller et al., 2005), which may have temporarily stimulated the proliferation of desert-like C_3 plants such as shrubs. Indeed, modern soils from the desert region (dominated by shrubs) in the MDB have relatively more negative $\delta^{13}\text{C}$ *n*-alkane values, suggesting more C_3 plants, compared to those soils from other regions in the MDB, confirming that this type of habitat may have increased around 43-37 ka, the period of the sharp vegetation change (Table S9.2 - Fig. S9.2). The reason why the vegetation change only lasted until 37 ka may be due to a new ecological equilibrium after the LQME and/or a decrease in the burning events. Indeed, comparison of levoglucosan AR (Fig. 9.2e), a marker for biomass burning events, with the $\delta^{13}\text{C}$ *n*-alkane record suggests that biomass burning only took place in the first 3 ka of the excursion. In general, after 54 ka the frequency in the burning events substantially increased, which is in agreement with previous studies (e.g. Bowler et al., 2003) that implied the presence and influence of humans in southeastern Australia only from this period onwards. Interestingly, the highest levoglucosan levels are recorded in the core during the LGM around 24-20 ka. The high levoglucosan values at these times may have been due to the more extensive aridity at that time, with fire conditions being more preponderant. Alternatively, the amount of terrestrial input was higher during the LGM (Fig. 9.2d) due to the proximity of the river mouth to the core site (Gingele et al., 2004) thereby leading to elevated AR of levoglucosan. In summary, our sediment *n*-alkane record of southeastern Australia suggests that vegetation change is unlikely to be the main driver of

the LQME in Australia as it followed the main period of the megafaunal extinction. Indeed, the sudden vegetation change recorded here appears to be a consequence of the LQME due to the decrease in herbivory pressure, perhaps aided by the stimulation of C₃ plants due to burning events. Other forms of human influence such as overhunting may have contributed to the LQME as the megafaunal extinction overlaps with the arrival of humans.

9.3 Material and Methods

Core MD03-2607, 32.95 m long, was taken during the AUSCAN cruise in 2003 and has previously been the subject of several investigations (Gingele et al., 2004; 2007; Gingele and De Deckker, 2005; Lopes dos Santos et al., 2012). Sediment samples were taken at 5 cm intervals for the upper 430 cm of the core, and below that at every 10 cm intervals for the rest of the core. The extraction of sediments and soils and subsequent separation into apolar, alkenone and polar fractions were carried out following methods described previously (Lopes dos Santos et al., 2012). The *n*-alkanes in the apolar fraction were analysed using a Hewlett Packard 6890 gas chromatograph, on a 25 m, silica column with 0.32 mm of diameter and coated with CP Sil-5 (thickness=0.12µm). The carrier gas was helium. The temperature program initiated at 70°C, increased first at a rate of 20°C min⁻¹ to 130°C, and next at a rate of 4°C min⁻¹ to the final temperature of 320°C, which was held for 10 minutes. Concentrations of *n*-alkanes were calculated through comparison with a squalane internal standard. AR was calculated based on concentrations, dry bulk density and sedimentation rates derived from the age model. Stable carbon isotopic composition of the *n*-alkanes was measured as described previously (Castañeda et al., 2009) with an average reproducibility of 0.5 ‰. Glycerol dialkyl glycerol tetraethers present in the polar fraction were measured using high pressure liquid chromatography/mass spectrometry (HPLC/MS) and the BIT index was calculated following methods described previously (Hopmans et al., 2004; Schouten et al., 2007). Levoglucosan was measured as described by Hopmans et al., 2012. Briefly, approximately 40 % of the samples were extracted with methanol using an Accelerated Solvent Extractor (100 °C, 1500 psi) and filtered through a sodium sulfate column and a regenerated cellulose filter. Identification and quantification of levoglucosan was achieved using an external standard with a Thermo HPLC/MS-MS using negative ion electrospray ionization in selected reaction monitoring mode. Reproducibility of the levoglucosan analyses was ±33%.

Acknowledgements

We thank J-B. Stuur for assistance in the field and J. Ossebaar, M. Kienhuis, M. Baas, M. Verweij and I. Rijpstra for analytical assistance. Research funding was provided by a VICI grant to SS from the Netherlands Organization of Scientific Research. Core MD03-2607 was obtained with a National Oceans Office and Australian Research Council grant, both awarded to PDD. Y. Balut from IPEV was instrumental in obtaining the core. Several of the ¹⁴C dates were obtained via an AINSE grant (07036) awarded to PDD.

Supplemental Figures and Table

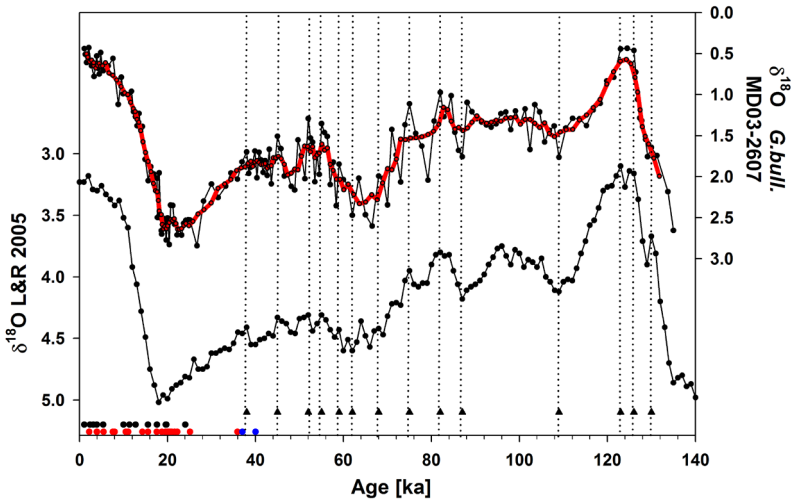


Fig. S9.1: Age model of core MD03-2607 (Gingele et al., 2004; Lopes dos Santos et al., 2012). The red line represents the smoothed line obtained by using a 5-point running mean. Black dots represent OSL dates, red dots represent ^{14}C dates, blue dots represent the two additional ^{14}C dates done in this study (see table S9.1) and triangles together with the dashed lines represent tie points between $\delta^{18}\text{O}$ record of *Globigerina bulloides* of this core and the global stack of benthic foraminifera (Lisiecki and Raymo, 2005).

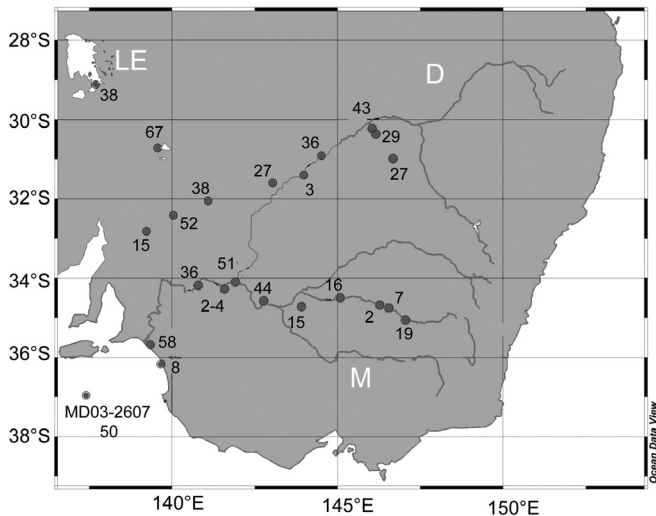


Fig. S9.2: Map showing the location of the soil samples taken in the Murray Darling Basin and sediment core MD03-2607. The values next to each dot represents the % C_4 plants reconstructed from the isotope mean of n -alkanes for each location referred in Table S2. LE =Lake Eyre, M =River Murray, D =Darling River.

Table S9.1: Radiocarbon ages for sediment samples at the core depths at which the vegetation excursion was observed (See Fig. S9.1)

| Sample depth (cm) | $\delta^{18}\text{O}$ inferred age (yr BP) | ^{14}C BP age | Calibrated age, BP one sigma | Calibrated age, BP two sigma |
|-------------------|--|------------------------|------------------------------|------------------------------|
| 490 | 39,870 | 32,600±250 | 36,465-36,900 | 36,271-37,467 |
| 528 | 41,730 | 35,215±275 | 39,395-40,347 | 38,965-40,693 |

Table S9.2: Coordinates, weighted mean isotopic composition of C_{29} - C_{33} *n*-alkanes and %C₄ inferred from the stable isotopes, from collected soils from the MDB and the uppermost sample of core MD03-2607.

| Soil | Latitude | Longitude | Weigh. Mean $\delta^{13}\text{C}$ <i>n</i> -alkanes [% ‰ , VPDB] | %C ₄ | Environment |
|--------|------------|------------|---|-----------------|--|
| 1 | -35.057816 | 147.052866 | -32.6 | 19 | Open <i>Eucalyptus</i> woodland and grassland |
| 2 | -34.754650 | 146.551050 | -34.2 | 7 | Treed river bank with some grasses |
| 3 | -34.681850 | 146.274500 | -34.9 | 2 | Open <i>Callitris</i> woodland and grassland |
| 4 | -34.496566 | 145.078366 | -33.1 | 16 | Red desert and few shrubs |
| 5 | -34.721950 | 143.912916 | -33.1 | 15 | Abundant salt bush on red soil |
| 6 | -34.578383 | 142.766783 | -29.3 | 44 | Treed river bank [billabong] with abundant grasses |
| 7 | -34.098516 | 141.917483 | -28.3 | 51 | <i>Eucalyptus</i> leaf litter + sporadic grass bed. |
| 8 | -34.274016 | 141.581666 | -34.9 | 2 | Abundant salt bush and grasses |
| 9 | -34.275033 | 141.581950 | -34.6 | 4 | Sporadic grasses and rare shrubs |
| 10 | -34.183900 | 140.791450 | -30.4 | 36 | grasses, sedges, <i>Sarcocornia</i> on edge of river |
| 11 | -35.685566 | 139.338766 | -27.4 | 58 | Grasses on edge of coastal lake |
| 12 | -36.171866 | 139.657800 | -34.2 | 8 | Black soil in Coorong region |
| 13 | -30.718683 | 139.567623 | -26.1 | 67 | Edge of Lake Frome, salt bushes and shrubs |
| 14 | -29.121914 | 137.692697 | -30.1 | 38 | Edge of Lake Eyre with salt bushes |
| 15 | -32.820077 | 139.229065 | -33.2 | 15 | Dense grasses and few salt bush (red soil) |
| 16 | -32.419023 | 140.041307 | -28.1 | 52 | Sparse shrubs on bare soil |
| 17 | -32.056407 | 141.091523 | -30.1 | 38 | Mostly grassland |
| 18 | -31.600410 | 143.040410 | -31.5 | 27 | Mostly grassland and shrubs |
| 19 | -31.406328 | 143.980922 | -34.8 | 3 | Thick grassland |
| 20 | -30.915312 | 144.517365 | -30.4 | 36 | Dry bushes but no grass |
| 21 | -30.229766 | 146.046164 | -29.4 | 43 | Abundant salt bush and few small trees |
| 22 | -30.369046 | 146.161075 | -31.3 | 29 | Tall trees and salt bush, but open landscape |
| 23 | -30.987106 | 146.679242 | -31.6 | 27 | Mixed trees, shrubs and few grasses |
| MD2607 | -36.960666 | 137.406500 | -28.4 | 50 | Core top |

References

- Alverson, K. D., Bradley, R. S. and Pederson, T. F., 2003. *Palaeoclimate, global change and the future*. (eds). Springer, Berlin, 221 pp.
- Andreasen, D.J., Ravelo, A.C., 1997. Tropical Pacific Ocean thermocline depth reconstructions for the last glacial maximum. *Paleoceanography* 12, 395-413.
- Armitage, S.J., Drake N.A., Stokes S., El-Hawat A., Salem M.J., White K., Turner P., McLaren S.J., 2007. Multiple phases of north African humidity recorded in lacustrine sediments from the fazzan basin, Libyan sahara. *Quaternary Geochronology* 2, 181–186.
- Batteen, M.L., Martinez, J.R., Bryan, D.W., Buch, E.J., 2000. A modeling study of the coastal eastern boundary current system off Iberia and Morocco. *Journal of Geophysical Research - Oceans* 105, 14173–14195.
- Bard, E., 1998. Geochemical and geophysical implications of the radiocarbon calibration. *Geochimica et Cosmochimica Acta* 62, 2025-2038.
- Bard, E., Rickaby, R.E.M., 2009. Migration of the subtropical front as a modulator of glacial climate. *Nature* 460, 380-U93.
- Bareille, G., Labracherie, M., Labeyrie, L., Pichon, J.-J., Turon, J., 1991. Biogenic silica accumulation rate during the Holocene in the southeastern Indian Ocean. *Marine Chemistry* 35, 537–551.
- Barrows, T.T., Juggins, S., 2005. Sea-surface temperatures around the Australian margin and Indian ocean during the last glacial maximum. *Quaternary Science Reviews* 24, 1017-1047.
- Behrensmeyer, A.K., 2006. Climate change and human evolution. *Science* 311 (5760), 476-478.
- Belkin, I.M., Gordon, A.L., 1996. Southern Ocean fronts from the Greenwich meridian to Tasmania. *Journal of Geophysical Research-Oceans* 101, 3675-3696.
- Berger, A.L., 1978. Long-Term Variations of Caloric Insolation Resulting from Earths Orbital Elements. *Quaternary Research* 9, 139-167.
- Berger, A., Loutre, M.F., 1991. Insolation values for the climate of the last 10 million years. *Quaternary Science Reviews* 10, 297–317.
- Bertrand, P., Shimmield, G., Martinez, P., Grousset, F., Jorissen, F., Paterne, M., Pujol, C., Bouloubassi, I., Buat-Menard, P., Peypouquet, J.P., Beaufort, L., Sicre, M.-A., Lallier-Vergès, E., Foster, J.M., Ternois, Y., Other Participants of the Sedorqua Program, 1996. The glacial ocean productivity hypothesis: the importance of regional temporal and spatial studies. *Marine Geology* 130, 1-9.
- Bi, X.H., Sheng, G.Y., Liu, X.H., Li, C., Fu, J.M., 2005. Molecular and carbon and hydrogen isotopic composition of *n*-alkanes in plant leaf waxes. *Organic Geochemistry* 36, 1405–1417.
- Bird, M.I., Summons, R.E., Gagan, M.K., Roksandic, Z., Dowling, L., Head, J., Fifield, L.K., Cresswell, R.G., Johnson, D.P., 1995. Terrestrial Vegetation Change Inferred from *n*-Alkane $\delta^{13}\text{C}$ Analysis in the Marine-Environment. *Geochimica et Cosmochimica Acta* 59, 2853-2857.
- Bird, M.I., Cali, J.A., 1998. A million-year record of fire in sub-Saharan Africa. *Nature* 394, 767-769.
- Boon, J.J., de Leeuw, J.W., 1979. The analysis of wax esters, very long mid-chain ketones and sterol ethers isolated from Walvis Bay diatomaceous ooze. *Marine Chemistry* 7, 117-132.
- Boon, J.J., Rijpstra, W.I.C., de Lange, F., de Leeuw, J.W., Yoshioka, M., Shimizu, Y., 1979. Black sea sterol- a molecular fossil for dinoflagellate blooms. *Nature* 277, 125-127.
- Boko, M., I. Niang, A. Nyong, C. Vogel, A. Githeko, M. Medany, B. Osman-Elasha, R. Tabo and P. Yanda, 2007: Africa. *Climate Change 2007: Impacts, Adaptation and Vulnerability. Contribution of Working Group II to the Fourth Assessment Report of the Intergovernmental Panel on Climate Change*, M.L. Parry, O.F. Canziani, J.P. Palutikof, P.J. van der Linden and C.E. Hanson, Eds., Cambridge University Press, Cambridge UK, 433-467.
- Bouimetarhan, I., Marret, F., Dupont, I., Zonneveld, K., 2009. Dinoflagellate cyst distribution in marine surface sediments off West Africa (17-6°N) in relation to sea-surface conditions, freshwater input and seasonal coastal upwelling. *Marine Micropaleontology* 71, 113-130.
- Bourles, B., Molinari, R.L., Johns, E., Wilson, W.D., Leaman, K.D., 1999. Upper layer currents in the western tropical North Atlantic (1989-1991). *Journal of Geophysical Research - Oceans* 104, 1361–1375.
- Bowler, J.M., Hope, G.S., Jennings, J.N., Singh, G., Walker, D., 1976. Late Quaternary Climates of Australia and New-Guinea. *Quaternary Research* 6, 359-394.
- Bowler, J. M., Johnston, H., Olley, J. M., Prescott, J. R., Roberts, R. G., Shawcross, W., & Spooner,

- N. A., 2003. New ages for human occupation and climatic change at Lake Mungo, Australia. *Nature* 421, 837-840.
- Bradley, R.S., 1999. *Paleoclimatology: Reconstructing Climates of the Quaternary*. Academic Press, San Diego, 610 pp.
- Bradt Miller, L.I., Anderson, R.F., Fleisher, M.Q., Burckle, L.H., 2006. Diatom productivity in the equatorial Pacific Ocean from the last glacial period to the present: A test of the silicic acid leakage hypothesis. *Paleoceanography* 21, PA4201-1-PA4201-12.
- Brassell, S.C., Comet, P.A., Eglinton, G., Isaacson, P.J., McEvoy, J., Maxwell, J.R., Thomson, I.D., Tibbetts, P.J.C., Volkman, J.K., 1980. The origin and fate of lipids in the Japan Trench. In: Douglas, A.G., Maxwell, J.R. (Eds.), *Advances in Organic Geochemistry* 1979. Pergamon Press, Oxford, pp. 375-392.
- Brassell, S.C., Eglinton, G., Marlowe, I.T., Pflaumann, U., Sarnthein, M., 1986. Molecular stratigraphy: A new tool for climatic assessment. *Nature* 320, 129-133.
- Brassell, S.C., Dumitrescu, M., The ODP Leg 198 Shipboard Scientific Party, 2004. Recognition of alkenones in a lower Aptian porcellanite from the west-central Pacific. *Organic Geochemistry* 35, 181-188.
- Brassell, S.C., 2009. Steryl ethers in a Valanginian claystone: Molecular evidence for cooler waters in the central Pacific during the Early Cretaceous? *Palaeogeography, Palaeoclimatology, Palaeoecology* 282, 45-57.
- Bray, E.E., Evans, E.D., 1961. Distribution of normal-paraffins as a clue to recognition of source beds. *Geochimica et Cosmochimica Acta* 22, 2-15.
- Broecker, W.S., 1982. Glacial to Interglacial Changes in Ocean Chemistry. *Progress in Oceanography* 11, 151-197.
- Broecker, W. S., and Peng T.-H., 1989. The cause of the glacial to interglacial atmospheric CO₂ change: A Polar Alkalinity Hypothesis, *Global Biogeochemical Cycles*, 3, 215–239.
- Brown, S.J., Elderfield, H., 1996. Variations in Mg/Ca and Sr/Ca ratios of planktonic foraminifera caused by postdepositional dissolution: Evidence of shallow Mg-dependent dissolution. *Paleoceanography* 11, 543-551.
- Brzezinski, M.A., Pride, C.J., Franck, V.M., Sigman, D.M., Sarmiento, J.L., Matsumoto, K., Gruber, N., Rau, G.H., Coale, K.H., 2002. A switch from Si(OH)₄ to NO⁻³ depletion in the glacial Southern Ocean. *Geophysical Research Letters* 29, 1564-1564-4.
- Calvo, E., Pelejero, C., De Deckker, P., Logan, G.A., 2007. Antarctic deglacial pattern in a 30 kyr record of sea surface temperature offshore South Australia. *Geophysical Research Letters* 34, L13707-1-L13707-6.
- Calvo, E., Pelejero, C., Pena, L.D., Cacho, I., Logan, G.A., 2011. Eastern Equatorial Pacific productivity and related-CO₂ changes since the last glacial period. *Proceedings of the National Academy of Science Early Edition*, 1-5.
- Canadell, J.G., Le Quéré, C., Raupach, M.R., Field, C.B., Buitenhuis, E.T., Ciais, P., Conway, T.J., Gillett, N.P., Houghton, R.A., Marland, G., 2007. Contributions to accelerating atmospheric CO₂ growth from economic activity, carbon intensity, and efficiency of natural sinks. *Proceedings of the National Academy of Sciences of the United States of America* 104, 18866-18870.
- Carlson, A.E., Clark, P.U., Haley, B.A., Klinkhammer, G.P., Simmons, K., Brook, E.J., Meissner, K.J., 2007. Geochemical proxies of North American freshwater routing during the Younger Dryas cold event. *Proceedings of the National Academy of Sciences of the United States of America* 104, 6556–6561.
- Carto, S.L., Weaver, A.J., Hetherington, R., Lam, Y., Wiebe, E., 2009. Out of Africa and into an ice age: On the role of global climate change in the late Pleistocene migration of early modern humans out of Africa. *Journal of Human Evolution* 56, 139–161.
- Castañeda, I.S., Mulitza, S., Schefuß, E., Lopes dos Santos, R.A., Sinninghe Damsté, J.S., Schouten, S., 2009. Wet phases in the Sahara/Sahel region and human migration patterns in North Africa. *Proceedings of the National Academy of Sciences of the United States of America* 106, 20159–20163.
- Castañeda, I.S., Schefuß, E., Pätzold, J., Sinninghe Damsté, J.S., Weldeab, S., Schouten, S., 2010. Millennial-scale sea surface temperature changes in the eastern Mediterranean (Nile River Delta region) over the last 27,000 years. *Paleoceanography* 25, PA1208-1-PA1208-13.
- Chang, P., Zhang, R., Hazeleger, W., Wen, C., Wan, X.Q., Ji, L., Haarsma, R.J., Breugem, W.P., Seidel, H., 2008. Oceanic link between abrupt changes in the North Atlantic Ocean and the African

- monsoon. *Nature Geoscience* 1, 444–448.
- Chiang, J.C.H., Cheng, W., Bitz, C.M., 2008. Fast teleconnections to the tropical Atlantic sector from Atlantic thermohaline adjustment. *Geophysical Research Letters* 35 L07704-1-5.
- Chikaraishi, Y., Naraoka, H., 2003. Compound-specific delta δD - $\delta^{13}\text{C}$ analyses of *n*-alkanes extracted from terrestrial and aquatic plants. *Phytochemistry* 63, 361-371.
- Christensen, J.H., B. Hewitson, A. Busuioic, A. Chen, X. Gao, I. Held, R. Jones, R.K. Kolli, W.T. Kwon, R. Laprise, V. Magaña Rueda, L. Mearns, C.G. Menéndez, J. Räisänen, A. Rinke, A. Sarr and P. Whetton, 2007: Regional Climate Projections. In: *Climate Change 2007: The Physical Science Basis. Contribution of Working Group I to the Fourth Assessment Report of the Intergovernmental Panel on Climate Change* [Solomon, S., D. Qin, M. Manning, Z. Chen, M. Marquis, K.B. Averyt, M. Tignor and H.L. Miller (eds.)]. Cambridge University Press, Cambridge, United Kingdom and New York, NY, USA.
- Claussen, M., Kubatzki, C., Brovkin, V., Ganopolski, A., Hoelzmann, P., Pachur, H.J., 1999. Simulation of an abrupt change in Saharan vegetation in the mid-Holocene. *Geophysical Research Letters* 26, 2037-2040.
- Cole, J.M., Goldstein, S.L., DeMenocal, P.B., Hemming, S.R., Grousset, F.E., 2009. Contrasting compositions of Saharan dust in the eastern Atlantic Ocean during the last deglaciation and African Humid Period. *Earth and Planetary Science Letters* 278, 257-266.
- Collister, J.W., Rieley, G., Stern, B., Eglinton, G., Fry, B., 1994. Compound-specific $\delta^{13}\text{C}$ analyses of leaf lipids from plants with differing carbon dioxide metabolisms. *Organic Geochemistry* 21, 619-627.
- Conkright, M.E., Locarnini, R.A., Garcia, H.E., O'Brien, T.D., Boyer, T.P., Stephens, C., Antonov, J.I., 2002. World Ocean Atlas 2001: Objective Analyses, Data Statistics, and Figures, CD-ROM Documentation. National Oceanographic Data Center, Silver Spring, MD.
- Crosta, X., Beucher, C., Pahnke, K., Brzezinski, M.A., 2007. Silicic acid leakage from the Southern Ocean: Opposing effects of nutrient uptake and oceanic circulation. *Geophysical Research Letters* 34, L13601-1-L13601-5, doi:10.1029/2006GL029083.
- Crosta, X., Romero, O.E., Ther, O., Schneider, R.R., 2012. Climatically-controlled siliceous productivity in the eastern Gulf of Guinea during the last 40 000 yr. *Climate of the Past* 8, 415-431.
- Crutzen, P. J., Andreae, M. O., 1990. Biomass burning in the tropics: Impact on atmospheric chemistry and biogeochemical cycles. *Science* 250, 1669-1678.
- De Deckker, P., Moros, M., Perner, K., Jansen, E., 2012. Influence of the tropics and de southern westerlies on glacial interhemispheric asymmetry. *Nature Geoscience* 5, 266–269.
- DeMenocal, P., Ortiz, J., Guilderson, T., Adkins, J., Sarnthein, M., Baker, L., Yarusinsky, M., 2000. Abrupt onset and termination of the African Humid Period: rapid climate responses to gradual insolation forcing. *Quaternary Science Reviews* 19, 347-361.
- DeMenocal, P., Ortiz, J., Guilderson, T., Sarnthein, M., 2000a. Coherent high- and low-latitude climate variability during the Holocene warm period. *Science* 288, 2198-2202.
- Denis E.H., Toney, J.L., Tarozo, R., Anderson, R.S., Roach, L.D., Huang Y, 2012. Polycyclic aromatic hydrocarbons (PAHs) in lake sediments record historic fire events: Validation using HPLC-fluorescence detection. *Organic Geochemistry* 45, 7-17.
- deNoblet, N., Braconnot, P., Joussaume, S., Masson, V., 1996. Sensitivity of simulated Asian and African summer monsoons to orbitally induced variations in insolation 126, 115, and 6 kBP. *Climate Dynamics* 12, 589–603.
- Diefendorf, A.F., Freeman, K.H., Wing, S.L., Graham, H.V., 2011. Production of *n*-alkyl lipids in living plants and implications for the geologic past. *Geochimica et Cosmochimica Acta* 75, 7472-7485.
- Drake, N.A., Blench, R.M., Armitage, S.J., Bristow, C.S., White, K.H., 2011. Ancient watercourses and biogeography of the Sahara explain the peopling of the desert. *Proceedings of the National Academy of Sciences of the United States of America* 108, 458-462, doi:10.1073/pnas.1012231108.
- Duplessy, J.C., Shackleton, N.J., 1985. Response of Global Deep-Water Circulation to Earths Climatic-Change 135,000-107,000 Years Ago. *Nature* 316, 500-507.
- Dupont, L.M., Jahns, S., Marret, F., Ning, S., 2000. Vegetation change in equatorial West Africa: time-slices for the last 150 ka. *Palaeogeography Palaeoclimatology Palaeoecology* 155, 95-122.
- Dymond, J., Suess, E., Lyle, L., 1992. Barium in deep-sea sediments: a geochemical proxy for

- paleoproductivity. *Paleoceanography* 7, 163–181.
- Eggins, S.M., Sadekov, A.Y., De Deckker, P., 2004. Modulation and daily banding of Mg/Ca in *Orbulina universa* tests by symbiont photosynthesis and respiration: a complication for seawater thermometry? *Earth and Planetary Science Letters* 225 411-419.
- Eglinton, G., Hamilton, R.J., 1967. Leaf Epicuticular Waxes. *Science* 156, 1322-1335.
- Elderfield, H., Greaves, M., Barker, S., Hall, I.R., Tripathi, A., Ferretti, P., Crowhurst, S., Booth, L., Daunt, C., 2010. A record of bottom water temperature and seawater $\delta^{18}\text{O}$ for the Southern Ocean over the past 440 kyr based on Mg/Ca of benthic foraminiferal *Uvigerina* spp. *Quaternary Science Reviews* 29, 160-169.
- Elias, V.O., Simoneit, B.R.T., Cordeiro, R.C., Turcq, B., 2001. Evaluating levoglucosan as an indicator of biomass burning in Carajás, Amazônia: a comparison to the charcoal record. *Geochimica et Cosmochimica Acta* 65, 267–272.
- Englebrecht, A.C., Sachs, J.P., 2005. Determination of sediment provenance at drift sites using hydrogen isotopes and unsaturation ratios in alkenones. *Geochimica et Cosmochimica Acta* 69, 4253-4265.
- Fabbri, D., Torri, C., Simoneit, B.R.T., Marynowski, L., Rushdi, A.I., Fabiańska M.J., 2009. Levoglucosan and other cellulose and lignin markers in emissions from burning of Miocene lignites. *Atmospheric Environment* 43, 2286-2295.
- Falkowski, P.G., 1997. Evolution of the nitrogen cycle and its influence on the biological sequestration of CO_2 in the ocean. *Nature* 387, 272-275.
- Ferguson, J.E., Henderson, G.M., Kucera, M., Rickaby, R.E.M., 2008. Systematic change of foraminiferal Mg/Ca ratios across a strong salinity gradient. *Earth and Planetary Science Letter* 265, 153-166.
- Fifield, L.K., Allan, G.L., Stone, J.O.H., Ophel, T.R., 1994. The ANU AMS system and research program. *Nuclear Instruments and Methods* 92, 85-88.
- Fink, D., Hotchkis, M., Hua, Q., Jacobsen, G., Smith, A.M., Zoppi, U., Child, D., Mifsud, C., van der Gaast, H., Williams, A., Williams, M., 2004. The ANTARES AMS facility at ANSTO. *Nuclear Instruments and Methods in Physics Research Section B: Beam Interactions with Materials and Atoms* 223-224, 109-115.
- Fischer, G. and Wefer G., 1999. *Use of Proxies in Paleoceanography: Examples From the South Atlantic*. Springer, New York 735 pp.
- Flores, J.-A., Bárcena, M.A., Sierro, F.J., 2000. Ocean-surface and wind dynamics in the Atlantic Ocean off Northwest Africa during the last 140 000 years. *Palaeogeography, Palaeoclimatology, Palaeoecology* 161, 459-478.
- Forster, P., Torroni, A., Renfrew, C., Rohl, A., 2001. Phylogenetic star contraction applied to Asian and Papuan mtDNA evolution. *Molecular Biology and Evolution* 18, 1864–1881.
- Francois, R., Bacon, M.P., Suman, D.O., 1990. Thorium 230 Profiling in Deep-Sea Sediments: High-resolution records of flux and dissolution of carbonate in the equatorial Atlantic during the last 24,000 Years. *Paleoceanography* 5, 761-787.
- Freeman, K.H., Hayes, J.M., Trendel, J.M., Albrecht, P., 1990. Evidence from Carbon Isotope Measurements for Diverse Origins of Sedimentary Hydrocarbons. *Nature* 343, 254-256.
- Freudenthal, T., Meggers, H., Henderiks, J., Kuhlmann, H., Moreno, A., Wefer, G., 2002. Upwelling intensity and filament activity off Morocco during the last 250,000 years. *Deep-Sea Research Part II-Topical Studies in Oceanography* 49, 3655-3674.
- Funasaki, H., Gilbertson, J.R., 1968. Isolation and identification of cholesteryl alkyl ethers from bovine cardiac muscle. *Journal of Lipid Research* 9, 766-768.
- Galloway, R. 1965. Late Quaternary climates in Australia. *Journal of Geology* 73, 603–618.
- Gambaro, A., Zangrando, R., Gabrielli, P., Barbante, C., Cescon, P., 2008. Direct determination of levoglucosan at the picogram per milliliter level in Antarctic ice by High-Performance Liquid Chromatography/ Electropray Ionization Triple Quadrupole Mass Spectrometry. *Analytical Chemistry* 80, 1649-1655.
- Ganachaud, A., Wunsch, C., 2003. Large-scale ocean heat and freshwater transports during the World Ocean Circulation Experiment. *Journal of Climate* 16, 696–705.
- Gao, Y., Kaufman, Y.J., Tanre, D., Kolber, D., Falkowski, P.G., 2001. Seasonal distributions of aeolian iron fluxes to the global ocean. *Geophysical Research Letters* 28, 29-32.
- Gasse, F., 2000. Hydrological changes in the African tropics since the Last Glacial Maximum. *Quaternary Science Reviews* 19, 189-211.

- Gaven, C., Hillairemarcel, C., Petitmaire, N., 1981. A Pleistocene lacustrine episode in Southeastern Libya. *Nature* 290, 131–133.
- Gingele, F.X., De Deckker, P., Hillenbrand, C.D., 2001. Late Quaternary fluctuations of the Leeuwin Current and palaeoclimates on the adjacent land masses: clay mineral evidence. *Australian Journal of Earth Sciences* 48, 867–874.
- Gingele, F.X., De Deckker, P., Hillenbrand, C.-D., 2004. Late Quaternary terrigenous sediments from the Murray Canyons area, offshore South Australia and their implications for sea level change, palaeoclimate and palaeodrainage of the Murray-Darling Basin. *Marine Geology* 212, 183–197.
- Gingele, F.X., De Deckker, P., 2005. Late Quaternary fluctuations of palaeoproductivity in the Murray canyons area, South Australian continental margin. *Palaeogeography Palaeoclimatology Palaeoecology* 220, 361–373.
- Gingele, F., De Deckker, P., Norman, M., 2007. Late Pleistocene and Holocene climate of SE Australia reconstructed from dust and river loads deposited offshore the River Murray Mouth. *Earth and Planetary Science Letters* 255, 257–272.
- Goering, J.J., Iverson, R.I., 1981. Phytoplankton distribution on the southeastern Bering Sea shelf. In: Hood, D.J., Calder, J.A. (Eds.), *The Eastern Bering Sea Shelf: Oceanography and Resources*. Volume 2. University of Washington Press, Seattle, pp. 933–946.
- Gong, C., Hollander, D.J., 1999. Evidence for differential degradation of alkenones under contrasting bottom water oxygen conditions: Implications for paleotemperature reconstruction. *Geochimica et Cosmochimica Acta* 63, 405–411.
- Goosse, H., Fichefet, T., 1999. Importance of ice-ocean interactions for the global ocean circulation: a model study. *Journal of Geophysical Research - Oceans* 104, 23337–23355.
- Goosse, H., Deleersnijder, E., Fichefet, T., England, M.H., 1999. Sensitivity of a global coupled ocean-sea ice model to the parameterization of vertical mixing. *Journal of Geophysical Research - Oceans* 104, 13681–13695.
- Govin, A., Holzwarth, U., Heslop, D., Ford Keeling, L., Zabel, M., Mulitza, S., Collins, J.A., Chiessi, C.M., 2012. Distribution of major elements in Atlantic surface sediments (36°N–49°S): Imprint of terrigenous input and continental weathering. *Geochemistry, Geophysics, Geosystems* 13, 1–23.
- Gregory, J.M., Dixon, K.W., Stouffer, R.J., Weaver, A.J., Driesschaert, E., Eby, M., Fichefet, T., Hasumi, H., Hu, A., Jungclaus, J.H., Kamenkovich, I.V., Levermann, A., Montoya, M., Murakami, S., Nawrath, S., Oka, A., Sokolov, A.P., Thorpe, R.B., 2005. A model intercomparison of changes in the Atlantic thermohaline circulation in response to increasing atmospheric CO₂ concentration. *Geophysical Research Letters* 32, L12703–1–5.
- Grousset, F.E., Parra, M., Bory, A., Martinez, P., Bertrand, P., Shimmield, G., Ellam, R.M., 1998. Saharan wind regimes traced by the Sr-Nd isotopic composition of subtropical Atlantic sediments: Last Glacial maximum vs today. *Quaternary Science Reviews* 17, 395–409.
- Grün, R., Eggins, S., Aubert, M., Spooner, N., Pike, A. W. G., & Muller, W., 2010. ESR and U-series analyses of faunal material from Cuddie Springs, NSW, Australia: implications for the timing of the extinction of the Australian megafauna. *Quaternary Science Reviews* 29, 596–610.
- Haarmann, T., Hathorne, E.C., Mohtadi, M., Groeneveld, J., Kölling, M., Bickert T., 2011. Mg/Ca ratios of single planktonic foraminifer shells and the potential to reconstruct the thermal seasonality of the water column. *Paleoceanography* 26, PA3218-1-PA3218-14.
- Haarsma, R.J., Campos, E., Hazeleger, W., Severijns, C., 2008. Influence of the meridional overturning circulation on tropical Atlantic climate and variability. *Journal of Climate* 21, 1403–1416.
- Harle, K.J., 1997. Late Quaternary vegetation and climate change in southeastern Australia: palynological evidence from marine core E55-6. *Palaeogeography Palaeoclimatology Palaeoecology* 131, 465–483.
- Harradine, P.J., Harris, P.G., Head, R.N., Harris, R.P., Maxwell, J.R., 1996. Steryl chlorin esters are formed by zooplankton herbivory. *Geochimica et Cosmochimica Acta* 60, 2265–2270.
- Harrison, S.P., 1993. Late Quaternary lake-level changes and climates of Australia. *Quaternary Science Reviews* 12, 211–231.
- Hattersley, P.W., 1983. The Distribution of C₃ and C₄-Grasses in Australia in Relation to Climate. *Oecologia* 57, 113–128.
- Hayes, C.T., Anderson, R.F., Fleisher, M.Q., 2011. Opal accumulation rates in the equatorial Pacific and mechanisms of deglaciation. *Paleoceanography* 26, PA1207-doi:10.1029/2010PA002008.
- Hennessy, K., B. Fitzharris, B.C. Bates, N. Harvey, S.M. Howden, L. Hughes, J. Salinger and

- R. Warrick, 2007: Australia and New Zealand. *Climate Change 2007: Impacts, Adaptation and Vulnerability. Contribution of Working Group II to the Fourth Assessment Report of the Intergovernmental Panel on Climate Change*, M.L. Parry, O.F. Canziani, J.P. Palutikof, P.J. van der Linden and C.E. Hanson, Eds., Cambridge University Press, Cambridge, UK, 507-540.
- Herbert, T.D., 2003. Alkenones as paleotemperature indicators. *Treatise on Geochemistry* 6, 1-44.
- Herfort, L., Schouten, S., Boon, J.P., Sinninghe Damsté, J.S., 2006. Application of the TEX₈₆ temperature proxy to the southern North Sea. *Organic Geochemistry* 37, 1715-1726.
- Herndl, G.J., Reinthaler, T., Teira, E., van Aken, H., Veth, C., Pernthaler, A., Pernthaler, J., 2005. Contribution of Archaea to total prokaryotic production in the deep Atlantic Ocean. *Applied and Environmental Microbiology* 71, 2303-2309.
- Hill, P.J., De Deckker, P., 2004. AUSCAN seafloor mapping and geological sampling survey on the Australian southern margin by RV Marion Dufresne in 2003: final project report. *Geoscience Australia Record 2004/4 (Petroleum and Marine Division)*, 1-144.
- Hinrichs, K.U., Schneider, R.R., Muller, P.J., Rullkotter, J., 1999. A biomarker perspective on paleoproductivity variations in two Late Quaternary sediment sections from the Southeast Atlantic Ocean. *Organic Geochemistry* 30, 341-366.
- Hippler, D., Eisenhauer, A., Nägler, T.F., 2006. Tropical Atlantic SST history inferred from Ca isotope thermometry over the last 140 ka. *Geochimica et Cosmochimica Acta* 70, 90-100.
- Hoefs, M.J.L., Versteegh, G.J.M., Rijpstra, W.I.C., de Leeuw, J.W., Sinninghe Damsté, J.S., 1998. Postdepositional oxic degradation of alkenones: Implications for the measurement of palaeo sea surface temperatures. *Paleoceanography* 13, 42-49.
- Hooghiemstra, H., Lezine, A.M., Leroy, S.A.G., Dupont, I., Marret, F., 2006. Late Quaternary palynology in marine sediments: A synthesis of the understanding of pollen distribution patterns in the NW African setting. *Quaternary International* 148, 29-44.
- Hopmans, E.C., Weijers, J.W.H., Schefuß, E., Herfort, L., Sinninghe Damsté, J.S., Schouten, S., 2004. A novel proxy for terrestrial organic matter in sediments based on branched and isoprenoid tetraether lipids. *Earth and Planetary Science Letters* 224, 107-116.
- Hopmans, E.C., Lopes dos Santos, R.A., Mets, A., Sinninghe Damsté, J.S., Schouten, S., 2012. A novel method for the rapid analysis of levoglucosan in soils and sediments. *Organic Geochemistry, In revision*.
- Horn, M.G., Beucher, C.P., Robinson, R.S., Brzezinski, M.A., 2011. Southern Ocean nitrogen and silicon dynamics during the last deglaciation. *Earth and Planetary Science Letters* 310, 334-339.
- Huang, Y.S., Lockheart, M.J., Collister, J.W., Eglinton, G., 1995. Molecular and isotopic biogeochemistry of the Miocene Clarkia Formation: Hydrocarbons and alcohols. *Organic Geochemistry* 23, 785-801.
- Huang, R.X., Cane, M.A., Naik, N., Goodman, P., 2000. Global adjustment of the thermocline in response to deepwater formation. *Geophysical Research Letters* 27, 759-762.
- Huang, Y., Dupont, I., Sarnthein, M., Hayes, J.M., Eglinton, G., 2000a. Mapping of C₄ plant input from North West Africa into North East Atlantic sediments. *Geochimica et Cosmochimica Acta* 64, 3505-3513.
- Hughen, K.A., Baillie, M.G.L., Bard, E., Beck, J.W., Bertrand, C.J.H., Blackwell, P.G., Buck, C.E., Burr, G.S., Cutler, K.B., Damon, P.E., Edwards, R.L., Fairbanks, R.G., Friedrich, M., Guilderson, T.P., Kromer, B., McCormac, G., Manning, S., Ramsey, C.B., Reimer, P.J., Reimer, R.W., Remmele, S., Southon, J.R., Stuiver, M., Talamo, S., Taylor, F.W., van der Plicht, J., Weyhenmeyer, C.E., 2004. Marine04 Marine Radiocarbon Age Calibration, 026 Cal Kyr BP. *Radiocarbon* 46, 1059-1086.
- Huguet, C., Kim, J.-H., Sinninghe Damsté, J.S., Schouten, S., 2006. Reconstruction of sea surface temperature variations in the Arabian Sea over the last 23 kyr using organic proxies (TEX₈₆ and U^K₃₇). *Paleoceanography* 21, 1-13.
- Huguet, C., Schimmelmann, A., Thunell, R., Lourens, L.J., Sinninghe Damsté, J.S., Schouten, S., 2007. A study of the TEX₈₆ paleothermometer in the water column and sediments of the Santa Barbara Basin, California. *Paleoceanography* 22 PA3203-1-PA3203-9.
- Huguet, C., Martrat, B., Grimalt, J.O., Sinninghe Damsté, J.S., Schouten, S., 2011. Coherent millennial-scale patterns in U^K₃₇ and TEX^H₈₆ temperature records during the penultimate interglacial-to-glacial cycle in the western Mediterranean. *Paleoceanography* 26, PA 2218-1-PA2218-10.
- Hutson, W.H., 1977. Transfer-Functions Under No-Analog Conditions - Experiments with Indian-

- Ocean Planktonic Foraminifera. *Quaternary Research* 8, 355-367.
- Imbrie, J. and Imbrie K. P., 1979. *Ice Ages: Solving the Mystery*. Enslow Publishers, Short Hills, NJ, 224 pp.
- Imbrie, J., Kipp, N.G., 1971. *A new micropaleontological method for quantitative paleoclimatology: Application to a Late Pleistocene Caribbean core, in The late Cenozoic Glacial Ages*. Yale Univ. Press, New Haven, Conn, pp. 71-181.
- IPCC, 2007. *Climate Change 2007: Synthesis Report. Contribution of Working Groups I, II and III to the Fourth Assessment Report of the Intergovernmental Panel on Climate Change* [Core Writing Team, Pachauri, R.K and Reisinger, A. (eds.)]. IPCC, Geneva, Switzerland, 104 pp.
- Jasper, J.P., Hayes, J.M., 1990. A Carbon Isotope Record of CO₂ Levels During the Late Quaternary. *Nature* 347, 462-464.
- Johnson, B.J., Miller, G.H., Fogel, M.L., Magee, J.W., Gagan, M.K., Chivas, A.R., 1999. 65,000 years of vegetation change in central Australia and the Australian summer monsoon. *Science* 284, 1150-1152.
- Jones, R., 1969. Fire-stick farming. *Australian National History* 16, 224-228.
- Jouzel, J., Masson-Delmotte, V., Cattani, O., Dreyfus, G., Falourd, S., Hoffmann, G., Minster, B., Nouet, J., Barnola, J.M., Chappellaz, J., Fischer, H., Gallet, J.C., Johnsen, S., Leuenberger, M., Loulergue, L., Luethi, D., Oerter, H., Parrenin, F., Raisbeck, G., Raynaud, D., Schilt, A., Schwander, J., Selmo, E., Souchez, R., Spahni, R., Stauffer, B., Steffensen, J.P., Stenni, B., Stocker, T.F., Tison, J.L., Werner, M., Wolff, E.W., 2007. Orbital and millennial Antarctic climate variability over the past 800,000 years. *Science* 317, 793-796.
- Karner, M.B., DeLong, E.F., Karl, D.M., 2001. Archaeal dominance in the mesopelagic zone of the Pacific Ocean. *Nature* 409, 507-510.
- Kemp, A.C., Horton, B.P., Donnelly, J.P., Mann, M.E., Vermeer, M., Rahmstorf, S., 2011. Climate related sea-level variations over the past two millennia. *Proceedings of the National Academy of Sciences of the United States of America* 108, 11017-11022.
- Kershaw, A.P., 1986. Climatic-Change and Aboriginal Burning in Northeast Australia During the Last 2 Glacial Interglacial Cycles. *Nature* 322, 47-49.
- Kershaw, A.P., D'Costa, D.M., McEwen Mason, J.R.C., Wagstaff, B.E., 1991. Palynological evidence for Quaternary vegetation and environments of mainland southeastern Australia. *Quaternary Science Reviews* 10, 391-404.
- Kienast, S.S., Kienast, M., Jaccard, S., Calvert, S.E., Francois, R., 2006. Testing the silica leakage hypothesis with sedimentary opal records from the eastern equatorial Pacific over the last 150 kyrs. *Geophysical Research Letters* 33, L15607-1-L15607-4.
- Kim, J.-H., Schouten, S., Buscail, R., Ludwig, W., Bonnin, J., Sinninghe Damsté, J. S., & Bourrin, F., 2006. Origin and distribution of terrestrial organic matter in the NW Mediterranean (Gulf of Lions): Exploring the newly developed BIT index. *Geochemistry Geophysics Geosystems* 7, 1-20.
- Kim, J.-H., Schouten, S., Hopmans, E.C., Donner, B., Sinninghe Damsté, J.S., 2008. Global sediment core-top calibration of the TEX₈₆ paleothermometer in the ocean. *Geochimica et Cosmochimica Acta* 72, 1154-1173.
- Kim, J.-H., Crosta, X., Michel, E., Schouten, S., Duprat, J., Sinninghe Damsté J.S., 2009. Impact of lateral transport on organic proxies in the Southern Ocean. *Quaternary Research* 71, 246-250.
- Kim, J.-H., Meer, J.v.d., Schouten, S., Helmke, P., Willmott, V., Sangiorgi, F., Koc, N., Hopmans, E.C., Sinninghe Damsté, J.S., 2010. New indices and calibrations derived from the distribution of crenarchaeal isoprenoid tetraether lipids: Implications for past sea surface temperature reconstructions. *Geochimica et Cosmochimica Acta* 74, 1-37.
- Klok, J., Baas, M., Cox, H.C., de Leeuw, J.W., Schenck, P.A., 1984. Loliolides and dihydroactinidiolide in a Recent marine sediment probably indicate a major transformation pathway of carotenoids. *Tetrahedron Letters* 25, 5577-5580.
- Koning, E., van Iperen, J.M., van Raaphorst, W., Helder, W., Brummer, G.-J.A., van Weering, T.C.E., 2001. Selective preservation of upwelling-indicating diatoms in sediments off Somalia, NW Indian Ocean. *Deep-Sea Research I* 48, 2473-2495.
- Könneke, M., Bernhard, A.E., de la Torre, J.R., Walker, C.B., Waterbury, J.B., Stahl, D.A., 2005. Isolation of an autotrophic ammonia-oxidizing marine archaeon. *Nature* 437, 543-546.
- Kumar, N., Anderson, R.F., Mortlock, R.A., Froelich, P.N., Kubik, P., Dittrich-Hannen, B., Suter, M., 1995. Increased biological productivity and export production in the glacial Southern Ocean. *Nature* 378, 675-680.

- Kuper, R., Kröpelin, S., 2006. Climate-controlled Holocene occupation in the Sahara: Motor of Africa's evolution. *Science* 313, 803-807.
- Kutzbach, J.E., Streetperrott, F.A., 1985. Milankovitch Forcing of Fluctuations in the Level of Tropical Lakes from 18 to 0 Kyr Bp. *Nature* 317, 130-134.
- Lalonde, K., Mucci, A., Ouellet, A., Gelinas, Y., 2012. Preservation of organic matter in sediments promoted by iron. *Nature* 483, 198-200.
- LaRoche, J., Breitbarth, E., 2005. Importance of the diazotrophs as a source of new nitrogen in the ocean. *Journal of Sea Research* 53, 67-91.
- Lea, D.W., Martin, P.A., Pak, D.K., Spero, H.J., 2002. Reconstructing a 350 ky history of sea level using planktonic Mg/Ca and oxygen isotope records from a Cocos Ridge core. *Quaternary Science Reviews* 21, 283-293.
- Lee, K.E., Kim, J.-H., Wilke, I., Helmke, P., Schouten, S., 2008. A study of the alkenone, TEX₈₆, and planktonic foraminifera in the Benguela Upwelling System: implications for past sea surface temperature estimates. *Geochemistry, Geophysics, Geosystems* 9, 1-19.
- Leider, A., Hinrichs, K.-U., Mollenhauer, G., Versteegh G.J.M., 2010. Core-top calibration of the lipid-based U^K₃₇ and TEX₈₆ temperature proxies on the southern Italian shelf (SW Adriatic Sea, Gulf of Taranto). *Earth and Planetary Science Letters* 300, 112-124.
- Le Quéré, C., Raupach, M.R., Canadell, J.G., Marland, G., Bopp, L., Ciais, P., Conway, T.J., Doney, S.C., Feely, R.A., Foster, P., Friedlingstein, P., Gurney, K., Houghton, R.A., House, J.I., Huntingford, C., Levy, P.E., Lomas, M.R., Majkut, J., Metz, N., Ometto, J.P., Peters, G.P., Prentice, I.C., Randeron, J.T., Running, S.W., Sarmiento, J.L., Schuster, U., Sitch, S., Takahashi, T., Viovy, N., van der Werf, G.R., Woodward, F.I., 2009. Trends in the sources and sinks of carbon dioxide. *Nature Geoscience* 2, 831-836.
- Li, Q., James, N.P., Bone, Y., McGowran, B., 1996. Foraminiferal biostratigraphy and depositional environments of the mid-Cenozoic Abrakurrie Limestone, Eucla Basin, southern Australia. *Australian Journal of Earth Sciences* 43, 437-450.
- Li, Q., McGowran, B., 1998. Oceanographic implications of recent planktonic foraminifera along the southern Australian margin. *Marine and Freshwater Research* 49, 439-445.
- Li, Q., Davies, P.J., McGowran, B., 1999. Foraminiferal sequence biostratigraphy of the Oligo-Miocene Janjukian strata from Torquay, southeastern Australia. *Australian Journal of Earth Sciences* 46, 261-273.
- Lisiecki, L.E., Raymo, M.E., 2005. A Pliocene-Pleistocene stack of 57 globally distributed benthic $\delta^{18}\text{O}$ records. *Paleoceanography* 20, PA1003-PA1003-17.
- Livingstone, D.A., 1975. Late Quaternary Climatic Change in Africa. *Annual Review of Ecology and Systematics* 6, 249-280.
- Lloyd, J., Bird, M.I., Vellen, L., Miranda, A.C., Veenendaal, E.M., Djagbletey, G., Miranda, H.S., Cook, G., Farquhar, G.D., 2008. Contributions of woody and herbaceous vegetation to tropical savanna ecosystem productivity: a quasi-global estimate. *Tree Physiology* 28, 451-468.
- Locarnini, R.A., Mishonov, A.V., Antonov, J.I., Boyer, T.P., Garcia, H.E., 2006. World Ocean Atlas 2005. In: Levitus, S. (Ed.), *Temperature, Volume 1*. NOAA Atlas NESDIS 61, U.S. Government Printing Office, Washington, D.C. 182 pp.
- Locarnini, R.A., Mishonov, A.V., Antonov, J.I., Boyer, T.P., Garcia, H.E., Baranova, O.K., Zweng, M.M., and Johnson, D.R., 2010. World Ocean Atlas 2009, Volume 1: Temperature, S. Levitus, Ed. NOAA Atlas NESDIS 68, U.S. Government Printing Office, Washington, D.C.
- Lopes dos Santos, R.A., Prange, M., Castañeda, I.S., Schefuß, E., Mulitza, S., Schulz, M., Niedermeyer, E.M., Sinninghe Damsté, J.S., Schouten, S., 2010. Glacial-interglacial variability in Atlantic meridional overturning circulation and thermocline adjustments in the tropical North Atlantic. *Earth and Planetary Science Letters* 300, 407-414.
- Lopes dos Santos, R.A., Wilkins, D., De Deckker, P., Schouten, S., 2012. Late Quaternary productivity changes from offshore Southeastern Australia: a biomarker approach. *Palaeogeography, Palaeoclimatology, Palaeoecology* 363-364, 48-56.
- Luthi, D., Le Floch, M., Bereiter, B., Blunier, T., Barnola, J.M., Siegenthaler, U., Raynaud, D., Jouzel, J., Fischer, H., Kawamura, K., Stocker, T.F., 2008. High-resolution carbon dioxide concentration record 650,000-800,000 years before present. *Nature* 453, 379-382.
- Lyle, M., Murray, D.W., Finney, B.P., Dymond, J., Robbins, J.M., Brooksforce, K., 1988. The record of late pleistocene biogenic sedimentation in the Eastern Tropical Pacific Ocean. *Paleoceanography* 3, 39-59.

- Lynch-Stieglitz, J., Adkins, J.F., Curry, W.B., Dokken, T., Hall, I.R., Herguera, J.C., Hirschi, J.J.M., Ivanova, E.V., Kissel, C., Marchal, O., Marchitto, T.M., McCave, I.N., McManus, J.F., Mulitza, S., Ninnemann, U., Peeters, F., Yu, E.F., Zahn, R., 2007. Atlantic meridional overturning circulation during the Last Glacial Maximum. *Science* 316, 66–69.
- Madureira, L.A.S. and Piccinini, A., 1999. Lipids as indicators of paleoclimatic changes, II: terrestrial biomarkers. *Revista Brasileira de Oceanografia*, 47, 115-125.
- Magee, J.W., Miller, G.H., Spooner, N.A., & Questiaux, D., 2004. Continuous 150 ky monsoon record from Lake Eyre, Australia: Insolation-forcing implications and unexpected Holocene failure. *Geology* 32, 885-888.
- Malmgren, B.A., Nordlund, U., 1997. Application of artificial neural networks to paleoceanographic data. *Palaeogeography Palaeoclimatology Palaeoecology* 136, 359-373.
- Mann, M.E., Zhang, Z.H., Hughes, M.K., Bradley, R.S., Miller, S.K., Rutherford, S., Ni, F.B., 2008. Proxy-based reconstructions of hemispheric and global surface temperature variations over the past two millennia. *Proceedings of the National Academy of Sciences of the United States of America* 105, 13252-13257.
- Marlow, J.R., Farrimond, P., Rosell-Melé, A., 2001. Analysis of lipid biomarkers in sediments from the Benguela Current Coastal Upwelling System (Site 1084). In: Wefer, G., Berger, W. H., Richter, C. (Eds.), *Proceedings of the Ocean Drilling Program, Scientific Results 175*, 1-26, doi:10.2973/odp.proc.sr.175.210.2001.
- Marlowe, I.T., Green, J.C., Neal, A.C., Brassell, S.C., Eglinton, G., Course, P.A., 1984. Long-Chain ($n\text{-C}_{37}\text{-C}_{39}$) alkenones in the Prymnesiophyceae. Distribution of alkenones and other lipids and their taxonomic significance. *British Phycological Journal* 19, 203-216.
- Marshall, A.G. & Lynch, A.H., 2006. Time-slice analysis of the Australian summer monsoon during the late Quaternary using the Fast Ocean Atmosphere Model. *Journal of Quaternary Science* 21, 789-801.
- Martens-Habbena, W., Berube, P.M., Urakawa, H., de la Torre, J.R., Stahl, D.A., 2009. Ammonia oxidation kinetics determine niche separation of nitrifying Archaea and Bacteria. *Nature* 461, 976-U234.
- Martinez, P., Bertrand, P., Shimmield, G.B., Cochrane, K., Jorissen, F.J., Foster, J., Dignan, M., 1999a. Upwelling intensity and ocean productivity changes off Cape Blanc (northwest Africa) during the last 70,000 years: geochemical and micropalaeontological evidence. *Marine Geology* 158, 57-74.
- Martinez, J.I., De Deckker, P., Barrows, T.T., 1999. Palaeoceanography of the last glacial maximum in the eastern Indian Ocean: planktonic foraminiferal evidence. *Palaeogeography Palaeoclimatology Palaeoecology* 147, 73-99.
- Matsumoto, K., Sarmiento, J.L., Brzezinski, M.A., 2002. Silicic acid leakage from the Southern Ocean: A possible explanation for glacial atmospheric $p\text{CO}_2$. *Global Biogeochemical Cycles* 16, 1-23, <http://dx.doi.org/10.1029/2001GB001442>.
- Mazeika, P.A., 1967. Thermal domes in eastern tropical Atlantic Ocean. *Limnology and Oceanography* 12, 537–539.
- McDougall, I., Brown, F.H., Fleagle, J.G., 2005. Stratigraphic placement and age of modern humans from Kibish, Ethiopia. *Nature* 433, 733–736.
- McIntyre, A., Molfino, B., 1996. Forcing of Atlantic equatorial and subpolar millennial cycles by precession. *Science* 274, 1867–1870.
- McManus, J.F., Francois, R., Gherardi, J.-M., Keigwin, L.D., Brown-Leger, S., 2004. Collapse and rapid resumption of Atlantic meridional circulation linked to deglacial climate changes. *Nature* 428, 834-837.
- Mellars, P., 2006. Going east: New genetic and archaeological perspectives on the modern human colonization of Eurasia. *Science* 313, 796-800.
- Mellor, G.L., Yamada, T., 1982. Development of a turbulence closure-model for geophysical fluid problems. *Reviews of Geophysics* 20, 851–875.
- Menzel, D., Hopmans, E.C., Schouten, S., Sinninghe Damsté, J.S., 2006. Membrane tetraether lipids of planktonic Crenarchaeota in Pliocene sapropels of the eastern Mediterranean Sea. *Palaeogeography Palaeoclimatology Palaeoecology* 239, 1-15.
- Meyers, P.A., 1994. Preservation of Elemental and Isotopic Source Identification of Sedimentary Organic-Matter. *Chemical Geology* 114, 289-302.
- Middleton, J.F., Bye, J.A.T., 2007. A review of the shelf-slope circulation along Australia's southern

- shelves: Cape Leeuwin to Portland. *Progress in Oceanography* 75, 1-41.
- Milankovitch, M., 1941. *Kanon der Erdbestrahlung und seine Anwendung auf das Eiszeitenproblem*. Royal Serbian Academy, Belgrade.
- Miller, G. H., Magee, J. W., Johnson, B. J., Fogel, M. L., Spooner, N. A., McCulloch, M. T., & Ayliffe, L. K., 1999. Pleistocene extinction of *Genyornis newtoni*: Human impact on Australian megafauna. *Science* 283, 205-208.
- Miller, G.H., Fogel, M.L., Magee, J.W., Gagan, M.K., Clarke, S.J., Johnson, B.J., 2005. Ecosystem collapse in pleistocene Australia and a human role in megafaunal extinction. *Science* 309, 287-290.
- Mills, M.M., Ridame, C., Davey, M., La Roche, J., Geider, R.J., 2004. Iron and phosphorus co-limit nitrogen fixation in the eastern tropical North Atlantic. *Nature* 429, 292-294.
- Mittelstaedt, E., 1983. The Upwelling Area Off Northwest Africa - A Description of Phenomena Related to Coastal Upwelling. *Progress in Oceanography* 12, 307-331.
- Mittelstaedt, E., 1991. The Ocean Boundary Along the Northwest African Coast - Circulation and Oceanographic Properties at the Sea-Surface. *Progress in Oceanography* 26, 307-355.
- Mix, A.C., 1989. Influence of Productivity Variations on Long-Term Atmospheric CO₂. *Nature* 337, 541-544.
- Mix, A.C., 1989a. Pleistocene paleoproductivity: evidence from organic carbon and foraminiferal species. In: Berger, W.H. (Eds.), *Productivity in the Ocean: Present and Past*, 313– 340 pp.
- Mohtadi, M., Oppo, D.W., Lückge, A., DePol-Holz, R., Steinke, S., Groeneveld, J., Hemme, N., Hebbeln, D., 2011. Reconstructing the thermal structure of the upper ocean: Insights from planktic foraminifera shell chemistry and alkenones in modern sediments of the tropical eastern Indian Ocean. *Paleoceanography* 26, PA3219-1-20.
- Mollenhauer, G., Kienast, M., Lamy, F., Meggers, H., Schneider, R.R., Hayes, J.M., Eglinton, T.I., 2005. An evaluation of ¹⁴C age relationships between co-occurring foraminifera, alkenones, and total organic carbon in continental margin sediments. *Paleoceanography* 20. doi:10.1029/2004PA001103 PA1016.
- Mollenhauer, G., Inthorn, M., Vogt, T., Zabel, M., Sinninghe Damsté, J.S., Eglinton, T.I., 2007. Aging of marine organic matter during cross-shelf lateral transport in the Benguela upwelling system revealed by compound-specific radiocarbon dating. *Geochemistry, Geophysics, Geosystems*. 8, 1–16.
- Monnin, E., Indermuhle, A., Dallenbach, A., Fluckiger, J., Stauffer, B., Stocker, T.F., Raynaud, D., Barnola, J.M., 2001. Atmospheric CO₂ concentrations over the last glacial termination. *Science* 291, 112-114.
- Moreno, A., Nave, S., Kuhlmann, H., Canals, M., Targarona, J., Freudenthal, T., Abrantes, F., 2002. Productivity response in the North Canary Basin to climate changes during the last 250000 yr: a multi-proxy approach. *Earth and Planetary Science Letters* 196, 147-159.
- Moros, M., De Deckker, P., Jansen, E., Perner, K., Telford, R.J., 2009. Holocene climate variability in the Southern Ocean recorded in a deep-sea sediment core off South Australia. *Quaternary Science Reviews* 28, 1932-1940.
- Mulitza, S., Bouimetarhan, I., Brüning, M., Freeseemann, A., Gussone, N., Filipsson, H., Heil, G., Hessler, S., Jaeschke, A., Johnstone, H., Klann, M., Klein, F., Küster, K., März, C., McGregor, H., Minning, M., Müller, H., Ochsenhirt, W.-T., Paul, A., Schewe, F., Schulz, M., Steinlöchner, J., Stuur, J.-B., Tjallingii, R., Dobeneck, T., Wiesmaier, S., Zabel, M., Zonneveld, K., 2006. Report and preliminary results of Meteor-cruise M65/1, Dakar-Dakar, 11.06- 1.07.2005. *Berichte aus dem Fachbereich Geowissenschaften der Universität Bremen* 252, 1-149.
- Mulitza, S., Prange, M., Stuur, J.-B., Zabel, M., von Dobeneck, T., Itambi, A.C., Nizou, J., Schulz, M., Wefer, G., 2008. Sahel megadroughts triggered by glacial slowdowns of Atlantic meridional overturning. *Paleoceanography* 23, PA4206-1-PA4206-11.
- Müller, P.J., Kirst, G., Ruhland, G., von Storch, I., Rosell-Mele, A., 1998. Calibration of the alkenone paleotemperature index (U^K₃₇) based on core-tops from the eastern South Atlantic and the global ocean (60°N-60°S). *Geochimica et Cosmochimica Acta* 62, 1757–1772.
- Müller, P.J., Fischer, G., 2001. A 4-year sediment trap record of alkenones from the filamentous upwelling region off Cape Blanc, NW Africa and a comparison with distributions in underlying sediments. *Deep-Sea Research Part I* 48, 1877–1903.
- Murphy, B.P., Williamson, G.J., Bowman, D.M.J.S., 2012. Did central Australian megafaunal extinction coincide with abrupt ecosystem collapse or gradual climate change? *Global Ecology*

- and Biogeography 21, 142-151.
- Nave, S., Freitas, P., Abrantes, F., 2001. Coastal upwelling in the Canary Island region: spatial variability reflected by the surface sediment diatom record. *Marine Micropaleontology* 42, 1-23.
- Nave, S., Salgueiro, E., Abrantes, F., 2003. Siliceous sedimentary record of the last 280 kyr in the Canary basin (NW Africa). *Marine Geology* 196, 21-35.
- Nicholson, S.E., Grist, J.P., 2003. The seasonal evolution of the atmospheric circulation over West Africa and equatorial Africa. *Journal of Climate* 16, 1013-1030.
- Niedermeyer, E.M., Prange, M., Mulitza, S., Mollenhauer, G., Schefuss, E., Schulz, M., 2009. Extratropical forcing of Sahel aridity during Heinrich stadials. *Geophysical Research Letters* 36 L20707-1-L20707-4.
- Niedermeyer, E.M., Schefuss, E., Sessions, A.L., Mulitza, S., Mollenhauer, G., Schulz, M., Wefer, G., 2010. Orbital- and millennial-scale changes in the hydrologic cycle and vegetation in the western African Sahel: insights from individual plant wax δD and $\delta^{13}C$. *Quaternary Science Reviews* 29, 2996-3005.
- Nürnberg, D., Bijma, J., Hemleben, C., 1996. Assessing the reliability of magnesium in foraminiferal calcite as a proxy for water mass temperatures. *Geochimica et Cosmochimica Acta* 60, 803-814.
- Ohkouchi, N., Kawamura, K., Taira, A., 1997. Fluctuations of terrestrial and marine biomarkers in the western tropical Pacific during the last 23,300 years. *Paleoceanography* 12, 623-630.
- Olivieri, A., Achilli, A., Pala, M., Battaglia, V., Fornarino, S., Al-Zahery, N., Scozzari, R., Cruciani, F., Behar, D.M., Dugoujon, J.-M., Coudray, C., Santachiara-Benerecetti, A.S., Semino, O., Bandelt, H.-J., Torroni, A., 2006. The mtDNA legacy of the Levantine early Upper Palaeolithic in Africa. *Science* 314, 1767-1770.
- Olley, J.M., Pietsch, T., Roberts, R.G., 2004. Optical dating of Holocene sediments from a variety of geomorphic settings using single grains of quartz. *Geomorphology* 60, 337-358.
- Opsteegh, J.D., Haarsma, R.J., Selten, F.M., Kattenberg, A., 1998. ECBILT: a dynamic alternative to mixed boundary conditions in ocean models. *Tellus series A: Dynamic Meteorology and Oceanography* 50, 348-367.
- Osborne, A.H., Vance, D., Rohling, E.J., Barton, N., Rogerson, M., Fello, N., 2008. A humid corridor across the Sahara for the migration of early modern humans out of Africa 120,000 years ago. *Proceedings of the National Academy of Sciences of the United States of America* 105, 16444-16447.
- Paillard, D., Labeyrie, L., Yiou, P., 1996. Macintosh program performs time-series analysis. *Eos* 77, 379.
- Park, B.-J., Park, S.-J., Yoon, D.-N., Schouten, S., Sinninghe Damsté, J. S., Rhee, S.-K., 2010. Cultivation of autotrophic Ammonia-oxidizing archaea from marine sediments in coculture with sulfur-oxidizing bacteria. *Applied and Environmental Microbiology* 76, 7575-7587.
- Pashynska, V., Vermeylen, R., Vas, G., Maenhaut, W., Claeys, M., 2002. Development of a gas chromatographic / ion trap mass spectrometric method for the determination of levoglucosan and saccharidic compounds in atmospheric aerosols. Application to urban aerosols. *Journal of Mass Spectrometry* 37, 1249-1257.
- Passlow, V., Wang, P., Chivas, A.R., 1997. Late Quaternary palaeoceanography near Tasmania, southern Australia. *Palaeogeography Palaeoclimatology Palaeoecology* 131, 433-463.
- Paul, A., Schafer-Neth, C., 2003. Modeling the water masses of the Atlantic Ocean at the last glacial maximum. *Paleoceanography* 1058. doi:10.1029/2002PA000783.
- Pearce, G.E.S., Harradine, P.J., Talbot, H.M., Maxwell, J.R., 1998. Sedimentary sterols and steryl chlorin esters: distribution differences and significance. *Organic Geochemistry* 28, 3-10.
- Pearson, P.N., Ditchfield, P.W., Singano, J., Harcourt-Brown, K.G., Nicholas, C.J., Olsson, R.K., Shackleton, N.J., Hall, M.A., 2001. Warm tropical sea surface temperatures in the Late Cretaceous and Eocene epoch. *Nature* 413, 481-487.
- Pena, L.D., Cacho, I., Ferretti, P., Hall, M.A., 2008. El Niño-Southern Oscillation-like variability during glacial terminations and interlatitudinal teleconnections. *Paleoceanography* 23, PA3101-8.
- Pepin, L., Raynaud, D., Barnola, J.M., Loutre, M.F., 2001. Hemispheric roles of climate forcings during glacial-interglacial transitions as deduced from the Vostok record and LLN-2D model experiments. *Journal of Geophysical Research-Atmospheres* 106, 31885-31892.
- Peters, K.E., Walters, C.C. and Moldovan, J.M., 2005. *The Biomarker Guide. Vol. I*, Cambridge University Press, Cambridge, 471 pp.
- Peterson, R.G., Stramma, L., 1991. Upper-level circulation in the South Atlantic Ocean. *Progress in*

- Oceanography 26, 1–73.
- Pether, J., 2012. *Proposed Sand Mine on Blaauwberg Farm (Cape Farm 88 and Cape Farm 91), near Melkbosstrand, City of Cape Town, Western Cape (Annexure B)*. AMATHEMBA Environmental Management Consulting. Ref E12/2/4/2-A2/305-3031/11
- Petit, J.R., Jouzel, J., Raynaud, D., Barkov, N.I., Barnola, J.M., Basile, I., Bender, M., Chappellaz, J., Davis, M., Delaygue, G., Delmotte, M., Kotlyakov, V.M., Legrand, M., Lipenkov, V.Y., Lorius, C., Pepin, L., Ritz, C., Saltzman, E., Stievenard, M., 1999. Climate and atmospheric history of the past 420,000 years from the Vostok ice core, Antarctica. *Nature* 399, 429-436.
- Pflaumann, U., Duprat, J., Pujol, C., Labeyrie, L.D., 1996. SIMMAX: A modern analog technique to deduce Atlantic sea surface temperatures from planktonic foraminifera in deep-sea sediments. *Paleoceanography* 11, 15-35.
- Pierau, R., Hanebuth, T.J.J., Krastel, S., Henrich, R., 2010. Late Quaternary climatic events and sea-level changes recorded by turbidite activity, Dakar Canyon, NW Africa. *Quaternary Research* 73, 385-392.
- Piotrowski, A.M., Goldstein, S.L., Hemming, S.R., Fairbanks, R.G., 2005. Temporal relationships of carbon cycling and ocean circulation at glacial boundaries. *Science* 307, 1933–1938.
- Piotrowski, A.M., Goldstein, S.L., Hemming, S.R., Fairbanks, R.G., Zylberberg, D.R., 2008. Oscillating glacial northern and southern deep water formation from combined neodymium and carbon isotopes. *Earth and Planetary Science Letters* 272, 394–405.
- Pitcher, A., Wuchter, C., Siedenberg, K., Schouten, S., Sinninghe Damsté, J.S., 2011. Crenarchaeol tracks winter blooms of ammonia-oxidizing Thaumarchaeota in the coastal North Sea. *Limnology and Oceanography* 56, 2308-2318.
- Prahl, F.G., Wakeham, S.G., 1987. Calibration of unsaturation patterns in long-chain ketone compositions for palaeotemperature assessment. *Nature* 330, 367-369.
- Prahl, F.G., Muehlhausen, L.A., Zahnle, D.B., 1988. Further evaluation of long-chain alkenones as indicators of paleoceanographic conditions. *Geochimica et Cosmochimica Acta* 52, 2303-2310.
- Prange, M., Schulz, M., 2004. A coastal upwelling seesaw in the Atlantic Ocean as a result of the closure of the Central American Seaway. *Geophysical Research Letters* 31, L17207. doi:10.1029/2004GL020073.
- Prescott, G. W., Williams, D. R., Balmford, A., Green, R. E., & Manica, E., 2012. Quantitative global analysis of the role of climate and people in explaining late Quaternary megafaunal extinctions. *Proceedings of the National Academy of Sciences of the United States of America* Early Edition 1-5; doi:10.1073/pnas.1113875109.
- Prideaux, G.J., Roberts, R.G., Megirian, D., Westaway, K.E., Hellstrom, J.C., Olley, J.I., 2007. Mammalian responses to Pleistocene climate change in southeastern Australia. *Geology* 35, 33-36.
- Prideaux, G.J., Ayliffe, L.K., DeSantis, L.R.G., Schubert, B.W., Murray, P.F., Gagan, M.K., Cerling, T.E., 2009. Extinction implications of a chenopod browse diet for a giant Pleistocene kangaroo. *Proceedings of the National Academy of Sciences of the United States of America* 106, 11646-11650.
- Rahmstorf, S., 2002. Ocean circulation and climate during the past 120, 000 years. *Nature* 419, 207–214.
- Rampen, S.W., Schouten, S., Koning, E., Brummer, G.-J.A., Sinninghe Damsté, J.S., 2008. A 90 kyr upwelling record from the northwestern Indian Ocean using a novel long-chain diol index. *Earth and Planetary Science Letters* 276, 207-213.
- Rampen, S.W., Willmott, V., Kim, J.-H., Uliana, E., Mollenhauer, G., Schefuß, E., Sinninghe Damsté, J.S., Schouten, S., 2012. Long chain 1,13- and 1,15-diols as a potential proxy for palaeotemperature reconstruction. *Geochimica et Cosmochimica Acta* 84, 204-216.
- Raynaud, D., Barnola, J.M., Souchez, R., Lorrain, R., Petit, J.R., Duval, P., Lipenkov, V.Y., 2005. Palaeoclimatology - The record for marine isotopic stage 11. *Nature* 436, 39-40.
- Reimer, P.J., Reimer, R.W., 2001. A marine reservoir correction database and on-line interface. *Radiocarbon* 43, 461-463.
- Reimer, P. J., Baillie, M. G. L., Bard, E., Bayliss, A., Beck, J. W., Blackwell, P. G., Ramsey, C. B., Buck, C. E., Burr, G. S., Edwards, R. L., Friedrich M., Grootes, P.M., Guilderson, T.P., Hajdas, I., Heaton, T.J., Hogg, A.G., Hughen, K.A., Kaiser, K.F., Kromer, B., McCormac F.G., Manning, S.W., Reimer R.W., Richards D.A., Southon, J.R., Talamo, S., Turney, C.S.M., van der Plicht, J., Weyhenmeyer, C.E., 2009. Intcal09 and Marine09 Radiocarbon Age Calibration Curves, 0-50,000

- Years Cal Bp. Radiocarbon 51, 1111-1150.
- Repeta, D.J., 1989. Carotenoid diagenesis in recent marine sediments: II. Degradation of fucoxanthin to loliolide. *Geochimica et Cosmochimica Acta* 53, 699-707.
- Repeta, D.J., Simpson, D.J., Jorgensen, B.B., Jannasch, H.W., 1989. Evidence for Anoxygenic Photosynthesis from the Distribution of Bacteriochlorophylls in the Black-Sea. *Nature* 342, 69-72.
- Repeta, D.J., McCaffrey, M.A., and Farrington, J.W., 1992. Organic geochemistry as a tool to study upwelling systems: recent results from the Peru and Namibian shelves. In Summerhayes, C.P., Prell, W.L., and Emeis, K.C. (Eds.), *Upwelling Systems: Evolution Since the Early Miocene*. Geological Society London Special Publications, 64:257-272.
- Richardson, P.L., Walsh, D., 1986. Mapping climatological seasonal variations of surface currents in the tropical Atlantic using ship drifts. *Journal of Geophysical Research - Oceans* 91, 537-550.
- Ridgway, K.R., Condie S.A., 2004. The 5500-km-long boundary flow off western and southern Australia. *Journal of Geophysical Research - Oceans* 109, C04017-1-C04017-18; doi:10.1029/2003JC001921.
- Ritchie, J.C., Eyles, C.H., Haynes, C.V., 1985. Sediment and Pollen Evidence for An Early to Mid-Holocene Humid Period in the Eastern Sahara. *Nature* 314, 352-355.
- Roberts, R.G., Flannery, T.F., Ayliffe, L.K., Yoshida, H., Olley, J.M., Prideaux, G.J., Laslett, G.M., Baynes, A., Smith, M. A., Jones, R., Smith B.L., 2001. New ages for the last Australian megafauna: continent-wide extinction about 46,000 years ago. *Science* 292, 1888-1892.
- Robinson, N., Cranwell, P.A., Finlay, B.J., Eglinton, G., 1984. Lipids of aquatic organisms as potential contributors to lacustrine sediments. *Organic Geochemistry* 6, 143-152.
- Rohling, E.J., Cane, T.R., Cooke, S., Sprovieri, M., Bouloubassi, I., Emeis, K.C., Schiebel, R., Kroon, D., Jorissen, F.J., Lorre, A., Kemp, A.E.S., 2002. African monsoon variability during the previous interglacial maximum. *Earth and Planetary Science Letters* 202, 61-75.
- Romero, O., Mollenhauer, G., Schneider, R.R., Wefer, G., 2003. Oscillations of the siliceous imprint in the central Benguela Upwelling System from MIS 3 through to the early Holocene: the influence of the Southern Ocean. *Journal of Quaternary Science* 18, 733-743.
- Romero, O.E., Kim, J.H., Donner, B., 2008. Submillennial-to-millennial variability of diatom production off Mauritania, NW Africa, during the last glacial cycle. *Paleoceanography* 23, PA3218-1-17.
- Rommerskirchen, F., Plader, A., Eglinton, G., Chikaraishi, Y., Rullkötter, J., 2006. Chemotaxonomic significance of distribution and stable carbon isotopic composition of long-chain alkanes and alkan-1-ols in C₄ grass waxes. *Organic Geochemistry* 37, 1303-1332.
- Rommerskirchen, F., Condon, T., Mollenhauer, G., Dupont, L., Schefuss, E., 2011. Miocene to Pliocene development of surface and subsurface temperatures in the Benguela Current system. *Paleoceanography* 26, PA3216-1-15.
- Rule, S., Brook, B.W., Haberle, S.G., Turney, C.S.M., Kershaw, A.P., Johnson, C.N., 2012. The aftermath of megafaunal extinction: Ecosystem transformation in Pleistocene Australia. *Science*, 1483-1486.
- Saito, T., Thompson, R.R., Breger, D., 1981. *Systematic index of recent and Pleistocene planktonic foraminifera*. University of Tokyo Press, Tokyo, 190 pp.
- Sanudo-Wilhelmy, S.A., Kustka, A.B., Gobler, C.J., Hutchins, D.A., Yang, M., Lwiza, K., Burns, J., Capone, D.G., Raven, J.A., Carpenter, E.J., 2001. Phosphorus limitation of nitrogen fixation by *Trichodesmium* in the central Atlantic Ocean. *Nature* 411, 66-69.
- Sarmiento, J.L., Gruber, N., Brzezinski, M.A., Dunne, J.P., 2004. High-latitude controls of the thermocline nutrients and low latitude biological productivity. *Nature* 427, 56-60.
- Sarnthein, M., Tetzlaff, G., Koopmann, B., Wolter, K., Pflaumann, U., 1981. Glacial and Inter-Glacial Wind Regimes Over the Eastern Sub-Tropical Atlantic and Northwest Africa. *Nature* 293, 193-196.
- Sarnthein, M., Thiede, J., Pflaumann, U., Erlenkeuser, H., Fiitterer, D., Koopmann, B., Lange, H., and Seibold, E., 1982. Atmospheric and oceanic circulation patterns off northwest Africa during the past 25 million years. In von Rad, U., Hinz, K., Sarnthein, M., and Seibold, E. (Eds.), *Geology of the Northwest African Continental Margin*: Berlin-Heidelberg-New York (Springer-Verlag), 545-603.
- Schefuß, E., Versteegh, G.J.M., Jansen, J.H.F., Sinninghe Damsté, J.S., 2001. Marine and terrigenous lipids in southeast Atlantic sediments (Leg 175) as paleoenvironmental indicators: initial results. In: Wefer, G., Berger, W. H., Richter, C. (Eds.), *Proceedings of the Ocean Drilling Program*,

- Scientific Results* 175, 1-34, doi:10.2973/odp.proc.sr.175.228.2001.
- Schefeuf, E., Ratmeyer, V., Stuut, J.-B.W., Jansen, J.H.F., Sinninghe Damsté, J.S., 2003a. Carbon isotope analyses of *n*-alkanes in dust from the lower atmosphere over the central eastern Atlantic. *Geochimica et Cosmochimica Acta* 67, 1757-1767.
- Schefeuf, E., Schouten, S., Jansen, J.H.F., Sinninghe Damsté, J.S., 2003. African vegetation controlled by tropical sea surface temperatures in the mid-Pleistocene period. *Nature* 422, 418-421.
- Schefeuf, E., Schouten, S., Schneider, R.R., 2005. Climatic controls on central African hydrology during the past 20,000 years. *Nature* 437, 1003-1006.
- Schkolnik, G., Rudich, Y., 2006. Detection and quantification of levoglucosan in atmospheric aerosols: A review. *Analytical and Bioanalytical Chemistry* 385, 26-33.
- Schmidt, M.W., Spero, H.J., Lea, D.W., 2004. Links between salinity variation in the Caribbean and North Atlantic thermohaline circulation. *Nature* 428, 160-163.
- Schmidt, M.W., Vautravers, M.J., Spero, H.J., 2006. Western Caribbean sea surface temperatures during the late Quaternary. *Geochemistry, Geophysics, Geosystems* 7, 1-17.
- Schmidt, S., De Deckker, P., Etcheber, H., Caradec, S., 2010. Are the Murray Canyons offshore southern Australia still active for sediment transport? *Geological Society of London, Special Publications* 346, 43-55, doi:10.1144/SP346.4.
- Schott, F.A., Brandt, P., Hamann, M., Fischer, R., Stramma, L., 2002. On the boundary flow off Brazil at 5-10°S and its connection to the interior tropical Atlantic. *Geophysical Research Letters* 29, 1840. doi:10.1029/2002GL014786.
- Schott, F.A., McCreary, J.P., Johnson, G.C., 2002a. Schallow Overturnig Circulations of the Tropical-Subtropical Oceans. *Geophysical Monograph* 147, 261-304.
- Schouten, S., Hoefs, M.J.L., Sinninghe Damsté, J.S., 2000. A molecular and stable carbon isotopic study of lipids in late Quaternary sediments from the Arabian Sea. *Organic Geochemistry* 31, 509-521.
- Schouten, S., Hopmans, E.C., Schefeuf, E., Sinninghe Damsté, J.S., 2002. Distributional variations in marine crenarchaeotal membrane lipids: a new tool for reconstructing ancient sea water temperatures? *Earth and Planetary Science Letters* 204, 265-274.
- Schouten, S., Hopmans, E.C., Sinninghe Damsté, J.S., 2004. The effect of maturity and depositional redox conditions on archaeal tetraether lipid palaeothermometry. *Organic Geochemistry* 35, 567-571.
- Schouten, S., Rampen, S.W., Geenevasen, J.A.J., Sinninghe Damsté, J.S., 2005. Structural identification of steryl alkyl ethers in marine sediments. *Organic Geochemistry* 36, 1323-1333.
- Schouten, S., Hugué, C., Hopmans, E.C., Kienhuis, M.V.M., Damsté, J.S.S., 2007. Analytical methodology for TEX₈₆ palaeothermometry by high-performance liquid chromatography/atmospheric pressure chemical ionization-mass spectrometry. *Analytical Chemistry* 79, 2940-2944.
- Schubert, C.J., Villanueva, J., Calvert, S.E., Cowie, G.L., von Rad, U., Schulz, H., Berner, U., Erlenkeuser, H., 1998. Stable phytoplankton community structure in the Arabian Sea over the past 200,000 years. *Nature* 394, 563-566.
- Sedwick, P.N., Church, T.M., Bowie, A.R., Marsay, C.M., Ussher, S.J., Achilles, K.M., Lethaby, P.J., Johnson, R.J., Sarin, M.M., McGillicuddy, D.J., 2005. Iron in the Sargasso Sea (Bermuda Atlantic Time-series Study region) during summer: Eolian imprint, spatiotemporal variability, and ecological implications. *Global Biogeochemical Cycles* 19, GB4006-1-11.
- Shackleton, N.J., Fairbanks, R.G., Chiu, T.C., Parrenin, F., 2004. Absolute calibration of the Greenland time scale: Implications for Antarctic time scales and for $\Delta^{14}\text{C}$. *Quaternary Science Reviews* 23, 1513-1522.
- Shah, S.R., Mollenhauer, G., Ohkouchi, N., Eglinton, T.I., Pearson, A., 2008. Origins of archaeal tetraether lipids in sediments: insights from radiocarbon analysis. *Geochimica et Cosmochimica Acta* 72, 4577-4594.
- Shanahan, T.M., Overpeck, J.T., Wheeler, C.W., Beek, J.W., Pigati, J.S., Talbot, M.R., Scholz, C.A., Peck, J., King, J.W., 2006. Paleoclimatic variations in West Africa from a record of late Pleistocene and Holocene lake level stands of Lake Bosumtwi, Ghana. *Palaeogeography Palaeoclimatology Palaeoecology* 242, 287-302.
- Shea, J.J., 2008. Transitions or turnovers? Climatically forced extinctions of *Homo sapiens* and Neanderthals in the east Mediterranean Levant. *Quaternary Science Reviews* 27, 2253-2270.
- Sicre, M.-A., Ternois, Y., Paterne, M., Boireau, A., Beaufort, L., Martinez, P., Bertrand, P., 2000.

- Biomarker stratigraphic records over the last 150 kyrs off the NW African coast at 25° N. *Organic Geochemistry* 31, 577-588.
- Sicre, M.-A., Ternois, Y., Paterne, M., Martinez, P., Bertrand, P., 2001. Climatic changes in the upwelling region off Cap Blanc, NW Africa, over the last 70 kyear: a multi-biomarker approach. *Organic Geochemistry* 32, 981-990.
- Siegenthaler, U., Stocker, T.F., Monnin, E., Luthi, D., Schwander, J., Stauffer, B., Raynaud, D., Barnola, J.M., Fischer, H., Masson-Delmotte, V., Jouzel, J., 2005. Stable carbon cycle-climate relationship during the late Pleistocene. *Science* 310, 1313-1317.
- Sikes, E.L., Howard, W.R., Samson, C.R., Mahan, T.S., Robertson, L.G., Volkman, J.K., 2009. Southern Ocean seasonal temperature and Subtropical Front movement on the South Tasman Rise in the late Quaternary. *Paleoceanography* 24, PA2201-1-PA2201-13.
- Simpson, C.D., Dills, R.L., Katz, B.S., Kalman, D.A., 2004. Determination of levoglucosan in atmospheric fine particulate matter. *Journal of Air and Waste Management Association* 54, 689-694.
- Simoneit, B.R.T., 2002. Biomass burning — a review of organic tracers for smoke from incomplete combustion. *Applied Geochemistry* 17, 129-162.
- Singh, G., 1983. *Late Quaternary vegetation and lake level record from Lake George, N.S.W., 18 +/- 2 ka*. In J. Chappell and A. Grindrod (eds), *Proceedings of the First CLIMANZ Conference, 1981*, Australian National University, p. 66.
- Sinninghe Damsté, J.S., Rijpstra, W.I.C., Schouten, S., Peletier, H., van der Maarel, M.J.E.C., Gieskes, W.W.C., 1999. A C₂₅ highly branched isoprenoid alkene and C₂₅ and C₂₇ *n*-polyenes in the marine diatom *Rhizosolenia setigera*. *Organic Geochemistry* 30, 95-100.
- Sinninghe Damsté, J.S., Schouten, S., Hopmans, E.C., van Duin, A.C.T., Geenevasen, J.A.J., 2002. Crenarchaeol: the characteristic core glycerol dibiphytanyl glycerol tetraether membrane lipid of cosmopolitan pelagic crenarchaeota. *Journal of Lipid Research* 43, 1641-1651.
- Sinninghe Damsté, J.S., Rampen, S., Rijpstra, W.I.C., Abbas, B., Muyzer, G., Schouten, S., 2003. A diatomaceous origin for long-chain diols and mid-chain hydroxy methyl alkanolates widely occurring in Quaternary marine sediments: Indicators for high-nutrient conditions. *Geochimica et Cosmochimica Acta* 67, 1339-1348.
- Smith, S.L., Codispoti, L.A., Morrison, J.M., Barber, R.T., 1998. The 1994-1996 Arabian Sea Expedition: An integrated, interdisciplinary investigation of the response of the northwestern Indian Ocean to monsoonal forcing. *Deep-Sea Research II* 45, 1905-1915.
- Smith, S.L., 2001. Understanding the Arabian Sea: Reflections on the 1994-1996 Arabian Sea Expedition. *Deep-Sea Research II* 48, 1385-1402.
- Spero, H.J., Bijma, J., Lea, D.W., Bemis, B.E., 1997. Effect of seawater carbonate concentration on foraminiferal carbon and oxygen isotopes. *Nature* 390, 497-500.
- Spero, H.J., Lea, D.W., 2002. The cause of carbon isotope minimum events on glacial terminations. *Science* 296, 522-525.
- Spooner, M.I., Barrows, T.T., De Deckker, P., Paterne, M., 2005. Palaeoceanography of the Banda Sea, and Late Pleistocene initiation of the Northwest Monsoon. *Global and Planetary Change* 49, 28-46.
- Spooner, M.I., De Deckker, P., Barrows, T.T., Fifield L.K., 2011. The behaviour of the Leeuwin Current offshore NW Australia during the last five glacial-interglacial cycles. *Global and Planetary Change* 75, 119-132.
- Sprengel, C., Baumann, K.H., Neuer, S., 2000. Seasonal and interannual variation of coccolithophore fluxes and species composition in sediment traps north of Gran Canaria (29°N 15°W). *Marine Micropaleontology* 39, 157-178.
- Stanley, S.M., 1999. *Earth System History*, W.H. Freeman and Company, New York, NY, 615 pp.
- Stephens, S.L., Martin, R.E., Clinton, N.E., 2007. Prehistoric fire area and emissions from California's forests, woodlands, shrublands, and grasslands. *Forest Ecology and Management* 251, 205-216.
- Still, C.J., Berry, J.A., Collatz, G.J., DeFries, R.S., 2003. Global distribution of C₃ and C₄ vegetation: Carbon cycle implications. *Global Biogeochemical Cycles* 17:1006,10.1029/2001GB001807.
- Stokes, S., Ingram, S., Aitken, M.J., Sirocko, F., Anderson, R., Leuschner, D., 2003. Alternative chronologies for Late Quaternary (Last Interglacial-Holocene) deep sea sediments via optical dating of silt-sized quartz. *Quaternary Science Reviews* 22, 925-941.
- Stouffer, R.J., Yin, J., Gregory, J.M., Dixon, K.W., Spelman, M.J., Hurlin, W., Weaver, A.J., Eby, M., Flato, G.M., Hasumi, H., Hu, A., Jungclaus, J.H., Kamenkovich, I.V., Levermann, A., Montoya,

- M., Murakami, S., Nawrath, S., Oka, A., Peltier, W.R., Robitaille, D.Y., Sokolov, A., Vettoretti, G., Weber, S.L., 2006. Investigating the causes of the response of the thermohaline circulation to past and future climate changes. *Journal of Climate* 19, 1365–1387.
- Stringer, C., 2000. Coasting out of Africa. *Nature* 405, 24–27.
- Stuiver, M., Reimer, P.J., 1993. Extended ^{14}C database and revised CALIB 3.0 ^{14}C age calibration program. *Radiocarbon* 35, 215–230.
- Sturman, S. and Tapper N., 1996. *The weather and climate of Australia and New Zealand*. Oxford University Press, Australia, pp. 1–476.
- Ternois, Y., Sicre, M.-A., Boireau, A., Conte, M.H., Eglinton, G., 1997. Evaluation of long-chain alkenones as paleo-temperature indicators in the Mediterranean Sea. *Deep-Sea Research Part I-Oceanographic Research Papers* 44, 271–286.
- Tipple, B.J., Pagani, M., 2007. The early origins of terrestrial C_4 photosynthesis. *Annual Review of Earth and Planetary Sciences* 35, 435–461.
- Tjallingii, R., Claussen, M., Stuut, J.B.W., Fohlmeister, J., Jahn, A., Bickert, T., Lamy, F., Rohl, U., 2008. Coherent high- and low-latitude control of the northwest African hydrological balance. *Nature Geoscience* 1, 670–675.
- Toggweiler, J.R., Dixon, K., Broecker, W.S., 1991. The Peru Upwelling and the Ventilation of the South-Pacific Thermocline. *Journal of Geophysical Research-Oceans* 96, 20467–20497.
- Turney, C.S.M., Flannery, T.F., Roberts, R.G., Reid, C., Fifield, L.K., Higham, T.F.G., Jacobs, Z., Kemp, N., Colhoun, E.A., Kalin, R.M., Ogle, N., 2008. Late-surviving megafauna in Tasmania, Australia, implicate human involvement in their extinction. *Proceedings of the National Academy of Sciences of the United States of America of the United States of America* 105, 12150–12153.
- Urey, H.C., 1947. The Thermodynamic Properties of Isotopic Substances. *Journal of the Chemical Society* 1947, 562–581.
- van Camp, L., Nykjær, L., Mittelstaedt, E., Schlittenhardt, P., 1991. Upwelling and boundary circulation off Northwest Africa as depicted by infrared and visible satellite-observations. *Progress in Oceanography* 26, 357–402.
- van der Kaars, S. & De Deckker, P., 2002. A Late Quaternary pollen record from deep-sea core Fr10/95, GC17 offshore Cape Range Peninsula, northwestern Western Australia. *Review of Palaeobotany and Palynology* 120, 17–39.
- Versteegh, G.J.M., Bosch, H.-J., de Leeuw, J.W., 1997. Potential palaeoenvironmental information of C_{24} to C_{36} mid-chain diols, keto-ols and mid-chain hydroxy fatty acids; a critical review. *Organic Geochemistry* 27, 1–13.
- Vidal, I., Labeyrie, L., Cortijo, E., Arnold, M., Duplessy, J.C., Michel, E., Becqué, S., van Weering, T.C.E., 1997. Evidence for changes in the North Atlantic Deep Water linked to meltwater surges during the Heinrich events. *Earth and Planetary Science Letters* 146, 13–27.
- Vogel, J.S., 1984. Performance of catalytically condensed carbon for use in accelerator mass spectrometry. *Nuclear Instruments and Methods in Physics Research Section B: Beam Interactions with Materials and Atoms* 5, 289–293.
- Volkman, J.K., Eglinton, G., Corner, E.D.S., Forsberg, T.E.V., 1980. Long-chain alkenes and alkenones in the marine coccolithophorid *Emiliana huxleyi*. *Phytochemistry* 19, 2619–2622.
- Volkman, J.K., Barrett, S.M., Dunstan, G.A., Jeffrey, S.W., 1992. C_{30} - C_{32} alkyl diols and unsaturated alcohols in microalgae of the class *Eustigmatophyceae*. *Organic Geochemistry* 18, 131–138.
- Volkman, J.K., Barrett, S.M., Dunstan, G.A., Jeffrey, S.W., 1993. Geochemical significance of the occurrence of dinosterol and other 4-methyl sterols in a marine diatom. *Organic Geochemistry* 20, 7–15.
- Volkman, J.K., Barrett, S.M., Dunstan, G.A., 1994. C_{25} and C_{30} highly branched isoprenoid alkenes in laboratory cultures of two marine diatoms. *Organic Geochemistry* 21, 407–413.
- Volkman, J.K., Barrett, S.M., Blackburn, S.I., Mansour, M.P., Sikes, E.L., Gelin, F., 1998. Microalgal biomarkers: A review of recent research developments. *Organic Geochemistry* 29, 1163–1179.
- Waelbroeck, C., Labeyrie, L., Duplessy, J.C., Guiot, J., Labracherie, M., Leclaire, H., Duprat, J., 1998. Improving past sea surface temperature estimates based on planktonic fossil faunas. *Paleoceanography* 13, 272–283.
- Webb, S., 2008. Megafauna demography and late Quaternary climatic change in Australia: A predisposition to extinction. *Boreas* 37, 329–345.
- Wefer, G., Berger, W.H., Richter, C., et al., 1998. *Proceedings of the Ocean Drilling Program, Initial Reports*, 175. College Station, TX (Ocean Drilling Program).

- Weijers, J.W.H., Schouten, S., Spaargaren, O.C., Sinninghe Damsté, J.S., 2006. Occurrence and distribution of tetraether membrane lipids in soils: Implications for the use of the TEX₈₆ proxy and the BIT index. *Organic Geochemistry* 37, 1680–1693.
- Weijers, J.W.H., Schouten, S., van den Donker, J.C., Hopmans, E.C., Damsté, J.S.S., 2007. Environmental controls on bacterial tetraether membrane lipid distribution in soils. *Geochimica et Cosmochimica Acta* 71, 703–713.
- Weldeab, S., Lea, D.W., Schneider, R.R., Andersen, N., 2007. 155, 000 years of West African monsoon and ocean thermal evolution. *Science* 316, 1303–1307.
- Wells, P.E., Wells, G.M., 1994. Large-Scale Reorganization of Ocean Currents Offshore Western-Australia During the Late Quaternary. *Marine Micropaleontology* 24, 157–186.
- Weltje, G.J., Tjallingii, R., 2008. Calibration of XRF core scanners for quantitative geochemical logging of sediment cores: Theory and application. *Earth and Planetary Science Letters* 274, 423–438.
- White, F., 1983. *The Vegetation of Africa, A Descriptive Memoir to Accompany the UNESCO/AETFAT/UNSO Vegetation Map of Africa* (United Nations Educational, Scientific, and Cultural Organization, Paris).
- Wien, K., Wissmann, D., Kolling, M., Schulz, H.D., 2005. Fast application of X-ray fluorescence spectrometry aboard ship: how good is the new portable Spectro Xepos analyser? *Geo-Marine Letters* 25, 248–264.
- Wilkins, D., 2009. Comparative optically stimulated luminescence (OSL) and AMS radiocarbon dating of Holocene lacustrine and marine deposits in southeast and southwestern Australia. PhD thesis, The Australian National University, Canberra. Australia.
- Wilkins, D., De Deckker, P., Fifield, L.K., Gouramanis, C., Olley, J., 2012. Comparative optical and radiocarbon dating of laminated Holocene sediments in two maar lakes: Lake Keilambete and Lake Gnotuk, south-western Victoria, Australia. *Quaternary Geochronology* 9, 3–15.
- Wilkinson, C. S., 1885. President's Address, Annual General Meeting. *Proceedings of the Linnean Society of N. S. W.* 9, 1207–1241.
- Williams, N.J., Harle, K.J., Gale, S.J., Heijnis, H., 2006. The vegetation history of the last glacial-interglacial cycle in eastern New South Wales, Australia. *Journal of Quaternary Science* 21, 735–750.
- Willmott, V., Rampen, S.W., Domack, E., Canals, M., Sinninghe Damsté, J.S., Schouten, S., 2010. Holocene changes in *Proboscia* diatom productivity in shelf waters of the north-western Antarctic Peninsula. *Antarctic Science* 22, 3–10.
- Wilson, W.D., Johns, E., Molinari, R.L., 1994. Upper layer circulation in the western tropical North Atlantic Ocean during August 1989. *Journal of Geophysical Research - Oceans* 99, 22513–22523.
- Winter, K., Smith, J.A., 1996. *Crassulacean Acid Metabolism: Biochemistry, Ecophysiology, and Evolution*, Springer, Berlin.
- Wooster, W.S., Bakun, A., McInain, D.R., 1976. The seasonal upwelling cycle along eastern boundary of North Atlantic. *Journal of Marine Research* 34, 131–141.
- Wroe, S. & Field, J., 2006. A review of the evidence for a human role in the extinction of Australian megafauna and an alternative interpretation. *Quaternary Science Reviews* 25, 2692–2703.
- Wu, J.F., Sunda, W., Boyle, E.A., Karl, D.M., 2000. Phosphate depletion in the western North Atlantic Ocean. *Science* 289, 759–762.
- Wuchter, C., Abbas, B., Coolen, M.J.L., Herfort, L., van Bleijswijk, J., Timmers, P., Strous, M., Teira, E., Herndl, G.J., Middelburg, J.J., Schouten, S., Sinninghe Damsté, J.S., 2006a. Archaeal nitrification in the ocean. *Proceedings of the National Academy of Science* 103, 12317–12322.
- Wuchter, C., Schouten, S., Wakeham, S.G., Sinninghe Damsté, J.S., 2006. Archaeal tetraether membrane lipid fluxes in the northeastern Pacific and the Arabian Sea: implications for TEX₈₆ paleothermometry. *Paleoceanography* 21 PA4208-1-PA4208-9.
- Xie, S., Nott, C.J., Avsejs, L.A., Volders, F., Maddy, D., Chambers, F.M., Gledhill, A., Carter, J.F., Evershed, R.P., 2000. Palaeoclimate records in compound-specific delta D values of a lipid biomarker in ombrotrophic peat. *Organic Geochemistry* 31, 1053–1057.
- Zarriess, M., Mackensen, A., 2010. The tropical rainbelt and productivity changes off northwest Africa: A 31,000-year high-resolution record. *Marine Micropaleontology* 76, 76–91.
- Zhang, R., 2007. Anticorrelated multidecadal variations between surface and subsurface tropical North Atlantic. *Geophysical Research Letters* 34, L12713. doi:10.1029/2007GL030225.
- Zhao, M., Eglinton, G., Haslett, S.K., Jordan, R.W., Sarnthein, M., Zhang, Z., 2000. Marine and

- terrestrial biomarker records for the last 35,000 years at ODP site 658C off NW Africa. *Organic Geochemistry* 31, 919-930.
- Zhao, M., Mercer, J.L., Eglinton, G., Higginson, M.J., Huang, C.-Y., 2006. Comparative molecular biomarker assessment of phytoplankton paleoproductivity for the last 160 kyr off Cap Blanc, NW Africa. *Organic Geochemistry* 37, 72-97.
- Zuppi, G.M., Sacchi, E., 2004. Hydrogeology as a climate recorder: Sahara-Sahel (North Africa) and the Po Plain (Northern Italy). *Global Planet Change* 40, 79-91.

Summary

Northwest (NW) Africa and Southeast (SE) Australia are regions which are particularly vulnerable to climate change. The predicted climate change for the future can lead to large change in temperatures and water supply, strong shifts in biodiversity and can compromise the food production of these areas. Research has been performed to investigate the impact of future climate change in these regions by climate modeling efforts but, unfortunately, several uncertainties remain with such predictions. One way to improve the results of the climate models is by testing them with paleoclimate data. In this thesis, organic proxies are used from marine sediment cores to reconstruct past environmental conditions in NW Africa and SE Australia. Three environmental parameters were studied, i.e. sea water temperatures, primary productivity and vegetation changes.

In sediments from the Guinea Plateau Margin (NW Africa), the $U^{K'}_{37}$ Index (based on long chain alkenones) was shown to be an efficient proxy for sea surface temperature (SST) reconstruction, while the TEX^H_{86} Index (based on glycerol dialkyl glycerol tetraethers) was shown to be related to thermocline temperatures. The record of SSTs ($U^{K'}_{37}$ Index) and thermocline temperatures (TEX^H_{86} Index) for the last 192 ka showed that periods of reduced Atlantic meridional overturning circulation (AMOC, based on ^{13}C of benthic foraminifera) coincide with a reduction in the near-surface vertical temperature gradient. Thus, variations in AMOC strength appear to be an important driver of the thermocline structure in the tropical Atlantic during this time period. Three independent organic proxies ($U^{K'}_{37}$, TEX^H_{86} and the LDI based on long-chain diols) were used to reconstruct seasonal SSTs for the last 135 ka in sediments from the Murray Canyons area on the coast of SE Australia. Comparison with SST estimates based on the modern analogue technique using foraminiferal assemblages shows that LDI inferred-temperatures compared well with the temperature of the warmest month, TEX^H_{86} with the temperature of the coolest month and $U^{K'}_{37}$ with mean annual temperature. An increase in TEX^H_{86} temperature estimates relative to the other proxies during deglaciations and interglacials indicated that either winter temperatures rapidly warmed, possibly due to an invigoration of the warm Leeuwin Current over the core site, or that there was a change in the growth season of the Thaumarchaeota, the source organism of the biomarkers used for TEX^H_{86} proxy.

Accumulation rates and concentrations of lipid biomarkers from various marine plankton classes were used to examine the changes in primary productivity at the above mentioned sites during the late Quaternary. In NW Africa, the relationship between primary productivity and iron supply from Sahara dust was evaluated. During the past 192 ka, total organic carbon (TOC) content and organic proxies for dinoflagellates, eustigmatophytes and haptophytes productivity revealed minima during interglacials and increased levels throughout glacial, Marine Isotope Stages (MIS) 3 and 5d. A positive correlation with sedimentary Fe was

observed, in particular during periods of high aridity on the continent. Thus, the productivity in the oligotrophic Guinea Plateau Margin is considerably influenced by the fertilization effect of the Sahara dust. To identify the impact of transport of nutrients from Southern Ocean waters on the primary productivity offshore SE Australia, a high-resolution planktonic foraminiferal $\delta^{13}\text{C}$ record was compared with the TOC content and biomarker records for *Proboscia* diatoms and haptophytes. Increases in primary productivity did not match periods of minima in planktonic foraminiferal $\delta^{13}\text{C}$, suggesting that the presence of the ^{13}C -depleted Southern Ocean waters in the Murray Canyons area did not stimulate productivity. Instead, the reconstructed periods of increased primary productivity are mainly thought to be due to stronger westerlies winds that brought dust to the core site and enhanced mixing of the water column during glacial periods. On the other hand, *Proboscia* diatom productivity is probably controlled by the transport of silicic acid to this area as increases in its productivity matched increased diatom productivity observed at some sites of the tropical equatorial Pacific. Finally, the abundance and structure of steryl alkyl ethers (SAE) were investigated in the core offshore SE Australia. The sedimentary record of these SAE show a rapid increase during glacial episodes and for those intervals characterized by a sharp decline in SST, suggesting that SAE may be related to marine eukaryotes that thrive when there is an influx of cold deep waters.

To assess changes in the vegetation of NW Africa and SE Australia, the stable carbon isotopic composition of plant leaf waxes were analysed. Sediments from the Guinea Plateau Margin reveal three periods (early Holocene, 50–45 and 120–110 ka) during the past 192 ka when the central Sahara/Sahel contained a higher percentage of C_3 plants, indicating wetter conditions than at present. A remarkably close correlation between $\delta^{13}\text{C}$ of benthic foraminifera and the plant wax *n*-alkane $\delta^{13}\text{C}$ records indicates a strong connection between variability in AMOC strength and vegetation type in the Sahara/Sahel region. The plant wax *n*-alkane $\delta^{13}\text{C}$ record of the SE Australian core reveals an increase in C_3 plant abundance during glacial periods and an extensive period (68–31ka) of generally high C_4 plant abundance that is punctuated by a sharp increase in C_3 vegetation at ~43 ka. This sharp increase in C_3 vegetation lasts ~5 ka and is characterized by increased levels of biomass burning as revealed by the quantification of levoglucosan, analysed using a novel method. Thus, this sharp vegetation change was likely caused by increased burning events and/or by substantially reduced herbivory as it follows the main period of the late Quaternary megafauna extinction in Australia.

This thesis demonstrates the benefit of applying multiple organic proxies on marine sediment cores to assess paleoenvironmental changes both in the marine environment as well as on the continent. It has thereby provided new insights in the cause and effect of environmental changes in marine and continental areas of NW Africa and SE Australia.

Samenvatting

Noordwest (NW) Afrika en zuidoost (ZO) Australië zijn gebieden die bijzonder gevoelig zijn voor klimaatveranderingen. De voorspelde klimaatverschuivingen kunnen leiden tot grote veranderingen in temperatuur, watertoevoer en biodiversiteit en leiden tot verminderde voedselproductie. Klimaatmodellen worden gebruikt om te voorspellen hoe het klimaat zal veranderen, maar deze voorspellingen zijn onderhevig aan grote onzekerheden. Een manier om deze modellen te verbeteren is ze te testen met paleoklimaatdata. In dit proefschrift worden organische indicatoren toegepast op mariene sedimentkernen om vroegere milieuocondities te reconstrueren van NW Afrika en ZO Australië. Drie milieuparameters werden in het bijzonder bestudeerd: zeewatertemperatuur, primaire productie en vegetatieveranderingen.

Voor sedimenten afkomstig van het continentale plat van Guinea (NW Afrika) werd aangetoond dat de $U^{K'}_{37}$ index (gebaseerd op langketige alkenonen) een goede indicator is voor oppervlaktezeewatertemperatuur (OZT) terwijl de TEX^H_{86} index (gebaseerd op glycerol dialkyl glycerol tetraethers) gerelateerd was aan temperaturen van de thermocline. De gereconstrueerde OZT ($U^{K'}_{37}$ index) en thermocline temperaturen (TEX^H_{86} index) van de laatste 192,000 jaar lieten zien dat perioden met een verminderde Atlantische Meridionale Omslaande Circulatie (AMOC; gebaseerd op het ^{13}C -gehalte van benthische foraminiferen) overeenkwamen met perioden gekenmerkt door een vermindering van de verticale temperatuurgradiënt. Variaties in de sterkte van de AMOC lijken dus een belangrijke sturing te zijn voor de structuur van de thermocline in de tropische Atlantische Ocean. Drie onafhankelijke proxies ($U^{K'}_{37}$, TEX^H_{86} en de LDI gebaseerd op langketige diolen) werden gebruikt om de OZT van verschillende seizoenen te reconstrueren van de laatste 135,000 jaar, gebruikmakend van sedimenten afkomstig van het Murray Canyons gebied voor de kust van ZO Australië. Een vergelijking van de verschillende OZT indicatoren met de moderne-analoog-techniek gebaseerd op foraminiferenassemblages laat zien dat LDI temperaturen vergelijkbaar zijn met de temperaturen van de warmste maand, de TEX^H_{86} temperaturen met de temperaturen van de koelste maand en de $U^{K'}_{37}$ temperaturen met de jaargemiddelde temperatuur. Een toename in TEX^H_{86} temperaturen ten opzichte van de andere OZT indicatoren gedurende de deglaciaties en interglacialen suggereert dat vooral de wintertemperaturen toenamen, mogelijk door een versterking van de warme Leeuwin Current, of een verandering in het groeiseizoen van de Thaumarchaeota (de microorganismen die de componenten die voor de TEX^H_{86} gebruikt worden synthetiseren).

Accumulatiesnelheden en concentraties van biomarker-lipiden van verschillende soorten marien plankton werden gebruikt om veranderingen in primaire productie te reconstrueren. Voor NW Afrika werd ook de relatie tussen primaire productie en de toevoer van ijzer via stof uit de Sahara woestijn geëvalueerd. Gedurende de afgelopen 192,000 jaar waren de hoeveelheden totale organische koolstof en biomarkers voor dinoflagellaten,

eustigmatophyten and haptophyten laag in de interglacialen en hoog in de glacialen en Mariene Isotopen Stadia 3 en 5d. Er werd ook een positieve correlatie gevonden met de hoeveelheid ijzer in sedimenten, vooral in periodes gekenmerkt door grote droogte op het continent. Dit betekent dat de productiviteit op het oligotrofe continentale plat van Guinea behoorlijk beïnvloed wordt door het bemestingseffect van stof afkomstig uit de Sahara woestijn. Om de invloed van nutriënten afkomstig uit de Zuidelijke Oceaan op de primaire productie voor de kust van ZO Australië te onderzoeken, werd er een hoge resolutie profiel van ^{13}C -gehaltes van planktonische foraminiferen vergeleken met de concentraties van organisch koolstof en biomarkers voor *Proboscia* diatomeeën en haptophyten. Perioden gekenmerkt door een toename in primaire productie kwamen niet overeen met perioden met een laag ^{13}C -gehalte van planktonische foraminiferen, hetgeen suggereert dat de aanwezigheid van ^{13}C -arm water uit de Zuidelijke Oceaan de productiviteit in het Murray Canyons gebied niet stimuleerde. De toegenomen primaire productie leek daarentegen meer toe te schrijven aan een toename in westelijke winden die stof naar het Murray Canyons gebied brachten en een grotere menging van de waterkolom veroorzaakte. Daarentegen werd de productiviteit van *Proboscia* diatomeeën beïnvloed door transport van kiezelzuur naar dit gebied omdat de toename in productiviteit overeenkomt met toegenomen productiviteit van diatomeeën rond de evenaar in de tropische Stille Oceaan. Tenslotte werden het voorkomen en de moleculaire structuren van sterol-alkylethers onderzocht in de kern voor de kust van ZO Australië. Deze sterol-alkylethers namen snel in concentratie toe gedurende de ijstijden en in periodes waarin er een snelle afname in OZT werd geobserveerd. Dit suggereert dat sterol-alkylethers afkomstig zijn van mariene eukaryoten die bloeien als er een toename is van koude diepe wateren in het oppervlaktewater.

Om vegetatieveranderingen in NW Afrika and ZO Australië te kunnen reconstrueren werd de stabiele koolstofsitoopsamenstelling van plantenwassen geanalyseerd. Analyse van de kern uit het continentale plat van Guinea toonde aan dat er drie perioden (vroeg Holoceen, 50,000 tot 45,000 en 120,000 tot 110,000 jaar geleden) in de afgelopen 192,000 jaar waren wanneer de Sahara/Sahel regio een hogere percentage aan C_3 -plant vegetatie (grasland) bevatte, daarmee nattere omstandigheden dan heden ten dage suggererend. Een opmerkelijk sterke correlatie tussen de ^{13}C -gehaltes van bentische foraminiferen en ^{13}C -gehaltes van *n*-alkanen afkomstig van plantenwassen werd vastgesteld, hetgeen een sterk verband tussen de variatie in de sterkte van AMOC en de type vegetatie in de Sahara/Sahel regio suggereert. Het ^{13}C -gehalte van *n*-alkanen uit de kern van ZO Australië laat zien dat er een toename in C_3 -plant vegetatie is gedurende ijstijden en een lange periode (68,000 tot 31,000 jaar geleden) van hoge hoeveelheden C_4 plant vegetatie. Deze periode werd onderbroken door een tijdelijke scherpe toename in C_3 -plant vegetatie rond ~43,000 jaar geleden. Deze toename duurde ~5,000 jaar en wordt gekenmerkt door een toename in vegetatiebranden, gereconstrueerd door de toename in de hoeveelheden levoglucosan in sedimenten. Deze

snelle vegetatieverandering werd dus waarschijnlijk veroorzaakt door vegetatiebranden en/of door de gereduceerde aantallen planteneters omdat de verandering volgde op de uitsterving van de megafauna in Australia.

Dit proefschrift laat de grote voordelen zien van het toepassen van meerder organische indicatoren op mariene sedimentkernen om de milieucondities op zowel land als in zee te reconstrueren. Dit heeft tot nieuwe inzichten geleid in de oorzaken en gevolgen van milieuveranderingen in de kustzee en op land van NW Afrika en ZO Australië.

Resumo

O noroeste Africano e o sudeste Australiano são áreas particularmente vulneráveis a mudanças climáticas. As mudanças climáticas previstas para o futuro nestas regiões podem levar a grandes alterações de temperaturas e abastecimento de água, fortes mudanças na biodiversidade e podem comprometer a produção de alimentos. Prévias pesquisas usando modelos climáticos foram executadas para investigar o impacto de futuras mudanças climáticas nestas regiões, mas infelizmente, várias incertezas permanecem em tais previsões. Uma forma de melhorar os resultados dos modelos climáticos é testá-los com dados climáticos do passado. Nesta tese, indicadores orgânicos são analisados em sedimentos marinhos para reconstruir condições ambientais ocorridas no noroeste Africano e no sudeste Australiano. Três parâmetros ambientais foram estudados: temperaturas da água do mar, produtividade primária e mudanças na vegetação.

Em sedimentos da margem continental da Guiné no noroeste Africano, o índice $U^{K'}_{37}$ (baseado em alquenonas de cadeia longa) mostrou-se um indicador eficiente para a reconstrução de Temperaturas da Superfície do Mar (TSM), enquanto que o índice TEX^H_{86} (baseado em glicerol tetraéters glicerol dialkil) mostrou-se estar relacionado com temperaturas do termoclina. O registo de TSMs ($U^{K'}_{37}$) e temperaturas do termoclina (TEX^H_{86}) para os últimos 192,000 anos mostrou que períodos de reduzida Circulação Meridional de Retorno do Atlântico, baseado em ^{13}C de foraminíferos bêntônicos, coincide com uma redução no gradiente vertical de temperaturas próximas à superfície. Assim, variações na força da Circulação Meridional de Retorno do Atlântico parece ser um importante mecanismo de controlo da estrutura do termoclina no Atlântico tropical durante este período de tempo. Por outro lado, três indicadores orgânicos independentes ($U^{K'}_{37}$, TEX^H_{86} e o LDI baseado em dióis de cadeia longa) foram usados para reconstruir TSMs dos últimos 135,000 anos em sedimentos da área dos canhões marinhos de Murray na margem continental do sudoeste Australiano. Comparações de TSMs estimadas por estes indicadores orgânicos com estimativas de TSMs baseadas na técnica analógica moderna de associações de foraminíferos planctónicos, mostrou que temperaturas inferidas pelo LDI compara-se bem com temperaturas do mês mais quente, TEX^H_{86} com temperaturas do mês mais frio e $U^{K'}_{37}$ com temperaturas médias anuais. Um aumento nas estimativas de temperatura do TEX^H_{86} relativo aos outros indicadores durante deglaciações e períodos interglaciais indicou, ou que temperaturas do inverno aqueceram rapidamente, talvez devido a um fortalecimento da corrente quente de Leeuwin sobre o local, ou que houve uma mudança na estação de crescimento do *Thaumarchaeota*, o organismo que produz os compostos base do TEX^H_{86} .

O índice de acumulação e concentrações de lipídios específicos de várias classes marinhas de plâncton foram usados para examinar as mudanças em produtividade primária nos locais acima citados durante o Quaternário tórdio. No noroeste Africano, o relacionamento entre

produtividade primária e o conteúdo de ferro no pó do Sahara foi avaliado. Durante os últimos 192,000 anos, o conteúdo total do carbono orgânico (TOC) e indicadores orgânicos para a produtividade de dinoflagelados, eustigmatofitas e haptofitas revelaram mínimas durante interglaciais e máximas durante glaciações e estágios isotópicos marinhos (MIS) 3 e 5d. Uma correlação positiva entre a produtividade primária e o conteúdo de ferro foi observado, em particular durante períodos de grande aridez no continente. Assim, a produtividade na margem continental da Guiné, caracterizada por condições oligotróficas, é consideravelmente influenciada pelo efeito de fertilização do pó do Sahara. Para identificar o impacto do transporte de nutrientes das águas do oceano Antártico na produtividade primária na margem continental do sudeste Australiano, um registo de alta resolução da composição isotópica de foraminíferos planctônicos foi comparado com o conteúdo de TOC e registos de indicadores orgânicos para a diatomácea do género *Proboscia* e haptofitas. Os aumentos em produtividade primária não combinaram com períodos de mínimos em $\delta^{13}\text{C}$ dos foraminíferos, sugerindo que a presença das águas do Oceano Antártico não estimulou a produtividade na área dos canhões marinhos de Murray. Em vez disso, os períodos de produtividade primária máxima foram durante períodos glaciais, provavelmente devido a ventos ocidentais mais fortes que trouxeram pó ao local e provocaram uma maior mistura da coluna de água, fertilizando as águas superficiais. Por outro lado, a produtividade da diatomácea do género *Proboscia* é provavelmente controlada pelo transporte de silício a esta área na medida em que aumentos em sua produtividade coincide com aumentos na produtividade de diatomáceas em alguns locais do Pacífico equatorial. Finalmente, a abundância e estrutura dos steril alkil éters (SAE) foram investigados na margem continental do sudeste Australiano. O registo sedimentário destes SAE mostra um aumento rápido durante episódios glaciais e intervalos caracterizados por um declínio drástico em TSM, sugerindo que SAE pode estar relacionado a eucariotas marinhos que prosperam quando há um influxo de águas profundas frias.

Para avaliar mudanças na vegetação do noroeste Africano e sudeste Australiano, a composição isotópica do carbono estável de lípidos encontrados na cera de folhas de plantas, e depositados posteriormente em sedimentos marinhos, foram analisados. Os sedimentos da margem continental da Guiné revelaram três períodos (Holoceno primário, 50,000–45,000 anos e 120,000–110,000 anos) durante os últimos 192,000 anos quando o Sahara/Sahel conteve uma percentagem mais alta de plantas com o mecanismo fotossintético do tipo C_3 , indicando condições mais húmidas que atualmente. Uma excepcional correlação entre registos isotópicos de foraminíferos bentônicos e *n*-alcanos encontrados nas ceras das plantas indica uma conexão forte entre a variabilidade na força da Circulação Meridional de Retorno do Atlântico e a vegetação na região de Sahara/Sahel. O registo isotópico de *n*-alcanos do sudeste Australiano revela um aumento em abundância de plantas do tipo C_3 durante períodos glaciais e um extenso período (68–31,000 anos) de alta abundância de plantas do tipo C_4 que é interrompida temporariamente por um aumento agudo em vegetação do tipo C_3 em ~43,000

anos. Este aumento agudo em vegetação do tipo C₃ dura ~5,000 anos e é caracterizado por níveis aumentados de queimadura da biomassa vegetal revelado pela quantificação de levoglucosano, analisado usando um novo método. Assim, esta mudança aguda de vegetação foi provavelmente causada por um aumento de fogos e/ou por uma drástica redução em herbívoros tendo em conta que segue o período principal da extinção da megafauna durante o Quaternário tórdio em Austrália.

Esta tese demonstra o benefício de aplicar múltiplos indicadores orgânicos em sedimentos marinhos para avaliar mudanças climáticas em ambientes marinhos assim como em ambientes continentais, provendo assim a comunidade científica, novos juízos na relação causa e efeito de mudanças ambientais em áreas marinhas *versus* áreas continentais do noroeste Africano e sudeste Australiano.

Acknowledgements

These last four years have been an amazing experience for me as I really enjoy performing this research and I had the opportunity to meet great people. This work would not be possible without the help and support of several people that directly or indirectly made this thesis a reality. Therefore, I would like to take this opportunity to show my gratitude to all of them.

First and foremost, I would like to thank my promoters Stefan Schouten and Jaap Sinninghe Damsté for the opportunity to work in the group, all the guidance, constructive criticism, article corrections and for the kind words on the good and less good moments. Special thanks go to Stefan Schouten for the endless patience to listen and answer my questions and all the scientific discussions. Your enthusiasm and support was definitely essential to push me forward.

Thank you to Patrick De Deckker for all the scientific comments and article corrections. Thanks very much for all the support and assistance during this 4 year and the great hospitality during the fieldwork in Australia.

I would like to thank all the others co-authors and people mentioned in the acknowledgements of the manuscripts for all the constructive comments and for the successful collaborations.

I am also very grateful to Jort Ossebaar, Michiel Kienhuis, Marianne Baas, Anhelique Mets, and Irene Rijpstra for all the lab, instruments and computer assistances. Beside all the help and knowledge you gave me, I really enjoy your friendship and the time we have been together.

Thanks to Ellen Hopmans for all the help with the levoglucosan analysis and all the support on the scientific and non scientific aspects. I also would like to thank you for letting me know about the RIK Bodylanguage gym, where I had very good moments.

I would like to thank Jung-Hyun Kim for giving me the possibility to participate in the PACEMAKER cruise and for all the understanding and support during my PhD. Thanks for the crew of the R/V Pelagia and participants of the cruise for providing everything to create a nice and work-efficient environment. Particularly, Claudia Zell, Denise Dorhout, Marianne Baas, Marcel Bakker, Ivo Witte and José Silva, a special thanks for the good conversations, moments and assistance during the cruise and during the time in Texel.

Special thanks go to all my office mates: Petra Schoon², Darci Rush, Thorsten Bauersachs and Anhelique Mets. Petra, thank you for your support and patience in the stressful moments, your endless friendship, your tolerance even after our constructive discussions ☺ and for always had been there in the good moments (in The Netherlands, Italy, Swiss, USA). Darci, thanks for always share your smile and always be there when I needed your help. Thorsten, thanks for being such a nice friend and colleague for the 2.5 years we shared office. It was inspiring to see your enthusiasm for science. Anhelique, thanks for being really supportive during the last phase of my PhD, for always answering my 'last minute' technical questions and for your tolerance with the heating of the room.

For all the members of the BGC group (tenure tracks, post-docs, PhDs, students, technicians and guests) a big thank you for all the nice moments, conversation and good

cakes we share inside and outside work. I feel a very lucky person to have the opportunity to get to know all of you. Special thanks go for some people (inside and outside the BGC group) that helped me with the work and/or to overcome the winters and the stress of the last year of PhD by sharing their friendship: Sebastiaan Rampen, Marcel van der Meer, Jan de Leeuw, Alina Stadniskaia, Monique Verweij, Danielle Schoen, Isla Castañeda, Francien Peterse, Angela Pitcher, Andrea Jaeschke, Joost Brandsma, Adam Klimiuk, Arjan Boere, Sabine Lengger, Nicole Bale, Cindy de Jonge, Sandra Heinzelmann, Yvonne Lipsewers, Daniela M'Boule, Martina Sollai, Lisa Warden, Cecile Blanchet, Laura Villanueva, Marta Rodrigo, Dorien Kool, Elisabeth Svensson, Sebastian Kasper, Kevin Donkers, Elisha Moore, Robert Gibson, David Chivall, Elda Panoto, Kees Booi, Ronald van Bommel, Cornelia Blaga, Kasia Sliwiska, Marita Smith, Els van Soelen, John Cluderay, Sharyn Ossebaar and Karel Bakker.

A big big hug goes to Margot Bik for all the friendship, laugh, support and constant care for me. I enjoyed very much sharing the house with you and the teas on the beach. Thanks very much also for all the work with reference manager.

I would like to thank Joke Mulder, Bert Aggenbach, and all the ICT, financial and technical departments for always being friendly and available to assist me.

For the Den Helder group and portuguese crew: Julie Ogier, Craig Grove, Lauren Grove, Catarina Leote, Pedro Frade, Veronica Willmot, Antje Müller, Silvia Santos, Jeremy Smith, Vânia Freitas, Filipe Amador, Sofia Saraiva, Luis Fernandes, Henrique Fernandes, Joana Cardoso, Ben Abbas, Inês Abbas, Cátia Carreira, Christian Lønborg, Catarina Silva and Catarina Cruzeiro. Very big thank you for all the dinners, wines and beers, 4 o'clock coffee breaks, visits to 'kermis', few visit to the SPOT, Teso boat trips together, for sharing the excitement of the arrival of new members in the group, good company and friendship. Julie, you and Craig have been always there for me and your friendship, support, calm and care made my life in Den Helder even more enjoyable. Big hug for everything ☺. Catarina Leote, adorei o tempo que dividimos casa em Den Helder, o ir ao cinema todas as semanas, as conversas até tarde e o bom almoço todos os dias. Fiquei sempre com muitas saudades tuas quando regressaste a Portugal. Um abraço.

During these four years some people in Maastricht and Delft also have supported me: Barbara Zarzycka and the Delft association, particularly Helga Cálix, Loreen Villacorte, Adrian Almoradie and Nuttakan Wongfun. Thank you all for your friendship and support since the time we did the master together.

Rotterdam was a welcome city for me with a lot of friendship, love and support. Djola obrigada por ter conseguid fazer ri e dam força cond menos nta espera. Bô ma bô família recebem super bem e mi é mut agradecida por tudo. Côrr obrigada pa tut morabeza enquant nteve de fim de semana na bo casa. Mana Filipa, Ti Djon e família um muitíssimo obrigada pa tud amor e cuidod na mi durante es quatro one, boces foi um autêntica família pa mi es temp tud. Otto, durante es quatro one no passa por muitos bons momentos. Obrigada por fca a nha lado támbé durante momentos mais difíceis. Bô paciência e carinho isdam a consegui terminá esse doutoramento. Ncá tem palavras pa expressa tont nta agradeceb.

Pa tut nha família, presentes e ausentes, um grande obrigada pa tut carinho e apoio. Mãe, Pai, Victor, Walter, Ruy, Teresa, Celene, Vivian e Tiago, parabéns pa es tese cnó escrevé.

Curriculum Vitae

Raquel Alfama Lopes dos Santos was born on the 10th of October 1979 in Mindelo, Cape Verde. After finishing high-school, she moved to Portugal to do her bacharel / licenciature in biology with a minor specialization in microbiology at the University of Coimbra. Soon after graduation in 2002, she started a half-year internship in water quality control at the University of Faro – Portugal. In 2003, she returned to Cape Verde and worked as a lecturer in a marine biology course at the Institute of Marine Sciences and Engineer in Mindelo. Later in 2006, she moved to The Netherlands to continue her studies at the UNESCO-IHE Institute for Water Education in Delft. At the end of her master in Environmental Sciences, she spent 6 months in the marine biogeochemistry and toxicology department at NIOZ Royal Netherlands Institute for Sea Research to perform her master thesis. After completing her master with distinction in 2008, she started her PhD in biogeochemistry at NIOZ in that same year. Her PhD focused on the application of multiple organic proxies in paleoclimate reconstructions and the results of that project are documented in this thesis.